ISSN 0236-2945

LIGHT & ENGINEERING

Volume 26, Number 3, 2018

Editorial of Journal
"Light & Engineering" (Svetotekhnika), Moscow

Journal “Light & Engineering” had been founded by Prof. Julian B. Aizenberg in 1993

LIGHT & ENGINEERING

СВЕТО ТЕХНИКА

Editorial of Journal “Light & Engineering/Svetotekhnika”

Moscow, 2018

Editorial Office:

Russia, VNISI, Rooms 327 and 334
106 Prospekt Mira, Moscow 129626

Tel: +7.495.682.26.54
Tel./Fax: +7.495.682.58.46
E-mail: lights-nr@inbox.ru
http://www.sveto-tekhnika.ru

Scientific Editors:

Sergei G. Ashurkov
Evgene I. Rozovsky
Raisa I. Stolyarevskaya
Art and CAD Editor
Andrei M. Bogdanov
Style Editor
Marsha D. Vinogradova

Light & Engineering" is an international scientific Journal subscribed to by readers in many different countries. It is the English edition of the journal "Svetotekhnika" the oldest scientific publication in Russia, established in 1932.

Establishing the English edition "Light and Engineering" in 1993 allowed Russian illumination science to be presented the colleagues abroad. It attracted the attention of experts and a new generation of scientists from different countries to Russian domestic achievements in light and engineering science. It also introduced the results of international research and their industrial application on the Russian lighting market.

The scope of our publication is to present the most current results of fundamental research in the field of illumination science. This includes theoretical bases of light source development, physiological optics, lighting technology, photometry, colorimetry, radiometry and metrology, visual perception, health and hazard, energy efficiency, semiconductor sources of light and many others related directions. The journal also aims to cover the application illumination science in technology of light sources, lighting devices, lighting installations, control systems, standards, lighting art and design, and so on.

"Light & Engineering" is well known by its brand and design in the field of light and illumination. Each annual volume has four issues, with about 80–140 pages per issue. Each paper is reviewed by recognized world experts.

To promote the work of the Journal, the editorial staff is in active communication with Thomson Scientific (Citation index) and other international publishing houses and agencies, such as Elsevier and EBSCO Publishing.

CONTENTS

VOLUME 26 NUMBER 3 2018

LIGHT & ENGINEERING

Light & Engineering
Vol. 26, No. 3, pp. 4–6, 2018

Svetotekhnika
No. 3, 2018, pp. 8–11

THE SCIENCE OF LIGHT ENGINEERING, FIELDS OF APPLICATION AND THEORETICAL FOUNDATIONS

Yulian B. Aizenberg[1,2] and Vladimir P. Budak[2]

[1] Russian Lighting Research Institute named after S.I. Vavilov, Moscow
[2] Editorial of Journal "Light & Engineering" (Svetotekhnika), Moscow
E-mail: julian.aizenberg@mail.ru, budakvp@gmail.com

ABSTRACT

The article discussed two important problems, which have not been addressed previously:

– The conceptual interpretation of lighting engineering, and the expansion of its definition beyond illumination, which has became widely accepted. An expanded concept of lighting engineering proposed by the authors includes all fields of application of optical radiation (light): illumination, irradiation, phototherapy (light therapy), light alarm systems, light location, light design, etc;

– The problem of developing the theoretical foundation of Lighting Engineering. Differences between three existing light theories are summarised. The first one is quantum theory, explaining all known light phenomena. The second one is wave theory based on the provision that light spreads in waves. The third theory is beam and photometric based on the light field theory, which is the most widely applied and simple for practical calculations and simulation.

Keywords: illumination, light irradiation, phototherapy, light location, power engineering, light design, light propagation theory, quantum, wave, beam or photometric

The formation and development of light engineering as an applied science occurred alongside the introduction of electric illumination, which was the most important stage of the second industrial revolution, characterising by the transition from steam to electric energy. From today's perspective, it is difficult to overestimate the introduction of electric illumination into our lives: society was no longer dependent on natural light and could create comfortable conditions for work, study and rest at any time. It would not be an exaggeration to say that electric illumination determined to a large extent the enormous scientific and technological progress of the twentieth century.

The generally accepted definition of light engineering science refers to an important but relatively narrow branch of industry. This industry is dedicated to the topics of generating optical radiation (light), its distribution in space and its application for illumination to create a visual image, non-visual exposure of people and other animals, the development of irradiating installations for plants, phototherapy (light therapy) and light alarm systems.

This definition is typical for the absolute majority of documents, books and journals, for the Light and Engineering professional description 05.09.07 of the Russian Federation State Commission for Academic Degrees and Titles and for training programmes of lighting engineers in all higher education institutions.

Telling is the name of the the International Commission on Illumination (CIE) as the scientific association for our field, as are the titles of all reputable lighting journals in the world: *Lighting Design + Application* (USA), *Journal of Lighting* (United Kingdom), *Lighting Research and Development* (United Kingdom), *Lux* (France), *Beleuchtung* (Germany), *Svetlo* (Czech Republic).

But *Lighting* means illumination, as well as *Beleuchtung*. The journals as *Leucos* (USA), *Licht* (Germany), *Lux* (France) and *Light & Engineering* (Russia) have a more holistic approach in to light in their title. The first two also consider the problem of illumination as their key topic.

And this is far from being accidental. Very few branches of science and engineering have are associated with such an impactful aspect of human existence and humanity as illumination. Between 10 % and 25 % of all electric energy generated in different countries and cities is consumed for illumination. Without illumination, cultural life, production and recreation would be impossible. The exploration of the oceans and space would also be impossible.

The introduction of electric illumination into our lives has demanded the development of light devices (LD) and illumination installations (II) calculation methods, methods to measure their characteristics, to determine illumination standards so that certain operations could be performed. A theoretical model of light was created as part of this process. This model was based on previous discoveries in astronomical photometry [1, 2]. Photometry (from the ancient Greek φῶς, or φωτός – light and μετρέω – measure) is an overarching scientific subject applicable to all branches of optics. It is the basis for the quantitative measurements of radiation field energy characteristics. A.A. Gershun [3] considered that the word "measurement" can also be interpreted in a broad sense, without reducing it to an experiment method, but considering the totality of theoretical and experimental questions relating to a quantitative comparison. Bouguer-Lambert's photometry was based on Kepler's ideas of light as a totality of rays [4]. Therefore, this model was named photometric and beam. The model was perfected in A.A. Gershun's works as a theory of the light field, which is being a space studied from the view point of the radiant energy transport happening therein [3].

The light field theory was developed at the same time and in parallel with the light electromagnetic (wave) theory, and later, with quantum electrodynamics. The connection between light field theory and light wave and quantum theories remained unqualified for a long time, which determined the attitude of physicists to it as an approximate, engineering and applied science. This connection was revealed in studies at the end of the twentieth century [5], which determined a hierarchy of three light theories in physics. The primary theory explains all light phenomena known for today: the quantum theory based on light as a collection of photons [6]. This theory is the most abstract, leading to difficulties in the interpretation of real measurements. If the number of photons is very large, their movement can be described as a wave process. This naturally leads to wave optics. In principle [7], wave and beam descriptions are equivalent to each other in the wave uniformity area: the ray is perpendicular to the wave in each point. Therefore, knowing the wave direction in space, the rays can be reassembled and vice versa. A uniformity (quasi-uniformity) condition of a field is its constancy in the wave length scale. If a wave direction changes abruptly in the wavelength scale, the field is non-uniform and its beam description is impossible. Light diffraction on a small opening is an example of this.

However, unveiling the connection between the three light theories showed that within their individual boundaries, each model has internal consistency and does not need any correction. Moreover, one should admit that the photometric beam model is correct in the majority of practical situations, and its deviations only appear in very fine experiments. The essence of the light field photometric model can be reduced to four main axioms [5]:

– The light field is a totality of arbitrary direction rays, along each of which light energy is transmitted. Therefore, spatial and angular power density of the transmitted energy is the luminance in a point of the light field along a set direction.

– The rays coming to the same point in space are independent (not coherent) of each other, which determines the absence of interference and additive luminance in the point.

– The time constant and the size of the radiation receiver are significantly greater than the radiation period and wavelength, which allows using wave field statistical moments when determining photometric values.

– Light fields are ergodic, which allows applying means (averages) to the photons, which is used in statistical optics to evaluate means for a specific implementation measured practically.

The light field theory goes significantly beyond illumination technology and serves as a language to describe almost any technological use of light. Therefore, the scope of lighting science is significantly wider than the problems of illumination. Op-

tical radiation is also used in light location, disinfection of drinking water and of industrial waste water, in deaeration, medicine, light design, solar power engineering and in many other applications.

Let us consider the boundaries of studies in the light engineering field and where the conditional boundary lies which separates lighting engineering from optics, laser engineering, radio engineering and astronomy.

Lighting science only considers the transport of incoherent radiation based on light field laws. This is the main fundamental difference of all lighting studies, developments and of their application in practice.

The purpose and definition of lighting engineering should be the development of light science within the boundaries of beam photometric ideas and its application for comfortable illumination, technological and medical contexts. ***Lighting Engineering*** is a field of science and technology, which takes as its subject the development of methods of generation and spatial distribution of optical radiation, as well as its transformation to other types of energy and its application for a variety of purposes.

The twenty-first century is a century of light. The scope of use for light continues to expand. The existence of a uniform international scientific and technological approach allows considering fundamental theoretical and applied problems in all spheres of light application from uniform first principles. It is noteworthy that *Svetotekhnika* / *Light & Engineering* is the only journal in the world, which publishes papers not just associated with illumination problems, but also the use of light for technological purposes within the boundaries of light field theory.

Modern lighting science and practice are based on the fundamentals of light field theory. However, in the context of rapid progress of adjacent fields of knowledge, lighting installations become automated systems, using light sources with LEDs and detectors, relays and other elements of automated control systems, taking into account the natural change of the surrounding light environment. Such technology is used, for example, in greenhouse facilities, poultry industry, water disinfection systems, etc.

Currently, studies may explore the processes and phenomena of visual and non-visual human perception. All of these are also based on the use of light, with light field theory is their physical foundation.

REFERENCES

1. Bouguer P. Optical tractate about light gradation, Moscow, The USSSR Academy of Science, 1950.

2. Lambert J.H., Photometria, sive de Mensura et Gradibus luminais, Colorum et Umbrae. Augsburg, 1760.

3. Gershun A.A. Selected manuscripts on photometry and lighting engineering / Moscow, G. Phys.-Math. P.H., Leningrad, 1958.

4. Kepler J. Ad vitellionem paralipomena, quibus astronomiae pars optica traditur de modo visionis, & humorum oculi usu, contra options& anatomicos. Frankfurt: C. Marnius & Heirs of J. Aubrius, 1604.

5. Apresyan L.A., Kravtsov Yu.A. Theory of radiation transfer: statistical and wave aspects/ Moscow, Science (Nauka), Main publisher house of phys.-math. literature, 1983.

6. Veklenko B.A. The Nature of the Photon and Quantum Optics// Light & Engineering, 2018, V.26, #2, pp. 4–13.

7. Born M., Wolf E. Fundamentals of Optics/ Second edition, Translation from Eng. To Russian Moscow, Science (Nauka), Main publisher house of phys.-math. literature, 1973.

Julian B. Ayzenberg, Prof. Dr. of Technical science, graduated from the Moscow Power Institute in 1954, General Editor of Svetotekhnika/ Light & Engineering Journal and chief researcher of VNISI named after S.I. Vavilov, Full Member of the Academy of Electro-technical Sciences of the Russian Federation, Honoured inventor of the RF

Vladimir P. Budak, Prof., Dr. of Technical Science, graduated from the Moscow Power Institute in 1981, Editor in-chief of Svetotekhnika/ Light & Engineering Journal, Professor of the Light and Engineering Chair of the Moscow Power Institute NRU, Corresponding member of the Academy of Electro-technical Sciences of the Russian Federation

Light & Engineering
Vol. 26, No. 3, pp. 7–13, 2018

Svetotekhnika
No. 1, 2018, pp. 40–44

RESULTS OF SPATIAL STRUCTURE OF ATMOSPHERE RADIATION IN A SPECTRAL RANGE (1.5−2) μm RESEARCH

Anton M. Mishchenko [1 *], Sergei S. Rachkovsky [2], Vladimir A. Smolin [2], and Igor V. Yakimenko [2]

[1] *Military Academy of Army Air Defence of Russian Armed Forces of Marshall of the Soviet Union A.M. Vasilevsky (MA AAD of RF AF),*
[2] *Smolensk Branch of the Moscow Power Engineering Institute NRU, Smolensk*
[*] *E-mail: kycu@mail.ru*

ABSTRACT

Results of experimental studying radiation spatial structure of atmosphere background non-uniformities and of an unmanned aerial vehicle being the detection object are presented. The question on a possibility of its detection using optoelectronic systems against the background of a cloudy field in the near IR wavelength range is also considered.

Keywords: optoelectronic systems, experimental studies, radiation spatial structure of atmosphere non-uniformities, IR spectral range

The last publications on study of atmosphere cloudy field radiation concern middle (3–5) μm and far infrared (8–13) μm wavelength (WL) [1–5]. In some foreign sources, data of space studies in IR spectrum on atmosphere composition and on weather forecasting are given in [6–10]. As to the data on atmospheres studies in the WL (1.5–2) μm, the publications are practically absent. And this fact interferes with solving a topical problem of detecting pilotless aircrafts (PLA) by means of passive optoelectronic systems.

In this regard, the authors have developed a technique of experimental studies of atmosphere radiation spatial structure non-uniformities in the WL (1.5–2) μm range with various cloud cover types. These studies were carried out in two stages:

• Record (measurement) of atmosphere radiance (R) fluctuation in Russia midland during winter and spring periods in the morning;

• The results processing in order to obtain statistical models describing principles of cloudy fields R fluctuation spatial structure.

To record R fluctuation of cloudy fields, a measurement computing system was developed, which basic element is a radiometer for the WL (1.5–2) μm spectral interval [11]. The radiometer contains as follows: a lens (Cassegrain's telescope), a rotated beam chopper driven by means of a step motor, an interference filter of (1.5–2) μm WL transmission band, a *PbS* photoresistor, and an electronic part (preamplifier, scale amplifier, low pass filter, analogue-digital converter, microcontroller and flash memory).

To evaluate parameters of the radiometer, calibration operations were made for the following purposes: to determine instant visual field, to plot calibration volt-thermal characteristics, to plot calibration volt-watt characteristics and to determine transmission coefficients of the radiometer channels, as well as to evaluate threshold sensitivity and expected measurement errors.

As a result of the performed operations, the following characteristics of the radiometer were determined: field width (20' × 20'), calibration volt-thermal characteristic; volt-watt characteristic, spectral characteristic in the WL (1.55–1.93) μm, transmission coefficient of the radiometer channel

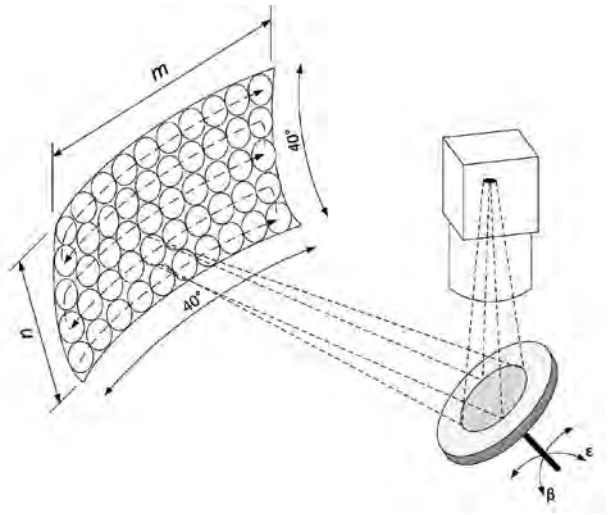

Fig. 1. A layout of scanning a cloudy field

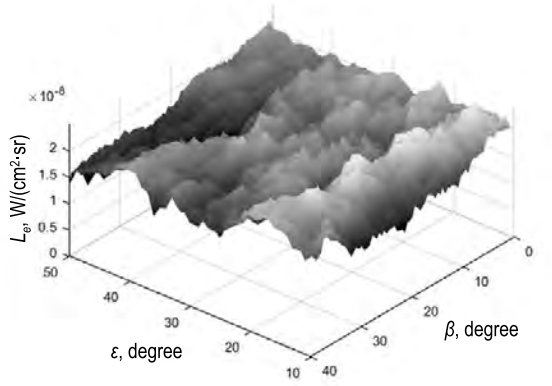

Fig. 2. A statistical model as a potential relief of radiance fluctuations average values distribution (L_e) of 4–6 points cumulus cloud cover (Cu)

($5.324 \cdot 10^7$ V·cm^2·strad/W), R threshold sensitivity ($6.411 \cdot 10^{-10}$ W/(cm^2·strad), R measurement error (10 %).

Control of step motors of the beam chopper and control of the scanning system mirror (Fig. 1) was implemented by a microcontroller. The commands came to the control unit via digital inputs (outputs) of the latter. Scanning sector of the selected atmospheric background (raster) fragment was provided within an interval to 40º in azimuth and within (10–50) º in altitude angle. The scanning mirror provided pass of one frame line within the selected fragment of atmospheric background for 5 s. During this time, in every 30', 80 R values of this background were recorded. Upon completion of the frame line scanning, a signal came to the step motor, the mirror changed tilt angle by 1°, and scanning was repeated in the opposite direction. In a preset number of pitches (lines), step motors returned scanning mirror to the initial position, and record of the taken frame using a replaceable flash carrier was performed. Then the cycle was repeated, and the next frame was recorded.

A statistical processing of the measurement results of cloudy field R fluctuations was carried out upon termination of the measurement series, which consisted in creation of a pack of frames (raster), on average by 30 pieces. In total, nine types of cloudy fields under day time conditions were studied: cumulus (Cu) of 1–3 points (87 pieces); cumulus (Cu) of 4–6 points (91 pieces); cumulus (Cu) of 7–9 points (93 pieces); stratocumulus (Sc) (84 pieces); altocumulus (Ac) (73 pieces); cirrocumulus (Cc) (85 pieces); stratiform (Stf) (123 pieces), cirrostratus (Cs) (118 pieces), cloudless sky (117 pieces). Totally 871 frames of cloudy fields were obtained.

Any such frame is a background image (BI) as a two-dimensional massif, which every element contains information on radiance level of the cloudy field in a selected direction. BI arrays can be a totality of lines and of columns (as matrices), an image in shades of grey or as a potential relief reflecting the spatial structure of atmosphere radiation non-uniformities.

Processing of the obtained BIs is carried out to obtain statistical models describing principles of R fluctuation of spatial structure of atmosphere cloudy fields. The BI processing results have shown that radiating non-uniformities of atmosphere cloudy fields are formed because of thermodynamic and turbulent atmospheric processes dependent on weather conditions. These non-uniformities have intrinsic angular dimensions and depend on cloud cover type, cloud amount, meteorological situation and day time.

After processing, the results are accumulated as packs of different type cloudy field BI frames and presented as matrices or as a potential relief of average values and dispersions (mean-square deviations) (RMSD) distribution. The obtained models can be considered to be statistical of the first type, which describe principles of spatial structure of atmosphere cloudy fields R fluctuations of the above named versions.

An analysis of the obtained statistical models of cloudy field radiance has shown that cumulus cloud cover (Cu) contains small-scale non-uniformities (Fig. 2). This can be explained by the fact that a cloudy Cu field has big vertical extent and in top

layers, ice crystals are contained, and in lower layers – water drops. As it is well-known [12], ice crystal reflection power in the WL (1.5–2) μm interval is higher than of water drops. Besides, a small increase of the R fluctuations average values and RMSD of a cloudy Cu field in the near-to-horizon area can be explained by influence of radiation reflection from Earth and from artefacts located on its surface.

Average values and dispersion (RMSD) of an altocumulus cloud cover (Ac) cloudy field R increase with increase of the altitude angle.

This result is explained by the fact that cloudy fields are formed at a big altitude and consist of ice crystals with a high reflection power in the WL (1.5–2) μm interval. And atmosphere influence in the near-to-horizon area increases because this area contains aerosols, which is absorbing a part of radiation.

In case of stratocumulus cloud cover (Sc), R average values and dispersion (RMSD) grow with increase of the altitude angle. This result is because of the fact that Sc type cloudy field is formed at a low height and mainly consists of water drops, which concentration increases in the near-to-horizon area as water drops to a great extent absorb WL radiation of the (1.5–2) μm interval [12].

During analysis of the obtained radiance statistical models for stratiform (St) cloud cover cloudy fields, it was revealed that average values and dispersion (RMSD) increase with increase of the altitude angle (Fig. 3). This is because St cloudy fields are formed at a low height and mainly consist of water drops, which concentration increases in the near-to-horizon area, and so they to a great extent absorb the considered type radiation [12].

Radiance average values and dispersions (RMSD) for stratiform cloudiness (Cs) cloudy fields are raise with increase of the altitude angle. This is because a Cs type cloudy field is formed at a big height and consists of ice crystals with high reflection power in the WL (1.5–2) μm interval. Reflection power decreases with reduction of altitude angle as distance between the measuring and computing system (MCS) and clouds increases; hence, radiation weakens because of absorption by atmosphere. A comparative low radiance value is explained by the fact that Cs type cloud structures are almost transparent.

Analysis results of the obtained statistical models of a clear sky hidden in morning haze have shown a high signal level. The reason of this is that

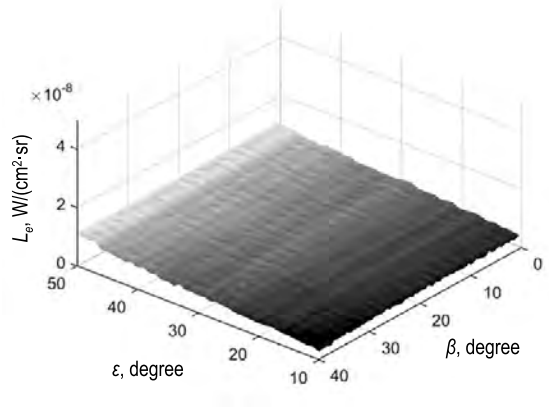

Fig. 3. A statistical model as a potential relief of radiance fluctuations average values distribution (L_e) of stratiform cloud cover (St)

despite a large water drop quantity determining the haze composition, optical thickness of the latter is insufficient for strong radiation absorption as, for example, in the event of St type cloud cover. Increase of average values and of dispersion (RMSD) with increase of the altitude angle, is caused by reduction of optical thickness of the haze absorbing radiation.

Measured R values in the event the sky is clear, are at the level of the radiometer intrinsic noise. A low signal level is generally caused by almost full absorption of the measured radiation and weak reflection because of a low aerosol concentration in the near-to-horizon area and of ice particles in upper atmosphere.

Thus, an analysis of the first type statistical models, presented as dependences of average values and RMSD fluctuations of cloudy field radiance on the observation angle, showed that radiation intensity depends on cloud formation height, on cloud composition (ice crystals or water drops), and on particle concentration (ice crystals or water drops). If clouds are located highly, they mainly consist of ice crystals with a high reflecting power in the WL (1.5–2) μm interval and, therefore with increase of the altitude angle, increase of cloudy field R fluctuation average values and RMSD is observed. If clouds are located low, they mainly consist of water drops, which intensely absorb radiation, and so cloudy field R fluctuation average values and RMSD of are not too large. Besides, a small increase of big vertical extent cloudy fields R fluctuation average values and RMSD in the near-to-horizon area (Cu) is due to effect of radiation reflection from Earth and from artefacts (buil-

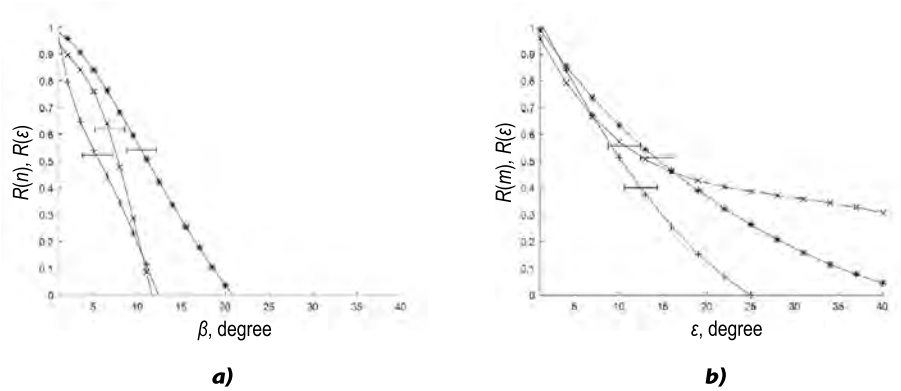

Fig. 4. Dependences of spatial correlation coefficient of a background image on angular shift linewise (a) and columnwise (b)

dings, trees, etc.) located on its surface. A dependence of cloudy field R fluctuation average values and RMSD on azimuth angles was observed with some types of cloud cover: cumulus (Cu), cumulonimbus (Cb), altocumulus (Ac), cirrocumulus (Cc), and cirrus (Ci).

Besides, an analysis of the obtained statistical models has shown that in depending on the non-uniformities size cloudy fields can be divided into two groups. The first one includes cloudy field types, which contain small-scale non-uniformities: cumulus (Cu), cumulonimbus (Cb), altocumulus (Ac), cirrocumulus (Cc) and cirrus (Ci). The second one includes large-scale non-uniformities, which size is more than dimensions of the obtained frames: stratiform (St), nimbostratus (Ns), stratocumulus (Sc), altostratus (As), and cirrostratus (Cs).

An analysis of the first type statistical models only allows understanding nature of the changes depending on the observation altitude angle, which does not allow estimating angular dimensions of cloudy field non-uniformities.

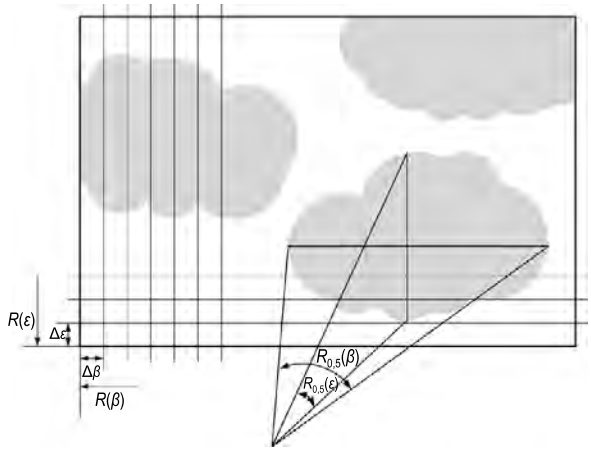

Fig. 5. An evaluation of cloudy field radiation spatial structure by correlation radiuses in horizontal and vertical directions, where $R_{0.5}(\varepsilon)$ *and* $R_{0.5}(\beta)$ are correlation radiuses of spatial correlation functions computed between lines (columns) of a background image; $\Delta\varepsilon$ and $\Delta\beta$ are angular discrete shifts when calculating spatial correlation functions for cumulus cloud cover (Cu)

To evaluate, how great these non-uniformities are, a correlation analysis of the first type models of different type cloudy field BI is necessary. The analysis should include calculation of mutual (spatial) correlation coefficients *R* and evaluation of their dependence on angular shift in two directions: linewise, and columnwise. The obtained dependences (Fig. 4) can be named statistical models of the second type reflecting principles of R fluctuation spatial structure. These dependences make it possible to estimate angular dimensions of cloudy field non-uniformities by the correlation radius value (angular values corresponding to the $0.5 \cdot R$ level).

The fulfilled analysis has shown that cloudy fields of stratiform (St), stratocumulus (Sc), nimbostratus (Ns) and cirrostratus (Cs) of cloud cover types have large-scale non-uniformities: more than 30°. An analysis of spatial correlation relations for cumulus type of cloud cover (Cu) has shown that altitude angle non-uniformity values are approximately identical for all cloud amounts and are equal to 7° – 18°. In the azimuth plane, non-uniformity values are similar 5° –15°.

A generalised analysis of all types of statistical models allowed revealing some features of cloudy field luminance characteristics in the WL (1.5–2) μm interval:

1. By statistical models, distributions of R fluctuations average values and RMSD of the first type cloudy fields have a trend of radiation intensity increase with increase of the observation altitude angle. Besides, they depend on formation height, cloud composition (ice crystals or water drops) and on particle concentration (ice crystals or water drops). They also allow dividing cloudy fields

Fig. 6. The turning device with two freedom degrees

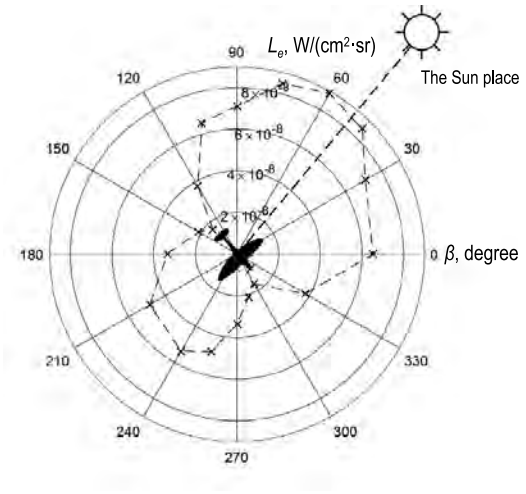

Fig. 7. A model as reflection indicatrix of a pilotless aircraft (altitude angle of its observation is 10°, position of the Sun is 50°)

by their R into two types: with small-scale structure and with large-scale non-uniformities.

2. Spatial correlation functions of cloudy field R fluctuations have valuable coefficients of spatial correlation between BI neighbour lines ($R_{n,\,n-1} \approx 0.9$) and columns ($R_{m,\,m-1} \approx 0.9$). And therefore, as soon as a point object appears in a neighbour line (for example, a PLA image) radiating in a selected WL, one can expect a noticeable change of spatial correlation coefficient between neighbour lines, and then also between neighbour columns. A point object being PLA image is a little size object, which image fits well into N pixels ($N \leq 5$) of the BI array [11].

Thus revelation of a line and a column, in which noticeable changes of spatial correlation coefficient are revealed, can serve to determine co-ordinates of a PLA within a BI cloudy field.

3. Angular dimensions of radiating non-uniformities of some type cloudy fields are limited by correlation radius values linewise and columnwise (Fig. 4). Therefore, dividing by width of PLA radiation spatial spectra and by extended radiating non-uniformities of cloudy fields is permissible.

4. Within BI segments with angular limitations equal to the correlation radiuses, spatial structure of cloudy field radiating non-uniformities linewise and columnwise is not subject to abrupt changes (Fig. 5) [12], i.e. can be considered to be uniform.

Thus, having obtained statistical models reflecting principles of a spatial structure (non-uniformity angular dimensions) of atmosphere cloudy field R fluctuations in the WL (1.5–2) μm, one can come to the second stage: study of PLA radiation energy characteristics.

There are several methods of experimental determination of PA radiance spatial distribution:

- Measurement method of PLA R while in flight. However, it is very complex to be implemented and requires a special equipment [13];
- Land-based method of measurement PLA R. It is measurement of PLA R in a preset WL using radiometric equipment moved around PLA.

To eliminate the main disadvantage of the latter (land-based) method, the PLA is fastened in a specially developed turning device with two freedom degrees (Fig. 6). This allows finding PLA reflection indicatrix (Fig. 7) not only in horizontal plane but also in case of changing its altitude angle position both in lower and in top hemispheres with switched-on, or switched off engine.

During the experiment studies, we have obtained PLA reflection indicatrix with one position of the Sun (azimuth 50°) and with observation angle of 10°. Later on, the studies will be continued to obtain PA radiation statistical models as indicatrices for various positions of the Sun and different observation angles.

Taking into account properties of the statistical models describing features of R fluctuation spatial structure (non-uniformity angular dimensions) of cloudy fields in the WL (1.5–2) μm interval, it is revealed that for some cloud cover types, PLA detection is possible by using the direct threshold method.

But for some types of cloud cover (for example, Cu and Cb) this method is ineffective as R of some areas of cloudy field can be higher than of the searched point object.

Therefore, another approach should be used to solve the problem of the point object detection against the background of cloudy fields. This approach is that the searched point object is found by an analysis of cloudy field spatial structure features. This principle of obtaining information (background principle) makes it possible to solve the detection problem in an absolutely new way and to widen the traditional threshold detection method in cases when the latter is ineffective, namely when luminance contrast between the point object and cloudy field is slight, and object's image size does not exceed an element of the BI array [14].

When implementing the background principle, the detection system should be agreed with features of the atmosphere radiation spatial structure, which is much simpler, because background is an object slowly changing in space and in time.

REFERENCES

1. Allenov A.M., Solovyov V.A. Correlation (spatial) relations between luminance fluctuations created by cloudy non-uniformities in the (8–13) μm interval / Proceedings of the IEM, 1995, Issue 25 (160): Atmosphere optics, pp. 3–15.

2. Allenov A.M., Solovyov V.A., Yakimenko I.V., etc. Studies of radiation of optical background in the (3–5) μm and (8–13) μm intervals / Proceedings of the IEM, 1996, Issue 26 (161), Physics of atmosphere, pp. 31–50.

3. Allenov A.M., Solovyov V.A., Yakimenko I.V. Structure of radiation of optical backgrounds in the (0.4–15) μm interval / Proceedings of the IEM, 1997, Issue 28 (163), Physics of atmosphere, pp. 3–41.

4. Allenov A.M., Ivanova N.P. Time changeability of the sky radiation spatial structure in the 8–13 μ interval with cumulus cloud cover / The Optical journal, 2001, V. 68, #3, pp. 43–44.

5. Allenov M.I., Solovyov V.A., etc. Stochastic structure of cloud cover radiation / SPb.: Gidrometeoizdat, 2000, 175 p.

6. Knapp H.W. et al. Discriminating between water and ice clouds using near- infrared AVIRIS measurements // Summaries of the ninth JPL Aerborne Earth Science workshop, 2000, Feb 23–25, JPL.

7. Clough S.A., Shephard M.W., Mlawer E.J., Delamere J.S., Iacono M.J., Cady-Pereira K., Boukabara S., Brown P.D. Atmospheric radiation transfer modelling: a summary of the AER codes // Journal of Quantitative Spectroscopy and Radiation Transfer, 2005, Vol. 91, Issue 2, pp. 233–244.

8. Huang B., Mielikainen J., Oh H., Huang H.L.A. Development of a GPU-based high-performance radiation transfer model for the Infrared Atmospheric Sounding Interferometer (IASI) // Journal of Computational Physics, 2011, Vol. 230, Issue 6, pp. 2207–2221.

9. Lieven C., Hurtmans D., Clerbaux C., Hadji-Lazaro J., Ngadi Y., Coheur P.F. Retrieval of sulphur dioxide from the infrared atmospheric sounding interferometer (IASI) // Atmospheric Measurement Techniques, 2012, Vol. 5, Issue 3, pp. 581–594.

10. Chen X., Wei H., Xu Q. Infrared atmospheric transmittance calculation model // Infrared and Laser Engineering, 2011, Vol. 40, Issue 5.

11. Mishchenko A.M., Rachkovsky S.S., Smolin V.A., Yakimenko I.V. Experimental studies of spatial distribution of atmospheric background intrinsic radiation in the infrared wave length interval // Radio Engineering, 2017, #2, pp. 119–125.

12. Kriksunov L.Z. Handbook on foundations of infrared facilities. – Moscow: Sovetskoye Radio, 1978, 400 p.

13. V.A. Solovyov et al. Experimental determination of infrared radiation of planes while in flight, [a monograph], scientific-and-theoretical publishing / Ministry of defence of the Russian Federation, Smolensk: MA AAD of RF, 2009, 83 p.

14. Yakimenko I.V. Methods, models and facilities of detecting air targets against atmospheric background using wide-angle optoelectronic systems. The second revised edition, SPb.: Lan, 2014, 176 p.

Anton M. Mishchenko,
an officer of the Russian army, graduated from the MA AAD of RF AF in 2009. At present, he is Adjunct of the of Chair "Special radio engineering systems" of the MA AAD of RF AF, an author of five scientific works and of one software product for a computer, his scientific interest field is image digital processing, observation systems of various wavelength intervals and study of target intrinsic radiation in the optical interval

Sergei S. Rachkovsky,
an engineer, graduated from the Moscow Power Engineering Institute in 1988. At present, he is an engineer of the Chair "Computer engineering" of the MPEI NRU branch in Smolensk, an author of two scientific works. His scientific interest field is electronics and microprocessor facilities, study of intrinsic radiation of atmosphere and of the underlying surface in the optical interval, as well as development of measuring equipment and general purpose industrial grade installations

Vladimir A. Smolin,
an engineer, raduated from the Moscow Power Engineering Institute NRU in 2013. At present, he is a teaching assistant of the Chair "Electronics and Microprocessor Facilities of the Moscow Power Enineering Institute NRU branch in Smolensk. A postgraduate student of the MPEI NRU, an author of 40 scientific and educational-and-methodical works, as well as of two invention patents. His scientific interest field is digital image processing, electronics and microprocessor facilities, and study of atmosphere intrinsic radiation in the optical interval

Igor V. Yakimenko,
Dr. of Technical Science, Associate Professor, graduated from the Smolensk highest zenith rocket engineering school (1985) and the MA AAD of RF AF (2006). At present, he is the Head of the Chair "Electronics and Microprocessor Facilities of the MPEI NRU branch in Smolensk, an author of more than 200 scientific and educational-and-methodical works, 11 invention patents and 22 software products for computers. His scientific interest field is digital image processing, computer vision and systems of artificial vision, observation systems in different spectral intervals, study of intrinsic radiation of atmosphere and of the underlying surface and of intrinsic radiation of targets in the optical interval

Light & Engineering
Vol. 26, No. 3, pp. 14–21, 2018

Svetotekhnika
No. 6, 2017, pp. 50–55

SIMULATION OF REFLECTED SOLAR RADIATION FOR ATMOSPHERE GAS COMPOSITION EVALUATION FOR OPTICAL REMOTE SENSING FROM SPACE

Mikhail Yu. Katayev[1] and Andrei K. Lukyanov[2]

Tomsk State University of Control Systems and Radio Electronics, Tomsk
E-mails: kataev.m@sibmail.com; hyena116@mail.ru

ABSTRACT

At present, in optical remote sensing of atmosphere from space, a new problem class appears: to determine little gas components (carbon dioxide, methane, etc.), which cause greenhouse effect. Concentration of these gases in atmosphere is less than one percent, which rigidly limits accuracy of satellite measurements and of simulating spatial concentration of the radiation (signal) flow reflected by Earth. In the article, a description of simulating signals received by satellite spectrometer in near-infrared spectrum region is given. The signals are solar radiation passed through an atmosphere layer and reflected from Earth surface. It is calculated based on parametrical radiation atmosphere scattering and absorption model, which takes into consideration both multidimensional atmosphere parameter structure and Earth surface relief. Accounting such information allows you to go from measurement of spatial radiation flux to calculations of gas concentration for an arbitrary geographical Earth surface point and for any time point. As an example, calculations for Fourier spectrometer for spectrum measurement near IR region with an average spectral resolution are presented. The spectrometer was installed on the *GOSAT* satellite of the Space Agency of Japan. A comparison of computed and of really measured values of the signal received by the satellite shows that deviation for the Sun zenith angle equal to 30° does not exceed 3 %.

Keywords: atmosphere, absorption, scattering, numerical model

1. INTRODUCTION

Satellite environment monitoring is a comprehensive and regular environment state observation system (Earth atmosphere and surface). Processing and analysis of the measurement results obtained during various time periods allows estimate trends of changing the state of Earth atmosphere or surface parameters under influence of natural and anthropogenic factors. A success of these data application in various science and practice fields depends on many components: on mathematical simulation of instrument measurement base, on radiation expansion in atmosphere (account of scattering and absorption effects), on reflections from Earth surface, on methods of the reverse problem solution, etc.

There are various ways of optical classification methods of atmosphere gas composition control from space. Depending on the used radiation source, optical methods are divided into passive (extra-atmospheric radiation sources, own and scattered atmosphere radiation) and active (laser and thermal sources). By physical effects of radiation interaction with environment, passive methods can be divided into three groups: 1) transmission (transparency method); 2) emission (own radiation method); 3) scattered radiation method. By experiment geometry, nadir and limb methods can be mentioned (Fig. 1). Active methods are divided into local and remote. Local (*in situ*) methods are measurements of some gas concentration in a given local point in relation to the obtained air specimens.

Difficulties of gas composition analysis using optical methods are as follows:

a) There are constantly two absorbing components in atmosphere (H_2O and CO_2), which absorption spectra cover practically all IR range, where main absorption bands of other atmospheric gases, both basic and anthropogenic are located;

b) Earth atmosphere is non-uniform in time and space by thermal, gas and aerosol composition;

c) Along with height structure of gas composition and atmosphere temperature, turbulent environment fluctuations are constantly present;

d) There is a mixture of aerosol particles in atmosphere, which is unstable and complex by the composition. These particles absorb and scatter radiation;

e) Most atmospheric gases have very little concentrations.

Nevertheless, optical methods are broadly applied in practice of atmosphere gas composition monitoring [1–5].

Among all mentioned methods, most widespread are passive methods of measuring atmosphere parameters. They have a number of advantages: a high sensitivity, a high spectral resolution and high measurement accuracy, absence of exposure on the examined objects, a high level of instrument base development, etc. The scheme B (Fig. 1) should be noticed, in which detector of the satellite device "looks" through atmosphere directly at the Sun, unlike scheme *C* (Fig. 1). Among all measurement geometries, an advantage of nadir version consists in a possibility to obtain continuous spatial fields of various atmosphere parameters with a good periodicity (from several hours to several days).

Optical measuring devices located onboard of spacecrafts are divided into multichannel devices (from several units to several tens channels) and hyper-spectral devices. Spectrometers and radio metres of various classes are referred to the first device type, and Fourier spectrometers most often belong to the second type. The Fourier spectrometers namely allow obtaining thousands of points with a high precision in spectral intervals from visible to infrared spectrum region. The obtained information reflects all peculiarities of radiation expansion in atmosphere.

Development of the instrument base and processing of the measurement results are connected with application of models including characteristics of the device, of atmosphere and of Earth surface. The models, as a rule, take into consideration influence of various factors not completely (dependence on latitude and longitude, on measurement time, etc.) and influence of physical processes (device noise, atmosphere fluctuations, height and space-time parameter value variation, etc.). From the other hand, account of many factors highly complicates the calculation models and requires a development of the special algorithms and involving of the correspondent computing facilities.

In this regard, there is a need to develop models, which with a sufficient accuracy allow imitating the signals measured by satellite optical devices, as well as applying this information to exercise methods of solving reverse problems of atmosphere optics [6, 7].

Abilities of modern hyper spectral satellite devices make it possible to solve fundamental problems of atmosphere physics, of climate, ecology, etc. During recent years, several devices of a high resolution were launched: *IASI* (MetOp satellite, the European Union) [8], SCIAMACHY (ENVISAT satellite, the European Union) [9], TANSO-FTS (GOSAT satellite, Japan) [10], which purpose is a recovery of information on atmosphere gas and aerosol composition.

Study of climate-forming parameters is an important fundamental problem. Gas and aerosol composition play an important role in forming various atmospheric processes. Study of aerosol influence on recovery of atmosphere gas composition information in global scale was a limiting factor, and there were no regular measurements covering a big territory.

Increase in concentration of some greenhouse gases (CO_2, H_2O, CH_4, N_2O, etc.) leads to changes of radiation properties of atmosphere and as a result, to Earth climate changes. Modern evaluations of various gases to atmosphere heating process contribution show that relative contribution of CO_2, CH_4, and N_2O is 60, 20 and 6 percents respectively. One of the climate change criteria is global warming, which is a process of gradual increase in average annual temperature of Earth atmosphere and of the World Ocean. A position of the Intergovernmental Panel on Climate Change (IPCC) of the UN is that since the beginning of industrial revolution (the second half of the 18th century) average on Earth surface temperature increased by 0.8 °C [11] and that a big part of the warming observed during the last fifty years is caused by the human ac-

tivity [12, 13]. Primarily, it was gas emission leading to the greenhouse effect: carbon dioxide (CO_2) and methane (CH_4). As a whole, reasons of climate changes remain unknown and require a study of radiation flows (ascending and descending), of gas and aerosol composition in atmosphere. In doing so, measurement points regularly and uniformly located over Earth surface are necessary. Such measurements are only possible using space methods.

And the former methods of interpreting satellite photometric information based to various extents on the curve-fitting method are hardly applicable since curve coincidence in thousands points cannot be achieved. From the other hand, measurement accuracy in each channel equal to not less, than 1 %, makes new strict requirements to radiation transfer model in atmosphere: the calculation accuracy should be also not less than 1 %. This leads to the fact that well developed methods of solving the radiation transfer problem for a plain layer of turbid environment become unacceptable. Under such conditions, a strict account of light scattering features in a three-dimensional environment is necessary: a vertical non-uniformity of atmosphere, a ragged cloud cover, an underlying surface profile.

Formerly, we made attempts to solve the problem of simulating solar radiation reflected from the surface [14]. In the proposed article, a development of some program is considered, which allows for any season and for any point of Earth surface computing the reflected solar radiation taking into account three-dimensional atmosphere structure.

2. PROBLEM DEFINITION

Radiation coming to a Fourier spectrometer receiver "looking" at nadir on Earth surface consists of two flows: solar radiation reflected by Earth surface, and solar radiation scattered over all atmosphere thickness. The ratio of these flow values depends on the solar declination angle: the more declination is, the more is contribution of the flow scattered in atmosphere. Having passed the way in atmosphere twice, total radiation flow received by the Fourier spectrometer contains information on gas composition and on atmosphere aerosol filling. A purpose of this work is calculation of solar radiation flows received by a satellite Fourier spectrometer in the spectrum near IR area [15], and comparison of the obtained values with the measurement results obtained by the GOSAT satellite[1]. When calculating the signal received by the satellite, use of new physical and mathematical models and methods is supposed. They not only increase the accuracy but also considerably accelerate the calculations.

Interaction of solar radiation with atmosphere leads to scattering and absorption. This interaction is quantitatively determined by properties of atmosphere gas composition and by aerosol types. The radiation, which was reflected from Earth surface or from clouds, depends on the surface relief, on the reflecting properties and on the temperature.

Some part of solar radiation, which has reached the satellite device, depends on the atmosphere absorbing properties and thus can be used to determine atmosphere gas composition.

3. MODEL DESCRIPTION

Solar radiation $I_0(\lambda)$ penetrates to Earth atmosphere under different angles depending on the season being subject to absorption and scattering by gases and by aerosol particles of atmosphere, as well as to reflection from clouds. Further reflection from Earth surface takes place, which is characterised by types, every of which has its own spectral distribution of reflection factor, and by the relief. The reflected radiation passing through atmosphere and incident to the satellite device input, which is consist of many components (Fig. 1). The scattering can be single-stage and multiple, and reflections can be not only from observed Earth surface but also from clouds, from a surface beyond visual field of the device, etc. Different components make different contributions to the signals received by the device [16].

In the signal $I(\lambda)$ received by the device installed at the *GOSAT* (further the GOSAT device), one can distinguish two main components: solar radi-

[1] *GOSAT* (*Ibuki*) is a satellite of remote Earth sensing, which aim is monitoring of greenhouse gases (*GOSAT* and *Ibuki* are the same but the first name is connected with an English phrase "*Greenhouse gases Observing SATellite"*, and *Ibuki* in Japanese is breath). The *GOSAT* is equipped with infrared detectors, based on which data determination of general concentration of carbon dioxide and of methane in atmosphere is possible. These are detector of greenhouse gas observation (TANSO-FTS) and detector of clouds and aerosols (TANSO-CAI). In the spectrum registered by *TANSO-FTS*, 1.6 μ and 2.0 μ bands in the spectrum near IR interval are used for observation of general concentration of CO_2 and CH_4. Total number of the spectral observation channels reaches 18,500.

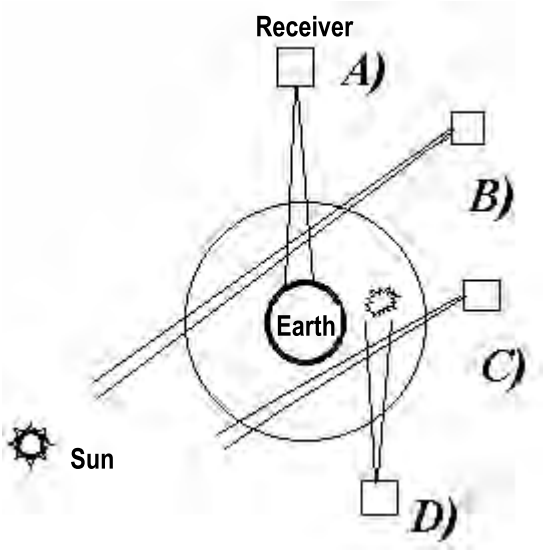

Fig. 1. Various versions of sounding atmosphere: *A)* nadir (method of thermal radiation – MTR); *C)* tangent (transparency method –TM); *C)* limb (MTI or method of reverse scattering – MRS) and *D)* emission

ation flow $I_1(\lambda)$ reflected from the surface and radiation single-stage flow $I_2(\lambda)$, which is scattered in atmosphere (Fig. 2), whereas other components make a little contribution (less than one percent) within $10^o < \theta_0 < 60^o$ interval of the Sun zenith angle change.

Taking into account geometrical factors, surface types and seasons, the signal received by the satellite is a multidimensional function of such parameters as spatial co-ordinates (x, y), wavelength λ, the Sun zenith angle θ_o, season t and altitude above sea-level h. With due regard for multidimensional formation of the signal registered by the satellite, it can be presented as [17],

$$I(\lambda) = I_1(\lambda) + I_2(\lambda), \tag{1}$$

where:

$$I_1(\lambda) = I_0(\lambda)\cos(\theta_0(t))r(\lambda,x,y) \\ R_{surf}(x,y)T(\lambda,x,y,\theta_0,H,t), \tag{2}$$

(See eqn 3 below)

$$\cos(\gamma) = \\ = -\mu_{sun}\mu_{sat} - \sqrt{(1-\mu_{sun})(1-\mu_{sat})}\cos(\theta_0), \tag{4}$$

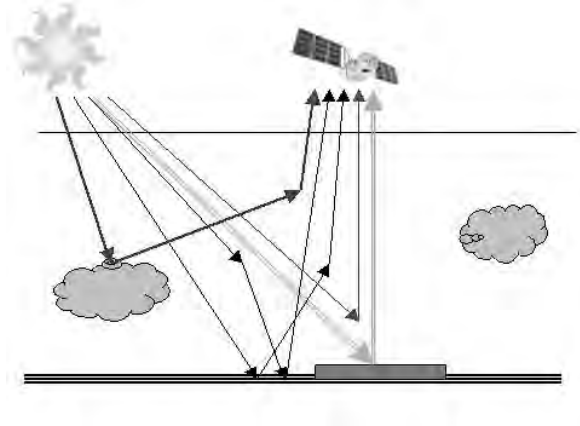

Fig. 2. Main components of the signal received by a satellite

where

$I_0(\lambda)$ is the radiation of the Sun beyond Earth atmosphere; $r(\lambda, x, y)$ is the spectral reflection factor of the surface; $R_{surf}(x, y)$ is the parameter responsible for relief; $T(\lambda, x, y, \theta_0, H, t)$ and $T(\lambda, x, y, \theta_0, h, t)$ are the atmosphere transmission along all optical route in atmosphere and at a given height h; θ_0 is the zenith angle of solar declination (in this work azimuth angle is not taken into consideration); t is the time, λ is the wavelength; x, y are co-ordinates of the point, α_{aer} and α_{mol} are attenuation factors due to aerosol and molecule scattering respectively; Ψ_{aer} and F_{aer} are characteristics of radiation scattering by aerosol (single-stage albedo and scattering function respectively); μ_{sun} and μ_{sat} are directions to the Sun and to the satellite for an observation point respectively ($\mu = 1/cos(\theta)$), H and H_0 are thickness of atmosphere (100 km) and height of a local place above sea level respectively.

Atmosphere transmission can be found according to the expression:

$$T(\lambda,x,y,\theta_0,h,t) = \\ +\exp\left(-m(\theta_0)\cdot\tau(\lambda,x,y,h,t)\right), \tag{5}$$

$$\tau(\lambda,x,y,h,t) = \\ = \int_{H_0}^{h}\begin{pmatrix}\alpha_{gas}(\lambda,x,y,h',t)+\\ +\alpha_{aer}(\lambda,x,y,h',t)+\\ +\alpha_{mol}(\lambda,x,y,h',t)\end{pmatrix}dh', \tag{6}$$

$$I_2(\lambda) = \frac{I_0(\lambda)}{\mu_{sun}}\int_{Ho}^{H}\left(\alpha_{mol}(\lambda,x,y,h,t)+\alpha_{aer}(\lambda,x,y,h,t)\psi_{aer}F_{aer}(\gamma)\right)T(\lambda,x,y,\theta,h,t)dh, \tag{3}$$

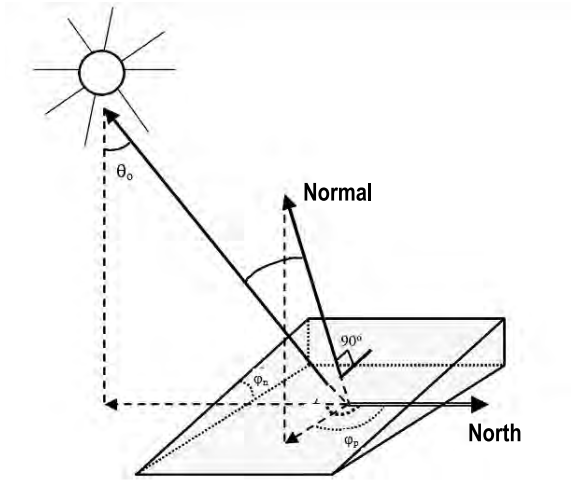

Fig. 3. Orientation layout of a site of Earth surface relative to visual field of the satellite device

where
$m(\theta_0) = 1/\cos(\theta_{sun}) + 1/\cos(\theta_{sat})$;
$\tau(\lambda, x, y, h, t)$ is the optical thickness of atmosphere;
$\alpha_{gas}(\lambda, x, y, h, t)$ is the gas attenuation factor.

Radiation attenuation by gases can be found from the expression:

$$\alpha_{gas}(\lambda, x, y, h, t) = \sum_{j=1}^{N} K_j(\lambda, h)\rho_j(x, y, h, t), \quad (7)$$

where $K_j(\lambda, h)$ is the absorption factor j because of gas, j = 1, …, N; $\rho_j(x, y, h, t)$ is the concentration profile of j gas at a preset height h and at a preset time t.

Radiation reflected towards the satellite device significantly depends both on the surface type (due to its spectral reflection factor) and on the relief (Fig. 2). Form factor, which takes into consideration relief parameters, is determined by expression [18]:

$$R_{surf}(x, y) = \cos(\varphi_p(x, y))/[\cos(\varphi_n(x, y)\cos(\theta_0)], \quad (8)$$

where θ_0 is the zenith angle of the Sun declination; φ_n is the tilt angle of a selected surface site; φ_p is the rotation angle of a selected surface site (Fig. 3).

4. DESCRIPTION OF THE SOFTWARE STRUCTURE

The problem of simulating radiation received by the satellite device is connected with calculation of direct and once scattered solar radiation and with reflection of radiation from Earth surface in spectral area of 1.5–2.0 μ. For each calculation part, its own priori information is necessary, based on which the calculation is carried out. This information should be global over space and should enclose time including at least one year. It should be noticed that a part of the information is one-dimensional, for example, spectra of reflection from different type surfaces, extra-atmospheric solar spectrum, etc. Another part is two-dimensional (Earth surface relief, Earth surface types (for example, water, wood, field, etc.). And meteorological information is four-dimensional. Therefore, before the calculation is performed, all priori information arrays are reduced to one network interconnected by space (*x, y, h)*, by wavelength λ and by time *t*. After this, calculation of the radiation received by the satellite Fourier spectrometer is made. A flow chart of the calculation program of the signal received by a satellite is given in Fig. 4.

For three flight days (along a preset trajectory), the GOSAT device obtains information from 12,600 geographical points (diameter of the observation spot is 10 km). In case when account of the points located over land is only carried out (about 4000 points), it is necessary to compute of about half a million points a year. For each geographical point, there are 18,500 spectral lines for three Fourier spectrometer channels. As a result, one should compute about 10^{10} spectral points during an acceptable time limit convenient for work, which, in our opinion, is no more than several hours. The last condition imposes rigid limitations on the calculation speed, with a minimum deviation of the model from real measured values of solar radiation reflected from the surface and received by the spectrometer.

Sets of priori data are formed of known sources of scientific information. For example, relief is taken from the *Shuttle radar topography mission* data [19]. Absorption by gases is calculated based on the *HITRAN* spectroscopic base [20], meteorological parameters are taken from the *NCEP* [21] base, aerosol extinction factor is taken from [22], and solar spectrum is from [23].

Within known calculation programs, the signals received by satellites are only calculated for one spatial point. The program, which we propose, allows calculating both for one point and along the satellite flight trajectory. For each point, a set of priori data (Fig. 4) is formed. Then for each set the program performs calculations of the signals re-

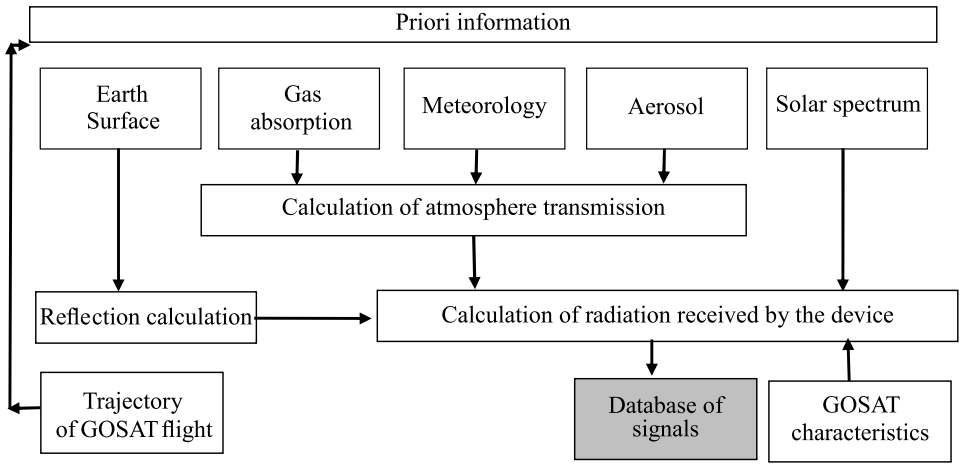

Fig. 4. Flow chart of the calculation program of the signal recieved by the satellite

ceived by satellites [24]. If data read-out and calculation acceleration techniques are not used, then processing time is long. Therefore we applied the *MMF* (Memory-Mapped Files) read out technologies and elements of parallel technologies. The *MMF* technology allows applications working with files as well as they work with dynamic memory. A numerical experiment performed to search number of optimum flows when changing data volume from 64 kb to 1 Gb and with use of the *MMF* technology, shows that for reading from a file, most effective number is 4–6 flows. A paralleling consisted in creation of elementary function groups and data sets for them, so that all computation nodes were loaded by calculations uniformly.

5. DESCRIPTION OF THE OBTAINED RESULTS

Because of its versatility, the considered task requires a bigger computational cost, which in its turn requires involving high-speed calculators, program technologies and algorithms. The flow chart presented in Fig. 4 was the basis of a program operating by means of a computing cluster with transfer of a part of algorithms into a parallel operation mode. It made it possible to perform mass calculations for a comparatively small time, which is now equal to 12 h. A comparison of calculation results of the radiation arriving to the GOSAT device with the values, which are really measured for two points under the conditions of an absence of clouds are given in Figs. 5–7. Figs. 5a and 6a show a spec-

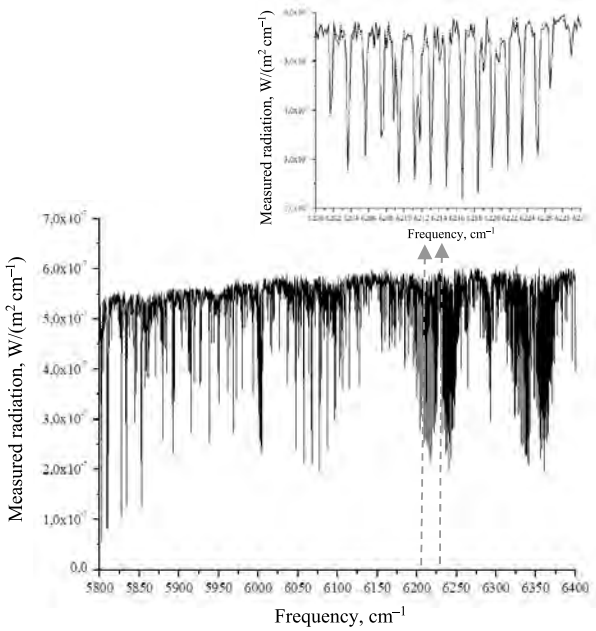

Fig. 5. Comparison of real (solid line) and computed (dashed line) of *GOSAT* signals (co-ordinates of a point are 23.003° N and 14.869° E – Sahara Desert)

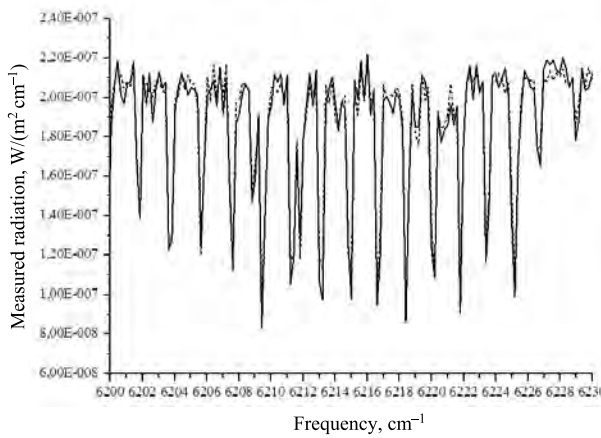

Fig. 6. Comparison of real (solid line) and *GOSAT* computed (dashed line) of *GOSAT* signals (co-ordinate of a point are 64.054 ^{0} N and 69.141° E – a northern tundra region)

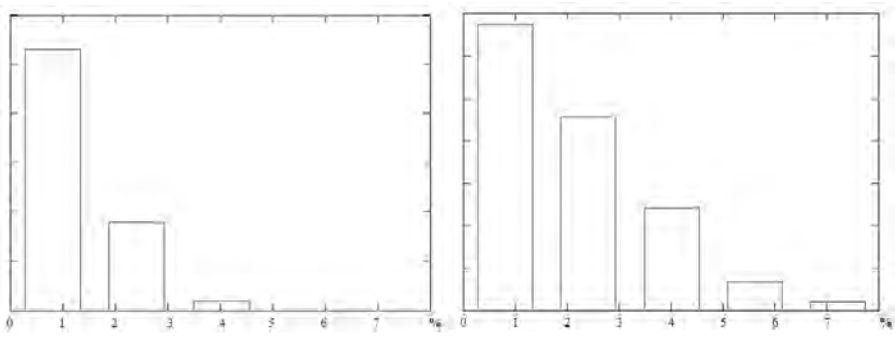

a) *b)*

Fig. 7. A histogram of deviation of the signal computed according to the model from the real signal with the Sun declination angles of 10° (a) and 60° (b)

tral radiation process in the second spectrometer channel within 1.6 μm, and Figs. 5b and 6b show a part of the spectrum within carbon dioxide absorption band, which is used to solve a reverse problem: to determine CO_2 general concentration.

One can see from the pictures that a difference of the model (computed) and of the real spectra takes place, and the main deviation reason is an unknown atmosphere state (meteorological parameters, gas and aerosol composition), as well as change of the surface reflective ability in the measurement point at a given atmosphere state. It should be noticed that for uniform surfaces, such as sand, the deviation is less, and for non-uniform, when surfaces of several types are in the device visual field, this error is just over.

As a whole, if also to take into consideration the Sun illumination angles relative to the surface, the main deviation values are within interval from (4–5)% to (10–15)% (Fig. 7).

The results given in Fig. 7 show that at big angles of the Sun declination, the calculation model of the radiation received by the satellite spectrometer gives a relatively big error when comparing with real signals, which is a consequence of a simple scattering model use. However, if to take into account that the proposed program system allows computing for a single-pass many data over Earth surface with a deviation from reality not worse than (5–10)%, then it is enough to carry out numerical experiments in order to exercise the reverse problem solution techniques, to develop devices and applications.

6. CONCLUSION

Use of space measuring equipment when solving practical problems makes new requirements to models of transforming solar radiation in the "earth surface- atmosphere" system taking into account a specific character of an instrument measurement base. Determination accuracy of the atmosphere optical characteristics depends on the mathematical model of radiation transfer and on the relevant priori information. To account factors influencing formation of the measured radiation when solving equation of radiation transfer in three-dimensional version, one should as much as possible completely take into consideration both: space-time environment fluctuations and features of the reflecting surface. The results of the presented work allow expanding possibilities of simulation programs of radiation transmission and transformation in atmosphere for a more precise solution of the optical remote sensing problems. Taking into account the multidimensional structure of space and time changing in the atmosphere parameters is a new element of the received by satellites signals calculating. Use of the atmosphere parameter model presentation limits accuracy of the calculated signals because of a considerable time and space averaging, which does not allow obtaining detailed information on signal variation. The proposed program makes it possible to compute the signals received by satellites for any spot of the globe and for any season. The obtained results give evidence of acceptability of the calculation quality of the received *GOSAT* signal ((5–10)% in comparison with the real measurement results). It should be notice that obtaining more precise results requires construction of a new model of aerosol scattering and reflection from the surface.

REFERENCES

1. Gushchin G.P. Studies of atmospheric ozone. Leningrad: Gidrometeoizdat, 1963, 289 p.

2. Khrgian A.H. Physics of atmospheric ozone. Leningrad: Gidrometeoizdat, 1973, 285 p.

3. Malkevich M.S. Optical studies of atmosphere from satellites. Moscow: Nauka, 1973, 303 p.

4. Kondratyev K. Ya., Timofeev Yu.M. Meteorological sounding of atmosphere from space. Leningrad: Gidrometeoizdat, 1978, 280 p.

5. Timofeev YU. M., Vasilyev A.V. Fundamentals of theoretical atmospheric optics. SPb., 2007, 152 p.

6. Hoffman N., Preetham A.J. Real-time light-atmosphere interactions for outdoor scenes. // Graphics programming methods, 2003, pp. 337–352.

7. Otterman, J. Single-scattering solution for radiative transfer through a turbid atmosphere. // Appl. Opt, 1978, Vol.1, No.17(21), pp. 3431–3438.

8. http://smsc.cnes.fr/IASI.

9. http://www.sciamachy.org.

10. http://www.gosat.nies.go.jp.

11. IPCC, Synthesis Report, Section 2.4: Attribution of climate change, in IPCC AR4 SYR2007.

12. Solomon S., Qin D., Manning M., Chen Z., Marquis M., Averyt K.B., Tignor M., Miller H.L. (eds). IPCC-2007: Climate Change 2007: The Physical Science Basis. // Cambridge University Press, Cambridge, United Kingdom and New York, NY, USA, 996p.

13. Pachauri R.K., Meyer L.A. (eds.) IPCC-2014: Climate Change 2014: Synthesis Report. Contribution of Working Groups I, II and III to the Fifth Assessment Report of the Intergovernmental Panel on Climate Change, IPCC, Geneva, Switzerland, 151p.

14. Katayev M. Yu. A program simulation system of solar radiation reflected from Earth surface /M. Yu. Katayev, I.V. Boychenko // TUSUR Reports, 2009, #1(19), Part1, pp. 88–95.

15. Krylov A.S., Vtyurin A.N., Gerasimova Yu.V. Data processing of infrared Fourier of spectroscopy. A textbook of methodics. Pre-print #832 Ф. Krasnoyarsk: Institute of physics of the Siberian Branch of the Russian Academy of Science, 2005, 48 p.

16. Hopfner M., Emde C. Comparison of single and multiple scattering approaches for the simulation of limb-emission observations in the mid-IR // Journal of Quantitative Spectroscopy & Radiative Transfer, 2005, Vol. 91, No. 3, pp.275–285.

17. Breon F., Frouin R., Gautier C. Downwelling longwave irradiance at the ocean surface: An assessment of in situ measurements and parameterizations // J. Appl. Meteorology, 1991, Vol. 30, No.1, pp.17–31.

18. Kane Van, R., Gillespie, A.R. Interpretation and topographic compensation of conifer canopy self-shadowing // Remote Sensing of Environment, 2008, Vol. 112, No. 10, pp.3820–3822.

19. Farr, T.G., Hensley, S., Rodriguez, E., Martin, J., Kobrick, M. The shuttle radar topography mission // CEOS SAR Workshop, Toulouse 26–29 Oct. 1999, Noordwijk, 2000, pp. 361–363.

20. Rothman, L.S., Gordon, I.E., Babikov, Y. et al. The HITRAN2012 Molecular Spectroscopic Database // Journal of Quantitative Spectroscopy and Radiation Transfer, 2013, Vol.130, No. 11, pp. 4–50.

21. http://www.ncep.noaa.gov/.

22. Hess, M., Koepke, P., Schult, I. Optical Properties of Aerosols and clouds: The software package OPAC // Bull. Am. Met. Soc., 1998, Vol. 79, No. 5, pp. 831–844.

23. Thuillier, G., Herse, M., Simon, P.C., Labs, D., Mandel, H., Gillotay, D., Foujols, T. The solar spectral irradiance from 200 to 2400 nm as measured by the SOLSPEC spectrometer from the ATLAS1–2–3 and EURECA missions // Sol. Phys., 2003, Vol. 214, No. 1, pp. 1–22.

24. Katayev M. Yu., Lukyanov A.K. Parallel technologies in the simulation problem of a satellite Fourier spectrometer signal // The Seventh Siberian conference on parallel and high-performance calculations. Report program and theses, November, 12–14, 2013, Tomsk: Publishing House of the Tomsk University, 2013, pp. 23–24.

Mikhail Yu. Katayev,
Dr. of technical science. He graduated from the Tomsk State University in 1984 with a specialisation as the optician-researcher engineer. At present, he is the Professor of the Chair of the automated control systems (ACS) at the Tomsk State University of Control Systems and Radio Electronics (TUSUR), professor of the Yurga Institute of Technology (branch) of National exploratory Tomsk Polytechnical University, scientific supervisor of the Centre of Earth space monitoring of the TUSUR

Andrei K. Lukyanov,
Ph.D. Graduated from the TUSUR with a specialisation of informatics and computer facilities (software) in 2010. Associate Professor of the Chair of the automated control systems (ACS) of the Tomsk State University of Control Systems and Radio Electronics (TUSUR)

Light & Engineering
Vol. 26, No. 3, pp. 22–28, 2018

Svetotekhnika
No. 1, 2018, pp. 56–61

ANALYSIS OF ERRORS IN THE RELIEF OF SCATTERING MICROSTRUCTURES IN LIGHT-CONDUCTING SYSTEMS MODELLING

Nikolai N. Bogdanov, Andrei D. Zhdanov, Dmitriy D. Zhdanov, and Igor S. Potyomin

The ITMO University (Saint Petersburg National Research University of Information Technologies, Mechanics and Optics), St. Petersburg
E-mail: nnbogdanov@corp.ifmo.ru

ABSTRACT

Main technological approaches to production of light-conducting systems with scattering microstructures are considered with a special attention to processing method of the optical material influence on geometrical parameters of the being formed microstructure. Relevance of it is caused by an insufficiency of studying influence of the microstructural scattering element configuration distortion on output luminance distribution of the light-conducting systems (because of the technological features of their production). As exemplified by a light-conducting system made by milling technology, a physically correct simulation of this system is carried out, and influence of the microstructure relief on output luminance distribution is shown. For the simulation, the *Lumicept* program system was used, which has provided physical correctness of the modelling results.

Keywords: light-conducting plate, scattering microstructures, micro-relief errors, illumination LED panels, computer simulation, luminance distribution, design, light-conducting illumination devices

1. INTRODUCTION

At present, about 20 % of all electric energy [1] generated in the world is consumed for illumination, which actualises the problem of power consumption decrease for all illumination devices (ID). In the world, a big attention is paid to design [2–4] and production [5, 6] of energy-effective and ergonomic special IDs with light-conducting systems. In particular, one can name thin LED panels, IDs of LCD display back illumination, IDs plane cabins, car interiors, dashboards and advertising panels among such IDs.

This subject attracts a great interest of such leading global manufacturers as *Asahi Kasei, Denso, Panasonic, Fuji-Film, Toshiba*, etc. So, Japanese company Denso manufactures a wide range of light-conducting IDs for dashboards based on the scattering element technologies [7]. Korean *Samsung* and *LG* based on scattering microelements manufacture optoelectronic devices of mass consumption [8, 9], and Russian companies Kvazar and VOLO develop light-conducting systems with scattering microelements for defence industry. Numerous patents concerning specific character of forming geometry and parametrical functions of scattering microstructural elements distribution, as well as publication in the leading scientific journals and proceedings of international conferences (*Proc. SPIE, Optical Engineering, Applied Optics, Optical Review*, etc.) on the problems of physically correct simulation and design of light-conducting IDs [10–13], give evidence of a great interest for the matter.

Uniformity of radiation distribution between light-conducting devices is provided by micro geometrical elements (light-scattering microstructures) deposited on the light-conducting element surface. Simulation of an optimum microelement structure

is rather complex problem requiring considerable computing resources. As a rule, the design results are configuration of the scattering elements, their co-ordinates and orientation on the light-conducting plate surface. One of the main problems of this type ID design is that the design results based on the physically correct laws of light propagation can differ from real lighting characteristics of the manufactured ID. The design errors can be explained by non-availability of the data on the light-conducting system production method and on the technological features of forming the scattering microstructures necessary to construct a correct model used when designing.

In this article, a method of simulating errors of production of scattering microstructures as exemplified by designing back illumination light-conducting IDs of LCD displays is proposed, and methods of forming micro geometrical elements with a description of possible defects of their production are considered.

2. DEPOSITION TECHNOLOGY OF MICRO GEOMETRICAL ELEMENTS ON AN OPTICAL SURFACE

The microelement size is usually tens micrometres, and special technologies are required for their production. Modern technological equipment allows forming microelements for lighting systems with a high precision and acceptable quality. There are several methods of microelements production. The main of them are hot forging, silk-screen printing, engraving and milling.

2.1. Hot Forging

The hot forging is a widespread process of manufacturing products from polymethyl methacrylate (PMMA) and polycarbonate. This method is usually applied to produce geometrical configurations, which size is tens and hundreds micrometres. By means of forging, formation of light-scattering microelements is possible. In this case, the surface thickness and quality high requirements can be applied. The hot forging is performed step by step. A workpiece of PMMA previously heated to the softening temperature (140–190ºC) is installed into the moulding machine, and then a contact is created between the optical surface and the compression mould, giving the workpiece a required configuration [14]. Upon the moulding completion, the finished product is cooled in the compression mould.

When pressing, wavy surface distortions (mechanical waves) can appear, which freeze up when cooling the workpiece [15]. Such distortions have a significant effect on light scattering by microstructures, which influences spatial luminance distribution of the light-conducting illumination devices and can result in a difference from the calculation distribution.

2.2. Silkscreen

The silkscreen printing is one more widespread technology for deposition of microstructures on a plain optical surface. It is also named stencil process.

This technology means light-scattering material deposition. The deposited material layer has thickness of several tens micrometres with a good endurance and durability.

During silkscreen printing, an emulsion layer is deposited on the product surface, and over it a light-scattering composition is applied through a special stencil plate. Using an UV radiation source, the emulsion layer is irradiated, and those sites of this layer where the radiation “fell into” are hardened, and other (unirradiated) sites are washed away. The light-scattering composition is forced through the mesh sites free of emulsion on the product surface when printing. Water and solvent painting compositions, plastisol UV paints and UV varnish can be used as light-scattering materials. The deposited compositions are hardened (polymerised) under UV radiation influence during the printing process.

The stencil plate in this case is usually made using a special mesh of nylon or metallic threads.

Silkscreen printing is considered to be quick and economic technology to manufacture light-conducting systems [16]. However, microstructures formed using it may be non-uniform and not identical, and their configuration may be far from the required [17].

2.3. Engraving and Milling

To perform a laser engraving on PMMA, a CO_2 laser with wavelength of 10.6 μ is used [18]. PMMA has a high absorption factor at this wave-

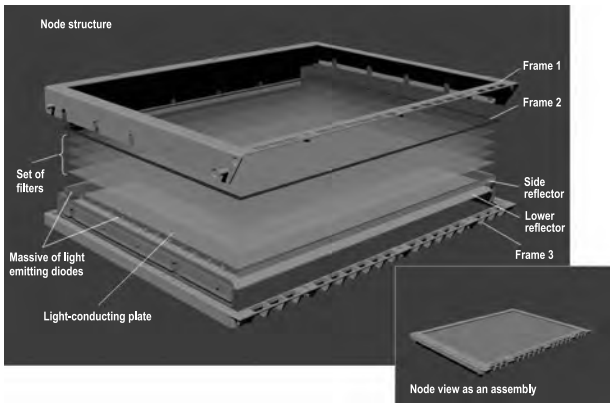

Fig. 1. ID (node) of back illumination of an LCD display

length, which allows (depending on the laser radiation flux) carrying out engraving or cutting the material. When exposing this radiation on a material, its evaporation occurs. Thickness of the evaporated layer depends on the radiation exposure time. Precision technologies used with modern laser machine tools allows moving the laser beam along the set lines with positioning accuracy of up to 25 μm, which makes it possible to obtain micro geometrical elements beginning from 250 μm size. Nevertheless, laser engraving has some disadvantages. In particular, it is impossible to obtain absolutely identical micro-relief over all surface of the material evaporation, and this influences the angular diagram of light scattering [19]. It is also possible to handle non-planar surface by means of a laser but the additional mechanical equipment is necessary to do it.

As for milling, one can produce microstructures of hundreds and thousands micrometre size using it. The milling treatment of a PMMA plain surface is widespread [20]. The milling cutter moves over the working field and cuts off a layer of the light-conducting plate in the locations of microstructure elements. The spent material residues are removed by air from the work-piece surface. The milling treatment can be also applied to produce curvilinear light-conducting systems. For this purpose, upon milling termination, one should give the work-piece a necessary form using a special attachment and then cool it. After these stages are completed, a curvilinear surface with light-scattering microelements is formed. To provide a high precision of microelement forming, high requirements are applied to sharpness of the cutting tool, to removal of the working out products and to cleanness maintenance on the treatment surface.

All above described microstructure manufacturing technologies have its own features, which should be taken into consideration when modelling. On the one hand, it can be residual products of burning when PMMA laser treatment is going on, bad repeatability of the microelement configuration, scratches on the surface due to operation of the milling cutter, etc. On the other hand, an incidentally oriented roughness can be formed (but not a specular surface), or it can be stiffened mechanical waves on the surface around the microelements. All of this significantly influences correctness of the constructed model and, if a maximum approach of the calculation results with work of the real systems is necessary, one should take into consideration all possible distortions. The authors set and solved the problem of correct simulating light-conducting systems with due to account for features of technologies of their production and with coordination of the simulation results with the real product. When solving such problems, some researchers chose a selection of parameters of bidirectional scattering function of element surface of the scattering microstructure [21]. In this article, an alternative approach to the correct simulation is offered.

3. AN EXAMPLE AND RESULTS

Let's consider a coordination of the measurement results of spatial luminance distribution over the light-conducting plate output surface with the

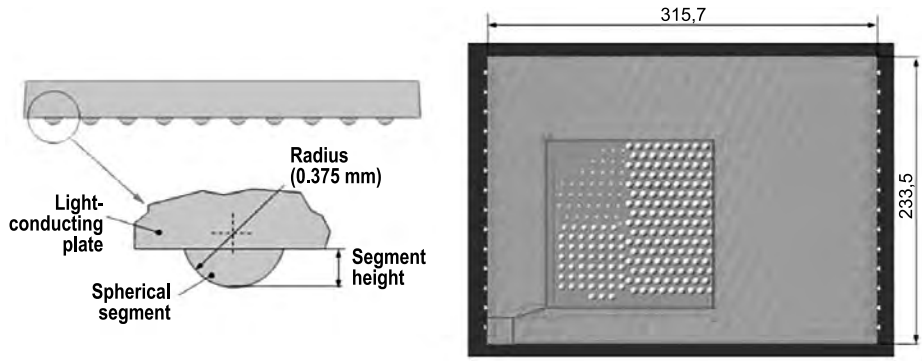

Fig. 2. Light-scattering microstructure

simulation results as exemplified by an ID project (node) of back illumination of an LCD monitor with end face input of the light radiation (Fig. 1).

A model of a light-conducting plate is parallelepiped of transparent PMMA (relative refractive index is the 1.49 and transmission factor is the 0.92) with overall length, width and thickness dimensions of (315.7×233.5×4) mm respectively. Under the light-conducting plate, a diffuse reflector is located (diffuse reflection factor is 0.89). On the plate surface, a microstructure as a massif of more than hundred thousand spherical segments of a constant radius (400 μm) but of an alternating height (Fig. 2) was set. Thirty light emitting diodes were located on both sides of the plate. They radiate in the visible interval and have luminous intensity distribution curve of D type.

The modelling was carried out using the *Lumicept* program system [22]. In comparison with the similar systems "ASAP" [23], "TracePro" [24], "LightTools" [25] and "SPEOS" [26], the *Lumicept* has the most effective algorithm of ray tracing and supports practically all possible from the view point of the beam optics physical effects of radiation propagation and light transformation on optical objects. The *Lumicept* has the most powerful and physically correct model of forming geometrical microstructures and their spatial distribution. Transformation of rays in the microelement geometrical model is also physically correct. All this makes the *Lumicept* an optimum tool for calculation design of complex IDs and of light scattering analysis in optical devices.

In this simulation example, a method of direct stochastic ray tracing was used. The output radiation parameter calculation was carried out using a model of luminance detector located in the plane of the light-conducting plate output edge. The detector model (Fig. 3) consisted of 713 cells (31×23). A cell size was equal to (10×10) mm, and integration cone angle was within ± 2º. The observation direction changed within – 60 to + 60º interval with a pitch of 15º.

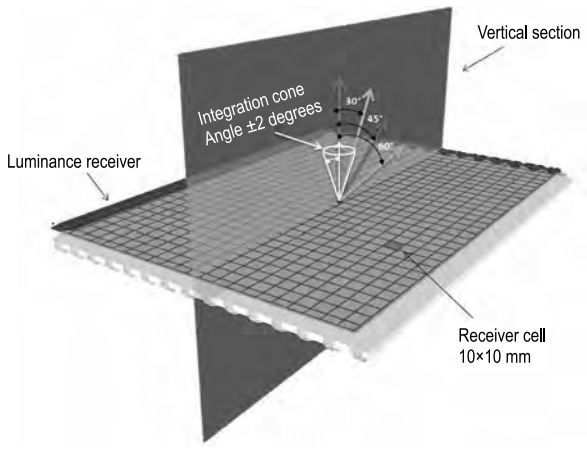

Fig. 3. Conditions of luminance distribution simulation over output surface of a light-conducting plate

During the first attempts of luminance distribution simulation, surface of each element of the scattering microstructure was set being completely smooth, i.e. without any micro-relief on it. The simulation results are presented in Fig. 4, where rise of the luminance level is well seen in the middle area of the light-conducting plate.

At the same time, the measured luminance distribution of the manufactured experimental specimen of the light-conducting plate with a scattering microstructure (Fig. 5) shows a noticeable luminance decrease in the middle area of the plate output edge, which significantly differs from the simulation results presented in Fig. 4. Such a measurement and simulation results discrepancy required to carry out an analysis to clarify its reasons.

As a result of the microscopic analysis of a separate microelement surface (Fig. 6, *a*) parallel grooves (Fig. 6, *b*) were found on it, which obviously arose when working the mould using a cutting tool. These grooves have a pronounced regularly directed structure, and this can quite lead to changes of angular distribution of light coming out of the

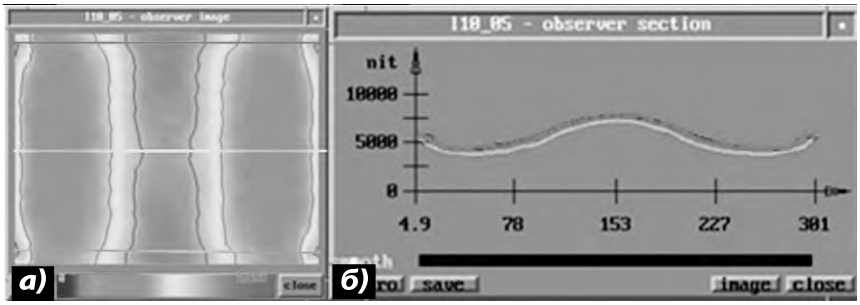

Fig. 4. Results of luminance distribution simulation over a light-conducting plate surface in the event of a completely smooth surface of micro-geometry elements: *a* – spatial distribution; *b* – distribution in the marked sections

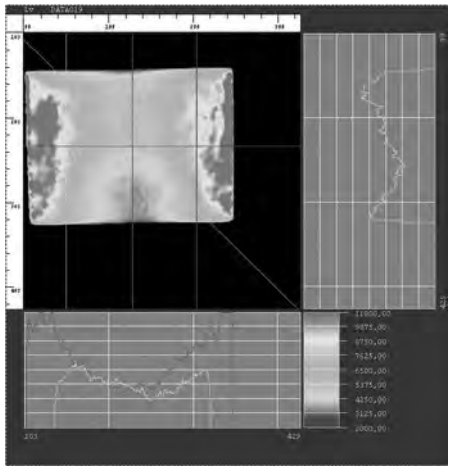

Fig. 5. A result of measuring luminance distribution over a manufactured specimen light-conducting plate output edge

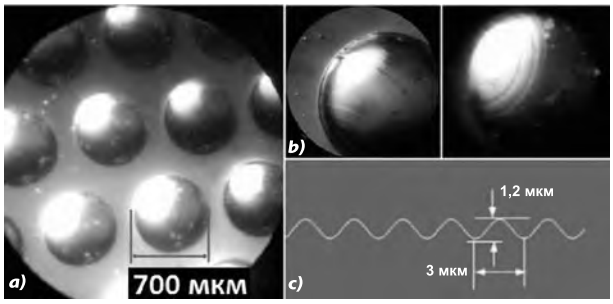

Fig. 6. Pictures of scattering elements microstructures (a) and of grooves on a microelement surface (b). Parameters of the groove relief (c)

plate and, thereby, have a significant effect on spatial luminance distribution. Unfortunately, exact measurements of either bidirectional scattering function [27], or of fine-grain relief on the spherical segment being a separate microgeometry element, not yet possible. Therefore, an attempt of reproduction of averaged parameters of the micro-relief observed in a microscope was made.

At the following simulation stage, a micro-relief consisted of sinusoidal grooves of 1.2 μm depth with the period of 3 μm (Fig. 6, *c*) was set on the surface of each element of microgeometry, which optical properties did not differ from the properties of the light-conducting plate.

In the first simulation experiment, micro-relief groove were placed in parallel to the longest side of the light-conducting plate, which corresponds to zero angle of the relief deviation. As it can be seen from Fig. 7(1), at different observation angles, luminance and its distribution on the plate edges is changing. During the second simulation experiment, direction of the micro-relief grooves was set with a deviation of 15º for all microstructural ele-

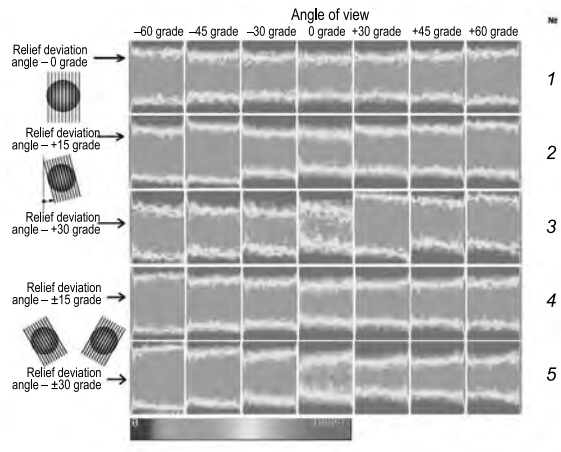

Fig. 7. Results of simulating output luminance distribution over the surface of a light-conducting plate taking into account micro-relief

ments. Respectively, it is seen from Fig. 7(2) that luminance distribution on the edges is asymmetric, and this is noticeable for observation angles of – 60,– 45, + 45 and + 60º. In the third simulation experiment, the relief for all microelements was turned by 30º. The correspondent luminance distribution (Fig. 7 (3)) strongly depends on the observation angle, and asymmetry is revealed stronger than in the previous experiment. This allows us to conclude that when changing micro-relief orientation, luminance distribution of the radiating light-conducting plate changes its symmetry for different observation angles. During the fourth simulation experiment, nature of micro-relief multidirectional orientation influence was verified. Each half part of the microelement massif is deviating off on + 15° and – 15° respectively. The obtained luminance distributions presented in Fig. 7 (4) save distribution symmetry. However, with increase of observation angle to – 60º, luminance on the light-conducting plate edges decreases.

The fifth simulation experiment differed from the fourth by the relief deviation angle (± 30°) only. In this case, with big observation angles (– 60º,– 45º), luminance decreases. When turning the micro-relief by ± 30°, at the observation angle equal to 0º, the simulation result repeats the measurement results of the light-conducting plate luminance distribution, wherein difference of luminance average values is equal to13 %.

Modelling experiment showed that an “addition” of a microstructural element micro-relief model allows coordinating calculation and measurement results among themselves. In that case,

spatial-and-angular luminance distribution depends on the micro-relief orientation.

4. CONCLUSION

Defects of light-conducting system optical surface, arising during manufacturing of microstructure diffusers, has a significant effect on the output light distribution, energy efficiency and ergonomics of an ID as a whole.

Therefore, to obtain correct results of light-conducting system simulation, it is necessary to know and take into consideration the features of microstructural scattering element formation technology.

As exemplified by simulation of an LCD display light-conducting plate with scattering microstructures performed using hot forging, it was found out that relief of microstructural elements influences the general luminance distribution. In spite of the fact that parameters of micro-relief arising on the surface of scattering microstructure elements almost cannot be exactly measured, several simulation experiments allow rather exactly selecting the micro-relief parameters for a further optimisation of this ID. Assuming that the technological process is stable, the obtained parameters of the micro-relief can be used for simulation and design of illumination systems, which light-scattering microelements are manufactured by a similar technology. The authors successfully solved the problem of a correct simulation of light-conducting systems taking into account the features of its production technology, and they developed an approach to simulation of output luminance distribution and to coordination of the results with the real luminance distribution. Use of the described method will help to improve quality of light-conducting system design in the future.

ACKNOWLEDGEMENT

The work is performed with financial support of a grant of the Russian Federal Property Fund #17–01–00363

REFERENCES

1. Shponkina Yu. Energy saving in electrical energy industry // ER, 2014, #3 (57), pp. 22–24.

2. Chang-Yi Li, Jui-Wen Pan “High-efficiency backlight module with two guiding modes” // Applied Optics, 2014, Vol. 53, # 8, pp. 1503–1511.

3. Young Chul Kim, Tae-Sik Oh, Yong Min Lee “Optimized pattern design of light-guide plate (LGP)” // Optica Applicata, 2011, Vol. XLI, No. 4, pp. 863–872.

4. Zhdanov D.D., Zhdanov A.D., Potyomin I.S. A quick method of constructing local equidistant distributions of micro geometrical objects of illumination systems // Optics and spectroscopy, 2015. #2, pp. 329–336.

5. Chao-Heng Chien, Zhi-Peng Chen “Design and fabrication of the concentric circle light guiding plate for LED-backlight module by MEMS technique” // Microsyst. Technol, 2007, #13, pp. 1529–1535, DOI 10.1007/s00542–006–0365-y.

6. Chiung-Fang Huang, Yung-Kang Shen, Yi Lin, Jen-Chang Yang “Luminance and brightness field distribution of light guiding plate for backlight panel (BLP) by micro moulding” // Polymers for advanced technologies, 2008, Vol. 19, Issue 12, pp. 1887–1893.

7. URL: http://denso.com/; http://denso-europe.com/products/information-safety-systems/instrument-clusters/ (addressing date: 5/20/2017).

8. United States Patent 13/562,888 July 31, 2012. Light emitting device and system providing white light with various colour temperatures / US20120293093 A1, Nov 22, 2012/ Kim; Yu-Sik. Samsung Electronics Co., Ltd. (KR).

9. United States Patent 15/048,476 Feb.19. 2016. Electronic device / US2017/0097614 A1, Apr.6, 2017/ Pilgoo Kang, Dongseuck KO and other. LG Electronics Inc.

10. United States Patent 14/918,591 October 21, 2015. Light guide plate, backlight module and display device / US9,557,469 B2 January 31, 2017/ Chang, Chia-Yin and other. Radiant Opto-Electronics Corporation.

11. Davenport T.L.R., Cassarly W.J. Optimizing Density Patterns to Achieve Desired Light Extraction for Displays // Proc. SPIE, 2007, Vol. 6342, p. 63420T.

12. United States Patent 14/632,377 February 26, 2015. Backlight module having a frame element, light bar, light guiding plate and light bar cover / US9,739,930 B2, August 22, 2017// Lo; Ching-I. INNOLUX CORPORATION.

13. Zhdanov D.D., Sokolov V.G., Potemin I.S., Voloboy A.G, Galaktionov V.A., Kirilov N. Modeling and Computer Design of Liquid Crystal Display Backlight with Light Polarization Film // Optical Review, 2014, Vol. 21, No. 5, pp. 642–650.

14. Cheng-Huan Yang, Sen-Yeu Yang “A high-brightness light guide plate with high precise double-sided microstructures fabricated using the fixed boundary hot embossing technique” // Journal of Micromechanics and Micro-engineering, 2013, Vol. 23, p. 035033.

15. Cheng-HsienWu and Chien-Hung Lu “Fabrication of an LCD light guide plate using closed-die hot embossing” // Journal of Micromechanics and Micro-engineering, 2008, Vol. 18, p. 035006.

16. Jen-Chin Yang, Chung-Ching Huang Using UV roll-to-plate imprint lithography to fabricate light guide plates with microdot patterns // Micro & Nano Letters, 2012, Vol. 7, Issue 3, pp. 244–247.

17. Peiyun Yi, Hao Wu, Chengpeng Zhang, Linfa Peng, Xinmin Lai “Roll-to-roll UV imprinting lithography for micro/nanostructures” // Journal of Vacuum Science & Technology B, 2015, Vol. 33, No. 6, p. 060801.

18. Tun-Chien Teng, Ming-Feng Kuo “Optical characteristic of the light guide plate with microstructures engraved by laser” // Proc. of SPIE, 2012, Vol. 8485.

19. Bogdanov N.N., Zhdanov A.D., Zhdanov D.D., Potemin I.S. Design of Ergonomic Illumination Systems for Cultural, Medical and Educational Facilities / EVA 2017 Saint Petersburg: Electronic Imaging and the Visual Arts: International conference, St. Petersburg, June 22–23, 2017: Conference Proceedings, St. Petersburg: ITMO university, 2017, pp. 106–111.

20. Luoa Xichun, Chenga Kai, Webba Dave, Wardle Frank “Design of ultra-precision machine tools with applications to manufacture of miniature and micro components // Journal of Materials Processing Technology, 2005, Vol. 167, pp. 515–528.

21. Tun-Chien Teng, Ming-Feng Kuo “Highly precise optical model for simulating light guide plate using LED light source” // Optics Express, 2010, Vol. 18, Issue 21, p. 22208.

22. Lumicept – Integra Inc. URL: http://www.integra.jp/en/products/lumicept (addressing date: 25.05.2017).

23. ASAP. URL: http://www.breault.com/software/software-overview.php (addressing date: 20.05.2017).

24. TracePro. URL: https://www.lambdares.com/tracepro/ (addressing date: 25.05.2017).

25. LightTools. URL: http://www.opticalres.com/lt/lt-prodds_f.html (addressing date: 19.05.2017).

26. SPEOS. URL: https://www.optis-world.com/product-offering-light-simulation-virtual-reality-software/SPEOS (addressing date: 21.05.2017).

27. Sokolov V.G., Zhdanov D.D., Potemin I.S., Garbul A.A., Voloboy A.G., Galaktionov V.A., Kirilov N. Reconstruction of scattering properties of rough air-dielectric boundary // Optical Review, 2016, Vol. 23, Issue 5, pp. 834–841, DOI: 10.1007/s10043–016–0250–6.

Nikolai N. Bogdanov, an engineer. At present, he is a senior engineer of Inter RAO LED Systems JSC, a postgraduate student of the Chair “Technology of visualisation” of the ITMO University (St. Petersburg State University of Information Technologies, Mechanics and Optics). His scientific interest field is illumination design

Andrei D. Zhdanov, an engineer, junior research worker of Scientific and Technical Computer Centre of IPM LLC, a postgraduate student of the Chair “Technology of visualisation” of the ITMO University. His scientific interest fields are computer graphics and virtual prototyping

Dmitriy D. Zhdanov, Ph.D., graduated from the Leningrad Institute of Precise Mechanics and Optics in 1984. At present, he is a Head of the Chair “Technology of visualisation” of the ITMO University. His scientific interests are: applied optics, computer graphics, lighting engineering

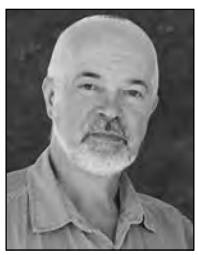

Igor S. Potyomin, Ph.D. graduated from the Leningrad Institute of Precise Mechanics and Optics in 1984. At present, he is a senior research associate of LLC Scientific and Technical Computer Centre IPM and Associate Professor of the chair “Technology of visualisation” of the ITMO University. His scientific interests are applied optics, computer graphics, lighting engineering

Light & Engineering
Vol. 26, No. 3, pp. 29–36, 2018

Svetotekhnika
No. 1, 2018, pp. 32–38

LIGHTING OF ENGINEERING STRUCTURES AND INDUSTRIAL FACILITIES: NEW ASPECTS OF THE TOPIC

Nicolai I. Shepetkov, George N. Cherkasov, and Vladimir A. Novikov

Moscow Architectural Institute – MARKHI (State Academy)
E-mail: n_shchepetkov@inbox.ru

ABSTRACT

This paper considers the fundamental problem of artificial lighting in various types and scales of industrial facilities, focusing on exterior lighting design solutions. There is a lack of interest from investors, customers and society in high-quality lighting design for industrial facilities in Russia, which in many cities are very imaginative structures, practically unused in the evening. Architectural lighting of various types of installations is illustrated with photographs. The purpose of the article is to draw attention to the aesthetic value of industrial structures, provided not only by the architectural, but also by a well-designed lighting solution.

Keywords: industrial objects, engineering structures, architecture, lighting, architectural lighting

Lighting engineering as a science emerged and developed primarily in the context of industrial production, because man has long understood that the results of his work and the quality of his life depend on the quantity and quality of light in the room where he works. For thousands of years people used natural illumination, limited by the sizes of expensive glazing in ancient times, because flame light sources in dark interiors did not produce a sufficient effect for production needs. It should be noted that the development of architecture was historically based on two objective factors: the structural construction capabilities of the covering dimensional spaces and their natural lighting. With the advent of electricity, the second factor has lost its need, but a the axiom of dependence of labour productivity on the quantity and quality of light remained. This became associated with specific content reflected in the normalisation and calculations of lighting, in improvement of evaluation criteria and design methods, in improving the quality of the light environment, significantly different from the natural light environment, in the expansion of contexts where lighting is always in demand. Interior lighting of industrial, transport and agro-industrial architecture is broad and well-researched topic, but it is constantly changing. Many industries are automated, and the role of man in them is changing constantly, but the human factor cannot be ignored under any circumstances. And this factor is primarily associated with visual perception, which depends on the quality of lighting.

Half a century ago in the USA and in other countries, controlled electric lighting drove the development of windowless shops, department stores, exhibition halls, sports and entertainment facilities, with no natural light inlets. A debate between professors V.A. Myslin and N.M. Gusev took place at the beginning of 1970s at a scientific conference in MARHI. The first posited that it was necessary to focus on creating comfortable visual conditions indoors with artificial lighting. The second argued that additional natural light is highly desirable for the psycho-physiological comfort of people in the room: the worker can look out of the window, see the natural world, the weather outside the window, the sun and the sky, the silhouettes of buildings, the crowns of trees. Today this point of view is no longer disputed. Later, Proff. G.N. Cherkasov proposed the idea of creating a favourable socio-psy-

Fig. 1 Group tour in the production hall (photo by G.N. Cherkasova)

chological environment inside industrial facilities, which could improve individuals' productivity [1, 2]. The concept comprised a set of interconnected classic and new, architectural, organisational and technical interventions in the interior and on site of the facility. This included: creating breakout spaces for short breaks on the shop floor, where they could be exhibited; establishing visual connections with the outside world through glazed openings (and today with the help of video screens); adjusting the light level and light spectrum at the beginning and end of each shift within the ranges set by health and comfort standards. New ideas for the formation of an interactive environment could be introduced in the process of work. For example: the video camera focuses on a worker at certain time intervals and the image projects onto the screens in the shop. This stimulates a level of responsibility, changes in emotional state, awareness of one's role in the production process and self-affirmation in the labour force. Changing images to other workers, creates a sense of belonging to the team, a level of personal connection within the technological space without separation from the workplace. It is

Fig. 3. "Glass manufacturing plantmanufactory" is a glowing factory of Volkswagen in Dresden

Fig.2 The glazed façade of the shop in Munich, BMW with a colour exteriorouter and interiorinner dynamic lighting in Munich

advised to use such video self-presentation briefly, selectively, at certain intervals in the shift, when there is a decline in performance, lapses in attention, fatigue before the end of the working day or a break in the work. Everything should be aimed at making people feel comfortable, getting satisfaction from their activities. The last few decades have seen the successful operation of modern industrial facilities, equipped with the latest technology, which provide tour opportunities for visitors, who can observe the production process, highly technical, and often quite beautiful equipment, the organisation and working conditions of people, the architecture and design of the environment, the effect of lighting (Fig. 1). Stained glass windows for workshops has become fashionable again (Fig.1), specifically so that the workshop and production process could be observed from the street outside even during the day-time, with intense indoor illumination, providing free workshop masterclass (Fig. 2). The industrial building extends to the red line, without a traditional fence. This is true in the case of the automobile assembly plant ("glass factory") in Dresden (Fig. 3), the winery "Protos" in Peñafiel (Spain), the brewery in Mytishchi (Russia), etc. When a group of tourists passes through the production facilities, it is advisable to use remote control "targeted" lighting, for short-term illumination of certain elements of equipment or work areas, focusing visitors' attention on the features of technological operations, safety, interior architecture and design of equipment, thus maintaining interest in the dynamic tour. The light can be controlled by a tour guide or programmed automatically. Specific solutions for light and colour, as well as sound, tactile and other sensory foci of the visitor's attention can

Fig. 4. Colour dynamic lighting of bridges:
a – Meiko East Bridge in Nagoya; b – St. Andrew walking in Moscow
(photo N. And. Shepetkov)

be applied as long as they do not interfere with the production process. The script and facilitation of such tours allows the visitor to become immersed in the atmosphere and space of production, making the industrial process a fascinating show, with the workplace as the central "hero".

The theme of lighting and lighting design of interiors of industrial buildings with different architecture and at various scales is extremely capacious, constantly relevant, structurally and technologically complex, and it is being studied continuously [3]. Another angle is the lighting design of industrial buildings as objects of the evening environment, forming part of the cityscape, historical and architectural, dominant and donor. Compared to public buildings, industrial facilities are rarely treated with artistic design, and when they are, this is often flawed. In fact, for many of these facilities, their large and original external form with proper lighting would do an honour to any city image. This is the case not only for industrial buildings, but also engineering structures – bridges (Fig. 4) and transport interchanges, CHP pipes, cooling towers and power line supports, hydroelectric dams and canals and locks, oil refineries and gas tanks, water towers and fire towers, railway depots and interchange hubs, river, sea and air ports, radar installations and TV towers, elevators, exhibition complexes (Fig. 5), etc. Many of them, especially older installations, located in residential areas, occupied by residential buildings, sports facilities, green spaces and recreational spaces, gradually are transformed into civic objects, starting a new functional and figurative life, preserved or modified in architectural form. In different cities around the world, and even beyond their borders, the architectural lighting of installations such as the Sayano-Shushenskaya and the Krasnoyarskaya hydroelectric

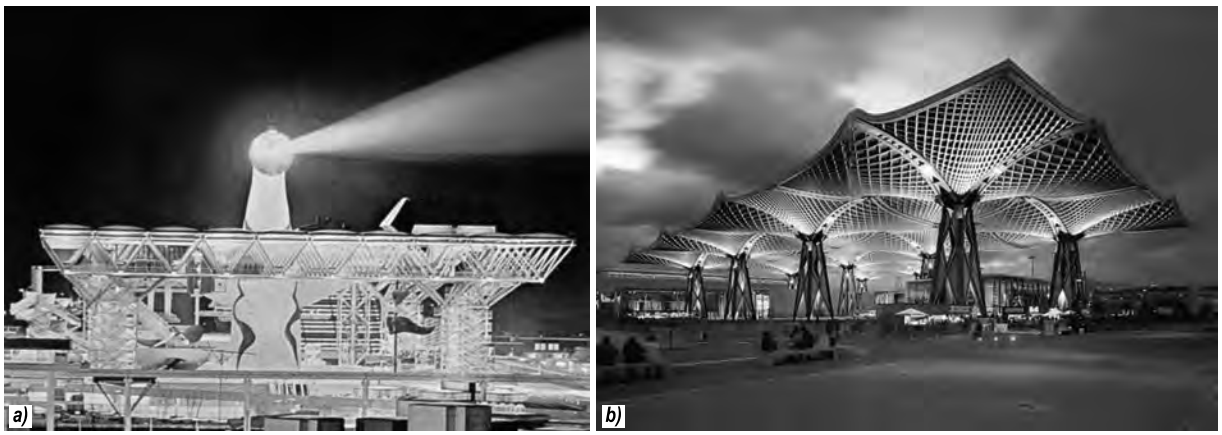

Fig. 5. Architectural lighting of exhibition facilities:
a – covering over the festival Area with the Sunsun Tower at EXPO-70 in Osaka;
b – exhibition pavilion " EXPO-200220002 in Hanover

Fig. 6. Architectural illumination of Krasnoyarskaya hydroelectric power station

power stations (Fig. 6), oil refineries, sewage treatment, and gas processing plants, become the topic of evening tours. In other cases, they appear like fantastic mirages, decorating the night landscape as seen from buses, trains, personal transport. For example: a chemical plant near the Dead Sea in Israel, is seen from afar as a bright spot of light in the darkness of the desert. The impression is enhanced by dynamically lit steam columns from the stacks. It is impossible to identify as an industrial object from afar. As you approach, it turns into a clear group of light verticals of open process equipment, reactor columns, cylindrical structures, stairs and bridges, winding pipelines. A competent system of electric lighting successfully reveals powerful architectonics, scale and energy of this 21st century (Fig. 7, (a). Even the basic mandatory technical and signal lighting of such plants make an impression on the unprepared observer. For example, driving in the evening towards Yaroslavl from the south reveals numerous electric lights and the live flames of the flared gas over the refinery stacks, which fascinate the eye. You can imagine even more powerful and sparkling complexes at night in the Tyumen

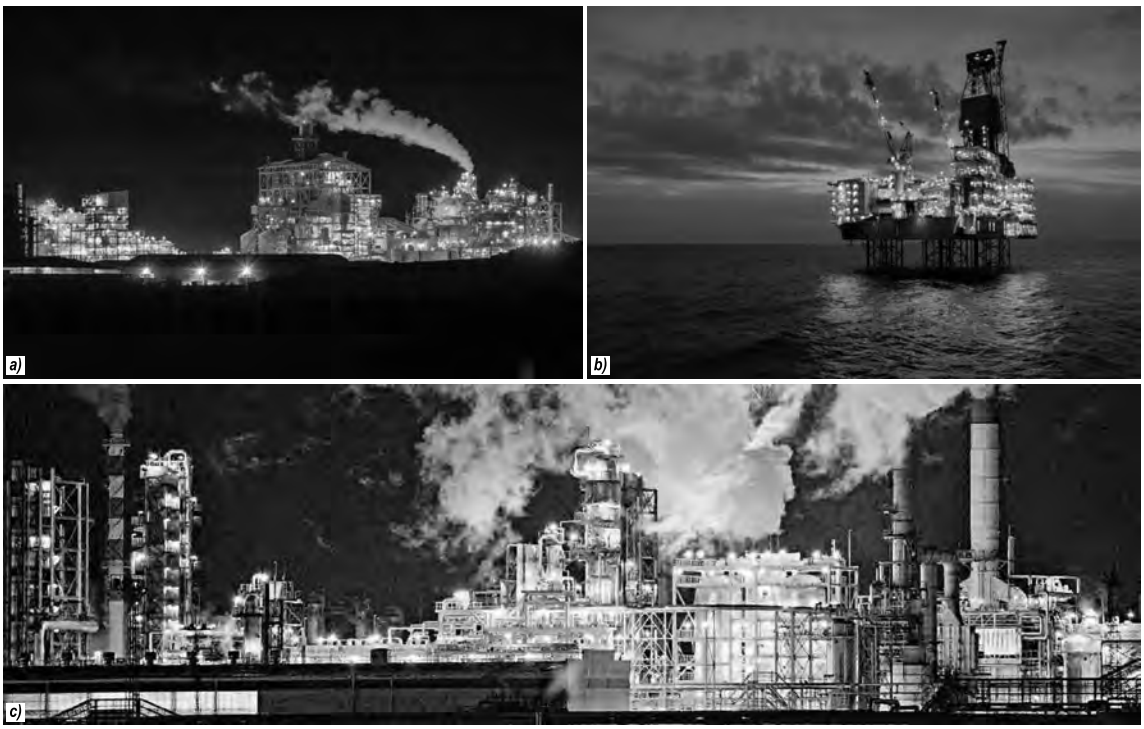

Fig. 7. Element of technological and signal lights in the night panoramic views of oil and gas, chemical and processing facilities:
a – chemical plant in the Sinai desert, Israel; b – oil platform in the North sea; c – complex of the company "Promtekhelektro" in Kstov (Nizhny Novgorod region.)

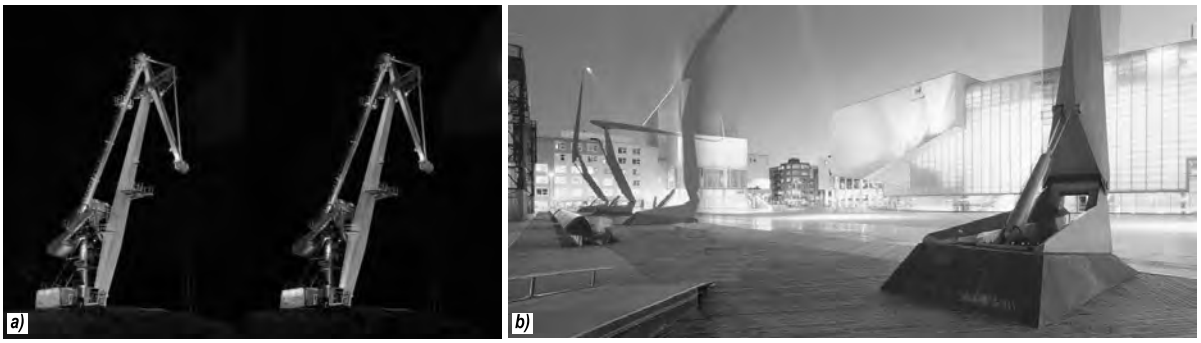

Fig. 8. Decorative lighting of port cranes as urban relics:
a – imitation of cranes at the Theatre square in Rotterdam;
b – port cranes in Murmansk, illuminated by colour light

region, in the endless tundra in the North of Russia, on oil platforms in the seas and Arctic ice (Fig. 7, b and c).

In many port cities of the world, the preferred technique of forming the light panorama was lighting, often coloured, of old port cranes, preserved as open air museum exhibits. They help people orientate themselves on embankments and the wider city space by their recognisable silhouettes and large scale. In Rotterdam, for example, the illuminated cranes in the old port inspired urban planners and designers in the 1990s to creatively interpret the image of cranes as kinetic lighting masts in the Theatre square [4]. Murmansk and other coastal cities follow the same example (Fig. 8).

The application of decorative lighting on in situ building cranes on large high-rise construction sites is increasingly used in Moscow, reviving the previously deserted and dark areas of the city territory.

Radio and television towers of different heights and designs are a known familiar silhouette of many large cities around the world. In Moscow there are two such towers – Ostankinskaya and Shabolovskaya (Shukhov). Shortly after its construction in 1967, the entire 500-metre tall Ostankinskaya tower was highlighted with searchlights and spherical discharge lamps on public holidays, according to a VNISI project. In 1996, the failed lighting system was replaced with a new one, using holiday and everyday stationary modes, metal-halogen lamps and mercury arc lamps (Fig. 9, a and b). These illumination devices were developed with our participation [4]. In 2016, “modern” designers

Fig 9. The modes of architectural illumination of Ostankino Television Tower in 1996 – 2017: fixed holidays (a) weekday and everyday (b) up to 2016, using the white light (N.I. Shchepetkov’s photo); modern coloured display mode, since 2016 (c)

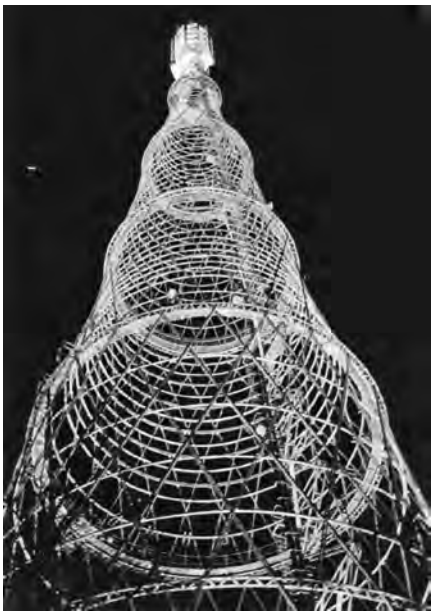

Fig. 10. Stationary two-colour floodlight lighting Shabolovskaya TV tower

added a diode mesh "stocking" onto the tower with a dynamically changing colour light pattern and temporarily preserved the unique ground system of aerial illumination made in the 1990s by Svetoservis (Fig. 9, c). The technically simple lighting of the elegant lattice of the Shukhov tower, flooded in 1997 by two-colour floodlight (Fig. 10), was often reconsidered in order to compete with the Eiffel tower in Paris; this was an initiative of Yuriy Lujkov, then Mayor of Moscow. However, all attempts to hang lighting equipment on the rusted structures of the tower were reasonably rejected by the Moscow office for the protection of monuments – we accounted for this and took it as given from the very beginning of the project [4].

Fig. 11. Light-graphic version of TV tower illumination and coloured lighting of Kantemirovsky bridge in St. Petersburg

And there are no other methods, except for intensifying the floodlight, changing its chromaticity and kinetics in this case. Perhaps the use of laser and/or narrow searchlight beams, typical for temporary (festive) light shows could be applied, because they can penetrate the tower structure without compromising its existence or creating a virtual light space around the tower, greatly increasing its scale and dominant role in the Moscow's light panorama. Illumination of unclad or monolithic structures of television towers in many cities of the world is fundamentally uniform, except that the latter allows for elements similar to the firmer: a light graphics of linear, dotted and dot colour, and dynamic patterns on their body (Figs. 11–13), as well as projection methods of video mapping.

Thermal power plant cooling towers, elevators, cylindrical oil storage tanks, cement and chemi-

Fig. 12. Lighting of the "pearl of the East" TV tower in Shanghai

Fig. 13. Lighting of a TV tower in Guangzhou

Fig.14. Lighting of the thermal power plant cooling tower in Brussels – one of the first media installation at the industrial facility

Fig. 15. Colour lighting of cooling towers CHP in Yekaterinburg

cal plants, gas tanks and water towers also large objects reflecting light in an urban context. Today, they rarely adorn the urban surroundings and industrial zones during the day, and are rather unpopular in artistic terms because of their unkept appearance, but at night they could become spectacular media screens. An example of this can be found in Brussels: an LED cord is mounted on a powerful hyperbolic-parabolic power plant cooling tower, running projections of a variety of colour animated images – flying birds, ornaments, text, etc. (Fig. 14). Our concept proposal from 2004 on the illumination of numerous cooling towers in Moscow [5] was not considered by the Moscow authorities but was implemented in Yekaterinburg and Samara (Fig. 15).

A similar story unfolded with the power lines in the area of Yaroslavl highway: in the tender for the lighting in 2011, we proposed to the Moscom-architecture and Dep-Tech to illuminate the power line supports with coloured light, forming a day silhouette panorama in the area of the platform "Severyanin" and in other areas of Moscow. The proposal has not yet been considered, although the delicate and beautiful designs of the supports deserve consideration. In the Moscow region, some power line supports in recent years have been painted with white and blue paint, which distinguishes them from the typical grey supports during the day. They can be seen from highways and from trains. Groups of such supports illuminated with coloured light, would play a powerful spatial-architectural, symbolic, informative and aesthetic role in the night space of the city.

Even more difficult for an urban solution and further adaptation to modern life are examples of the preservation and conversion of large industrial facilities, for example, metal production plants. In the West of Germany in the industrial Ruhr, many steel plants from the 19th and 20th centuries were not destroyed after the Second World War, but turned into a kind of tourist centres. One of the symbolic, attractive, accessible and effective methods of

Fig. 16. Coloured lighting technology Park in a reopened steel mill in Duisburg

this transformation was their coloured architectural lighting (Fig. 16). It is a pity, that this technique is almost unused in Russian practice, because many industrial enterprises in Moscow (and beyond) have been leaving, or are leaving the city, leaving behind the objects of historical industrial architecture. In some cases, the facades of the buildings, which have transformed into functional civic buildings, offices, museums or residential, are still illuminated, but their choice and style of lighting is very random, not referring to the functional-figurative beginning of the original architecture. Elsewhere, in the republican, regional and district cities, the situation is even worse.

Meanwhile, urban civil construction investors have long realised that good architectural lighting increases the prestige and reputation of the facility – it or its product is more expensive and quickly sold or rented. The modest cost of lighting has a relatively quick payback period. Today, it is difficult to find a small town of regional scale, and even a village where there is no shining light form private business, some advertising, windows and even facades. From our professional point of view, this light must not only be "shiny" and bright, but also informative and artistic. Lighting design in Russia in the field of architecture is clearly inferior to lighting design in the architecture of life. This is not favourable, since most of an adult's active life is devoted to work.

REFERENCES

1. Cherkasov G.N. Architectural aspects of psychological climate organization at industrial enterprise // Industrial construction. 1975, № 12, pp. 23–25.

2. Cherkasov G.N. Some of the features of modern architecture. Architecture and construction. ACADEMIA // 2017,№ 2, pp. 37–43.

3. Ilyina E. A., Chestukhina Tn. Special assessment of workplace lighting, Svetotekhnika, 2017, № 2, pp. 23–27.

4. Shepetkov N.I. Lighting design of the city. – M.: Architecture-C, 2006.

5. Shepetkov N.I. About creating a new light-the silhouette of the city, "Architectural science and education. Abstracts of the scientific conference dedicated to the 60th anniversary of Victory in the great Patriotic war". – M.: Architecture-C, 2005, 73 p.

Nikolai I. Shechepetkov,
Dr. of Architecture, Professor.
Graduated from the Moscow Institute of Architecture in 1965. Head of the Department of "Architectural physics", Moscow Institute of architecture (SA). Laureate of the State Prize of the Russian Federation (for architectural lighting in Moscow). Corresponding member of the Academy of Natural Sciences, member of the editorial Board of the journals "Svetotekhnika" and "Light & Engineering"

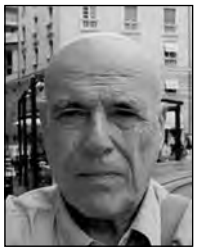

George N. Cherkasov,
Dr. of Architecture, Professor. Graduated from the Moscow Architectural Institute in 1958. Professor of the chair of "Architecture of industrial structures" of Moscow Institute of Architecture (SA). Honoured architect of the Russian Federation and honorary worker of higher professional education of the Russian Federation

Vladimir A. Novikov,
Dr. of Architecture, Professor. Head of the Department "Architecture of rural settlements" MARHI. Honorary architect of Russia and honorary worker of higher professional education of Russia

Light & Engineering
Vol. 26, No. 3, pp. 37–43, 2018

Svetotekhnika
No. 5, 2018

DEVELOPMENT OF LED LIGHT SOURCES IN LANDSCAPE LIGHTING

Zhiqiao WANG

School of Art Yangtze University, Jingzhou Hubei 434000, China;
E-mail: zhangque8@yeah.net

ABSTRACT

An LED light source, which is extensively used in landscape design, has played a good role in its application due to its characteristics and advantages. On the basis of cost-effectiveness analysis, green lighting energy-saving technologies that use LED light sources in landscapes are analyzed, as well as the key factors that affect the cost-effectiveness of various stakeholders. Results show that the cost-effectiveness analysis method is effective for evaluating the DSM technology. Moreover, the application of LED light source in landscape lighting has great feasibility. This study provides some theoretical reference for the promotion of green lighting energy-saving technology.

Keywords: LED, illumination, cost-effectiveness, DSM technology, cluster analysis method, analytic hierarchy process (ANP)

1. INTRODUCTION

By 2050, approximately 75 % of the world's population will be living in urbanized areas. Urbanization leads to energy crisis and environmental issues, as well as lifestyle changes. These trends cause the lighting industry to undergo a major transformation. The rapid development of LEDs has made this revolution possible not only because the energy-saving characteristic of LED lighting meets the requirements of the form; moreover, the dynamic changes not only further suit the needs of the market but also able to render the lights under night conditions [1]. Garden landscapes are ideal paradise and motivation for people. A garden fully embodies people's yearning and desire for a free life. It is a concentrated expression of aesthetic cognition and thinking applied by humans in the transformation of nature and the use of natural processes to create a living environment [2]. Landscape stones are typically used for hard landscape. Although these stones have dull appearance, they seem to emanate life after artificial selection and stacking, such that they look natural. These stones ingeniously imply the natural and philosophical views of "harmony between man and nature." Strong and weak light changes, colour matching, and strong irradiation are fully used in garden lighting, which increases the brilliance of garden flowers, trees, and landscape buildings at night, thereby fully expressing the characteristics of night scenes and fully displaying the design style of an architecture or landscape to achieve elegant lighting atmosphere [3]. Lighting designers often use several urban architectural and square lighting methods to redesign traditional gardens, such that peaceful and distant natural garden landscape becomes distraught, noisy, and exceedingly bright and modern gardens are always full of sound and light effects [4].

2. STATE OF THE ART

Garden lighting designs should have specific use of lights to ensure that distinctive buildings, sculptures, flowers, rocks, and mountains have different appearance during daytime. A quiet and tranquil atmosphere is present in the light and shadow created by light. However, nightscape lighting designs should meet a series of ecological and psychological requirements to avoid problems, such as

glare and light pollution. Night scene lighting must meet the professional and artistic fusion to ensure that political and cultural qualities, artistic heritage, and historical background of a city or township are appropriately reflected. Meanwhile, the lighting design should express a rich landscape culture and reflect its cultural heritage [5]. China has no noticeable development trend of garden lightings until the 1990s. The subject of lighting that time was buildings, and garden landscapes only needed basic lighting functions. Moreover, landscape lighting is only utilized during festivals. The lighting was specifically used for a short time and its method was simple. Simple objects mostly used contour and floodlighting. With the active development of science and technology, garden landscapes have gradually expanded to its full range [6]. Lighting techniques and designs have also become increasingly complex and diverse. From the use of a single layer to the utilization of integrated light sources, the three-dimensional collocation of various lighting fixtures has enabled the current variety of lighting technologies to emerge in an endless stream. "Green lighting" is a new lighting approach proposed after the 1990s on the basis of the perspective of energy conservation and environmental protection [7].

3. METHODOLOGY

3.1. Establishment of LED Lighting Indicator System and Determination of Indicator Weight

The emergence of white LED at the end of the 20th century has attracted widespread attention. It is the fourth generation of light source for the purpose of green lighting. With the continuous advancement of LED technology in recent years, LED light sources are gradually replacing traditional light sources in urban landscape lighting. Hence, LED lights are increasingly favoured by designers because of its advantages, such as good concealment, low power, concentrated light, and controllability [8]. However, thus far, LED light source has no evident advantage over traditional light sources in several areas, such as road and hotel interior lightings; hence, people must not rapidly adopt this technology. In recent years, designers have continuously conducted theoretical research on the lighting of garden sketches. Researchers extensively use plants as examples to investigate their changes in light and shadow. However, research on this subject is relatively rare. In the cluster analysis method, we must clearly classify the criteria and weights. First, we need to establish a judgment matrix that represents the aforementioned level as a benchmark. Then, we compare the relative importance of the two-level indicators. Judgment matrix A is adopted in this study, where $a_{ij} = 1/a_{ji}$ and $a_{ii} = 1$, $1 \le i \le j \le n$. The matrix weights and the product M_i of the elements of each row of judgment matrix A are calculated as follows:

$$M_i = \prod_{j=1}^{n} a_{ij}, i = 1,2,3,4...n. \quad (1)$$

The n^{th} root value of each row M_i is calculated as

$$\bar{W}_2 = \sqrt{M_2},\ i = 1,2,3,4...n. \quad (2)$$

Vector $(\bar{W}_1, \bar{W}_2, ...\bar{W}_N)^T$ is normalized, and W_i denotes the weight coefficient value of each obtained index, as expressed as follows:

$$W_i = \frac{\bar{W}_i}{\sum_{j=1}^{n} \bar{W}_j}. \quad (3)$$

Then, consistency check is performed. Practically, the judgment matrix should satisfy the general consistency, and consistency check is required. We can prove that the judgment matrix is logically reasonable to continue analyzing the results only through inspection. The maximum eigenvalue is calculated as

$$\lambda_{\max} = \sum_{i=1}^{n} \frac{(AW)_i}{nW_i}. \quad (4)$$

Then, the consistency index *CI* is calculated as

$$CI = \frac{\lambda_{\max} - n}{n-1}. \quad (5)$$

The corresponding average random consistency index *RI* is obtained on the basis of the difference of various orders of the judgment matrix, as shown in Table 1.

Table 1. An Average Random Consistency Index RI

n	1	2	3	4	5	6	7	8	9
RI	0	0	0.58	0.89	1.12	1.26	1.36	1.41	1.46

First, the consistency ratio *CR* is calculated and analyzed. The consistency of the judgment matrix is

considered acceptable when $CR < 0.1$. Meanwhile, when $CR > 0.1$, the consistency requirement is not met; hence, the judgment matrix must be revised. Finally, the index system weight determination and consistency check are performed. Three criteria indicators, namely, consumption, profit, and user indicators of the mobile environment are set under the consumer value evaluation index. The result corresponded with the matrix A_1 after comparing the first-class indicators by using the available questionnaire number.

$$A_1 = \begin{bmatrix} 1 & 3 & \frac{1}{3} \\ \frac{1}{3} & 1 & \frac{1}{5} \\ 3 & 5 & 1 \end{bmatrix}. \quad (6)$$

A step-by-step calculation can be performed to obtain each index. In addition, we interviewed nine experts in related fields to establish a mobile consumer segmentation model. After calculating the weights of the indicators provided by each expert, the weights of the final indicators are identified using the arithmetic average method. The statistics of the final results of the first-level indicators of value evaluation are not listed due to the limited space. Table 2 shows the final weight of the analytic hierarchy process (AHP).

We use AHP to analyze and compare the competitiveness of Jiangmen with the developed cities of the LED industry, such as Shenzhen, Dongguan, Zhongshan, and Foshan in the Pearl River Delta. Therefore, the indicators are transformed into a hierarchical structure (Fig. 1).

3.2. Lighting Cost-Effectiveness Analysis

The cost-effectiveness of lighting is analyzed. During user cost analysis, users participate in the LED green lighting energy-saving project to pay the additional cost by replacing incandescent lamps with energy-saving lighting products, that is, direct costs or increased equipment purchase fees, which can be expressed as

$$Cc = \sum_{j \in J, k \in K} (C_{c(j,k)} n_{(j,k)} N_{(j,k)}), \quad (7)$$

where

$$C_{c(j,k)} = (P_j - Q_j / Q_b P_b) / (p_b - p_j), \quad (8)$$

where C_c is the total direct cost of the user in yuan/W, k is the collection of user categories (such as residents, shopping malls, hotels, and restaurants) participating in the green lighting energy-saving project, and j is the collection of green lighting products. At present, a large number of mature and simple lighting energy-saving measures use compact fluorescent lamps (commonly known as energy-saving lamps) instead of incandescent lamps or electronic ballasts instead of ordinary magnetic ballasts for fluorescent lighting. $C_{c(j,\,k)}$ is the direct cost of the use of the seventh type green lighting product for the k^{th} user to save 1 W electricity, yuan/W; and $N_{(j,\,k)}$ is the number of users who are interested in replacing the original lighting products with the seventh type of green lighting products. The corpse and

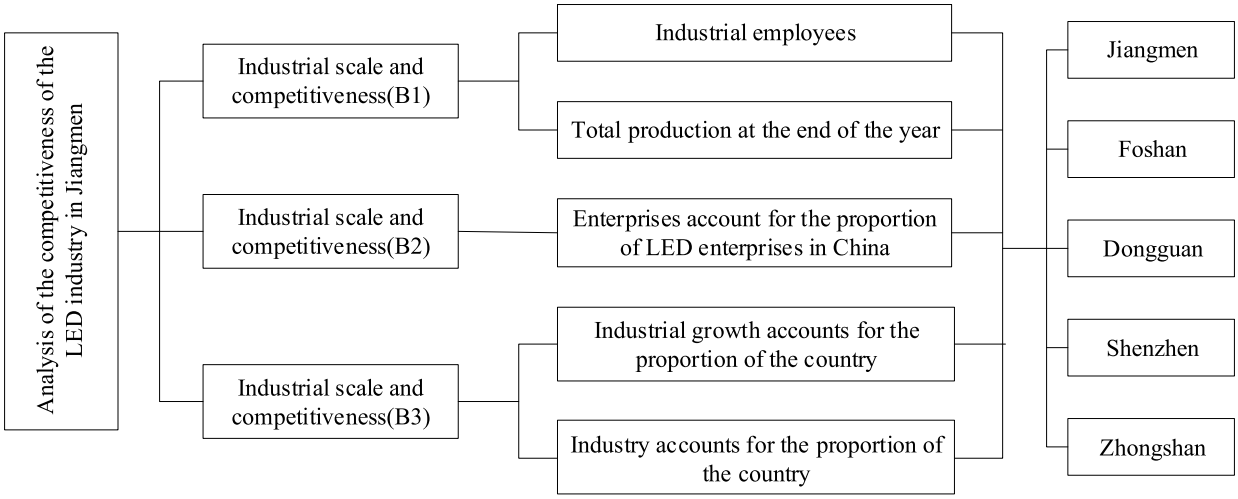

Fig.1. Hierarchical structure diagram

Table 2. Indicators for the Comprehensive Competitiveness Evaluation System of the LED Industry in Jiangmen

	First level index	Two level index
The comprehensive competitiveness of the LED industry in Jiangmen	Industrial scale and competitiveness Industrial growth competitiveness Competitiveness of industrial market	Number of industrial employees (only)
		Total production at the end of the year (billion yuan)
		Industrial GDP at the end of the year (billion yuan)
	First level index Industrial scale and competitiveness Industrial growth competitiveness	Average growth rate of industrial value in the past three years
		Enterprises account for the proportion of LED enterprises in China (cy0)
		Industry production accounts for the proportion of national output (%)
	Competitiveness of industrial market	Industrial output accounts for the proportion of LED industry in China
		Industrial growth accounts for LED growth in the country (%)
		The export value of the industry accounts for the proportion of the export value of the region (%)

cadaver are the market prices of the original lighting products and the seventh type of green lighting products, respectively. Q_b and Q_j are the average life of the original lighting products and the seventh type of green lighting products, *h*, respectively. P_b and P_j are the power of the original lighting products and the seventh type of green lighting products, in W, respectively. In addition, N_0 is the total number of users in a certain area, and $i_{(j,\,k)}$ is the participation rate of the k^{th} user who is willing to replace the original lighting product with the j^{th} green lighting product. In the user benefit analysis, the benefit accumulated by users through the use of energy-saving lighting products is the energy-saving benefit during the product life cycle accumulated by all the different types of users participating in the green lighting energy-saving project. The power-saving benefits that users receive during the life cycle of green energy saving lighting products are as follows:

$$B_{c(j,k)} = \Delta W_{c(j,k)} P_k, \tag{9}$$

where

$$\Delta W_{c(j,k)} = (p_b - p_j) Q_j n_{(j,k)} N_{(i,k)} \times 10^{-3}, \tag{10}$$

$B_{c(j,k)}$ is the power-saving benefit obtained by the k^{th} user through the use of the seventh type of green lighting products; $\Delta W_{c(j,k)}$ is the amount of electricity used by the k^{th} class user for the j^{th} green lighting product, kW·h; and P_k is the lighting power consumption of the k^{th} user, yuan/(kW·h). The static investment recovery period of the users who utilize various types of energy-saving technologies is one of the key factors that affect the willingness of users to participate in the DSM measure. The static investment payback period for users who utilize green lighting products is expressed as

$$T_j = \frac{P_j - Q_j / Q_b P_b}{P_k h_j (p_b - p_j) \times 10^{-3}} = \frac{C_{c(k,j)}}{P_k h_j \times 10^{-3}}, \tag{11}$$

where h_j is the daily illumination time of the seventh type of green lighting product, h/d.

3.3. Association Rule Algorithm

The Apriori algorithm mines item sets through constant construction and filtration. Each screening requires a scan of all the raw data. Therefore, scanning the original data multiple times is necessary. When the size of the original data is large, the efficiency is relatively low. Thus, scholars have found ways to reduce the number of scans of the original data, simplify the strategy of mining frequent

Table 3. Average Random Consistency Index R (1000 Positive Reciprocal Matrix Calculation Results)

Matrix order	1	2	3	4	5	6	7	8
R.I.	0	0	0.52	0.89	1.12	1.26	1.36	1.41
Matrix order	9	10	11	12	13	14	14	15
R.I.	1.46	1.49	1.52	1.54	1.56	1.58	1.58	1.59

item sets, simplify calculations, and shorten the time consumption. To avoid the defects of the Apriori algorithm, Han et al. proposed the frequent pattern (FP)-growth algorithm. This algorithm does not generate candidate frequent item sets but only scans the original data twice. Compression of raw data through FP-tree data structure is increasingly efficient. Therefore, the FP-growth algorithm is an efficient algorithm for mining frequent item sets in the case of large data size.

The FP-growth aims to construct an FP-tree with frequent item sets to retain the item set information during the first pass scan. Then, the FP-tree is divided into several conditional libraries, which are then mined. The FP-growth algorithm mainly involves two steps, namely, FP-tree construction and recursive mining. The FP-tree construction compresses the transactions in the original data to an FP-tree via two data scans. The FP-tree is similar to a prefix tree, and the paths of the same prefix can be shared to compress the data. Then, the FP-tree is used to identify the conditional pattern base and FP-tree of each items, and the recursive mining condition of the FP-tree acquires all the frequent item sets. Similarly, we use the examples provided previously to describe the main steps of the FP-growth algorithm in detail.

The FP-tree is initially constructed. The entire database is scanned; hence, the frequent item sets and their support for a single item is $\{a\}:5,\{b\}:4,\{c\}:6,\{d\}:7,\{e\}:1$.

The minimum support number is set to 1, and the result is presented in descending order as A = $\{\{d\},\{c\},\{a\},\{b\}\}$ S. Hence, the FP-tree can be constructed. First, an empty root node is established. Then, the database is scanned for the second time. Finally, a branch for each order is created in accordance with the previous support order. For example, a, d, and e are present in Order No. 1. Hence, the order is three branches d(7)–a(5) according to the support degree. The empty node is connected to d, which is connected to a; the branch node corresponding to Order No. 2 is d(7)–b(4). Meanwhile, a header table (Header Table) is created. The project, its support, and its nodes are recorded to facilitate traversal in the subsequent mining. The constructed FP-tree and item header table are shown in Fig. 2.

Then, the FP-tree is recursively mined.

4. RESULT ANALYSIS AND DISCUSSION

Simulation experiments are conducted through the BP neural network to design the most energy efficient lighting installation scheme that satisfies the illumination standard value. Generally, the lighting fixture installation position and power in different environments will have a certain lighting effect.

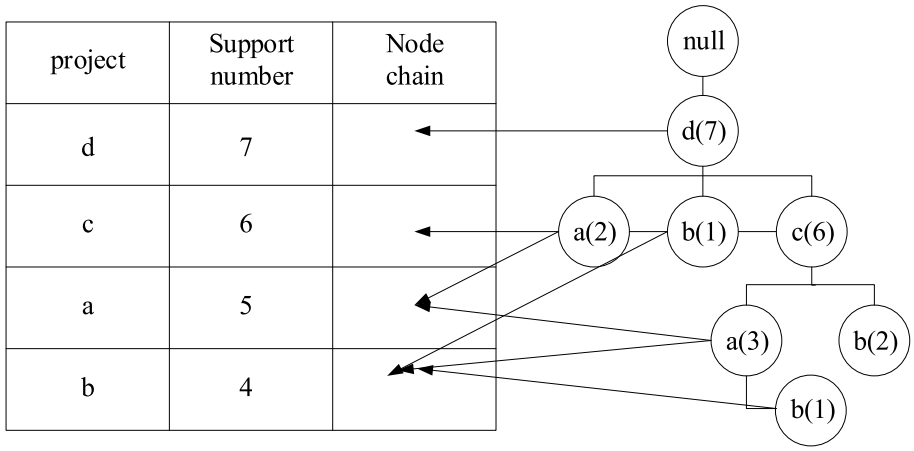

Fig.2. Header Table and FP-tree

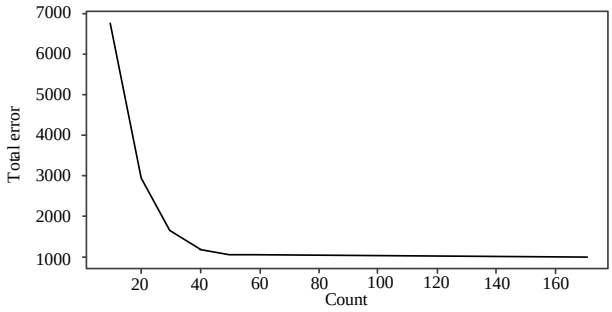

Fig.3. BP neural network algorithm (a)

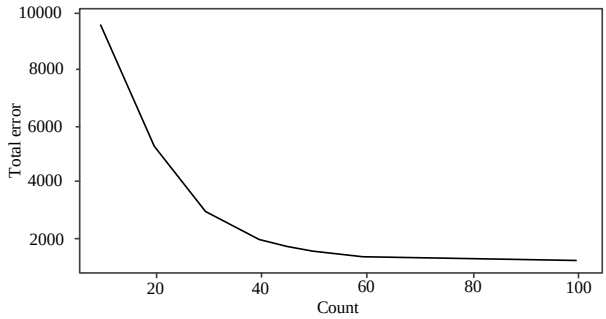

Fig.4. BP neural network algorithm (b)

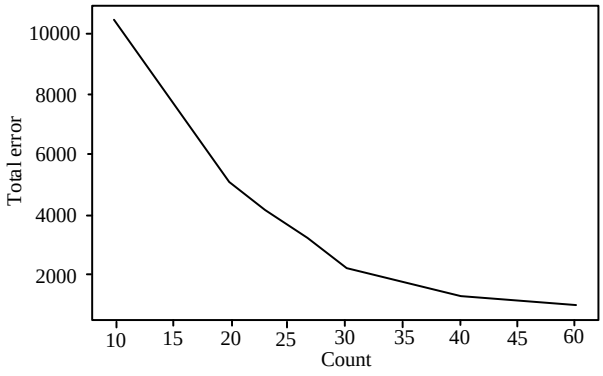

Fig.5. BP neural network algorithm (c)

A model is established using the BP neural network, and the illuminance standard and the luminaire power are defined as the input quantities. Furthermore, the installation position of the luminaire is defined as the output quantity, and the training is performed. We select a classroom in as an experimental object. The input data of the BP algorithm is normalized, the input and output parameters of the network are determined, and the selection and determination of the parameters are selected according to actual conditions. The data used in the test show that the input quantities are the lighting brightness and the lamp power, whereas the output are the minimum horizontal and vertical spacing (in cm) of the lamps installed in the selected classroom. The default size of the classroom is 12 m × 9 m. Evaluations can be performed on data modified for classrooms of various sizes. During the test, fluorescent lamps are used as test fixtures. The 16 W LED lamp used for this design is generally the same as the fluorescent lamp 40 W in illumination. Thus, the simulation of the 40 W lamps can be the basis for the installation position of the lamp in the design. The total error of the training obtained after running multiple times is shown in Figs. 3, 4, 5. The error of the algorithm is graphically displayed every 10 iterations.

The condition pattern base for each item is created starting with the last item (lowest support) in the header table. All paths that contain the project are calculated, and the project's prefix path is the conditional mode base. For example, if the path of b item is d–b, c–a–b, c–b, d–c-b, and b, then the prefix path is d, d–c–a, c, and d–c, that is, the condition mode base of item b. Then, the condition tree of the project is constructed using the set of conditional schema bases of the project with minimum support. All combinations of frequent item sets are generated on the basis of the condition tree. Let the minimum support number be 1. For b, the resulting frequent item set is {b, d}{b, c}. The numbers of support for these frequent item sets are 2 and 3. The results obtained through the Apriori algorithm are the same. However, the FP-growth algorithm has its disadvantages. Given that the algorithm recursively generates conditional databases and FP-trees, it consumes a large amount of memory. This large memory consumption is the main problem of this algorithm. The advantages of the recommendation based on association rules are its simplicity and perceptivity; moreover, it can imitate an actual shopping scene and does not need knowledge related to the product while possibly exploring the potential interests of users and purchase stimulations. However, computational complexity is a considerable drawback of association rule mining. With the increase in the size of frequent item sets, especially in the case of large data sets, the cost of mining will also increase. Nevertheless, given the same minimum support, confidence, and other constraints for the same data set, the association rules obtained by the Apriori and FP-growth algorithms are exactly the same.

Finally, the test results are obtained, which can be used to meet the illuminance requirement if a 40 W lamp is selected in a 12 m × 9 m classroom. Five and six fixtures can be installed in the X- and

Y-axis ranges, respectively. The entire classroom requires 30 lamps.

5. CONCLUSION

At present, lighting designers often use several urban architectural lighting and square lighting methods in designing traditional gardens and construct garden landscapes. Traditional gardens are originally peaceful, distant, and natural but become distraught, noisy, and saturated with light. Garden landscapes are consistently full of modern gardens with sound and light effects. Hence, relevant data in the overall design of the system are reviewed in this study. Then, the current status in the development of the green lighting technology of LED light source and its advantages, composition, and development overview are evaluated. The existing LED light source green lighting systems are analyzed inside and outside the country. The overall design ideas and programs are formed in combination with the current condition of landscape lighting in China. The cost-effectiveness of the green lighting energy-saving technology is investigated on the basis of the cost-effectiveness method by using LED light sources in the landscape. The method provides a theoretical basis and technical guidance for the implementation of the green lighting project. The results show that the cost-effectiveness analysis method is effective for evaluating the DSM technology. The method can also be applied to other DSM measures. Therefore, conducting a quantitative cost-effectiveness study is worthwhile to evaluate the feasibility of a certain DSM measure.

REFERENCES

1. Farahat A, Florea A, Lastra J L M, et al. Energy efficiency considerations for LED-based lighting of multipurpose outdoor environments. IEEE Journal of Emerging and Selected Topics in Power Electronics, 2015. V3, #3, pp.599–608.

2. Leccese F. Remote-control system of high efficiency and intelligent street lighting using a ZigBee network of devices and sensors. IEEE transactions on power delivery, 2013. V28, #1, pp.21–28.

3. Xu, X., Xie, L., Li, H., & Qin, L. Learning the route choice behaviour of subway passengers from AFC data. Expert Systems with Applications, 2018. #95, pp. 324–332.

4. Basker D K, Cortes O A H, Brook M A, et al. 3D Nonlinear Inscription of Complex Microcomponents (3D NSCRIPT): Printing Functional Dielectric and Metallodielectric Polymer Structures with Nonlinear Waves of Blue LED Light. Advanced Materials Technologies, 2017. V2, #5, p.1600236.

5. Haiying Li, Xian Li, Xinyue Xu, Jun Liu, Bin Ran. Modeling departure time choice of metro passengers with a smart corrected mixed logit model – A case study in Beijing. Transport Policy. 2018, #69, pp.106–121.

6. Pimputkar S, Speck J S, DenBaars S P, et al. Prospects for LED lighting. Nature photonics, 2009. V3, #4, p.180.

7. De Rossi F, Pontecorvo T, Brown T M. Characterization of photovoltaic devices for indoor light harvesting and customization of flexible dye solar cells to deliver superior efficiency under artificial lighting. Applied Energy, 2015. V156, pp.413–422.

8. Wang L, Wang X, Kohsei T, et al. Highly efficient narrow-band green and red phosphors enabling wider color-gamut LED backlight for more brilliant displays. Optics Express, 2015. V23, #22, pp.28707–28717.

Zhiqiao WANG
received his Master Degree from Wuhan University in 2012, and received his bachelor degree from Huazhong University of Science & Technology in 2004. Now, he is working as a lecturer in Yangtze University. His current research interests include digital art design, landscape design and interior design

Light & Engineering
Vol. 26, No. 3, pp. 44–50, 2018

Svetotekhnika
No. 5, 2018

APPLICATION AND DEVELOPMENT OF LED DISPLAY IN SPORTS FIELD

Jing LIU

Beihang University, Department of Physical Education, Beijing, 100191, China;
E-mail: irxcva78961171@126.com

ABSTRACT

LED screens have become a must-have for modern large-scale sports venues and are indispensable equipment for major sports events. Therefore, the application and development of LED display in the field of sports are studied. The LED dot matrix is selected as the display system of the automatic track circle system of the sports track competition. By analyzing the display principle of the display screen pair code and Chinese characters applied in the sports field, an algorithm is proposed to develop the application of the display screen in the sports field for the sports field. The application display provides a reference for character and Chinese character display. The debugging result is consistent with the expected goal, and the number of displays and the number of additions and subtractions can be realized by keyboard operation, and the remaining number of laps of the athlete is correctly displayed.

Keywords: LED display, sports field, development research

1. INTRODUCTION

After entering the 21st century, as one of the main information distribution media, the LED display industry and technology have made some progress [1]. Its use in the sports industry is to serve sports competitions. Therefore, in product research and development, it should first meet the requirements of sports competitions, and can play the role of timing scoring in sports competitions, and timely broadcast the contestants' competition results and related materials, which is the main role that LED display screens can enter the sports industry at the beginning. In addition, it has a strong rendering effect in the sports game highlight playback, real-time broadcast, background image, etc., and can create a very lively atmosphere [2]. The LED display panel is used as a display method for controlling semiconductor light emitting diodes to display a series of information such as text, graphics, images, animations, quotes, videos, etc. [3]. Compared with other terminal displays, it has the advantages of high brightness, long life cycle, large visual range, easy interface, and support software [4]. It has gradually become one of the must-have facilities for contemporary large stadiums, and the use of more LED screens in important sports is an indispensable device. The display system of the stadium should be able to display the event information clearly and correctly, and use multimedia technology to show the situation of the competition and render the atmosphere of the scene. Therefore, the paper has a very important practical value for the use and development of LED display in the sports industry.

2. STATE OF THE ART

Western exploration of LEDs is early, generally analyzing the materials, colours, and brightness of LEDs. China's more well-known enterprises include Shenzhen Ai Biesen and Huizhou Desai. Compared with Western countries, domestic research is biased. Late, it is basically the exploration of LEDs by the Chinese Academy of Sciences and some schools. However, the countries that widely use

LED displays are basically in Asia, such as China, South Korea, Japan, etc., and Europe and the United States [5]. Along with the continuous advancement of LED technology, a large number of stadiums have replaced LEDs and CRT displays with LED displays, and the displayed information has been converted from past figures into text, images, and videos [6]. The LED display of the stadium serves as the main means of game information display and live broadcast of the game. It is connected with the game's timing and scoring system, plays the player's game results and related materials, publishes sports information, and displays text animation and video images, which is one of the most important information dissemination vehicles on the scene and is the "soul" device in many facilities of the stadium [7]. In the 43rd World Table Tennis Championships held in Tianjin, China in 1995, a huge LED screen of more than 1,000 square meters is used. At the opening ceremony of the Beijing Olympic Games in 2008, the dream world created by LED and projector has already amazed the audience. At present, the high-standard stadium LED display has gradually become one of the necessary facilities, and the demand for LED screens in the stadium has been increasing. At this stage, the design technology, control technology, manufacturing process and usage level of domestic LED display screens are close to international standards, and the production cost is significantly less than that of international products [8].

3. METHODOLOGY

3.1. Gray-Scale Modulation Model Algorithm Based on LED Display in Sports Field

Generally speaking, indoor gymnasiums must have one or two LED displays installed, which can be hung on the wall. The display should be serviced by sports competitions, which can be seen by most people. It is assumed that the venues are large in scale and there are more seats in the audience. Then, it is possible to install a number of combined display screens in the central part of the venue. For example, the Wukesong Basketball Hall in Beijing uses a multi-piece combination display system. The whole system consists of a "funnel screen", a ring screen and a timing score control system. Among them, the display screen is installed in the central part of the venue weighs 22 tons. Because it looks like a funnel, it is called a "funnel screen." It is divided into five layers, with a net height of 9.042 meters and a maximum diameter of 11 meters. Generally speaking, only one LED display is installed in the outdoor venue. It is more reasonable to set it above the southern stands, facing the north, so as to prevent direct sunlight from affecting the effect. The display of the outdoor venue has high requirements for brightness. In the direct sunlight, the audience needs to see the content above. Similarly, it should have strong wind, defence, and anti-corrosion and lightning protection capabilities. The interior has good ventilation and heat dissipation. The size should be determined according to the size of the site, the space and the audience capacity. In addition, the venue is brighter and the viewing range is larger. Therefore, the specifications and brightness of the LED screen should be clearly defined according to the actual situation, which refers to Table 1 for specific settings.

Table 1. Determination of the Size of the Frame of the Stadium LED Display

Stadium audience capacity	LED display frame size
1,0000seats or less	3000mm(height)×10000mm (length)
2000~3000 seats	5000mm(height)×15000mm (length)
3000~4000 seats	7000(height)×20000mm (length)
More than 8,000 seats	8000(height)×25000mm (length)

The number of pixels of the LED display, N_{LEF}, can be calculated from the width and height of the display for:

$$N_{LEF} = N_w \times N_h . \quad (1)$$

Among them, N_w represents the width of the display screen in the model, and N_h represents the height of the display screen in the model. From the perspective of the driver chip, the number of pixels of the LED display is N_{LEF}. It can also be expressed as:

$$N_{LEF} = N_{ic} \times N_{ch} \quad (2)$$

Table 2. Proportion of Brightness Loss Within of the Reference Time

$\frac{\Delta N_{latch}}{N_{latch}}$	1	2	3	4	5
32	3.03	5.88	8.57	11.11	13.51
64	1.54	3.03	4.48	5.88	5.88
96	1.03	2.04	3.03	4.00	7.25
128	0.78	1.54	2.29	3.03	4.95
192	0.52	1.03	1.54	2.04	3.76
256	0.39	0.77	1.16	1.54	1.91

Wherein, N_{ic} represents the number of driving chips used for one channel of data, and N_{ch} represents the number of channels included in each driving chip. If the latch length is defined as N_{Iatch}, obviously:

$$N_{Iatch} = N_{ic} \times N_{ch}. \tag{3}$$

For a data link with a length of N_{Iatch}, the time required for the migration is τ_{Iatch}:

$$\tau_{Iatch} = \frac{1}{f_{clk}} \times N_{Iatch}. \tag{4}$$

In actual engineering use, there will be some idle clocks in the gap between each two shift operations. The shift gap is used for timing adjustment, which is recorded as ΔN_{Iatch}, so the time required to transfer data once is τ_0, which is expressed as:

$$\tau_0 = \frac{1}{f_{clk}}(N_{Iatch} + \Delta N_{Iatch}). \tag{5}$$

Here τ_0 is defined as the reference time of the scan, also known as a time slice, which is an important parameter based on the time slice gray modulation. It can be seen that in the case where the scan clock is constant, the reference time increases as the length of the shift increases. If the reference time is kept constant, the scan clock needs to increase as the length of the shift increases. The latch signal is a very narrow level signal, and the number of scan clocks is recorded as N_{LE}, which is a part of the middle of ΔN_{Iatch}. During the benchmark time, the bandwidth utilization and bandwidth loss rates are:

$$\begin{cases} \eta_{BL} = \dfrac{N_{latch}}{N_{latch} + \Delta N_{latch}} \times 100\% \\ \eta_{\Delta BL} = \dfrac{N_{latch}}{N_{latch} + \Delta N_{latch}} \times 100\% \end{cases}. \tag{6}$$

Table 2 shows the ratio of luminance loss in the reference time. The first behaviour is the shifting gap. The range is from 1 to 5. The first column is the shifting length. The range is from 32 to 256. The other parts are the luminance loss during the reference time. It can be seen that when the transfer length is constant, the brightness loss in the reference time increases with the increase of the transfer gap; when the transfer gap is constant, the brightness loss decreases as the transfer length increases. In practical engineering applications, the transfer gap is generally set to be adjustable, in order to obtain better bandwidth utilization, if there is no special explanation about the calculation of the transfer gap mentioned later, take $N_{Iatch} = 3$, at this time, if the transfer length is 256, the bandwidth loss rate is 1.16 % in the reference time. If the gray level of the display screen is n bit, the single primary colour image data is represented as D[(n-1):0], and each bit of data is represented as D[n-1], D[n-2], …, D[1], D[0]. During the reference time, the relationship between the stored serial data sequence D[x] and the data bits can be expressed as:

$$D[x] = \bigcup_{i=0}^{N_{LED}-1} D_i[x], (0 \le x < n). \tag{7}$$

From equation 7, when x=0, $D[0]=\{D_0[0], D_1[0],..., D_{N_{LED-1}}[0]\}$, the serial data that is sequentially transferred in a time slice is indicated.

3.2. Time Matching Algorithm

The core of the LED display is the scan clock. The scan clock is like the human blood, driving all the display logic. This section expresses the relationship between the gray parameters based on the scan clock and gray level. In order to realize the gray level modulation of the LED display screen and obtain the preferred scanning clock, according to the gray level modulation model, the gray level modulation process is divided into basic gray level modulation and extended gray level modulation, and an optimization is proposed by analyzing the relationship between the parameters. The selection method of scan clock and the concept of scan clock redundancy are summarized on the basis of this. Finally, the gray level model is verified and implemented by the hardware platform. According to the grayscale modulation model, the grayscale modulation process is divided into basic grayscale modulation and extended grayscale modulation. The basic gray level refers to the gray level generated by the reference time τ_0 as the minimum modulation period. If the refresh rate of the LED display is f_{frame}, the period of one frame of data is T_{frame}:

$$T_{frame} = \frac{1}{f_{frame}}. \tag{8}$$

The frame period includes the maximum number of time slices n_{int}:

$$n_{\text{int}} = \frac{T_{frame}}{\tau_0}. \tag{9}$$

Thus, the basic gray level number N_{int} is:

$$N_{\text{int}} = fix(\log_2 n_{\text{int}}). \tag{10}$$

Expanding the gray level means that the gray level is generated with the minimum response pulse width τ_{oe} as the minimum modulation period within the reference time τ_0. Thus, the reference time contains 20. The number is n_{fra} for:

$$n_{fra} = \frac{\tau_0}{\tau_{oe}}. \tag{11}$$

This will result in an expanded gray level number of N_{fra}:

$$N_{fra} = fix(\log_2 n_{fra}). \tag{12}$$

The LED display gray level n is a superposition of the basic gray level and the extended gray level:

$$n = N_{\text{int}} + N_{fra}. \tag{13}$$

The performance of the LED display control system is closely related to the selected driver chip. The maximum scan clock and minimum response pulse width are directly affected by the parameters of the driver chip itself. Table 3 lists the driver chip parameters of four different manufacturers. It can be seen from Table 3 that the scan clock of the driver chip is below 35 MHz. On the one hand, the excessive scan clock may exceed the limit speed of the driver chip itself, and on the other hand, the PCB layout and layout of the display module are also higher. The minimum response pulse width is above 30 ns. Too small pulse width time will cause the driver chip to not respond correctly. Therefore, the driver chip can limit the grayscale parameters to:

$$\begin{cases} \tau_{oE} \geq 30 \text{ ns} \\ f_{clk} \leq 35 \text{ MHz} \end{cases}. \tag{14}$$

The minimum response pulse width of the driver chip is the effective width at which channel can be opened under the condition that the linearity of all channel output currents can be maintained. If the given pulse width is less than the minimum response pulse width, the channel output does not respond or the response is non-linear. If the given pulse width is greater than or equal to the minimum response pulse width, the channel output can respond correctly. Due to the unevenness of the chip manufacturers, the technical specifications given by the manufacturer are also incorrect. Therefore, after selecting the driver chip, the minimum response pulse width of the driver chip must be tested, and the value used is slightly larger than the test value (5-l0) ns. It to some extent offsets the inconsistency of the chip pulse width response. The driver chip on the LED display module adopts TI's TLC59282, the serial data input is given a high level; the clock is l0MHz; the latch is a periodically changing pulse with a period of 13 ns and a high level width of 200 ns. The given response pulse width is 40 ns. These are all implemented by FPGA programming. According to the technical ma-

Table 3. Parameters of Small Driver Chip

Driver chip model	MB15024	TCL59282	SMI6126	SD16739
Minimum response pulse width, ns	70	30	30	30
Maximum scan clock, MHz	25	35	25	30

nual, τ_{oe} is 40 ns as the pre-test object, and the channel output response of 10 groups of chips is tested. The response result is up to 41.8 ns, deviating from the given pulse width of 4.5070, and other response results are greater than the given pulse width of 40 ns. This deviation is mainly caused by the chip itself and can be corrected by the late point-by-point uniform correction technique.

It is analyzed by formula (10) and formula (15) and their associated formulas. For each level of basic gray level, the number of reference time slices needs to be increased by 2 times. The methods and analysis can be taken as follows: the scan clock is doubled, but it cannot be breaking through the limitations of the drive chip itself on the clock frequency. Halving the length of the transfer or halving the number of scan lines will result in a reduction in the control range of the control system. The refresh rate is halved, which affects the visual effect. In general, the increase in the reference gray level will be limited by the performance of the device, and will also bring other performance degradation. The method and analysis that can be taken for each level of gray level expansion is as follows below. The minimum response pulse width is halved, but it cannot break the minimum time that the driver chip itself can respond. The scan clock is halved or the transfer length is doubled, which results in a halving of the basic gray level, which is of no practical significance. In the gradation modulation, after the parameters are preferably determined, the gradation control can be performed. Here, a time slice matching algorithm is adopted, that is, the time slice occupied by the high-weight data bits is split, and the low-weight data bit time slice is mixed and modulated in combination with the case that the total number of time slices is the same. In order to better understand the time slice split, when the gray modulation model parameters n=14, m=9, the latch sequence and the blanking sequence are respectively:

$$L_x = \begin{cases} 1, x < 9 \\ 2^{x-9}, x \geq 9 \end{cases} (0 \leq x < 14). \qquad (15)$$

4. RESULT ANALYSIS AND DISCUSSION

When the minimum pulse width is selected as 40 ns and the refresh rate is 600 Hz, the relationship between the gray level, the shift length, and the relationship between the scan clocks is as shown in Fig.1, in which the scan clock is changed between 1 and 30 MHz. The storage length varies between 16 and 512.

As can be seen from Fig. 1, the gray level varies between 14 bit and 15 bit, 14 bit is mostly, 15 bit is less, and the distribution is concentrated on several strips of radiation. The upper right picture shows the amplification of the low-speed clock area. It can be seen that when the transfer length is less than 200, the fluctuation of the gray level distribution fluctuates greatly. In the area above 200, the gray level changes relatively smoothly. The lower left image is an enlargement of the area with a small transfer length. The 16–64 area is selected. It can be seen that the gray level of the area changes the same as the upper left picture.

Fig. 2 is a state in which the gradation level exhibits disordered fluctuations in the low-speed clock region where the transfer length is small. During the whole modulation period, the time slice matching algorithm realizes that the LED lights up according to a certain rule, so that the LED does not appear bright or off for a long time, thereby achieving

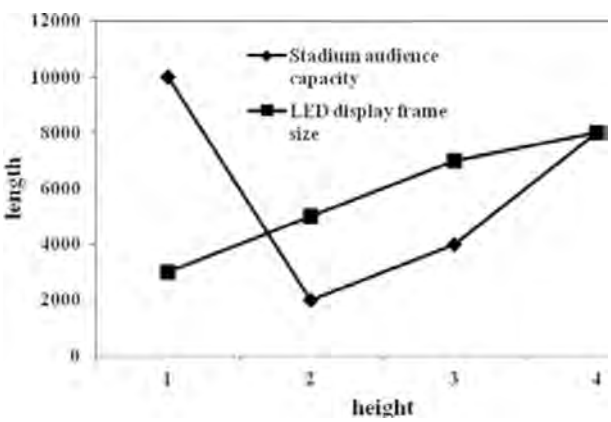

Fig.1. Determination of the size of the frame of the stadium LED display

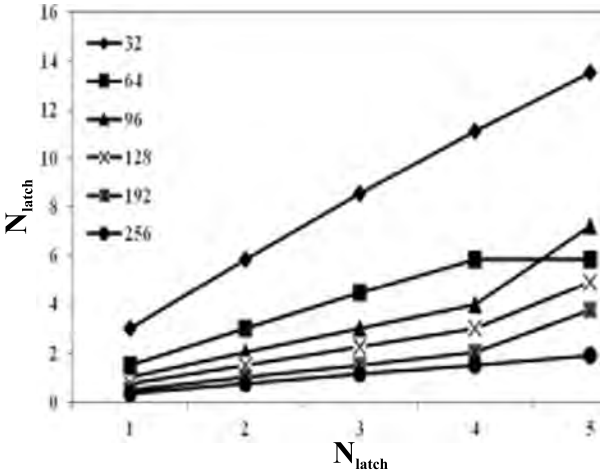

Fig.2. Proportion of brightness loss within the reference time

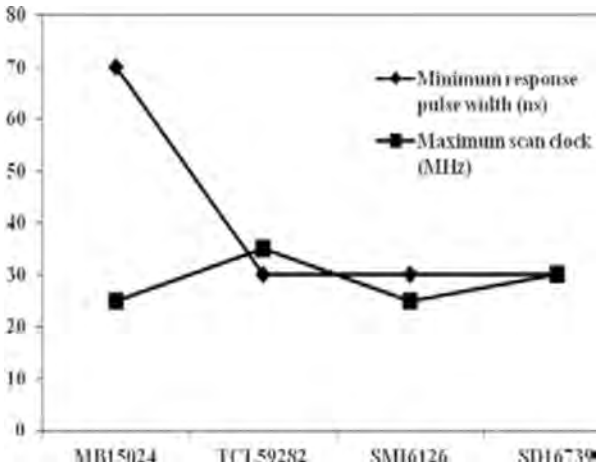

Fig.3. Parameters of small driver chip

the purpose of reducing the flickering of the display screen. In this section, based on the characteristics of LED gray-scale modulation, an evaluation strategy based on the flash frequency factor is proposed to qualitatively evaluate the flickering of the screen. This method evaluates different time slice combinations and belongs to the category of gray-scale modulation algorithms. The human eye produces a flickering effect on the rapidly changing optical signal. Since the LED is off and on, when the LED changes frequency is not fast enough, the human eye can perceive a noticeable flickering feeling. When the frequency of change is high, due to the visual inertia of the human eye, the observer will no longer feel flicker, and usually will not cause flicker, that is, the frequency at which the human eye can feel a stable picture, called the critical flicker frequency. The critical flicker frequency of the human eye is related to many factors: the brightness of the blinking picture; the higher the brightness is, the higher the critical flicker frequency is. The amplitude of the flicker: the larger the amplitude is, the more obvious the flicker is perceived by the human eye. When the amplitude is smaller than the brightness that can be resolved by the human eye, the observer will not feel the flicker. Observation time, short-term observation is not obvious to the flicker, and it is easier to feel the flicker when observed for a long time.

For the area of the image, the larger the angle of view is observed by the human eye, the higher the critical flicker frequency is; the frequency at which the LED light is on and off at the same brightness and refresh rate. With the rapid development of displays, people are increasingly demanding displays. The degree of flickering of the screen has certainly become a hot issue of concern. Fig. 3 reflects the subjective evaluation of the display effects of different types of displays under different conditions. The observation results show that when the outdoor display brightness is greater than 4000 cd/m^2, it is better to use a refresh rate above 400 Hz; when the brightness is less than 4000 cd/m^2, it is better to use a refresh rate above 240 Hz. The degree of flicker is not enough to measure by the refresh rate, because in the case of the same refresh rate, the difference in the gray-scale modulation algorithm is different. The time T occupied by arbitrarily selecting two adjacent time slices in the LED working waveform is regarded as one sub-period. Among them, the high level indicates that the LED display is lit, the time is T_1, and the low level indicates that the LED is off and the time is T_Z. There are many factors affecting the flash factor. Here are the effects of different modulation factors m, different matching parameters g and different matching combinations on the flash factor. According to the above analysis method, other parameters can be analogized, such as the influence of different gamma on the flash factor. Using the evaluation strategy of the flash frequency factor, the design parameters can be relied upon to avoid artificial subjective speculation.

5. CONCLUSION

A method for selecting the preferred gray control parameters suitable for engineering applications is provided. According to the gray modulation model, the gray level modulation is divided into basic gray level modulation and extended gray level modulation, and a preferred scan clock is given. The

selection method and the concept of scan clock redundancy are given. The maximum scan clock redundancy can be used as an indicator to judge the hardware performance of the control system. In addition, on this basis, the optimization method of LED display control parameters is summarized, which provides sufficient theoretical guidance for the design of LED display control system. A time slice matching algorithm is proposed to improve the stability of the displayed image and reduce the stroboscopic effect. After determining the optimization parameters, the optimization parameters can be used to implement the gray-scale modulation algorithm to achieve the purpose of optimizing performance. Here, through the time slice matching algorithm, the arrangement of the time slices can be relied upon to make the LEDs turn on and off more evenly, thereby achieving the purpose of reducing the flickering of the display screen. At the end of the paper, an evaluation strategy based on the flash frequency factor is also presented, which can be used to judge the results of time-scale gray-scale modulation, which provides an important basis for the update and improvement of the algorithm.

REFERENCES:

1. Ahn H A, Hong S K, Kwon O K. An Active Matrix Micro-Pixelated LED Display Driver for High Luminance Uniformity Using Resistance Mismatch Compensation Method. IEEE Transactions on Circuits and Systems II: Express Briefs, 2018. V65, #6, pp.724–728.

2. Chun J, Lee M. Developing a SEIL (Smart Enjoy Interact Light) bag utilizing LED display. International Journal of Clothing Science and Technology, 2016. V28, #2, pp.233–253.

3. Delabrida S, D'Angelo T, Oliveira R A R, et al. Wearable HUD for Ecological Field Research Applications. Mobile Networks and Applications, 2016. V21, #4, pp.677–687.

4. Bai Y, Welk G J, Nam Y H, et al. Comparison of consumer and research monitors under semistructured settings. Medicine & Science in Sports & Exercise, 2016. V48, #1, pp.151–158.

5. Ellis B J, Volk A A, Gonzalez J M, et al. The meaningful roles intervention: An evolutionary approach to reducing bullying and increasing prosocial behavior. Journal of research on adolescence, 2016. V26, #4, pp.622–637.

6. Roy R, Hebden L, Kelly B, et al. Description, measurement and evaluation of tertiary-education food environments. British Journal of Nutrition, 2016. V115, #9, pp.1598–1606.

7. Konstantinidis E I, Billis A S, Mouzakidis C A, et al. Design, implementation, and wide pilot deployment of FitForAll: an easy to use exergaming platform improving physical fitness and life quality of senior citizens. IEEE journal of biomedical and health informatics, 2016. V20, #1, pp.189–200.

8. Xu, X., Xie, L., Li, H., & Qin, L. Learning the route choice behavior of subway passengers from AFC data. Expert Systems with Applications, 2018. #95, pp. 324–332.

Jing LIU,
Master of Physical Sport Training, Lecturer. Graduated from the Northwest Normal University in 2004. Worked in BeiHang University. His research interests include Physical education and Sports training, Sports Humanity Education

Light & Engineering
Vol. 26, No. 3, pp. 51–57, 2018

Svetotekhnika
No. 5, 2018

DETECTION AND ANALYSIS OF LED DISPLAY SYSTEM IN LARGE STADIUMS

Xiaodong YI and Min ZHOU*

School of Physical Education, Sichuan University, Chengdu, Sichuan, 610065, China;
**E-mail: dhxutxo4636@126.com*

ABSTRACT

As the mainstream products of flat panel display, LED screen is becoming more and more popular, which has been widely used in the display system of large gymnasium. The detection of LED display system in large stadium is analyzed. Based on the large LED display in Jingzhou stadium, the qualification of LED display system after installation is tested. A scanning line seed filling algorithm is proposed and used to collect the gray value in the connected domain of the lamp and obtain the average gray value of the light point, so that the LED display system of the large gymnasium is detected. The experimental results show that a reasonable LED display and adjustment scheme can ensure the installation of LED display system in large gymnasium in line with the requirements of the national standard.

Keywords: stadiums and gymnasiums, LED, system testing, OSTU algorithm

1. INTRODUCTION

LED display is the latest information media tool. It has the following advantages: long life cycle, less energy consumption, large visibility range, long viewing distance, etc. [1]. At present, it has a wide range of use, for example, securities trading, finance, stations, stadiums, road traffic, airport flights, dispatching command centres, and shopping malls, advertising media and other public places. Compared with LCD, this LED display has the characteristics of low price and high brightness. And standard cell boards can be used to assemble the size of their own requirements [2]. Lighting is a key component in the construction of sports venues. The design must meet the specific needs of the venue and provide lighting conditions for recreational activities, competition activities, training activities and cleaning activities. Whether the lighting effect is good or not is directly related to the fairness of the game, the effect of broadcasting, the safety of the players and the atmosphere of the scene. However, for large scale gymnasiums, the detection of LED display system is also crucial [3]. The detection of the display system plays a very important role in the lighting. The design of the horse track for controlling the lighting equipment is closely related to the specialties of architecture, structure and electricity [4]. Because it is necessary to examine the LED display system in the design and construction of sports venues, it is necessary to understand the core technology and create a scientific display and detection system to help promote the intelligent development of the gymnasium [5]. Therefore, the detection of large LED display has a very important practical value.

2. STATE OF THE ART

In the LED production company of China, when the display system is tested, the LED display unit is opened to use the human eye to check it. However, this kind of manual detection relies on the subjectivity of the individual, and it is difficult to ensure the credibility of the test. On the other hand, the human eye may cause harmful damage to the high bright-

ness LED display panel [6]. In the west, the development of test facilities for display screen lighting units is early. However, the test target is not uniform and the facilities are expensive. For example, Japanese enterprises are testing the luminous effect of light-emitting devices. This is to ensure the unity of production and invest tens of millions of dollars to develop an automatic inspection, acquisition, correction and production line [7].

In China, Shenzhen elephant horizon Photoelectric Technology Co., Ltd. invested about six hundred thousand in developing a set of module detection system. However, its detection efficiency is not high, and is limited to internal applications only. Other manufacturers are slow in testing, but only for internal use. The rest of the manufacturers did not invest in the development of the display module's testing facilities. In September 3, 1997, China's Ministry of Electronics Industry issued the general specification for display, and has begun to practice. In May 1998, the relevant commission commissioned the Nanjing Luo Pu company to formulate the "screen display test method", which is finalized to promote the steady development of the industry [8]. The LED display test method divides the performance of the LED display, such as light and power, electricity and so on. The methods of testing are categorized. However, this method is clear after the module is assembled into LED display screen. However, the way of testing is not clearly defined. If the detection of LED display module cannot be standardized, it will be harmful to the detection of LED display unit. After the screen, the effect will also be adversely affected.

3. METHODOLOGY

3.1. Image Denoising Algorithm Based on LED Display System Detection

In the process of collecting, acquiring and transmitting images of a unit panel of LED display, the influence of the input conversion device and the surrounding environment is input. For example, the fluctuation of light intensity, the unevenness of the sensitivity of the photosensitive element, the quantization noise generated during the digitization process, the camera shake fixed on the bracket caused by the machine vibration, the fluctuation of the power supply, the shot noise introduced by the CCD device itself, etc. This makes it inevitable that the digital images acquired in the detection system contain a wide variety of noises and distortions. These noises will bring many difficulties to image processing. It has a direct impact on image segmentation, feature extraction, image recognition and other image processing operations. Therefore, real-time collection of images needs to be filtered first.

In a large number of experiments, it is found that the image captured by the camera is seriously affected by discrete impulse noise and discrete salt and pepper noise. Median filtering is a nonlinear signal processing technique that can effectively suppress salt and pepper noise. The basic principle of median filtering is to replace the gray value of a point in a digital image or a digital sequence with the median value of a point in a neighbourhood. The surrounding pixels are closer to the true value, thus eliminating the isolated noise points. The method is to use a two-dimensional sliding template with some structure to sort the pixels in the template according to the size of pixels. Two dimensional data sequences are generated monotonically (or descending). The two-dimensional median filter output is:

$$g(x,y) = med\{f(x-k, y-l), (k,l) \in w\} \qquad (1)$$

Among them, $f(x, y)$ and $g(x, y)$ are original and processed images respectively. w is a two-dimensional template. Usually 2 * 2, 3 * 3 area, generally used window. Median filtering can preserve the details of the image while removing noise. In addition, the median filter is easy to self adapt, so that its filtering performance can be further improved. Therefore, the median filtering method is adopted to remove noise, and the width of the filter window is 3 * 3 area.

3.2. OSTU Algorithm Based on Image Segmentation

Image segmentation is one of the key technologies in digital image processing and computer vision. The purpose is to separate the target from the background and provide a basis for subsequent classification and recognition. The image segmentation methods are divided into the following categories: segmentation methods based on threshold include region based segmentation, edge based segmentation, and segmentation based on specific theories.

Threshold segmentation is one of the most commonly used image segmentation methods. Scholars at home and abroad have done a lot of research and put forward a variety of methods to select ICJ values. Among these methods, the early OSTU method proposed by Otsu is most concerned. It uses an exhaustive search method to select a gray threshold so that the variance between the background and the target is the maximum. Later, Reddi and Morii did not use the original exhaustive search method, and a fast search iteration method was proposed. Because of the low signal-to-noise ratio (SNR) of image, the segmentation results of OSTU algorithm are not very satisfactory. In order to solve the above problem, Liu Jianzhuang uses the idea of two-dimensional histogram proposed by Abutaleb to select the closed value by an average gray level two-dimensional histogram, so that the segmentation effect is obviously improved. But the system needs real-time processing on the one hand, and it can directly observe the large SNR of the picture in the system. Therefore, the system adopts one-dimensional OSTU algorithm for image segmentation. The segmentation principle of the next one dimensional OSTU algorithm is first introduced. For the M * N size gray image, *f (x, y)* is the gray value of the image at the *(x, y)* point and the gray level is *L*. *p(k)* is the frequency of the gray value of *k*, and then there is:

$$p(k) = \frac{1}{M \times N} \sum_{f(i,j)=k} 1. \tag{2}$$

Assuming that the background and target of the image segmented by the gray value *T* are $\{f(i,j) \le t\} \setminus \{f(i,j) > t\}$, the proportion of the background part is:

$$\omega_0(t) = \sum_{0 \le i \le t} p(i). \tag{3}$$

The proportion of the target part:

$$\omega_1(t) = \sum_{t \le i \le L-1} p(i). \tag{4}$$

The number of points in the target part:

$$N_1(t) = MN \sum_{t \le i \le L-1} p(i). \tag{5}$$

Background mean:

$$\mu_0(t) = \sum_{0 \le i \le t} \frac{p(i)}{\omega_0(t)}. \tag{6}$$

Target mean:

$$\mu_1(t) = \sum_{t \le i \le L-1} i \frac{p(i)}{\omega_1(t)}. \tag{7}$$

Total mean:

$$\mu = \omega_0(t)\mu_0(t) + \omega_1(t)\mu_1(t). \tag{8}$$

The formula for finding the best threshold by using the largest class variance is as follows:

$$g = \arg \max_{0 \le t \le L-1} \{\omega_0(t)[\mu_0(t) - \mu^2] + \\ + \omega_1(t)[\mu_1(t) - \mu]^2\}. \tag{9}$$

After the partition threshold is determined, the definition is:

$$f(x,y) = \begin{cases} 0; f(x,y) < g \\ 255; other \end{cases}. \tag{10}$$

Thus the image segmentation is completed. As shown in Fig.1, the result of threshold segmentation for indoor model is calculated by the above method, and the best segmentation threshold is gray level.

Since the glass mirror surface of the display panel will have some particles and the glow of the display unit after the light is lit, the image edge of the two valued image will be scattered with some noise areas, such as the sharp corner of the edge of the lamp area in the lower image. The elimination of these noises is based on the introduction of morphological image processing to handle the edges of these regions. There are four basic operations in morphology: dilation, decay, candlestick opening and closing operations. When *A* and *B* are collections of *Z2*, *A* is defined as $A \oplus B$ by *B* expansion:

$$A \oplus B = \{Z \left| (\hat{B})_z \cap A \ne \otimes \right.\}. \tag{11}$$

This formula is based on the mapping of the *B* relative to its origin and the displacement of the image by *Z*. A is expanded by *B* as a set of all displacement *Z*, so that at least one element of $\hat{B}$ and *A* is overlapped. The use of pairs of rotting candles is the collection of points contained in all translations. One of the simplest uses of rotting candles is to eliminate irrelevant details from two valued images. Dilation and rotten worms are mutually ex-

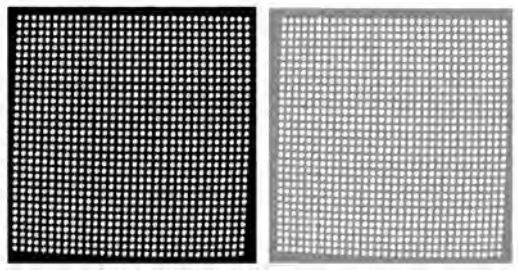

Fig.1. Images before and after threshold method segmentation

clusive for set complement operation and reflection operation.

3.3. Experimental Setup

The planning site for Jingzhou cultural and sports centre is 29.6 hectares, with a total construction area of about 33 thousand and 600 square meters. The LED large screen of the Main Gymnasium of Sports Centre is adopt two P7.62 indoor full colour LED displays, each display area is 93.352m^2. The display screen is installed on the wall of the main hall's 5-J axis and the 15-J shaft respectively, which is installed by the embedded structure of the box body. The swimming pool uses a P7.62 indoor full colour LED display with an area of 30.482m^2. The display screen is installed on the wall of the 1-F axis of the swimming pool, which is also installed with an embedded structure of the box.

The LED display system is located in the gymnasium of Jingzhou sports centre. The long axis of the site is north-south, with a fixed stand around it, and the rostrum is on the west side. A total of two LED display screens are installed on the venue, which are installed on the north and south ends of the audience auditorium, respectively, with three primary colours (full colour) LED display. According to the methods stipulated by the GB/T 29458–2012 (sports venues LED display requirements and test methods) standard, the brightness uniformity of the two sets of the three base colour LED displays of the stadiums and gymnasiums is measured respectively. The average temperature of the field environment is 29.40C, and the relative humidity is 76 %. LED full colour screen basic information is shown in Table 1.

According to the size of the display screen and the location of the display screen, the monitoring points of the display screen are set up. According to the size of the actual display screen, in order to ensure the rationality of the display system detection, the display area is divided into nine areas. And the monitoring points are set up. The maximum brightness of LED display is a basic rigid index in LED detection project. In engineering projects, first of all, luminance should meet the contract requirements. At the same time, many screen manufacturers in China are also concerned about this project goal. In the process of luminance detection, the key to luminance detection is to find the optical axis of the display screen. Because of the huge display screen of Jingzhou Sports Centre, in order to ensure a good visual effect for the audience in the field, the LED display panel with high hanging height is usually installed with a certain degree of tilt in addition to a certain height. So, finding the optical axis is the first task to test the brightness. On the other hand, it is necessary to ensure that the display screen is in a reasonable operating time range when testing the brightness of the display. Try to avoid the brightness attenuation and surface area caused by LED long time use, resulting in a decrease in brightness of the display screen.

Table 1. LED Full Colour Screen Basic Information

Size	Length	13664 mm
	Width	6832mm
Full colour screen (two sets)	type	P7.62 7.62mm LED
	Pixel spacing	7.62mm
	Pixels	17222 point /m^2
	Maintenance	Backstage maintenance
	Installation method	Wall hanging
	Supplier	***

Homogeneity refers to the combination of the intensity uniformity of the pixel, the brightness uniformity of the display module and the brightness uniformity of the module in the display screen. These three indicators play a great role in the production inspection of manufacturers. Due to the influence of environmental factors on the installation of LED display screen, the difficulty of detecting the uniformity of the whole screen is greatly increased. It is mainly because of the difficulty in measuring the light intensity of the outdoor pixels

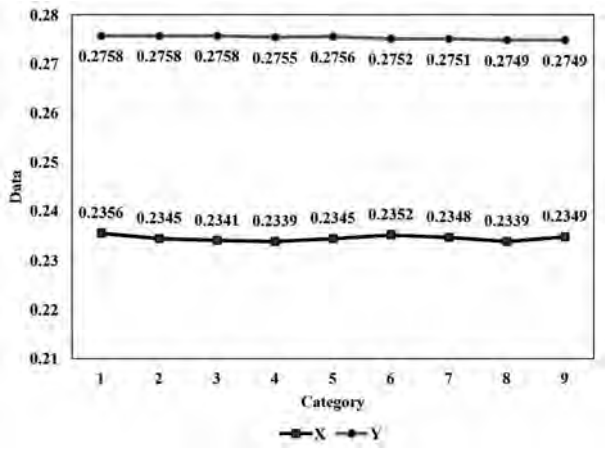

Fig.2. Results of colour coordinate detection in white field

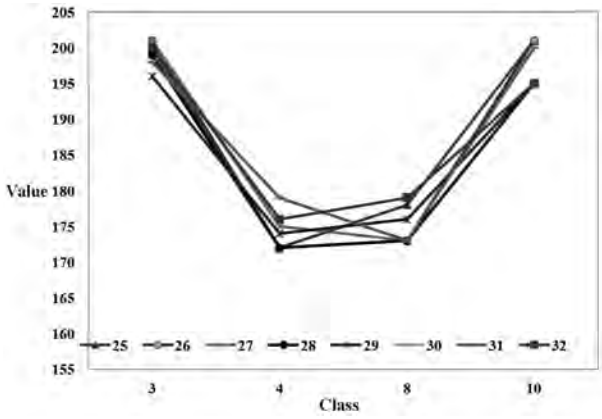

Fig.3. Gray-scale contrast between red super-light area between near area

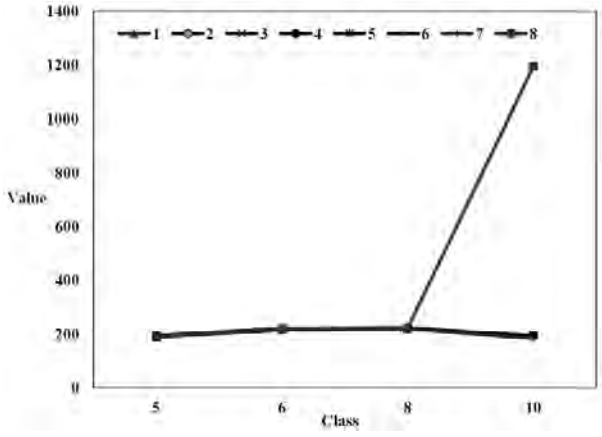

Fig.4. Gray-scale contrast between green dark-light area between near area

and the confusion of the installation definition of the display module. So the field detection is only pertinent, and it does not have the actual significance of the detection.

Contrast is an optical performance indicator of LED display detection, which mainly reflects the brightness of the display, and can also reflect the influence of the environment on the brightness of the display screen. Therefore, when measuring the brightness contrast of LED display, it is necessary to measure according to the different contents of the scene, and set up different scenes for measuring.

4. RESULT ANALYSIS AND DISCUSSION

With the improvement of the LED display control technology, the display can adjust every colour of the display in the process of use, so that the display screen is displayed in a smooth and perfect condition. According to the LED display test method, its detection technology is the white field colour of the highest gray level and the most luminance display, reflecting the brightness of the R G and the brightness of the three colours in the brightest spot. The average value of *x* coordinates of the test points is 0.2346, the minimum value is 0.2339, and the maximum value is 0.2356. The average value of *y* coordinates is 0.2754, the minimum value is 0.2749, and the maximum value is 0.2758. The *x* coordinate colour deviation is 0.001. *y* coordinate colour deviation is 0.0005.

The main luminescence of LED displays is the luminance of LED luminous tubes. At the same time, the main wavelength of the LED tube is related to the current of the LED display and the junction temperature difference of the semiconductor. The general LED luminous tube is tested at ambient temperature 25^0C and working current 20mA. Environmental changes can give a certain impact on testing, so there will be some errors in on-site inspection. The display shows the function test results as shown in the Table 2.

After on-site monitoring, the brightness, contrast, brightness uniformity, white field chromaticity coordinates, display installation position and number finger, display control, display characters of Jingzhou Sports Culture Centre super large LED information release screen system meet the relevant requirements of GB/T 29458–2012 (requirements and test methods for LED display in Gymnasium).

A problem with the cell board, when the cell board displays red, there is a super bright problem in a certain area, the light in the red frame. When the unit panel displays green, there is a dark magic problem in a certain area, such as the lights

Table 2. Display Non-Screen and Non-Functional Detection

Project	Detection result
Display position and quantity of display screen	The site is set up with two flat LED displays, which are installed on the north and south ends of the long axis of the field, and the two screens are all three base colours (full colour).More than 95 % of the audience can meet the maximum sight distance.
Display character	The two LED displays on the site can display characters or Chinese characters on the whole screen, and a small 16 dot matrix Chinese character is less than 12 lines, and the distance between lines is not less than the character 1/1D.The association can display 36 Chinese characters.
Display control	Two LED displays can display the game time and the standard clock; it can display the time of the game in real time and the result of the competition. The content of the display can be manually switched; the video display screen, the text and picture, the animation, the present live image can be automatically switched between each other and handover manually.
Maximum sight distance and character height	The top two characters of the LED display are 0.38M and the maximum sight distance 131.1m.

in the green box. A dead light appeared when the cell board showed blue. The collection is red super bright area, green dark light area and adjacent area gray value.

Red, green, and blue question lights are marked respectively. Through Figs. 2–4 and combined with fault items, workers can quickly identify problems and make timely repairs. Since the centred coordinates of each lamp area correspond to the unit plate coordinates of a lamp, the function of automatically generating the plate coordinates of the wrong lamp point in the system is also set. On the one hand, the marks in the wrong pictures can help the workers to identify the wrong pictures quickly. The unit plate coordinates of the generated error points can be used to query and confirm the error problem. Because the following problems will directly cause a single pixel anomaly, multi pixel anomaly, single light often brightens, so the following problem is considered only when designing the wrong document. The document can be used as a reference document for maintenance, and the maintenance worker can quickly finish the maintenance after accurate positioning.

5. CONCLUSION

After ten years of development, China's industry has developed to a large scale. In the process of domestic industry construction, the standardization and standardization of products have long been highly concerned. The screen test method was officially introduced last year. In spite of the specification of brightness in this document, there is no standardized facility to detect the differences in the brightness of each lamp in the display unit or by the way of personal work detection. The display unit detection system based on machine vision is introduced. In this system, the display unit pictures are taken by the camera, and each lamp in the display unit is collected by the digital image processing technology and the computer vision technology. And the lamp is determined according to the gray level criterion. The main contents are as follows:

– In order to carry out real-time and fast detection, the hardware circuit structure of real-time display and real-time shooting of display unit is designed;

– The choice of camera and lens is the most important part of the hardware device, which determines the quality of the picture taken by the camera. After comparing the parameters of each camera and lens, the camera and lens suitable for the system are selected;

– In order to reduce the noise pollution caused by the hardware and the external environment, the median filtering method is used to filter the salt and pepper noise in the pictures taken.

REFERENCES

1. Kozacki T, Chlipala M, Makowski P L. Color Fourier orthoscopic holography with laser capture and an LED display. Optics express, 2018. V26, #9, pp.12144–12158.

2. Ahn H A, Hong S K, Kwon O K. An Active Matrix Micro-Pixelated LED Display Driver for High Lu-

minance Uniformity Using Resistance Mismatch Compensation Method. IEEE Transactions on Circuits and Systems II: Express Briefs, 2018. V65, #6, pp.724–728.

3. Kim D S, Im S K, Shigeta T, et al. High resolution LED display using a new rendering method with color sub-pixel architecture. Electronic Imaging, 2016, #20, pp.1–4.

4. Xu, X., Xie, L., Li, H., & Qin, L. Learning the route choice behavior of subway passengers from AFC data. Expert Systems with Applications, 2018. #95, pp. 324–332.

5. Lv X, Loo K H, Lai Y M, et al. Energy-Saving Driver Design for Full-Color Large-Area LED Display Panel Systems. IEEE Trans. Industrial Electronics, 2014. V61, #9, pp.4665–4673.

6. Zhang K, Peng D, Lau K M, et al. 25-5: Distinguished Student Paper: Fully-Integrated Active Matrix Programmable UV and Blue Micro-LED Display System-on-Panel (SoP). SID Symposium Digest of Technical Papers. 2017. V48, #1, pp.357–361.

7. Hong Y, Lee B, Byun J, et al. 19-3: Invited Paper: Key Enabling Technology for Stretchable LED Display and Electronic System. SID Symposium Digest of Technical Papers. 2017. V48, #1, pp.253–256.

8. Ejzak G A, Dickason J, Marks J A, et al. 512$\ times $512, 100 Hz Mid-Wave Infrared LED Microdisplay System. Journal of Display Technology, 2016. V12, #10, pp.1139–1144.

Xiaodong YI,
Master of Physical Education, Lecturer, Graduated from Sichuan University in 2009, working in Sichuan University, his interest include Sports and Physical Education

Min ZHOU,
Master of Physical Education, Lecturer, Graduated from Sichuan University in 2014, working in Sichuan University, his interest include Sports and Physical Education

Light & Engineering
Vol. 26, No. 3, pp. 58–65, 2018

Svetotekhnika
No. 6, 2018, pp. 20–26

A CORRECT ILLUMINATION OF AN ESCALATOR IS A SET OF RADICAL SOLUTIONS

Leonid G. Novakovsky and Sergei A. Feofanov

PHAROS-ALEF LLC, Moscow
E-mail: pharos-alef@yandex.ru

ABSTRACT

An analysis of escalator areas illumination of the Moscow underground is given. Disadvantages of the existing illumination system are shown, and ways of their elimination are proposed using upgrading illumination devices with preservation of a "historical" image of the latter.

Keywords: light environment, psychophysiological disorders of vision perseption apparatus, escalator inclination, operation and emergency illumination

1. INTRODUCTION

Illumination of the Moscow underground station space, being most complex system ensuring safety of transportations and maintenance of the railways and all infrastructures with elements of cultural heritage, is a very specific problem, which solution is more similar to museum illumination.

As these objects are a part of the general architectural project, their illumination should be implemented within the context of solving the problem for the whole system as a dual formation. The first subsystem is "external environment – entrance hall – escalator – central hall –platform – car", and its exposure element is a passenger. The second subsystem is "platform – tunnel" and its exposure element is a train driver, Fig.1.

Here we deal with the first subsystem, in which among the station areas requiring illumination alignment the most contradictory elements are escalators, as shows analysis. It is going on because illuminance at the passengers faces changes repeatedly for a short time interval, for example, more than threefold. Besides, one should notice that such illumination, when all elements of the system are identical by illuminance, is ideal. As *PHAROS-ALEF LLC* studies together with representatives of escalator service and with power supply service of Moscow underground showed, the situation is complicated by imperfection of the existing principle of the escalator inclination illumination, which does not allow reaching modern illuminance standards predetermined by the requirements [1].

Respectively, due to features of the traditional illumination devices (ID) structures installed on escalators, a principled revision of illumination approach of this station area is necessary.

A complexity of solving this problem is aggravated by the fact that design of escalator luminaries are different and most of them requires a change of the diffuser structure, and in doing so, one should not change their appearance, otherwise, should not distort a "historical" image of the stations.

Implementation of emergency illumination using light emitting diodes isn't less important, but this requires special developments.

And finally, a support of psychological comfort determined by colour temperature of light environment is necessary: this parameter of light sources should be changed from (3700–4200) *K* in the morning to (2800–3200) *K* in the evening (i.e. taking into account the human circadian cycles).

Solution of all specified problems should be implemented along with power consumption decrease, which was a very difficult technological problem

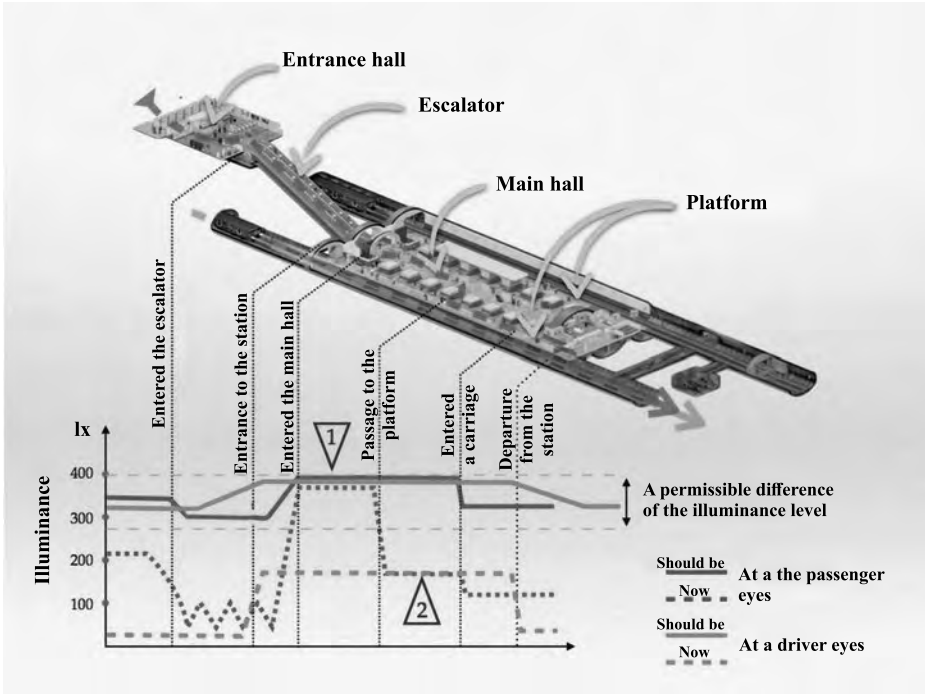

Fig. 1. Layout of illuminance distribution over a station space

until recently. Emergence and quick development of powerful LED light sources allows the successful overcoming obstacles on this way and solving some other problems of illumination upgrade. One of these problems, for example, alignment of illuminance in tunnels, on platforms, and at central halls is already solved based on adaptive IDs of the rolling stock [2], which were developed by PHAROS-ALEF LLC and tested at the Moscow underground.

It is clear that the proposed underground illumination upgrade should be provided with a minimum range of as much as possible unified IDs and light sources taking into account features of their service maintenance.

This work is dedicated namely to solving all above listed illumination upgrade problems at the Moscow underground.

2. AN ANALYSIS OF THE LIGHT ENVIRONMENT STATE IN ESCALATOR AND PRE-ESCALATOR AREAS OF THE MOSCOW UNDERGROUND STATIONS

As it was already noticed, a specific position in the underground illumination is held by escalators. It is specific, because illumination of this area practically adapts a passenger either for visual work in the street, or for underground light environment (halls, platforms, etc.). For this reason, considerable differences in illuminance are not desirable for passenger eyes. So, they are not allowed [1]. However, the real situation obviously contradicts this limitation. As the measurements show (Table 1), illuminance on steps and passenger eyes while escalator driving is different at different stations depending on the using ID structure, on their location, on ceiling type, on the vault inclination, and, which is most important, the illuminance does not meet the adopt standards anywhere. So, maximum illuminance at a passenger's eyes (324 lx) is at Baumanskaya station, and minimum (10 lx) is at Kievskaya radial; maximum illuminance on a step (169 lx) is at Baumanskaya, and minimum (4 lx) is at Sportivnaya station.

On one escalator with traditional ID structures, (floor lamps with spherical diffusers), the illuminance fluctuates from 340 lx to 186 lx when moving downwards and from 160 lx to 312 lx when moving upwards, i.e. illuminance at passengers' eyes changes more than 1.7 and 1.95 times respectively when passing one ID. And when using floor lamps with semi-spherical diffuser IDs, it changes from 44 lx to 14 lx when moving downwards and from 53 lx to 19 lx when moving upwards (the changes are 3.1 and 2.7 times respectively). These changes are very much, whereas they should be no more than 1.5 [1], and each such change happens during five seconds

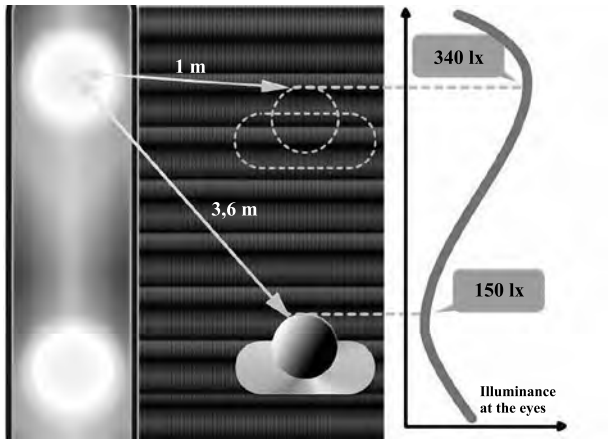

Fig. 2. Layout of illuminance change at passengers' eyes when escalator moving

Fig. 3. Arrangement of escalator area illumination at Sretensky Boulevard station

and total number of the changes for one escalator descent or ascent reaches 15–18.

Similar results were also obtained at escalators using IDs with other types of diffusers: matte long cylindrical, matte short cylindrical and transparent cylindrical. A reason of such illumination changes is in an essential change of the distance between an ID and a passenger when moving along with an escalator. A scheme of illuminance change at a passenger eyes when moving along with an escalator is shown in Fig. 2.

Besides, within a normalised area, (an escalator at the step level should have illuminance no less than 100 lx [1]), the measured illuminance practically at all stations was lower than the standard.

It was also dependent on the following:

– On the distance to the IDs (for example, at VDNKH station it was from 15 lx to 58 lx);

– On the ID types used (for example, when using IDs with spherical diffusers at Elektrozavodskaya station it was from 18 lx to 63 lx, and

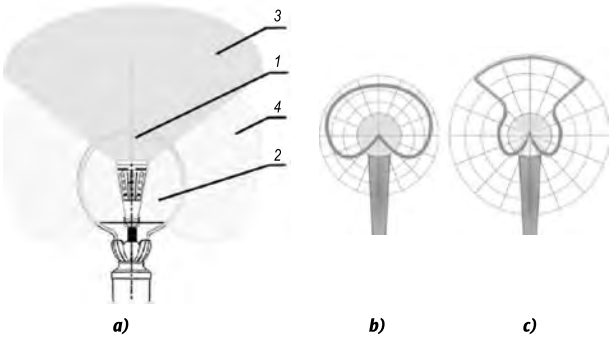

Fig. 4. Escalator standing lamp:
a – a proposed structure; *b* – radiation indicatrix for traditional implementation, *c* – radiation indicatrix for implementation of the proposed structure

when using IDs with semi-spherical diffusers at Sportivnaya it was from 10 lx to 28 lx;

– On power of the light sources (for example, for IDs with the same diffuser at Marksistskaya it was from 17 lx to 78 lx, and at Pushkinskaya – from 51lx to 130 lx).

3. A CORRECT ESCALATOR ILLUMINATION IS A SET OF RADICAL SOLUTIONS

3.1. A Basic Technological Solution of Escalator Illumination

A desire to reduce illuminance changes led to development of a new principle of escalator illumination and of the structures implementing it at Sretensky Boulevard, Mehzdunarodnaya and Spartak stations.

In these versions, illumination in a reference area is made by radiation of an ID installed on the balustrade re-reflected from of the vault surface inclination, which excludes its of ID direct radiation into passengers' eyes.

By the light distribution nature, balustrade IDs (luminaires) installed at Sretensky Boulevard station (Fig.3) met the requirements [1]. This meeting is not complete, because relation of luminous fluxes in the top and lower hemispheres is not the best. The calculations show that to provide the standard illuminance, ID luminous flux towards the ceiling in this case should be not less than 5000 lm.

An analytical simulation and practical implementation of such a "balustrade" illumination confirm a possibility to solve the set problems but requires new IDs, which are not suitable to be used at old stations because of their stylistic features.

Nevertheless, it turns out possible to solve this problem using all permissible ID versions of an escalator balustrade without changing their historical image [3, 4]. So, in the most widespread escalator ID versions of the first stations of Moscow underground made as floor lamps with spherical diffusers (Fig. 4), top and lower parts of diffusers should have different transmission factors, lower parts should have a small, and top parts should have a big transmission factor. Such diffusers should have two areas, one of which (area *1)* should be almost transparent (with a big transmission factor), and the second one (area *2*) should be matte (with a small transmission factor). In doing so, the light source should direct most part of luminous flux *3* to area *1* illuminating the escalator inclination vault with a minimum attenuation and forming a necessary illuminance on the escalator steps using the reflected light. In this case, a part of luminous flux *4* (5–6 times lesser) should be directed to the diffuser area *2*. As a result, with a switched on ID, the diffuser looks like an entirely luminous body.

Wherein dazzle of the passengers is completely eliminated as most part of luminous flux is limited by a cone, which generators are always located out of passenger eyes (Fig. 5) passing the IDs, and illuminance distribution along the balustrade vault ceiling is uniform enough and comfortable for the perception.

A visualisation of illuminance distribution (Fig. 6) shows that stripes created by the IDs will not be sighted within the visual field.

As it was already noticed, luminous flux reflected from the escalator vault ceiling creates a sufficient illuminance on the escalator steps without visual discomfort (due to the created illuminance of (350–400) lx as it is in the station and in the entrance halls). Absolute illuminance values and their distribution in operation illumination mode were calculated according to the DiaLUX program with use of a specially developed LED lamp, which appearance and technical specifications are given in Fig. 7 and in Table 2.

In the case, when traditional escalators IDs have other structure, such technological solutions are also implemented without special problems (Fig. 8).

3.2. Emergency Illumination

A specific position in the station escalator area illumination system of the underground is held by emergency illumination, requirements to which assume ID operation based on alternate and direct current in voltage intervals of (60–160) V and 127 V ± 10 %.

In this case, standard illuminance on the escalator steps should be not less than 10 lx.

It is clear, that solution of this problem requires use of a special equipment to control and connect IDs to operation and emergency circuits.

Fig. 5. A proposed illumination layout of an escalator: visualisation of escalator inclination illumination principle

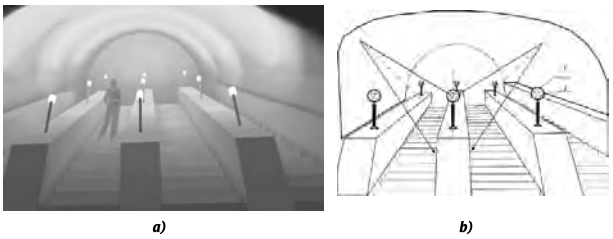

Fig. 6. Illuminance distribution on an escalator balustrade vault:
a – visualisation of illuminance on the vault, *b* – ray path

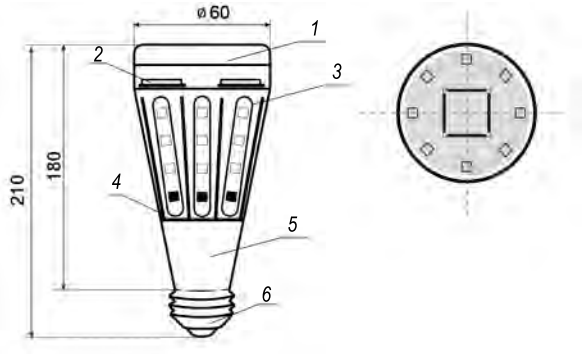

Fig. 7. Appearance of a LED lamp for general and emergency illumination of escalator inclinations:
1 – matte diffuser, *2* – matrix of the main illumination, *3* – line of diffuser decorative illumination, *4* and *5* – case, *6* – socle *E27*

Table 1

№	Station	Light device type		Illuminance, lx												
				Steps (standard: 100 lx at any point)							Passenger eye level				
				At the edge (on the left)		At the centre		At the edge (on the right)			Vertical			Horizontal	
				Min.	Max	Min	Max	Min	Max	$E_{max}/E_{min} \leq 1,5$	Min	Max	Relation	Min	Max
1	2	3	4	5	6	7	8	9	10	11	12	13	14	15	16
1	Prospekt Mira-ring		Up Down	26 26	33 33	54 30	40 48	23 23	35 28	2,35 2,08	53 50	80 96	1,5 1,92	52 50	92 76
2	Dinamo		Up Down	20 18	21 52	23 33	34 78	24 19	35 50	1,75 4,3	37 40	140 230	3,78 5,75	45 40	130 105
3	Belorusskaya		Up Down	27 41	34 58	36 64	38 84	27 65	29 70	1,4 2,04	50 190	69 210	1,38 1,1	45 90	42 78
4	VDNKH		Up Down	27 25	43 32	40 37	58 74	15 28	24 33	3,86 2,96	44 37	60 100	1,36 2,7	69 67	95 115
5	Baumanskaya		Down	99 90	120 110	132 120	169 158	87 86	110 105	1,94 1,83	160 186	312 324	1,9 1,74	208 170	363 346
6	Electrozavodskaya		Up Down	33 30	43 44	39 40	63 70	18 23	33 31	3,5 3,04	50 70	134 124	2,68 1,77	76 70	120 115
7	Alekseevskaya		Up Down	21 17	36 26	20 21	22 23	15 17	17 18	2,4 1,52	47 50	85 85	1,8 1,7	45 42	59 60
8	Universitet		Up Down	34 20	40 30	14 22	20 30	12 19	15 33	3,3 1,73	33 49	60 112	1,8 2,28	41 35	52 65
9	Komsomolskaya-radial		Up Down	40 35	57 40	34 35	38 40	36 32	52 34	1,6 1,25	78 89	131 121	1,7 1,35	82 84	126 110
10	Komsomolskaya-ring		Up Down	21 12	22 30	19 17	24 34	22 15	37 25	1,94 2,0	66 73	133 142	2,01 1,94	45 55	126 103
11	Kievskaya-radial.		Up Down	9 8	17 15	13 8	22 15	10 8	15 10	2,44 1,88	20 10	46 23	2,3 2,3	26 26	45 32
12	Prospekt Mira-radial	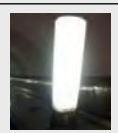	Up Down	76 64	83 90	83 85	96 97	86 72	110 77	1,45 1,51	160 210	230 280	1,43 1,3	181 186	210 206
13	Semyonovskaya		Up Down	52 35	60 60	52 52	74 87	33 44	77 62	2,49 2,48	80 95	243 216	3,03 2.27	105 92	160 183
14	Sportivnaya		Up Down	10 4	19 15	18 19	28 26	11 11	21 16	2,8 6,5	19 14	53 44	2,7 3.1	16 19	31 47

1	2	3	4	5	6	7	8	9	10	11	12	13	14	15	16
15	Vorobyovy Gory		Up Down	10 11	19 15	18 19	28 26	11 11	21 16	2,8 2,36	19 14	53 44	2,78 3,14	16 19	31 47
16	Cherkizovskaya		Up Down	4530	83 50	34 42	83 110	30 50	70 101	2,77 3,67	95 113	309 551	3,25 4,88	126 110	420 432
17	Kievskaya-ring		Up Down	9 9	11 12	13 13	15 15	9 9	11 11	1,6 1,6	27 30	33 45	1,2 1,5	16 20	17 27
18	Tverskaya		Up Down	78 58	109 62	76 70	106 110	63 45	70 85	1,68 2,4	95 140	240 270	2,5 1,93	150 120	179 195
19	Mayakovskaya (the short escalator)	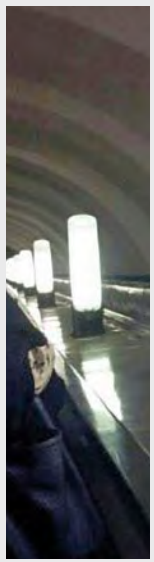	Up Down	18 17	26 21	34 26	53 35	27 20	48 22	2,9 2,05	46 41	115 105	2,5 2,56	39 49	103 67
20	Mayakovskaya (the long escalator)		Up Down	22 36	32 64	27 61	35 93	28 28	42 43	1,9 3,3	44 65	63 125	1,43 1,9	62 63	82 159
21	Pushkinskaya		Up Down	51 65	73 105	80 85	116 160	85 76	130 127	2,55 1,88	130 171	400 390	3,07 2,28	137 132	319 251
22	Marksistskaya		Up Down	17 23	60 45	18 26	66 41	13 22	78 25	6,0 2,04	41 47	230 125	5,61 2,66	37 32	138 60
23	Okhotny Ryad		Up Down	52 13	85 20	43 24	76 50	35 23	60 51	2,4 3,9	45 67	161 261	3,57 3,9	60 79	180 148
24	Kitay-gorod		Up Down	54 81	58 104	76 100	104 152	79 66	105 115	1,94 2,3	145 153	210 235	1,44 1,53	149 107	167 185
25	Lubyanka		Up Down	36 57	42 98	51 54	78 88	37 60	78 113	2,16 2,1	85 137	279 310	3,28 2,26	121 117	239 216
26	Sukharevskaya		Up Down	38 27	82 75	48 77	79 143	31 52	45 109	2,64 5,3	114 121	404 369	3,54 3,05	108 100	178 200
27	Belyaevo		Up Down	11 11	27 15	31 13	42 31	35 15	49 39	4,4 3,54	49 63	231 157	4,7 2,49	53 33	77 73
28	Sretensky Bulvar	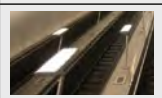	Up Down	35 27	43 30	36 32	47 52	32 40	38 48	1,46 1,92	45 59	61 70	1,35 1,18	90 95	115 110
29	Spartak	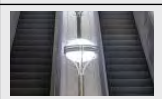	Up Down	19 29	26 50	24 65	61 123	17 19	50 51	3,5 6,4	54 60	94 114	1,74 1,9	52 84	92 170
30	Mezhdunarodnaya		Up Down	52 50	90 91	75 63	93 115	76 84	95 109	1,82 2,3	41 94	67 200	1,63 2,13	50 107	85 214

(**Red** – does not meet the standards, black – normal, **blue** – not normalised)

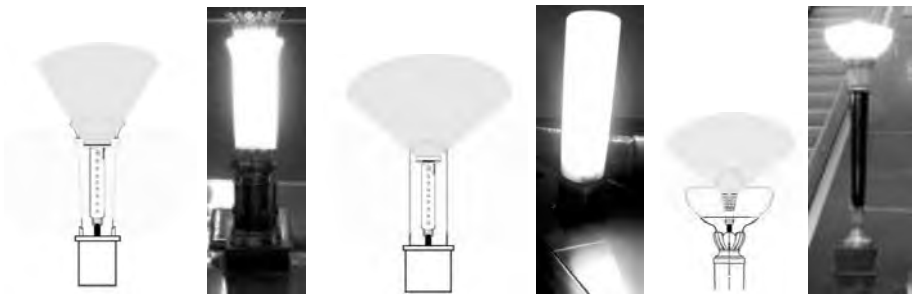

Fig. 8. Layout of a special LED lamp operation in structural versions of traditional escalator luminaires in the operation illumination mode:
a – with a matte diffuser closed from top, *b* – with a matte diffuser opened from top, *c* –with a semi-spherical diffuser

Functioning of such IDs with light emitting diodes in illumination operation mode assumes a shared use of areas *1* and *2* of the diffusers and lamps (Fig. 4 and 8), and illumination emergency mode supposes use of area *2* only.

Fig. 9 shows illuminance distribution on escalator steps in emergency mode according to the proposed solution. It is clear from the figure that the solution provides a comfortable illuminance for passenger evacuation and for recovery work, which is six times higher than the current limit [1].

3.3. Designation of an Escalator Moving Part Dimensions

Modern requirements to safety demand a designation of escalator moving part. Today this requirement in some cases is implemented using installation of a blue LED stripe, which use is inadmissible by medical parameters [5] and is forbidden due to fulfilment form [1]. For example, such a stripe is installed at the ring station Prospect Mira.

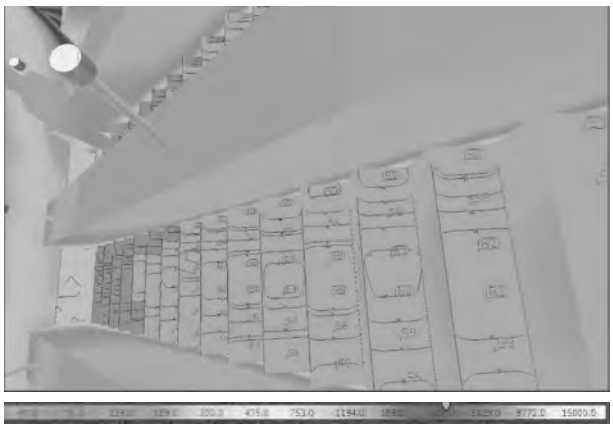

Fig. 9. Illuminance distribution (lx) on an escalator step in the emergency illumination mode

To eliminate the negative effect, replacement of the radiation colour with the correspondent green LED stripe in a diffusing shell can be used.

3.4. Adaptive Illumination of Escalators

The general trend of developing illumination systems is adaptation of the formed light environment towards psychophysiological functions of a person. So, in view of the light sources development level, construction of such systems changing ID colour temperature depending on day time, i.e. of the systems, which take into consideration psychophysiological state of a passenger, is possible already today.

Such a system can be implemented based on LED matrices with a variable correlated colour temperature (Fig. 10).

4. DEVELOPMENT OF THE REGULATORY BASE

An analysis of the stated in paragraph 3 shows that today, there is a technological basis to upgrade illumination of all areas of underground station space including escalators. However, its implementation is impossible without development of the correspondent standards taking into consideration not only the labour protection requirements of the underground personnel but also the passengers' protection requirements. And it is obvious that the set of the controlled lighting parameters should be considerably expanded in this regard. For example, along with escalator step illuminance, this set should include illuminance at the passengers' eyes.

Besides, it is advisable to exclude eye contact with direct radiation of an observer not only from LED light sources but also from fluorescent lamps,

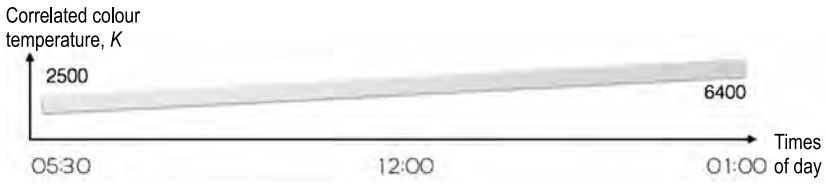

Fig. 10. Time change of correlated colour temperature T_{cc} of LED lamps for adaptive illumination systems

which, due to the luminous flux ripple, are much more harmful than LED light sources. And there are many such reasons and recommendations concerning comfort of the passengers.

5. CONCLUSION

• The presented materials confirm a possibility to upgrade illumination of all areas of the station space, including escalators based on the existing technology facilities.

• Illumination upgrade of the escalator areas requires a revision of the light environment formation methods.

• The proposed escalator space illumination version and the correspondent structural solution allow preserving historical image of the used IDs.

• The modernisation work of the specified illumination requires a revision of sanitary standards and of service regulations of the underground.

REFERENCES

1. Sanitary regulations of underground operation СП 2.5.1337–03. Sanitary and epidemiologic rules (according to the Resolution of the Chief state health officer of the Russian Federation of 4/30/2010 #50).

2. Novakovsky L.G. Illumination of the rolling stock is a key problem of forming light environment of the underground // Svetotekhnika, 2011, #4, pp. 8–14, 16–21.

3. Novakovsky L.G., Kazovsky N.I., Kanevsky A.V., Peselis Yu. A. A luminaire of underground escalator balustrade // Application for PM #2017107716, 3/9/2017.

4. Novakovsky L.G., Miras Jan-Pierre, Allash E.H. A light device to form light beam / Invention Patent #159921. 2016. Bulletin #5.

5. Kaptsov V.A., Deynego V.N. Blue light of light emitting diodes is a new hygienic problem // Analysis of risk for health, 2016, #1(13), pp. 15–25.

Leonid G. Novakovsky,
Ph.D. He is graduated from the MAMI in 1969, Director of PHAROS-ALEF LLC at present

Sergei A. Feofanov,
Ph.D. He is graduated from the MADI in 2005 and Senior research associate at PHAROS-ALEF LLC at present

Light & Engineering
Vol. 26, No. 3, pp. 66–73, 2018

Svetotekhnika
No. 5, 2018

EVALUATION MODEL OF LIGHTING ENVIRONMENT FOR SUBWAY STATION SPACE BASED ON BACK-PROPAGATION NEURAL NETWORK

Wenhao DUN

School of Civil Engineering & Architecture of Wuhan University of Technology / Hubei Institute of Fine Arts, 430000, Wuhan, Hubei, China;
E-mail: 26978991@qq.com

ABSTRACT

BP neural network is a new computer technology, which has natural advantages in the study of lighting environment evaluation model of subway station space. With the implementation of energy conservation and emission reduction, how to establish a suitable calculation model for the lighting environment of subway station space is also a hot research field. Firstly, the development trend of subway and the research status at home and abroad is introduced, then the specific application method of BP neural network is expounded, the evaluation criteria and evaluation model of space lighting environment of subway station is established. BP neural network is used to establish the corresponding mathematical model, through the weight calculation, the appropriate evaluation system is established, and finally the model is used to verify it.

Keywords: BP neural network, subway station, lighting environment evaluation, intelligent algorithm

1. INTRODUCTION

The development of the subway is a far-reaching theme, Nowadays, the comfort and convenience of travel is emphasized in the whole world, and the interior lighting environment design of metro also plays an important role in the overall comfort design and development of metro [1]. At present, China's metro is mostly imported or jointly developed from other countries in the interior lighting environment design of trains, foreign lighting design is mainly used, and the lighting reference value and evaluation basis conforming to China's national visual environment are lacking [2]. At that same time, the design only bases on meet physical parameters such as illuminance and the like in lighting design, lacks subjective feel evaluation on the visual environment of the high-speed train's passengers. In particular to the visual psychology scale of "visual brightness", " visual illuminance", " visual concentration point" that sort of things [3]. There is a lack of reasonable consideration on the colour temperature of the light source of subway indoor lighting, only using the evaluation method which accords with the colour temperature feeling of foreign passengers. The problems of high physical il-

Fig.1. Lighting environment of a subway station

lumination and poor actual illumination effect exist in the structural design, installation mode and spatial scale of the lamp, in particular, the problem of the space installation scale of the indirect lighting device leads to the problems of large brightness contrast of the light source, uncomfortable glare and so on [4]. Therefore, the research of this paper has important practical significance to solve the problem of interior lighting environment design of subway in China. At the same time, the research on this aspect can provide a reference for designers, which has a strong practical significance [5].

2. START OF THE ART

BP neural network is an artificial intelligence algorithm, at the beginning of the 20th century, people studied the layout and structure of the animal brain, found that the brain is made up of a large number of neurons connected to each other. Complex non-linear information can be processed in parallel in such systems, known as neural networks [6]. Through the simulation and reference of animal neural network, scientists put forward the concept of artificial neural network [7]. The essence of artificial neural network is an algorithm model, like animal brain, artificial neural network is composed of a large number of artificial neurons [8]. The structure and function of these artificial neurons are very simple, but they can be connected to each other and form a network to achieve very powerful functions [9]. Artificial neural network can learn independently, self – perfect, and process complex nonlinear information in parallel. It has a very broad application prospect in solving complex problems such as thinking, reasoning and consciousness [10]. Therefore, it is of great significance to use BP neural network algorithm to study the evaluation model of lighting environment in subway station space.

3. METHODOLOGY

3.1. Evaluation Criteria for Spatial Lighting Environment of Subway Stations

The evaluation of space lighting environment of subway station under fluorescent lighting is mainly based on the function of lighting. The main purpose of the lighting is to meet the physical characteristics of the light environment required by space users to accurately identify the surrounding environment and the route to the subway station space. And LED has the characteristics of high light efficiency, long life, adjustable light, which is applied to the lighting environment created by subway station space lighting. Besides meeting the functional requirements, its energy-saving characteristics are more prominent. Therefore, in order to study the evaluation system suitable for subway station space lighting environment, it is necessary to combine the characteristics of lighting function and energy saving to conduct in-depth study, the theoretical model of spatial lighting environment evaluation system for metro station is constructed. The weight of each index in the model is solved by particle swarm optimization, and the advantages and disadvantages of lighting environment under two kinds of light sources are obtained from the model and field investigation. A subway station lighting environment is shown in Fig. 1.

3.2. Subway Station Spatial Lighting Environment Evaluation Model

The evaluation index of space lighting environment of subway station mainly includes two kinds of indexes: functional index and energy-saving index, among which the functional index is divided into two categories: light environment and space environment. The light environment factors include illuminance level, illuminance uniformity, luminance distribution, glare index, colour temperature, colour rendering index, illumination induction, recognition, etc. Lighting energy saving includes lighting power density (LPD) value, energy saving lamps and lanterns, new energy utilization. The evaluation index system for evaluating the spatial lighting environment of the subway station is obtained after three rounds of expert consultation by using the Delphi method, in which a total of 16 indicators are included: illuminance level, illuminance uniformity, luminance level, luminance distribution, glare, colour temperature, colour rendering, illumination induction, recognition, stereoscopic impression, environmental coordination, illumination artistry, control strategy, control mode, LPD, energy-saving lamps and lanterns, The analytic hierarchy process is used to decompose a complex decision-making problem into several interrelated levels. The hierarchical structure diagram of spatial lighting environment evaluation of metro station is shown in Fig. 2.

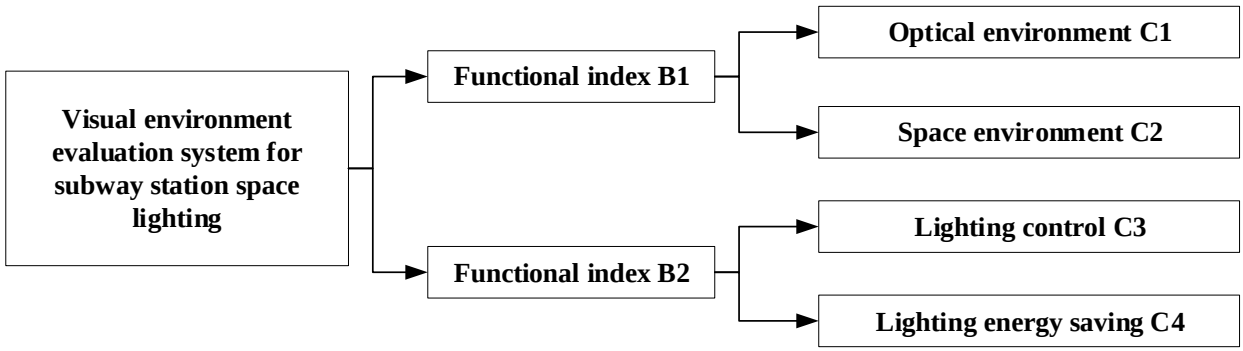

Fig.2. Hierarchical structure of subway station space visual environmental assessment

3.3. BP Neural Network Model

The interconnections between artificial neurons form is a directed graph, and the structural diagram of artificial neurons is shown in Fig. 3.

The corresponding real number for each connection is referred to as the connection weight; the set of weights may be considered as long-term memory. There are two main types of connection weights, excitation and suppression, positive connection weights for excitation and negative connection weights for suppression. The connection of weights is the feature description of artificial neural network. At time *t*, the corresponding value of the artificial neuron is called the state of the artificial neuron, also called the excitation value of the artificial neuron, if a certain artificial neuron is represented by u_j, then its state is represented by *x*, and *X(t)* represents a set of neuronal states of a certain amount. State set can be expressed by continuous function or discrete function. It can be bounded function or unbounded function. This set may have solution in some real field or finite solution. In practical applications, generally take two values, with 0 and 1, or – 1 and 1 to represent two states, there are some cases need to take the value in the continuous real number. Information is passed through each neuron to obtain an output signal, which is passed through the connection weights to the other connected neurons. The output signal value depends on the state of the neuron. This interaction is a function of the output transformation from function f_j to the neuron u_j.

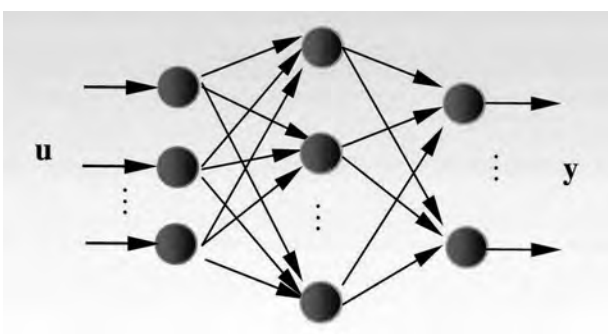

Fig.3. BP neuron structure diagram

The calculation formula of nerve source is presented in equation 1.

$$Z_j(t) = f_j(x_j(t)), \tag{1}$$

where $Z_j(t)$ represents the output signal of the neuron u_j, and *f* represents a component function.

By grouping artificial neurons in this layer, and taking each neuron group as a whole, the batch control of artificial neurons is realized, and the network operation speed is accelerated. For example, the use of lateral inhibition mechanism to make some artificial neurons in a state of no output, and can have the largest output in the layer of artificial neurons selected.

An interconnected network can connect any two artificial neurons. Belonging to this kind of network is Hopfield network and Boltzmann machine. In networks without feedback, the signal processing function stops as the signal passes through the artificial neuron. Starting from the initial state, the signal will change several times, and finally achieve dynamic balance, the structure and characteristics of the network is different, and finally the reached state is not the same.

The reasonable determination of the weight is the premise of correct evaluation. After determining the comprehensive evaluation index of spatial lighting visual environment of subway station, the weight of each index becomes an important part of the evaluation system research, and its accuracy is more related to the correctness and scientific character of the final evaluation results. Based on this,

Table 1. Classification Scale for Comparison of Evaluation Indicators

Scale value	Relative comparison	Scale value	Relative comparison
1	A is as important as B	1	A is as important as B
3	A is more important than B tip	1/3	A is a little less important than B
5	A is more important than B	1/5	A is not B important
7	A is much more important than B	1/7	A is much less important than B
9	A is more important than B	1/9	A is far from B

we intend to use analytic hierarchy process to build hierarchical structure, establish the initial judgment matrix, use particle swarm optimization to solve the index weight, establish the urban subway station spatial lighting environment evaluation system model. The calculation flow is shown in Fig. 4.

Analytic hierarchy process is an effective method to determine the weight vector, when calculating weights by analytic hierarchy process. The function $f(x,y)$ represents the importance scale for the ratio of x to y in general. If $f(x,y)>1$, x is more important than y, otherwise y is more important than x. Table 1 shows the scale values of grade division for comparison of evaluation indicators.

In the current application, the judgment matrix given by the scale of 1–9 is difficult to achieve consistency, so that the judgment matrix is inconsistent with the actual judgment thinking, the calculation distortion of the relative weight is caused. This is also the current multi-decision-making problems need to be solved and challenges. Through the study of the initial judgment matrix, in order to check the consistency of the initial judgment matrix, get a reasonable weight vector, we need to build a proper consistency correction model, and use intelligent algorithm to optimize the solution, quickly get the judgment matrix and the corresponding weight vector can pass the consistency check. The obtained judgment matrix is fed back to the experts to evaluate whether the modified matrix is within an acceptable range in practice and whether a group of weight vectors obtained by solving the nonlinear model can be used as the weight of each evaluation index required to solve the practical problem. If the expert opinion is positive, the modified judgment matrix is acceptable; On the other hand, the parameters need to be reset and solved, again to verify, until recognized by the experts.

The calculation formula of the objective function is shown in equation 2.

$$\min Y = \sum_{i=1}^{n}\sum_{j=1}^{n}[\lambda_1(x_{ij}-a_{ij})^2 + \lambda_2(x_{ij}-\omega)^2], \quad (2)$$

where λ is the weight value, a is the weight matrix and y is the target function value. The smaller y in the objective function is, the better it is. It shows that the adjusted amplitude is relatively small and the modified matrix quality is higher when the consistency condition is satisfied. Wherein λ_1 and λ_2 are weight factors, and the assignment is mainly determined according to the specific requirements in practice, on the one hand, the compliance degree of the expert judgment matrix, on the other hand,

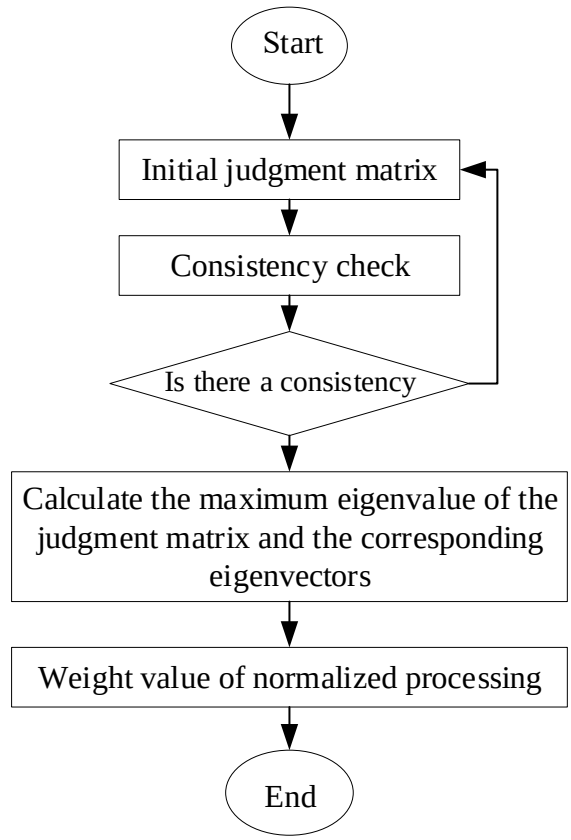

Fig.4. Index weight calculation process

Table 2. Visual Environmental Assessment System of Subway Station Space

Standard layer B	Index layer C	Evaluation index D	Index weight
Functional index B1	Optical environment Cl	Illuminance level D1	0.0901
		Illumination uniformity D2	0.0729
		Luminance level D3	0.1015
		Luminance distribution D4	0.1184
		Glare D5	0.0620
		Colour temperature D6	0.0881
		Chromaticity D7	0.0219
		This visual induction D8	0.0743
		Identifiability D9	0.1024
	Space environment C2	Stereoscopic D10	0.0199
		Environmental coordination D11	0.0139
		Photoperiod D12	0.0124
Energy saving index B2	Lighting control C3	Screwing strategy D13	0.0454
		Screwing method D14	0.0503
	Lighting energy saving C4	Lighting power density D15	0.0755
		Energy saving luminaire D16	0.0511

the requirement degree of meeting the consistency index. The main goal of the solution of the model is to meet the consistency index, so the degree of meeting the consistency index requirements is higher than the degree of following the expert judgment matrix. In the process of original expert judgment matrix correction for each element adjustment of a constraint index, the smaller θ is the better. A_{ij} is the element of initial judgment matrix, x_{ij} and w_i are the elements of judgment matrix with good consistency and corresponding index weights.

After a lot of research, BP neural network algorithm and particle swarm optimization are combined to solve the least squares consistency correction model of analytic hierarchy process, so, as to obtain the judgment matrix with good consistency. Revise the index weight from both subjective and objective aspects to improve the accuracy of the index weight. The basic principle is that there are M particles in D – dimensional space, the motion space of particles is the solution space, the objective function value to be optimized is the fitness of particles, the position vector of particles represents the variables in the solution space of optimization problems, and the motion process of particles is the search process of solutions.

The formula for calculating the particle position is shown in equation 3:

$$x_i = (x_{i1}, x_{i2}, ..., x_{iD}). \tag{3}$$

The calculation formula of particle velocity is shown in equation 4.

$$v_i = (v_{i1}, v_{i2}, ..., v_{iD}). \tag{4}$$

The formula for calculating the optimal position is shown in equation 5.

$$G^0 = \min\{f(P_1^0), ..., f(P_i^0), ..., f(P_M^0)\}, \tag{5}$$

where G is the optimal position of matrix.

3.4. The Construction of Subway Station Space Lighting Environment Evaluation System

The judgment matrix and the sorting weight vector obtained by the particle swarm optimiza-

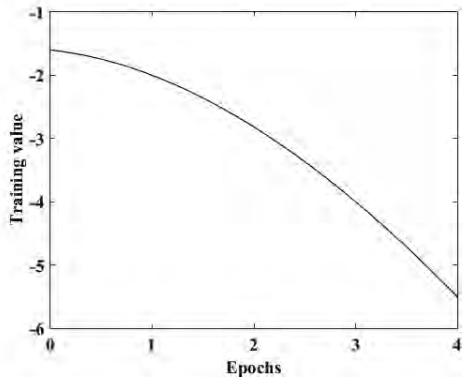

Fig.5. First class parameter training diagram

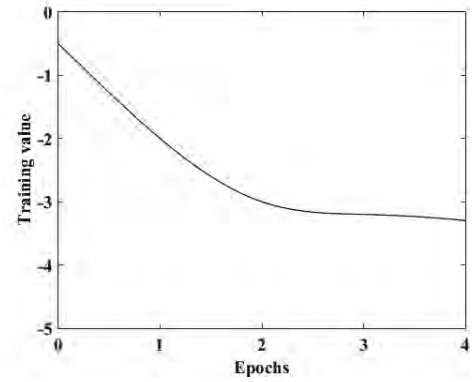

Fig.6. Second class parameter training diagram

tion algorithm are fed back to the experts of the initial judgment matrix, and the experts believe it is acceptable. Therefore, the modified judgment matrix is taken as the final judgment matrix, and the weight vector obtained by solving the model is taken as the weight of each evaluation index, thus the comprehensive evaluation model of lighting environment in subway station space is constructed. As shown in Table 2.

4. RESULT ANALYSIS AND DISCUSSION

The model-based inspection and evaluation method is a method based on the design process, mainly through lighting simulation design software. Its advantages are easy operation, fast and reliable acquisition of index data similar to the actual project. Foreign mature professional software: AGI32, DIALux, LightStar, Lummenmicro, Autolux, Inspire, etc. DIAlux is mainly used for inspection, mainly because the software support Chinese, easy to operate, easy to master, and pay attention to the accuracy of the calculation, lighting error is only 3 % ~ 7 %. There are many manufacturers supporting optional lighting libraries, which can support the calculation of light environment and three-bit light distribution simulation diagram in different scenes, can output including illuminance, brightness value contour, data analysis report and lamps and lanterns of light distribution, unified glare index, lighting scene power density and other data. The model-based inspection and evaluation method is mainly realized: detecting the power consumption of large-space lighting scheme and the implement ability of lighting effect, then a metro model of a standard island platform layer based on foundation structure in China is studied.

The learning of sample pattern P by neural network is to minimize E. In the secondary test of the index, the evaluation data (experts' evaluation) obtained by the Delphi method is taken as a training set to form a matrix of P, The E value is taken as a matrix of T formed by training samples, the number of input layers is M of parameters, the number of output nodes is 1, and the number of hidden layers is $L = 2m + 1$. And set the learning accuracy e = 0.0001, training times n = 1800, weight adjustment parameter α = 0.5, offset adjustment parameter β = 0.8.

The training results of the primary parameters are shown in Fig. 5, and the values of the results are shown in Table 3.

The training results of the secondary parameters are shown in Fig. 6, and the values of the results are shown in Table 4.

The use of BP neural network method is mainly to test the relationship between the relatively complex two to four parameters, Fig. 5 shows that due to the number of first-order parameters input is small, the number of training steps is very small. On that other hand, the high value of the primary parameter e can be used as a reference only in the

Table 3. Level BP Parameters Training Results and Delphi *E* Value Comparison Table

Parameter	Design process	Electricity consumption measurement	Lighting effect
The training results	0. 8998	0.7385	0. 7973
Expected output	0. 9000	0.7400	0.8000

Table 4. Two Parameters of BP Training Results and Delphi *E* Value Comparison Table

Parameter	Subway characteristics	Lighting specification	Selection of lighting	Lighting control	Illumination calculation	Lighting consumption	Other consumption	Test standard
Training results	0.3192	0.8783	0.8795	0.8056	0.7407	0.8466	0.5198	0.7591
Expected output	0.3200	0.8800	0.8800	0.8000	0.7400	0.8400	0.5200	0.7600

case where it is determined as an index. The capacity grade of the secondary parameter is more in line with the standard of BP neural network method. By processing a large number of data, the BP training result E value is compared with the expected output E value of Delphi method, that is, the correctness of the previous index screening is verified by using objective data.

The results from the above table show that the *e* value trained by BP neural network method is basically consistent with the *e* value calculated by Delphi method. The relative error range of secondary parameters is 0.11 % ~ 0.78 %, and all of them are within the allowable error range. Therefore, it can be comprehensively determined that the previously determined index set is feasible and accurate. The index parameters of secondary confirmation were consistent with those of Delphi method. The number and quality of learning samples affect the learning performance of neural network model to a great extent. The samples selected in our research are slightly less, but the results are still more accurate after calculation. Therefore, if we increase the number of learning samples on this basis, we will achieve more accurate and good results.

5. CONCLUSION

With the development of computer technology, it has been widely applied to some problems in real life environment. Therefore, aiming at the problem of comprehensive evaluation of lighting environment in metro station space, this paper uses the theoretical knowledge of light environment, environmental psychology and fuzzy mathematics to construct the theoretical model of comprehensive evaluation of lighting environment in metro station space. The model is applied to the comprehensive evaluation of the lighting environment of the subway station space of Shenzhen metro line 2 illuminated by LED light sources and Shenzhen metro line 3 illuminated by fluorescent lamps. According to the questionnaire of each index on the spot and the model, the optimal lighting environment is obtained, the rationality of the selected index in the model and the validity of the index weight are verified by combining the subjective investigation result and the model theoretical data. Thus, the evaluation model has universal applicability, provides model reference for the future evaluation of subway station space lighting environment, and provides theoretical basis for subway station space lighting design. Indoor lighting environment is a multi-factor comprehensive lighting environment, and the field of indoor environment lighting, which is dominated by artistic lighting, needs further study.

REFERENCES

1. Englund S R, O'brien J J, Clark D B. Evaluation of digital and film hemispherical photography and spherical densiometry for measuring forest light environments. Canadian Journal of Forest Research, 2000. V30, #12, pp.1999–2005.

2. Poorter L, Arets E J M M. Light environment and tree strategies in a Bolivian tropical moist forest: an evaluation of the light partitioning hypothesis. Plant Ecology, 2003. V166, #2, pp.295–306.

3. Hernandez Duran T, Ravela N, Sanchez Rivero S, et al. Evaluation of Different Light Conditions in the Working Environment for Handling Photosensitive and Thermolabile Compounds. Journal of AOAC International, 2015. V98, #6, pp.1491–1495.

4. Mills P R, Tomkins S C, Schlangen L J M. The effect of high correlated colour temperature office lighting

on employee wellbeing and work performance. Journal of circadian rhythms, 2007. V5, #1, p.2.

5. Haiying Li, Xian Li, Xinyue Xu, Jun Liu, Bin Ran. Modeling departure time choice of metro passengers with a smart corrected mixed logit model – A case study in Beijing. Transport Policy. 2018, #69, pp.106–121.

6. Li D H W, Lam J C. Evaluation of lighting performance in office buildings with daylighting controls. Energy and buildings, 2001. V33, #8, pp.793–803.

7. Iwata T, Tokura M, Shukuya M, et al. A pilot experiment on a method for evaluating acceptability of a daylit luminous environment. Journal of Thermal Biology, 1993. V18, #5–6, pp.555–559.

8. Xu, X., Xie, L., Li, H., & Qin, L. Learning the route choice behavior of subway passengers from AFC data. Expert Systems with Applications, 2018. #95, pp. 324–332.

9. Stansbury J, Mittelsdorf A M. Economic and environmental analysis of retrofitting a large office building with energy-efficient lighting systems. Environmental management, 2001. V27, #6, pp.909–918.

10. Aghemo C, Fabbri M, Verso V L, et al. Visual perception in aircraft cockpit under real ambient lighting conditions: A procedure for the evaluation of readability and legibility. Perception ECVP abstract, 2009. V38, pp.181–181.

Wenhao DUN,
on-the-job doctor and lecturer. Graduated from school of civil engineering and architecture, Wuhan university of technology. Work in Wuhan university of technology, research direction is underground engineering lighting design

Light & Engineering
Vol. 26, No. 3, pp. 74–80, 2018

Svetotekhnika
No. 1, 2018, pp. 69–73

FEATURES OF ARTIFICIAL ILLUMINATION OF HISTORICAL AND MODERN LANDSCAPE COMPOSITIONS

Alexander N. Belkin [1] and Victoriya V. Dormidontova [2]

[1] University of Civil Engineering (NRU MGSU), Moscow
[2] Mytishchi branch of the MSTU of N.E. Bauman (MGUL), Moscow oblast, Mytishchi
E-mail: an.belkin@mail.ru; v.dormidontova@mail.ru

ABSTRACT

The article is dedicated to the problem of artificial illumination of landscape compositions. As exemplified by the Château de Vaux-le-Vicomte palace and garden ensemble of the *XVII*th century and by the National memorial complex of the *11*th September 2001, features of artificial illumination of historical and modern landscape compositions are considered. Methods of revelation of existing planning and spatial elements in historical gardens are described. Merits and demerits of use of modern technological capabilities of artificial illumination are shown.

Keywords: artificial illumination, landscape, composition, space, methods

The illumination problem of landscape compositions is topical from the moment of home gardens emergence. First, it was caused by a need of convenient and safe movement within the garden space and then, by a desire to prolong a possibility of its aesthetic perception. The historical landscape gardening spaces were an extension of the palace. In the evenings, the gardens lived life to the full: the people feasted, danced, listened to music and enjoyed theatre in open garden rooms. Therefore in the gardens, evening illumination with candles and torches was always envisaged. So, for example, the Sea Theatre of Villa Garzoni was illuminated with torches, which faun sculptures held in their highly raised hands. The theatrical performances were often arranged in gardens afloat with fireworks [1]. Candles installed along paths revealed the planning patterns, the torches illuminated supporting walls, lace and water parterres, sculptures, fountains, theatrical scaffolding and stages. Until now, the evening candle lighting in Château de Vaux-le-Vicomte attracts tourists from all over the world. Here they can observe, how the famous immense ensemble is gradually absorbed by darkness and then, also gradually, it appears reviving by lighted sparks, which is beginning a dialogue with the star sky. And all of this is an apparent picture of art harmony with nature.

Today, the artificial illumination of the landscape gardening compositions with a considerable set of technological facilities is a particular complex genre of the light design. But unfortunately, technological capabilities do not always provide aesthetic qualities. Trees wired by the LED bulbs with best intentions, suddenly turn into stumps of the branches shining against the background of night sky. A familiar and pleasant space of the traditional boulevard formed by alleys disappears. It is destroyed by light tunnels, brightly illuminated arches, figures of animals, by stiffened light “fountains” and many other things. A public garden in front of facade of a well illuminated architecture memorial is quite often filled with high and fatly ornamented arches, which are brightly illuminated and coloured; however, they block the best view on a remarkable composition. A thoughtless festive illumination from temporary turns into long-term and its rich bad taste turns the city environment into a persuasive buffoonery. It destroys the thought-over, carefully built,

expressive historical and modern gardens, buildings and ensembles.

This is a childhood of the light design, with often awkward attempts of developing a new toy by a child, for whom any action is a discovery not burdened with knowledge. A theoretical foundation of the light design began to develop relatively recently, and one should notice works of N.I. Shchepetkov [2–4] as the most important among works of other researchers. The big attention to the subject of illumination of the city landscape environment is attracted by a desire to develop new technological capabilities, to use visual illusions in architectural composition [5–7], as well as desire to remind easily forgotten lessons of the past.

A purpose of this work is features understanding and revelation of composition methods of the successful artificial illumination of two landscape compositions: the historical and the modern.

Artificial illumination of the Château de Vaux-le-Vicomte palace and garden being a remarkable ensemble (Fig. 1) belonging to Nicolas Fouquet, who was finance superintendant of Louis XIV. The estate has old traditions and is an example of a masterful combination of utility and of decorative effect. The Vaux estate constructed during five years reached us "untouched" despite wars, revolutions and changes in tastes, which took place for three and a half centuries of the European history [8]. And today every Saturday, two thousand candles are lighted in the garden, recreating the situation of a magnificent festival on August 17, 1661, which was the opening day of the estate and the day, when it was visited by the king Louis XIV (Fig. 2).

Fig. 1. An appearance of the Château de Vaux-le-Vicomte ensemble (URL: http//www.vaux-le-vicomte.com)

To create his estate, N. Fouquet involved architect L. Levaou, artists N. Poussin and C. Le Brun. And for the garden arrangement, A. Le Nôtre was invited [9]. Well educated Fouquet brought together a group of outstanding persons of different art types who when creating the Château de Vaux-le-Vicomte ensemble to a large extent had created the French classicism itself. Here a composition method system was for the first time used, which formed a new type of the spatial arrangement, as well as an aesthetic approach system of a new style. For the managing director of the France finance, nothing seemed to be too huge, too beautiful or too expensive. The estate, which was spreading out over 500 hectares, turned out magnificent. Magnificent buildings, gardens, cascades are an axial composition extended from North to South for 1.5 km [10, 11].

But a source of the funds spent to create this masterpiece was too obvious. And this excited anger of the young envious king. Less than in a month after the festival, on September 5, 46-year-old Fouquet was arrested, accused of embezzlement of public funds and flung in prison, where he died 19 years later. All experts working in Château de Vaux-le-Vicomte together with the pupils were transferred

Fig. 2. Lighting of candles in Château de Vaux-le-Vicomte (URL: http//www.vaux-le-vicomte.com)

Fig. 3. The lace parterre in Château de Vaux-le-Vicomte (URL: http://www.lenotre.culture.gouv.fr/fr/de/index.htm)

Fig. 4. A revelation method using dotted contours (URL: http//www.vaux-le-vicomte.com)

to Versailles. The Château de Vaux-le-Vicomte garden is an alternation of lace and water partners, channels and grottoes decorated with vases and sculptures. But the new style and distinctive "manner" of Andre Le Nôtre were not created by a set of elements and a high degree of their decorative effect. This set was already used in terrace gardens of the Italian Renaissance and medieval French gardens: covered alleys (berceau), pergolas, channels, broderie level spaces – (broderie means embroidery, lace) (Fig. 3) [1].

The main feature of Château de Vaux-le-Vicomte was an immense expressly horizontal composition subject to the axis, along which a wide 1.5-kilometre perspective was built. Height of all vertical elements, i.e. rows of trimmed plants, sculptures, bosquet walls and even of the palace is insignificant in comparison with width and depth of the observed space involved in the composition.

The palace surrounded with a channel is located in the northern estate part. Its southern facade is turned to the garden. The palace is the centre of the composition. From the palace, along the main composition axis, an open integral space decorated with a sequence of lace and water level spaces is spreading. However, the "soaring continuity" is an optical illusion. As the garden was arranged at several levels, harmony of horizontal planes is interrupted by channels, cascades and a grotto crossing the main perspective and composition axis creating deep vertical partitioning of the space and enriching the perception. According to increase the distance from the palace, the areas and elements are rhythmically enlarged, the pattern becomes simpler. The open space is flanked by trimmed bosquet walls forming green halls. The main perspective is closed with a transverse channel and with a plastically cultivated hill, at which top Heracles's statue is installed in the perspective convergence point. Thus Le Nôtre changed not elements but the nature of their spatial interrelations, partitioning scale, proportions and composition scale as a whole.

In the 17th century, the garden was illuminated with candles and torches and fireworks were arranged in feast days. Flame of the candles placed in a metric principle, emphasised contours of the main garden paths and of the level space pools. Evening illumination revealed the planning but shifted focus, emphasised plasticity of the palace facades, and integral level space garden composition was turned into a dotted waving flickering mirage [10, 11].

Due to the dotted candle arrangement with equal intervals, the architectural and park ensemble became light, aerial and more integral. As if thousands glow worms having flied out from the palace windows, plashed in the pools, ran on the fountain edges, hid and giggled in the lace arabesque labyrinths (Figs. 2 and 4). A fabulous atmosphere increased expressiveness of the ensemble.

Garden and park art has always been opened for all news and provided its spaces for experiments. So, Château de Vaux-le-Vicomte today also tries fresh technological capabilities of art illumination on itself. At present, not only candles but also electricity is solving problems of art revelation of historical composition at night using different light scenarios in different cases (Fig. 5).

At normal weekends, low-key, restrained illumination of the road network using lighted candles designates boundaries of the basic elements reproducing the historical illumination.

Within these contours, low ground luminaires located at the level space part angles "pull out" an-

Fig. 5. An evening view of the palace from Sheaf fountain (URL: http//www.vaux-le-vicomte.com)

gular fragments of the broderie level spaces from darkness turning the huge composition into a dialogue of "fragmentary phrases" and giving human imagination a chance to finish drawing the rest independently.

In holidays, the illumination is more decorative but keeps less to be elusive. To reveal lace arabesques, a tight moisture-proof LED tape is used with a monochrome yellow glow repeating their pattern. It also outlines external contour of the lace level space. The same tape is used to emphasise spherical crowns of the trimmed plants (Fig. 6). With other scenarios, a LED tape is applied in combination with low ground luminaires. The luminaires are located along the level space main axis and directed perpendicularly to it, with their white glow stripes, reveal top plane of the arabesques, which are cut off from boxwood (Fig. 7). Besides, contours of large elements: terraces, supporting walls and ladders underlined with LED tapes articulate the garden space giving together with the illuminated palace facade the third dimension of the majestic composition.

Fig. 7. A revelation method by "filling" (URL: http//www.vaux-le-vicomte.com)

Fig. 6. A configuration revelation method using linear draughtsmanship by light (URL: http//www.vaux-le-vicomte.com)

Fireworks, although they are historical but seem a vulgar invasion, which in a barbarian way disturb integrity, adequacy and silent harmony of the ensemble, instantly turn it into chaos and force to expect fading the sparks and a gradual return of the recognizable configurations of the palace and garden (Fig. 8).

Illumination of the Château de Vaux-le-Vicomte ensemble shows that in case of a restrained and proportional use of modern technological facilities, the main problem, which is a revelation of the historical composition features, can be successfully solved. Moreover, different illumination scenarios can enrich perception of the ensemble art image.

Light design of the 11th September National memorial and museum in New York is beyond the framework of a just local illumination and revelation of an architectural and landscape composition. An initial reaction was a light installation on the

Fig. 8. Destruction method (URL: http//www.vaux-le-vicomte.com)

Fig. 9. 11th September National memorial and museum (URL: http//www.pvpla.com)

Fig. 10. 11th September National memorial and museum with evening illumination (URL: http//www.pvpla.com)

tragedy place named "Dedication using light" (*Tribute in Light*). On September 13, 2001 President of Arnell Group Innovation Company presented the installation idea to heads of Consolidated Edison Energy Company serving New York. The project was developed by architects J. Bennet, G. Bonevardy and R. Nash Good, as well as by artists J. Leverdyer and P. Mioda. The installation has been created by a company specialising in high power lighting installations. Already in half of a year, two "light towers" appeared. They were lighting installations with 44 powerful searchlights with a xenon lamp in everyone. These temporary installations operated during a month, and since 2003 the searchlights are switched on annually on September 11, and in fine weather, their light can be seen at a distance of 100 km. Since 2008, the installation power supply generators use a biodiesel powered by utilised oil from local restaurants.

In 2003 an international competition on the memorial of the World Trade Centre project as a tribute to the memory of the terrorist attacks victims on September 11, 2001 was announced. On January 6, 2004 the winner was selected. It was the Reflecting Absence project. Construction of the Memorial began in 2006 according to the project of an architect Michael Arad and a landscape architect Peter Walker. It was completed in 2011 [12–17].

The memorial ensemble has a public garden appearance and is located at the place of the destroyed towers of the World Trade Centre. Main elements of the memorial composition are two deep squares in plan pools at the Twin Tower places. Along inner steel surfaces of their walls, water streams, covers the bottom with a thin layer and disappears in bottomless wells. The pools are surrounded with reading desks of bronze plates along their perimeters with names of 2,983 victims. The garden composition around is a visible embodiment of the silence moment. Metric rows of horizontal lawns are followed with a metronome of strict rows of white oaks and eucalyptuses (Fig. 9). Later on, under the pools, a museum was constructed, which was opened on May 21, 2014.

In evening and night time, art illumination significantly increases imaginative expressiveness of this minimalist composition (Fig. 10). First of all, bright light illuminates water flows violently streaming along the pool walls, which turns them into flows of fire lava as an eternal reminder about the tragedy burning souls of the visitors (Fig. 11). Among the trees, standing lamps with a dull glow are accidentally on purpose scattered. The yellow glow makes an impression of commemorative candles.

Despite the installation high price, annually including September 11, 2017 powerful great light columns virtually recreate the towers against the background of the dark sky (Fig. 12). In the considered case of modern architectural and landscape composition, illumination not only reveals planning and spatial volumetric configurations but also creates new configurations supplementing the composition and new "night" dominants transforming daytime perception. The illumination also takes part in formation of an art image.

CONCLUSION

When designing illumination of historical and modern architectural and landscape compositions, different problems are solved: in the first case illumination is a facility to reveal the existing configu-

Fig. 11. A method of light imaginative expressiveness using colour (URL: http//guruturizma.ru/ memorial-911-v-nyu-jorke)

Fig. 12. A method of creating new virtual configurations using light (URL: http//www.shutterstock.com/ … / stock-photo-twin-towers-memorial

ration, in the second case, it is a facility of a new form shaping.

In historical compositions, one should save and reveal valued composition features of a memorial applying illumination facilities, which do not deform both: the space as a whole and configurations of separate planning and volumetric elements. As exemplified by the artificial illumination of the17th century ensemble "Château de Vaux-le-Vicomte", one can notice methods of revealing landscape composition with light as follows: creation of a dotted contour of basic volumetric and planning elements; linear draughtsmanship of most important elements; emphasis of plant geometrical configuration surfaces (dot and plane).

When designing modern architectural and landscape compositions, illumination initially is a form shaping method. In the above considered case of artificial illumination of the 11 September National memorial and museum in New York, light initially was the only form shaping facility. It also initiated its spatial composition and to a large extent determined it. The composition in the day-time expresses a silent grief and a rest state. The light design methods are directly purposed to create an art image. Scenario of evening illumination causes a sharp emotional pain due to lighting among trees yellow sparks of standing lamps as commemorative candles, which turn water of the pools into streaming fiery lava, and due to constructing virtual phantom towers. From the day-time reality we are transferred to an illusory metaphoric space created by light and by its colour.

Illumination facilities of architectural and landscape objects should correspond to the time of their creation, to the technologies and materials, to the rhythm, pace of life and to the life features. Therefore, use of torches and candles is pertinent to illuminating historical objects. And use of modern facilities should be limited and careful. Modern objects do not limit the illumination facilities choice. Everything that is available from the technological point of view is pertinent.

REFERENCES

1. Dormidontova V.V. History of landscape gardening styles: a study guide// Moscow: Arkhitektura-C, 2004, 207 p.

2. Shchepetkov N.I. Light design of a city// Moscow: Arkhitektura-C, 2006, 320 p.

3. Shchepetkov N.I. Interspace of light design / Theses of reports of the International scientific and practical conference of higher-education teaching personnel, young scientists and students "Science, edication and experimental design"// Moscow: MARKHI, 2014, pp. 350–352.

4. Shchepetkov N.I. Evolution of light design in Baku / / Svetotekhnika, 2015, #5, pp. 47–51.

5. Savelyeva L.V. Light as an instrument of creation of virtual images in architecture // Svetotekhnika, 2014, #6, pp.15–19.

6. Solovyyov A.K. Physics of environment// Moscow: Association of building high education institutions, 2015342 p.

7. Tsvetkova I. Landscape illumination: dialogues about eternal // Landscape Architecture Design, 2007, #1, pp. 60–61.

8. Sefrioui A. Vaux-le-Vicomte// Paris: Scala, 2008, 64 p.

9. Belkin A. N. I only thought about honour and glory of France // Development and economics, 2013, #8, pp. 216–219.

10. URL: http://www.lenotre.culture.gouv.fr/fr/de/index.htm (addressing date: 2/10/2017).

11.URL: http//www.vaux-le-vicomte.com (addressing date: 2/10/2017).

12. Dormidontova V.V. Stages of forming gardens of the 21st century // Architecton: news of high education institutions, 2012, #1(37).

13. URL: http://archvuz.ru/2012_1/19 (addressing date: 2/10/2017).

14. Dormidontova V.V. Minimalism in the garden art // Architecton: news of high education institutions, 2012, #2(38).

15. URL: http://archvuz.ru/2012_2/17 (addressing date: 2/10/2017).

16. URL: http//www.pvpla.com (addressing date: 2/15/2017).

17. URL: http//guruturizma.ru/memorial-911-v-nyu-jorke (addressing date: 2/15/2017).

18. URL: http//www.shutterstock.com/…/stock-photo-twin-towers-memorial (addressing date: 2/15/2017).

Alexander N. Belkin,
Ph.D., Professor, graduated from the Town Development and Architecture faculty of the Chisinau Polytechnic Institute with a specialisation “Architecture”. At present, he is a professor of the Chair “Design of Buildings and Constructions” of the University of Civil Engineering (NRU MGSU), a member of the Russian Union of Architects

Victoriya V. Dormidontova,
Ph.D., Pofessor, graduated from the Town development and architecture faculty of the Chisinau Polytechnical Institute with a specialisation “Architecture”. At present time, she is a professor of the Chair “Landscape Architecture and Landscape Gardening construction” of the Mytishchi branch of the MSTU of N.E. Bauman (MGUL), a member of the Union of Architects of Russia and of Moscow association of landscape architects

Light & Engineering
Vol. 26, No. 3, pp. 81–87, 2018

Svetotekhnika
No. 2, 2018, pp. 6–10

ON THE EFFICIENCY OF LIGHTING BY LEDS IN VISUAL WORK

Svetlana A. Amelkina, Olga E. Zheleznikova, and Lyudmila V. Sinitsyna

Ogarev Mordovia State University, Saransk
E-mail: sarstf@mail.ru

ABSTRACT

It is experimentally found that LEDs illumination does not cause a negative influence on visual organs and human body as a whole. It is shown that changes of visual organ functional indices for visual operations are within the correspondent boundaries of physiological fluctuations and have a reversible nature. Integral indices of LEDs illumination efficiency from visual working capacity and visual fatigue degree are estimated. A practical importance of the obtained results is shown.

Keywords: light emitting diodes (LEDs) illumination, comprehensive technique, experimental research installation, visual functions, visual fatigue, visual working capacity, lighting efficiency

1. INTRODUCTION

Light emitting diodes (LEDs) allowed expanding technological capabilities of illumination devices (ID) with significantly improved energy and operational characteristics. In modern illumination regulation documents, LEDs are specified as recommended to be applied for production rooms, public buildings and in communal rooms of residential buildings. And interest in medical and biological aspects of new LED technologies [1] also increases.The possibility of LED use in order to create a favourable illumination conditions requires weighty evidence, which can be only obtained by comprehensive studies of LED illumination (LEDI) influence on visual organs and on the human body as a whole. In that case, vital questions both of direct danger of visual organ damage due to LED radiation, and of possible consequences of LEDI artificial illumination long action on psychophysiological and physical human health are considered.

A purpose of this work is evaluation of LEDI influence on visual organs and on visual operation efficiency indices.

An important stage of this work was creation of an experimental study installation of general illumination (ESI) in laboratory #316 of the Institute of Electronics and Lighting Engineering of Ogarev Mordovia State University (Ogarev MSU).The laboratory consists of four rooms: one of them is intended for study of observers (with 0.7, 0.5 and 0.3 reflection factor of ceiling, walls and floor respectively). And three others are used for experiment studies; ID with LEDs are mounted in two of them, and ID with fluorescent lamps (FLs) are placed in the third, Fig. 1.When comparing illumination versions, the ID with FLs is used as the basic[1].

For ESI, according to the requirements [2], luminaires with LEDs *Cap Flat 66–16*[2] and ДВО12–38–001 *Prizma*[3] were selected, as well as luminaires with FLs ЛВО 04–4×14–041 *PRS*[3]. Luminaires correlated colour temperature T_{cc} were equal to 3000, 4000 and 5000 *K*. Photometric and spectrocolori-

[1] This is because FLs are most studied light sources (LS) of mass application on psychophysiological and hygienic exposure of their radiation on human organisms.

[2] Their manufacturer is NepesRus Russian-Korean LLC company (of LEDs of own production).

[3] The manufacturer is Ardatov Lighting Factory JSC (LEDs of *Seoul Semiconductor* production).

Fig. 1. Rooms for examination and experimental studies

metric parameters of the selected luminaires were measured in the Ogarev MSU Lighting Metrology Collective Use Centre. Their spectral distributions, luminous intensity distribution curves and colour rendition indexes R_a are given in Figs. 2–5.

In order to meet the requirements [3], illumination versions were simulated previously within the *DIALux* program, Fig. 6. Change of illuminance *E* on the working surface was reached by use of ballast and of control units adjusted according to the *DALI* protocol respectively. The studies were carried out at three *E* levels: 200, 400 and 1000 lx.

To evaluate LEDI conditions influence on indexes of visual organ state and on the human body as a whole, a comprehensive technique, which has been special developed, was used [4].

An analysis of the existing techniques for determination of some indices allowed selecting most appropriate methods for the objectives: a LEDI condition efficiency evaluation when implementing visually intensive operations. So changes of the functional state of a visual organ were estimated based on the following studies: of accommodation – muscleand receptor systems of visual organs and of the central link of visual organs.

Before the studies were begun, a group of volunteer students at the age of 20–25 years was examined in the Republican Ophthalmologic Hospital of Saransk. The examination included determination of refraction and visual acuity, as well as computer tomography of eye retinas. All selected observers had mainly emmetropic refraction, visual acuity of both eyes was equal to 1.0, and colour perception was without any pathology.

Sixty persons as the selected observers were divided into two groups in a random way, 30 persons each group: a reference group was intended for FL illumination (FLI) experiments and the main group was used for LEDI lighting experiments. The observer and experiment number were determined on the basis of the requirements to obtain statistical-

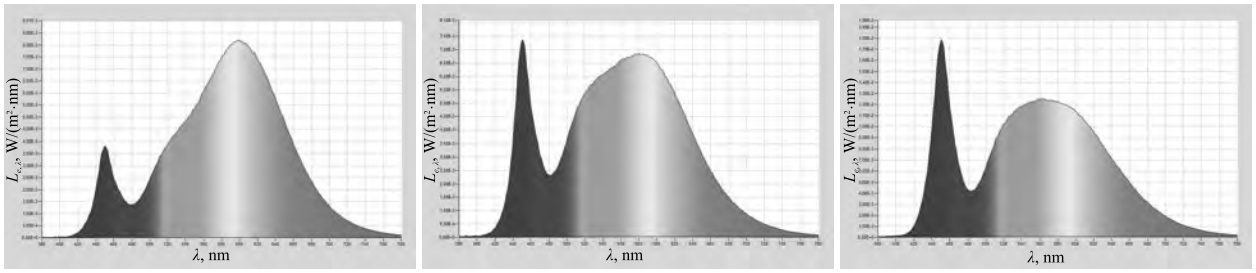

a) *b)* *c)*

Fig. 2. Spectra of *Cap Flat* 66–16 luminaires with T_{cc} = 3000 K(a), *Cap Flat 66–16* with T_{cc} =4000 K (b) and ДВО 12–38–416 with T_{cc} = 5000 K (c)

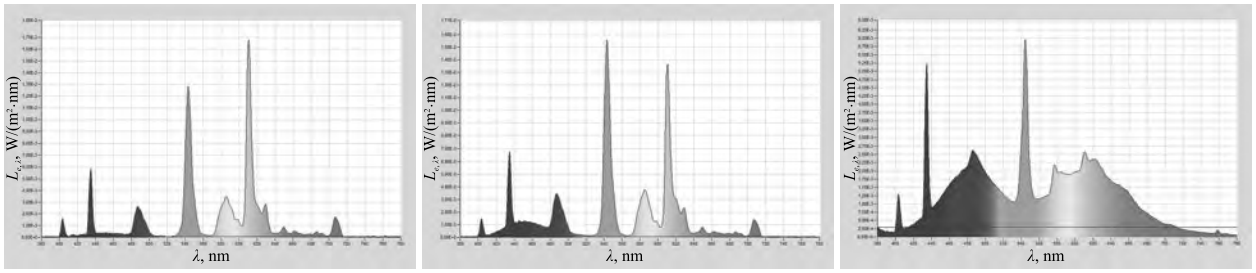

a) *b)* *c)*

Fig. 3. Spectra of ЛВО 04–4×14–041 PRS luminaires with FL *T5 FH 14W HE* (T_{cc} =3000 K)of*Osram*production(a), ЛВО 04–4×14–041 *PRS* with FL *Master TL5 HE14W*(T_{cc} =4000 K) of *Philips*production (b) and ЛВО 04–4×18–041 PRS with FL *T8 L18W* (T_{cc}=5000 K) of *Osram*production*(c)*

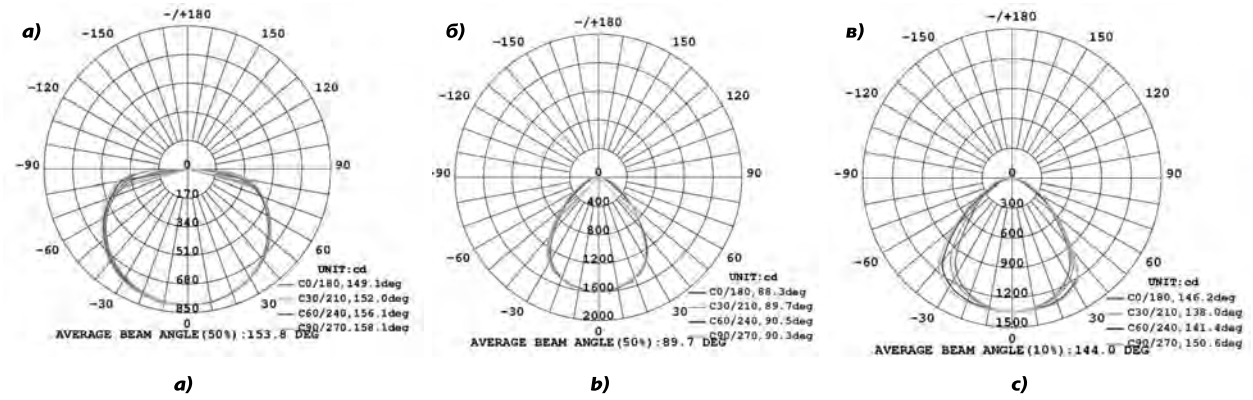

Fig. 4. Luminous intensity curves of luminaires *Cap Flat* 66–16 (a), ДВО 12–38–416 (b) and ЛВО 04–4×14–041 *PRS* with FL *T5 (c)* in four meridian planes

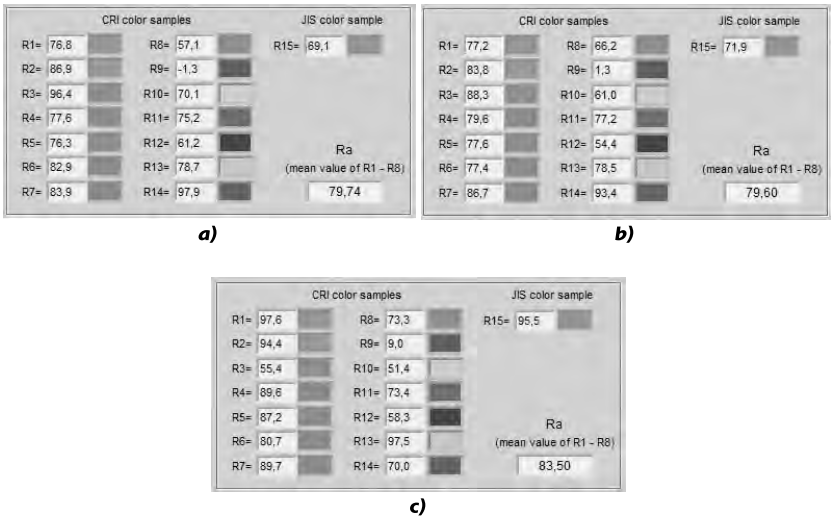

Fig. 5. Colour rendition indices of luminaires *Cap Flat* 66–16 (a), ДВО 12–38–416 (b) and ЛВО 04–4×14–041 *PRS*withFL*T5*of *Master TL5 HE14W*(T_{cc} =4000 K) *Philips (c)*

ly reliable data and based on regulation of the studies duration. The experiment plans and each group work schedules were developed. In doing so, daily human biorhythms were taken into consideration. As a functional load, one and a half hour duration visually intensive work of a proof-reading type with paper texts was used. A calculation of curvilinear figure areas (an intellectual component) was also included.

In all illumination versions during the experiments, indices of illumination quality did not exceed the normalised values [3]: *UGR* integrated factor was equal to 10–14, and illuminance ripple factor was (0.2–0.6)%.

Before the studies began, all observers were trained during 10 days according to the study technique sufficient for stable results to be obtained.

Upon termination of the studies, the reference and basic groups of the observers were repeatedly examined in the Republican Ophthalmologic Hospital of Saransk in order to determine, whether LEDI negatively influenced their visual organs.

Plan of the experiment provided for measuring absolute accommodation volume (AAV), time of achromatic adisparopia, critical flicker frequency (CFF) using the КПФК-99 special computer system), and arterial pressure. The listed measurements should be made under the set illumination conditions before and after the visual operations. At the end of the work, the observers filled in personal questionnaires of subjective estimation of the illumination conditions[4].

Besides, before and after the visually intensive work, colour discrimination thresholds of the observers were measured by means of anomaloscope

[4] This was a specially developed questionnaire of subjective estimation with questions on the main characteristics of the illumination versions (LEDI or FLI), on radiation colour rendition properties and on psycho-emotional state of the observers.

Fig. 6. Simulation of room illumination for experimental studies (using the *DIALux*)

AH-59, and projections of visual organ blind spot by the campimetry method in the monocular mode were also measured [5].

2. EXAMINATION OF VISUAL ORGANS

The results of the examination showed an AAV reduction during visually intensive operations in the considered illumination versions (Tables 1 and 2).

Determination of the AAV change reliability as a visual load result according to *Student's t-criterion* with $p<0.05$ showed that practically in all illumination versions, shifts of the AAV values are reliable and do not exceed the limits of natural variations of this factor of accommodative function of visual organs (0.5–1.5 dioptres).

Spectral composition influence on change of the considered accommodation factor at a constant E level according to *Student's t-criterion*is revealed in the compared versions withT_{cc} = 4000 K and with all E levels. And with T_{cc} =5000 K it was revealed with E=200 lx and E=400 lx. AAV maximum values were recorded with LEDI. AAV excess after work with LEDI in comparison with basic illumination version (FLI) at T_{cc}=4000 K and with E in range (200–1000) lx was 0.6–0.7 dioptres, ((6.3–8.4)%), and at T_{cc}=5000 K and E in interval (200–400) lx, it was equal to (0.5–0.7) dioptres, ((6.0–8.0)%).

Therefore it was found out that visual organ accommodation with LEDI is better (at T_{cc} about 4000 K and 5000 K), which is explained by a greater activity of ciliary muscle and probably is connected with LED spectrum [6].

The correlated colour temperature influence on the achromatic adisparopia period at the constant E, when working in the versions being compared, is very essential. The achromatic adisparopia period was longer with LEDI both before, and after the work. This shows that more favourable conditions for visual organ accommodation-muscle apparatus operation are with LEDI than with FLI.

When retina state estimating by the computer tomography data, it was found out that after the experiment end, foveola profile for the both groups of observers (reference and basic) remained and retina architectonics was not disturbed. And a statistical processing of the study results did not reveal statistically significant differences between the studied indices ($p>0.05$ according to the Student's *t-criterion*); id est., retina state of the observers remained without reliable changes.

Studies of the blind spot projection area showed that retina fatigue estimated proceeding from peripheral sight state leads to a reliable increase of physiological area of the blind spot after an intensive visual work. Interval of optic nerve disc projection increase in relation to initial for FLI versions was equal to (6.57–12.06)%, and for LEDI versions

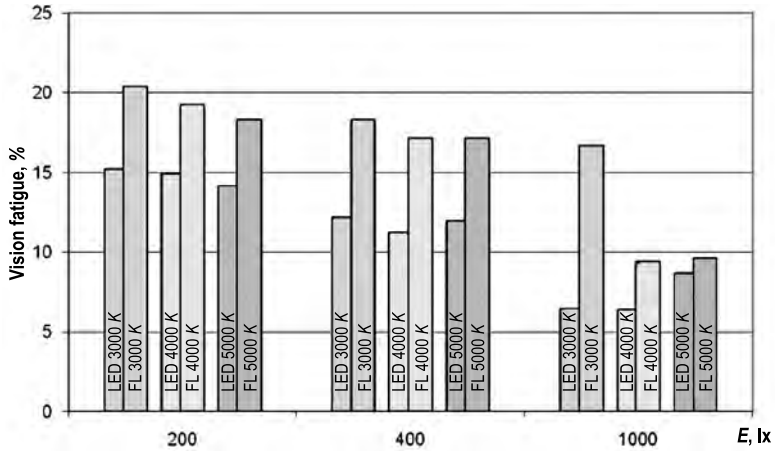

Fig. 7. Visual fatigue (by means of the achromatic adisparopia method)

Table 1. Change of AAV after visual loads at different LEDI versions

E, lx	T_{cc}, *K*	Beforework		Afterwork		Correlationcoefficient	
		OOV, diopters, $\overline{x}$	Confidenceinterval, $t \cdot \sigma_{\overline{x}}$	OOV, diopters, $\overline{x}$	Confidenceinterval, $t \cdot \sigma_{\overline{x}}$	*r* (between "before" and "after" work)	*p*(*r*)
200	3000	8.70	0.10	8.40	0.21	0.75	<0.05
400		9.00	0.21	8.80	0.12	0.85	<0.01
1000		9.90	0.16	9.70	0.19	0.73	<0.05
200	4000	9.40	0.13	9.00	0.16	0.66	
400		9.70	0.17	9.50	0.19	0.65	
1000		10.10	0.13	10.20	0.18	0.14	–
200	5000	9.30	0.11	8.70	0.15	0.79	<0.05
8.70		9.70	0.13	9.40	0.18	0.66	
1000		10.00	0.22	9.80	0.24	0.63	

Table 2. AAV change after visual loads at different versions of FLIs

E, lx	T_{cc}, *K*	Before work		After work		Correlation coefficient	
		AAV, diopters, $\overline{x}$	Confidenceinterval, $t \cdot \sigma_{\overline{x}}$	AAV, diopters, $\overline{x}$	Confidenceinterval, $t \cdot \sigma_{\overline{x}}$	*r* (between "before" and "after" work)	*p*(*r*)
200	3000	8.60	0.21	8.20	0.12	0.73	< 0.01
400		8.80	0.20	8.60	0.10	0.69	< 0.05
1000		9.60	0.14	9.40	0.10	0.74	< 0.01
200	4000	8.80	0.14	8.30	0.16	0.69	< 0.05
400		9.10	0.15	8.80	0.10	0.77	< 0.01
1000		9.80	0.14	9.60	0.12	0.85	< 0.001
200	5000	8.70	0.29	8.20	0.27	0.63	< 0.05
400		9.10	0.17	8.70	0.23	0.83	< 0.001
1000		9.70	0.10	9.40	0.07	0.72	< 0.05

it was equal to (3.87–10.77)%. A comparison of the studied parameter dynamics showed that with T_{cc} =3000 K, visual fatigue (VF) with LEDI was lesser than with FLI (p< 0.05).

It was revealed during the experiments that colour discrimination threshold change for different illumination versions had different natures. It follows from the obtained results that when visual system are working under FLI and LEDI conditions, functional states of the retina are not identical, which was obviously connected with photochemical reactions in the retina. And this can be slowed and accelerated under radiation influence in different parts of the visible spectrum. Influence of LED radiation is revealed only on retina *b*-receptors at T_{cc}= 4000 K and E= 1000 lx, as well as at T_{cc}= 5000 K and E = 400, 1000 lx (p< 0.05). For other illumination versions, LS radiation influence on r-, g- and b- receptors was insignificant; that can be explained by nature of visual tasks: work with achromatic objects.

Studies of the state of the visual organ central link before work according to the CFF method did not allow revealing most preferable illumination version: *Student's t*-criteriondid not confirm difference reliability in all studied E and T_{cc} intervals. Thus it is found out that CFF values with LEDI and FLI are hardly distinguishable.

The results of the studies have showed that CFF decrease during the experiments is connected with visually intensive work. This process is reversible: at the beginning of the next day, the parameters restored to the initial values. Id est., LEDI did not influence oppressively on the central nervous system state.

3. DETERMINATION OF LEDI EFFICIENCY INTEGRAL INDICES BY VISUAL WORKING CAPACITY AND VISUAL FATIGUE

Visual working capacity was estimated by the correction task method. A special tests were used for this purpose: correction tasks consisted of Cyrillic letters using a random number generator: contrast of the tests was negative.The observers worked with the tests within two minutes: they deleted a set letter, which was found in certain combinations. According to the test results, visual working capacity coefficient I was calculated, which takes into consideration sign number looked through during the test, and quality coefficient taking into consideration properly deleted signs and made mistakes [7]. A study result analysis showed LEDI advantages in providing a greater visual working capacity. The greatest I value was with LEDI at T_{cc} = 4000 K. So, in comparison with FLIs, it was by 11.8 %, 14.9 % and 12.4 % respectively higher with E= 200, 400 and 1000 lx.

The obtained pair correlation coefficient r confirmed ($p< 0.05$) presence of a positive interrelation between AAV and I after visual work. This allowed assuming that a certain contribution to I increase with LEDI was made by a better work of the accommodation-muscle apparatus.

Results of work quality study showed that when visual loading, the quality level decreased. However, decreasing accuracy coefficient proceeding from the *Student's t*-criterium was only reliable under the LEDI conditions with T_{cc} =4000 K (E = 400 lx and 1000 lx) and with T_{cc} = 5000 K (E = 400 lx). Differences of the work quality when comparing LEDI and FLI versions appeared to be insignificant.

The visual fatigue was estimated by the time threshold dynamics of the achromatic adisparopia. In doing so, VF factor A was calculated as follows:

$$A = (1 - \frac{t_j}{t_i}) \cdot 100\%,$$

where t_i and t_j are durations of achromatic adisparopia before and after visual work respectively.

Calculation results (Fig. 7) have shown that with LEDI during 1.5-hour visually intensive work a lesser VF took place. The least VF in case of LEDI was at T_{cc} = 4000 K, 5000 K and E= 400 lx.

Reliability of T_{cc} influence on VF was proved in all studied illumination versions with $p< 0.05$ by the *Student's t*-criterion.

An analysis of illumination efficiency integral indices proceeding from visual working capacity showed that LEDI conditions facilitated a greater visual working capacity and a lesser VF.

An analysis of the obtained results reliably confirmed the fact LEDI does not influence negative visual organs and visual working capacity indices (age group of 20–25 years).The studies performed under different illumination conditions (LEDI and FLI) revealed both a close connection of sight functions with compensatory and adaptive reaction of an organism, and stability of the adaptive systems responsible for regulation of sensitivity of visual organs and of human body as a whole. The study results can be used to develop practical recommendations for LEDI application.

Finally one should notice that the work on LEDI hygienic evaluation requires a continuation.

REFERENCES

1. Light environment for people: science, industry and law // Svetotekhnika, 2016, #1, pp. 45–49.

2. GOST P 54350–2015 Illumination devices. Lighting requirements and test methods.

3. Building regulations СП 52.13330.2016 Natural and artificial illumination

4. Zheleznikova O.E., Amelkina S.A., Sinitsyna L.V., Kiryukhina S.V. Development of a comprehensive technique to estimate LED illumination conditions influence on state of human visual organs and organism as a whole // Natural and technical sciences, 2013, #5 (67), pp. 249–257.

5. Aksenova S.V., Kulikova M.P., Zheleznikova O.E., Sinitsyna L.V., Amelkina S.A. A method of visual fatigue determination / Patent of Russia #2534910. 2014. Bulletin #34.

6. Kuchma V.R., Teksheva L.M., Sukhareva L.M., etc. Hygienic basis of light emitting diode use in artificialillumination systems. – Moscow: Scientific Centre of Children Health Federal State Budgetary Institution of the Russian Academy of Medical Science, 2013, 246 p.

7. A practical on labour physiology / Editored by K.S. Tochilov. Leningrad: Publishing house of the Leningrad State University, 1970, 251 p.

Svetlana A. Amelkina,
Ph.D., Associate Professor, graduated from the Lighting Faculty of the MSU of N.P. Ogarev in 1989. At present, she is an Associate Professor of the Lighting Engineering Chair of the MSU of N.P. Ogarev

Olga E. Zheleznikova,
Ph.D., Associate Professor, graduated from the Lighting Faculty of the MSU of N.P. Ogarev in 1989. At present, she is a Head of the Lighting Engineering Chair of the MSU of N.P. Ogarev and an honoured worker of the higher school of Republic of Mordovia

Lyudmila V. Sinitsyna,
Ph.D, Associate Pprofessor, graduated from the Lighting Faculty of the MSU of N.P. Ogarev in 1989. At present, she is Associate Professor of the Lighting Engineering Chair of the MSU of N.P. Ogarev

Light & Engineering
Vol. 26, No. 3, pp. 88–94, 2018

Svetotekhnika
No. 5, 2018

PRACTICE AND DISCUSSION ON LIGHTING DESIGN OF URBAN LANDSCAPE BRIDGE

Wenting ZHANG* and Jianjun WNAG

Chang'an University, Xi'an, Shaanxi, 710061, China;
**E-mail: 209959209@qq.com*

ABSTRACT

The design status of an urban landscape bridge lighting system was analyzed via system analysis. Through the evaluation of eight two-level, 24 three-level, and five four-grade indexes on the basis of three aspects, namely, design process, electricity consumption calculation, and lighting effect. The hierarchy framework and index relationship of the entire system were clearly defined. Many angles reflected the links involved in the design of bridge lighting system. The neural network method was used in verifying the screening results to provide a comprehensive indicator specimen for establishing the evaluation system of the system. On the basis of the knowledge and experience of experts, information was processed, and the subjective influence and uncertainty of human calculation could then be reduced.

Keywords: urban landscape, bridge, lighting, Delphi method, ter Faye Fa screening method, neural network method

1. INTRODUCTION

Urbanization and urban landscape designs revolve around the city. In the past, development of bridges involved natural stone beams or plants. Trees were commonly utilized to cross rivers and streams. People used artificial bricks and rattan materials to construct passages in relatively complex environments. With the current development of technology, bridges are developed using special materials and have unique designs with strong structure. Bridges have a single traffic function but have unique structures [1]. With the development and progress of society, lighting has gradually developed from its basic to artistic and quality functions, thereby achieving high-quality vision that satisfies the functional requirements of lighting [2]. Bridges are important structures of urban traffic. These structures across urban rivers are one of the elements of a city. The river itself is also a component of a city. Numerous civilizations begin with rivers flowing to a city. For example, Nanjing on the Huaihe River from Qing Dynasty, Guangzhou on the Pearl River, and Tianjin on the Haihe River. The city centre is the key point of every city's landscape, whether daytime landscaping or night lighting landscape enhances the colour of a city [3]. The bridge on the Urban Central River is different from the city's building. Buildings in most cities are often large, and constructing enhanced buildings is possible. Developing nightscape lighting project involves many attempts with high chance of failure [4]. Therefore, evaluating the lighting engineering of urban landscape bridges is important.

2. STATE OF THE ART

A bridge in a city affects the urban space and the life of people. The longitudinal development of bridges in different periods reflects the changes and levels of social and urban improvements. It also denotes the development in the fields of science, technology, and aesthetics [5]. The night landscape engineering of a bridge is accompanied by the challenge of new lighting requirements due to new technolo-

gy of structural mechanics supported by the bridge itself. Meanwhile, the progress of lighting technology and equipment also has high modification requirements. With the development of social culture, conforming to the general needs of the masses becomes difficult due to the people's increasing aesthetic standards [6]. At present, local and international research on theories and methods of bridge and bridge lighting design has achieved certain results. However, many projects in China have poor quality due to the speed of urban construction. Some of these designs are inconsistent with the development of urban planning, and the connections between the design and construction are poor because of several subjective reasons. The lighting of bridges is an important landscape of the city centre. The entire display directly affects the image of a city and the daily life of people [7]. Along with the development process of a city, a bridge night scene project should not only compete with regard to beauty but also with times; hence, constant upgrade is necessary, which requires the research and summary of the same bridge project to provide information for upgrading. The overall cost of a bridge night lighting project is large; however, sometimes the effect is not so good. The two designs involve additional manpower and material resources. Therefore, the practice and discussion of the design of urban landscape bridge lighting has practical importance.

3. METHODOLOGY

3.1. Preliminary Screening of ter Faye Fa Index

In comparison with other methods that tend to delete concepts, ter Faye Fa is a screening method with direction verification. Therefore, the preliminary screening of the electrical efficiency of the lighting system of a bridge was implemented using the Delphi method. Ter Faye Fa is a method that uses expert knowledge and experience. Experts were consulted with regard to the design of evaluation indicators and statistical processing and they provided feedback after the consultation. When the expert opinion is consistent after the poll, the final target was determined [8]. Ter Faye Fa is an internationally recognized forecasting and decision-making method for establishing a system engineering evaluation system. Anonymous method was not utilized to obtain information from an expert. The experts can modify the initial feedback within a specified time. After collecting all the information, the feedback data were processed mathematically according to ter Faye Fa's criterion, and the index was initially determined. The ter Faye Fa's main criterion is described below. The expert opinion concentration degree E reflects the recognition degree of the experts to the index. The feedback score of experts was provided, and the weighted average of the number of participated experts is follows:

$$E = \frac{1}{m}\sum_{i=1}^{m} a_i , \tag{1}$$

where m is the number of experts, and a_i is the feedback score. The degree of divergence of expert opinion δ denotes the degree of divergence among experts in a certain factor and is expressed as follows:

$$\delta^2 = \frac{1}{\text{m-1}}\sum_{i=1}^{m} (a_i - E)^2 . \tag{2}$$

The restricted values of E and δ can be set to E_0 and δ_0, respectively depending on a specific problem. When equations 3 and 4 are satisfied, the index is retained.

$$E_1 > E_0 , \tag{3}$$

where E_i is the concentration value obtained by using specific indicators, and E_0 is the set concentration limit value.

$$\delta_i < \delta_0, \tag{4}$$

where δ_i is the discrete-time value obtained for a specific index, and a is the set of discrete-time limits. The experts involved were four lighting design experts, two lighting experts, two pedestrians, and two bridge lighting management staff. Given that the degree of evaluation of each electricity efficiency index is relatively vague, the evaluation Table 1 of the degree of impact was set. As shown in the table, the score system does not adopt the 10 % or the percentage system because it is evaluated according to the maximum or percentage system. When determining the weight ratio, the information (i.e., the number of [0, l]) was expressed as a percentage that needed to be normalized. Apart from the evaluation of seve-

Table 1. Evaluation of the Influence Degree of Electric Effect

Influence degree	Not very important	Slightly important	Very important	Obviously important	Absolutely important
Score value	0.1	0.3	0.5	0.7	0.9

Table 2. Level Evaluation Parameter of the Table Method

Expert code	01	02	03	04	05	06	07	08	09	10	δ	E
Design process	0.9	0.9	0.9	0.9	0.9	0.9	0.9	0.9	0.9	0.9	0	0.9000
Electric effect measurement	0.9	0.5	0.7	0.9	0.5	0.9	0.7	0.9	0.7	0.7	0.158	0.7400
Lighting effect	0.7	0.9	0.9	0.7	0.9	0.9	0.5	0.7	0.9	0.9	0.141	0.8000

Table 3. Two-stage Evaluation Parameter of the Table Method

Expert code	01	02	03	04	05	06	07	08	09	10	δ	E
Subway characteristics	0.3	0.3	0.3	0.3	0.3	0.3	0.9	0.3	0.5	0.5	0.114	0.3200
Lighting specification	0.7	0.9	0.9	0.9	0.9	0.9	0.7	0.9	0.9	0.9	0.063	0.8800
Selection of lighting	0.9	0.9	0.9	0.9	0.9	0.9	0.7	0.9	0.9	0.9	0.063	0.8800
Lighting control	0.9	0.9	0.9	0.0	0.7	0.9	0.7	0.7	0.7	0.7	0.105	0.8000
Illumination calculation	0.7	0.7	0.7	0.9	0.7	0.9	0.7	0.7	0.7	0.7	0.084	0.7400
Lighting consumption	0.7	0.9	0.9	0.7	0.9	0.9	0.7	0.9	0.9	0.9	0.097	0.8400
Other losses	0.3	0.5	0.5	0.5	0.5	0.7	0.7	0.5	0.5	0.5	0.114	0.5200
Test standard	0.7	0.5	0.9	0.7	0.7	0.9	0.7	0.7	0.9	0.9	0.135	0.7600

ral special indicators, describing conditions with regard to [0, l] values is impossible. Hence, normalization is redundant and unnecessary.

The screening criteria of the ter Faye Fa were set. When the two bits after the decimal point were half adjusted and E is greater than 0.4, an index was assigned to the index set. Thus, the value was only used as an auxiliary reference value. When the degree of divergence is large, the information is collected again until its value reaches a small stable state. Tables 2–4 show the expert evaluation information, E value, and eight values for all levels of indicators, respectively. The 10 experts were anonymous and numbered 01–10. The index at the left side of the table and the number of tables intersected by experts and numbers were scored.

Table 2 presents the evaluation value of the one-level Delphi method. The E value of the three indicators is between 0.7 and 0.9, and they show the importance of the expert opinion. The small a value denotes the consensus of the experts. The design process, electrical efficiency calculation, and lighting effect are used as the evaluation index system. Table 3 depicts the evaluation value of the two-level Delphi method. Among them, the E value of the seven indexes is between 0.5 and 0.9, whereas that of the subway characteristic is 0.32. According to the set of screening criteria, the subway characteristic index should be removed; hence, the subway characteristics are not included in the index set. Meanwhile, the corresponding statistical results of the three-level indicators will not be included. There-

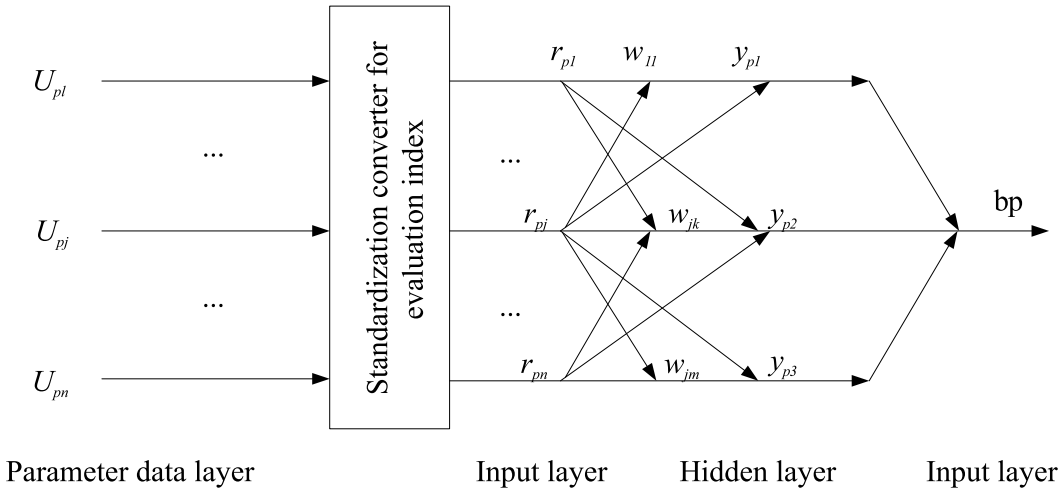

Fig.1. Principle diagram of the BP neural network method

fore, the lighting standard, selection, control, calculation, and consumption of lighting and other losses and verification standards are used as evaluation indicators in the second level.

Given that the lamps and lanterns are covered with additional indicators, the four-level indicators of the luminaire should be evaluated. The five indicators met the requirements and were classified into index sets. By screening the indicators using the Delphi method, three one-level, seven two-level, 20 three-level, and five four-level indicators were present.

3.2. Index Verification Based on Neural Network Method

The basic principle of artificial neural network is similar to that of a human brain. The BP neural network approach is used as the two-confirmation method of the index. In view of the nonlinear relationship between the indexes of the bridge lighting electric effect system, the trained neural network provides the expert evaluation idea of the network through the method of connection right. It can achieve a suitable output to the input of the non-centralized sample and can accomplish an approximation function. Moreover, the network can well simulate the quantitative evaluation of experts. Hence, subjectivity and uncertainty in the evaluation can be avoided. Fig.1 shows the diagram of the principle of BP neural network.

n represents the input node (i.e., the number of evaluation indicators), *m* denotes the number of hidden nodes, and $\mathrm{U}_{p1},\mathrm{U}_{p2},...,\mathrm{U}_{pn}$ is the evaluation index value of the P sample model on the $X=\{x_1,x_2,...,x_n\}$ of the evaluation index, remember $\overline{\mathrm{U}}_{\mathrm{P}}$. The formula is as follows:

$$\overline{\mathrm{U}}_{\mathrm{P}}=\{\overline{\mathrm{U}}_{\mathrm{P1}},\overline{\mathrm{U}}_{\mathrm{P2}},...,\overline{\mathrm{U}}_{\mathrm{Pn}}\}^{\mathrm{T}}=(\overline{\mathrm{U}}_{\mathrm{Pj}})_{\mathrm{h\times n}}, \tag{5}$$

where r_{p1}, r_{p2},...,r_{pn} is the evaluation vector $\bar{r}p$ after quantizing the standard converter of *X* upper body, which can be expressed as follows:

$$\bar{r}p=\{\mathrm{r}_{\mathrm{p1}},\mathrm{r}_{\mathrm{p2}},...,\mathrm{r}_{\mathrm{pn}}\}, \tag{6}$$

where $w_{jk}\,(j=1,2,...,n;k=1,2,...,m)$ is the connection weight between the first nodes of the input layer and the *k* node of the hidden layer, $y_{pk}\,(k=1,2,...,m)$ is the output of the hidden layer (*k* node) of sample mode *P*, $w_k\,(k=1,2,...,m)$ is the connection weight between the *k* node and its output layer, and BP is the output of sample pattern *P*. The algorithm of the BP neural network evaluation was described using the sigmoid function, which is expressed as follows:

$$f(x)=(1+\exp(-x))^{-1}. \tag{7}$$

The output y_{pk} of the hidden layer sample pattern *P* is calculated as:

$$y_{pk}=f(\sum_{j=1}^{n}w_{jk}r_{pj}-\theta_k), \tag{8}$$

where $k=1,2,...,m;\theta_k$ represents the bias value of the hidden layer (*k* node). The output $b`_p$ of the output layer sample pattern *P* is calculated as:

$$b`_p=f(\sum_{k=1}^{m}w_k y_{pk}-\theta), \tag{9}$$

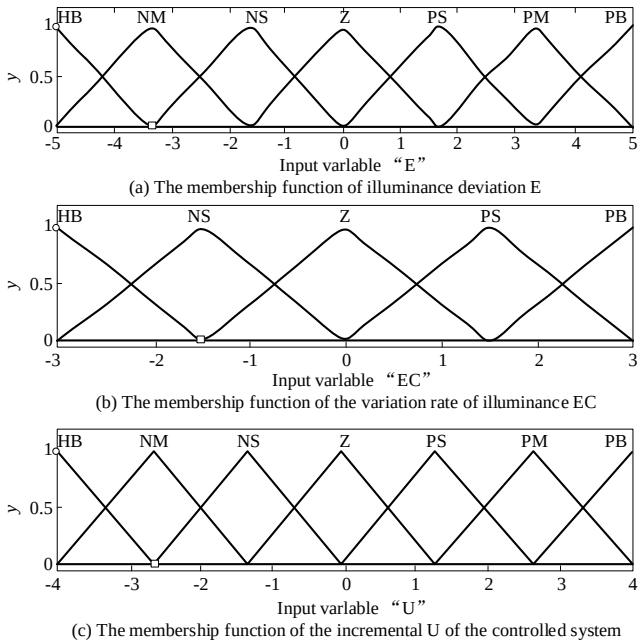

(a) The membership function of illuminance deviation E

(b) The membership function of the variation rate of illuminance EC

(c) The membership function of the incremental U of the controlled system

Fig.2. Subordinate function of the fuzzy controller

where θ represents the offset value of the output layer (or node). The trainer of the BP neural network is based on the process of error back propagation and correction, and it defines the total error function of the actual output $b`_p$ of the *h* sample pattern. The expected output mass is *E*, as shown as follows:

$$E = \sum_{p=1}^{h} (b`_p - b_p)^2 / 2. \qquad (10)$$

4. RESULT ANALYSIS AND DISCUSSION

4.1. Research on fuzzy feedback controller

The input/output variable of the feedback controller is determined. In this design, the feedback controller is a two-dimensional fuzzy controller, that is, the double input and output mode. The input variables are the illuminance deviation *E* and the deviation rate *Ec*. The output is the controlled system increment. This method not only can ensure the stability of the control system but also reduce overshoot and vibration. The membership function *M* for the input/output variable is determined. A membership function is a fuzzy set that should be applied to address practical problems. Accurate construction of membership functions can lead to the full usage of the key of fuzzy sets. The triangular membership function is used in the system, and the MATLAB fuzzy toolbox is used to identify the GUI function editor. Fig. 2 shows an example of a fuzzy controller.

The characteristics and factors of the input/output variables are selected. For this fuzzy controller, the domain of the input variable, according to the experience of the expert, should be "PB" for the maximum value of the language if the value of the system deviation *E* is more than or equal to 20 lx. The value of *E* is less than or equal to 20 lx, which is "NB". Therefore, the range of *E* is [–20, 20], and the fuzzy set theory domain is [–5, 5]. The value of the quantizing factor *Ke* is 0.25. Generally, *E* of fuzzy controller input variables is not equal to the range of deviation in the system operation. A limiter should be added in the actual control to ensure that the error is within the allowed range.

Similarly, the domain and the controller output and error variation factors can be determined according to the standards of illumination design for civil buildings, the illumination principle of indoor working lighting system, and the international vision ergonomics principle. The standard illumination value is 420 lx, and the luminance area of the luminaire is set to [300, 500]. Therefore, the ratio factor *Ku* of the controller output should be 5. Moreover, error changes must be set according to the actual requirements, where *KEC* is equal to 0.01 in this controller.

In the actual control, the continuous domain should be discrete. For example, the fuzzy set theory domain of *E* error is divided into seven grades, and each grade corresponds to a fuzzy subset. That is {–5, –4, –3, –2, –1, 0, 1, 2, 3, 4, 5} correspond to (NB, NM, NS, ZO, PS, ZO). Then, the elements in the domain were determined and the membership degrees of the fuzzy linguistic variables are identified.

The fuzzy control rule is the core of fuzzy controller, reflecting the knowledge collection of a particular control problem. In the formulation of the fuzzy rules, the following requirements should be met. For the perceptibility, the fuzzy control model should constantly be able to obtain a suitable control function for the each reasoning of process state.

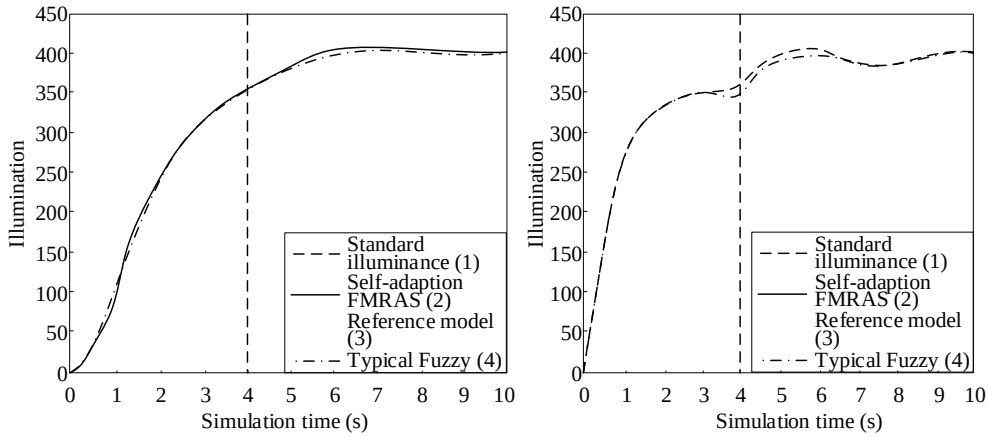

(a) First order contrast diagram (b) Two order contrast diagram

Fig.3. Improved adaptive simulation results

This characteristic is called "completeness," which indicates that a runaway situation does not exist for the number of fuzzy control rules. If the input of a fuzzy controller has *m*, the numbers of fuzzy classifiers for each input are *n1, n2, …, nm*; and the maximum possible fuzzy rule number is *Nmax* = n1, n2, …, nm. The actual number of the fuzzy control numbers depends on many factors. The general principle is to minimize the number of rules to simplify the design and implementation of fuzzy controllers.

In lighting control, the illumination value is mainly affected by natural light. When natural lighting is high, the lamps in the classroom must be closed. Meanwhile, when natural lighting is low, the lamps and lanterns in the classroom must be opened, and the standard value of illumination is guaranteed. This study focuses on the actual lighting control. Fuzzy control table rules, combined with the actual situation and the experience of manual lighting control, can be obtained. The *E, EC,* and *U* were the fuzzy linguistic variables of illumination deviation e, deviation rate *EC*, and output *u*, respectively. This table represents control rules, such as if (*E is* NB) and (*EC is* NB), then (*U* is PB)). Practically, the result must be transformed into a fuzzy control response table. The method of the fuzzy logic control is used to calculate all the input languages *M* (*E, EC*) after quantization and calculate the output table generated by the fuzzy controller of each state. The method is placed in the computer in the form of "file." When a real-time control is performed, determining the control strategy from the file based on the input information is convenient. The fuzzy inference method is used as follows. First, the fuzzy relation *R* is obtained. Then, the fuzzy output is obtained using the synthetic reasoning method according to the input deviation and the variation rate of the deviation. Finally, the fuzzy quantity is transformed to the exact quantity via anti-fuzzification. Thus, the design of the fuzzy feedback controller is complete.

4.2. Simulation and Analysis

The step size is set, and simulation is performed. This simulation compares the classical fuzzy control with the improved adaptive FMRAS to verify the progressiveness and experimentation of the improved model and ensure that the control rules and quantization factors of the input/output variables are the same. The results are shown in Fig. 3. Fig. 3(a) presents the result of the performance comparison between the improved adaptive FMRAS and classical fuzzy control in the first-order system. Fig. 3(b) shows the comparison of the performance results of the improved adaptive FMRAS and the classical fuzzy control under the two-order system.

As shown in the figures, in comparison with the typical fuzzy controllers commonly used at present, the adaptive FMRAS has the following advantages: good tracking performance, high steady-state accuracy, small overshoot, and high response speed. It can meet the illumination requirement of the bridge and achieve the design goal.

5. CONCLUSION

Designs of urban landscape bridge lighting are the growing concern of the public. Night landscape lighting project is important regardless of the structural design and implementation. ZigBee techno-

logies, such as embedded ARM, sensor, and other lighting systems, are combined to design a city landscape bridge lighting control system. Through the evaluation of eight two-level, 24 three-level, and five four-grade indexes on the basis of three aspects, namely, design process, electricity consumption calculation, and lighting effect, the hierarchy framework and index relationship of the entire system are clearly defined. Many angles reflect the links involved in the design of bridge lighting system, providing an omni bearing indicator specimen for establishing the evaluation system of the bridge lighting system. The neural network is used to validate the screening results. The information is processed on the basis of the knowledge and experience of the experts, and the subjective impact and uncertainty of human weighting can be reduced.

ACKNOWLEDGEMENT

Fund Project: Fund Project of National Science Foundation of China (51208054), Special Fund Project of Fundamental Research Fees of Central Collages

REFERENCES:

1. Hale J D, Davies G, Fairbrass A J, et al. Mapping lightscapes: spatial patterning of artificial lighting in an urban landscape. PloS one, 2013. V8, #5, p.61460.

2. Haiying Li, Xian Li, Xinyue Xu, Jun Liu, Bin Ran. Modelling departure time choice of metro passengers with a smart corrected mixed logit model – A case study in Beijing. Transport Policy. 2018, #69, pp.106–121.

3. Johansson E, Emmanuel R. The influence of urban design on outdoor thermal comfort in the hot, humid city of Colombo, Sri Lanka. International journal of biometeorology, 2006. V51, #2, pp.119–133.

4. Hayden D. Urban Landscape History. The People, Place, and Space Reader, 2014, p.82.

5. Lee Y C, Ahern J, Yeh C T. Ecosystem services in peri-urban landscapes: The effects of agricultural landscape change on ecosystem services in Taiwan's western coastal plain. Landscape and Urban Planning, 2015. V139, pp.137–148.

6. Gaston K J, Davies T W, Bennie J, et al. Reducing the ecological consequences of night-time light pollution: options and developments. Journal of Applied Ecology, 2012. V49, #6, pp.1256–1266.

7. Wuren G, Yang X, Xia J. To Explore the Urban Landscape Lighting Development in China – Taking the City of Shanghai as an Example. Acta Oeconomica, 2015. V65, #s2, pp.251–265.

8. Garrido-Jiménez F J, Magrinyá F, del Moral-Ávila M C, et al. The Relationship Between Urban Morphology and Street Lighting Operating Costs: Evidence from Medium-sized Spanish Cities. Applied Spatial Analysis and Policy, 2017. V10, #3, pp.381–399.

Wenting ZHANG,
mainly engaged in the research of traffic planning and urban landscape at School of architecture in Chang'an University, Shaanxi Province, China

Jianjun WANG,
Prof., Ph.D., Department of Traffic Engineering, School of Highway at Chang'an University, Shaanxi Province, China. The main study filed is the traffic planning and traffic safety

Fig. 2. Panorama of evening Astana. Photo of D. Chistoprudov, *http://www.titus.kz/*

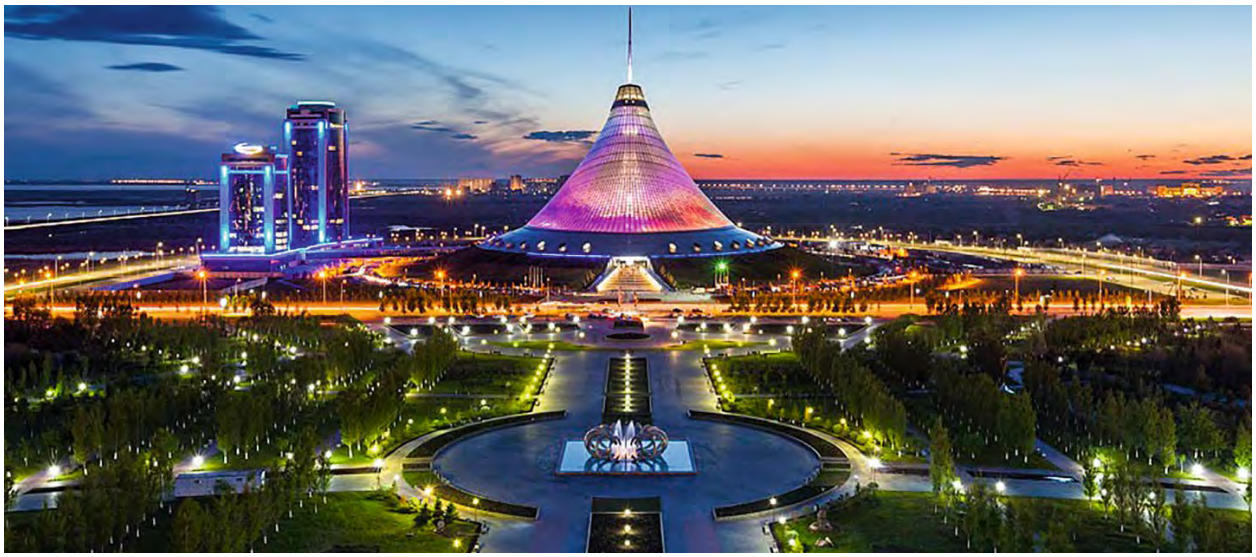

Fig. 5. An evening view of the Khan-shatyr shopping and entertaining centre. Photo of D. Chistoprudov, *http://www.titus.kz/*

Fig. 7. Evening illumination of the Kazakhstan national pavilion of the international specialised EXPO-2017 exhibition. Photo of the EXPO-2017 official site *http://www.expo2017astana.com/*

Fig.2 The glazed façade of the shop in Munich, BMW with a colour exteriorouter and interiorinner dynamic lighting in Munich

Fig. 5. Architectural lighting of exhibition facilities:
a – covering over the festival Area with the Sunsun Tower at EXPO-70 in Osaka;
b – exhibition pavilion " EXPO-200220002 in Hanover

Fig. 6. Architectural illumination of Krasnoyarskaya hydroelectric power station

Fig. 7. Element of technicaltechnological and signal lights in the night panoramic views of oil and gas, chemical and processing facilities:
a – chemical plant in the Sinai desert, Israel; b – oil platform in the North sea; c – complex of the company "Promtekhelektro" in Kstov (Nizhny Novgorod region.)

Fig. 16. Coloured lighting technology Park in a reopenedrevitalized steel mill in Duisburg

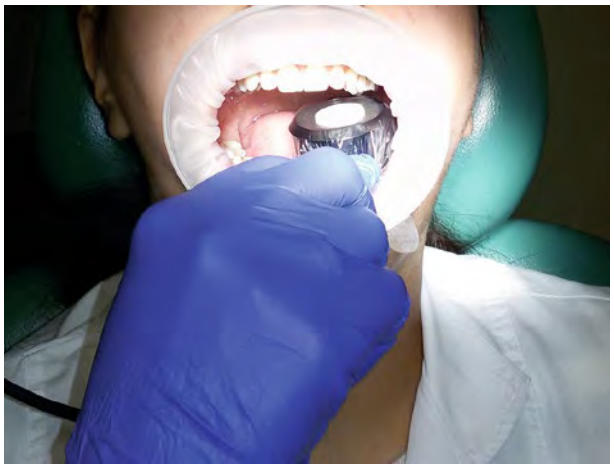

Fig. 1. The illuminance measurement at the lower molar occlusal surface

Fig. 5. Colour filter for LED headlights

Fig. 8. Dental LED turbine handpiece

Fig. 3. Dental unit operating light

Fig. 4. LED headlight

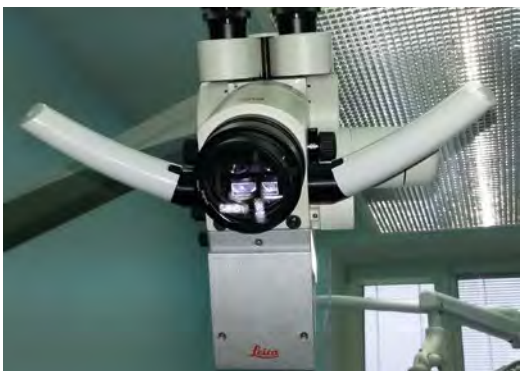

Fig. 6. Dental operating microscope

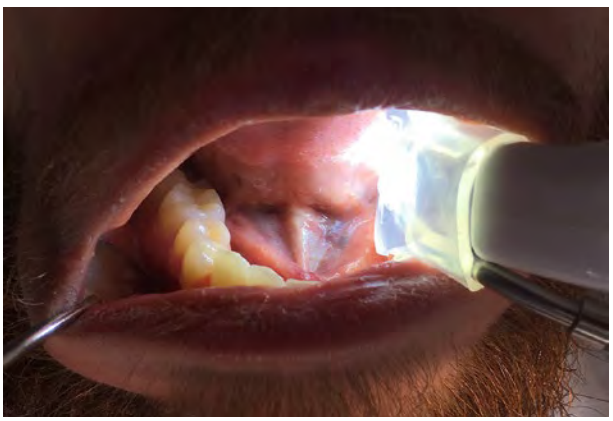

Fig. 9. Intraoral suction&lighting system MaxBite

Light & Engineering
Vol. 26, No. 3, pp. 99–108, 2018

Svetotekhnika
No. 3, 2018, pp. 24–31

OPTIMIZATION METHODS FOR SPECTRAL SYNTHESIZING OF A TUNEABLE COLOUR LIGHT SOURCE

Nina Carli[1], Armin Sperling[2], and Grega Bizjak[1]

[1] University of Ljubljana, Faculty of Electrical Engineering,
[2] Physikalisch-Technische Bundesanstalt, Braunschweig, Germany
E-mail: grega.bizjak@fe.uni-lj.si

ABSTRACT

A method for a tuneable colour light source (TCLS) output spectrum synthesizing is described. A TCLS is a multi-channel LED light source, which is able to mimic and produce different spectral distributions and can be used for the realization of different spectra, e.g. the spectra of different CIE standard illuminants. The synthesizing of output spectrum is actually an optimization problem of tuning the output spectrum of a TCLS to the target spectrum. It is also a so called constrained problem as output spectrum is produced by adding the weighted spectra of used light sources (e.g. single-colour LEDs) and due to the fact that there is no "negative light". Because of that usual optimization methods like least square method cannot be used. A novel synthesizing method based on a constrained optimization process was developed and tested on the laboratory TCLS to be used for calibration purposes. The developed synthesizing method, described in this paper, gives good results but comparison with more simple methods shows that also these can be successfully used.

Keywords: LED, tuneable colour light source, synthesized spectral power distribution, constrained least squares problem

1. INTRODUCTION

Tuneable colour light sources (TCLS) are suitable for different purposes and can be used in laboratories or in our everyday lives. TCLS are actually multi-channel light sources based on LEDs, which are able to mimic spectral power distributions (SPDs) of different light sources and also different CIE Standard Illuminants, even those which are only defined by mathematical models.

Spectra of modern light sources based on light emitting diodes (LEDs) are much different from spectra of classical light sources. To reduce measurement uncertainty of new LED based products, measurement equipment (photometers) should be calibrated not only with sources providing the spectrum of CIE Standard Illuminant A but also with sources providing a spectrum which is very close to the one intended to be measured. That is why a TCLS can be very useful in a photometric laboratory. As it is designed to simulate any chosen spectrum, it can be used for calibrations of equipment with varying spectra, so reducing the number of different calibration light sources in use in a laboratory. But as it will be used for calibration it is important that such a laboratory TCLS is able to produce various SPDs with defined and stable photometric or colorimetric parameters like luminance, correlated colour temperature (CCT), colour coordinates (x, y), or colour rendering index (CRI).

To be able to utilize the TCLS, described in [1], for calibration and research purposes a new set of LEDs was installed, and a new control program was written. The main purpose of the TCLS will be the calibrations of measurement devices at a series of different spectra, so the TCLS needs to enable fast and precise setting of the wanted spectrum.

The core of the control program is a synthesizing process for TCLS output spectrum. It needs to give the best possible solution; in our case this is an output spectrum which should be as close to the target spectrum as possible and in an acceptably short time. As the TCLS output spectrum needs to be very close to the target spectrum, the synthesizing process was based on an optimization method where the difference between output and target was used as an optimization criterion. The development and testing of the synthesizing process is described below.

2. SYNTHESIZING OF THE SPECTRUM

The idea behind the TCLS based on LEDs was to build a device capable of producing any wanted spectrum in the spectral range covered by the LEDs. The initial version of the TCLS was built with the help of an integrating sphere equipped with 24 different so-called monochromatic LEDs installed in a circle around the output port so as to illuminate the back of the sphere. Although called monochromatic, used LEDs actually emit a narrow bandwidth of light with FWHM (Full width at half maximum) between 15 nm and 35 nm as it can be seen in Fig. 3.

The LEDs are placed so that they cannot be seen directly from the output port. As shown in Fig. 1, the output port of the TCLS is also equipped with a baffle tube containing four apertures to minimize the entrance of stray light from the environment into the sphere. In the sphere, the spectra of LEDs used are mixed by multiple diffuse reflections and the output port provides access to a uniform luminous area approximating the synthesized spectrum. A multi-channel DC power supply is used to control each LED individually by a set current. The DC power supply is connected to the PC via a GPIB bus, which enables the LEDs control by computer program. The sphere also includes a fibre-optic port for a spectroradiometer, which is connected to the same PC. The measured spectral data is processed by the control program written in a LabVIEW environment, which can be used to control and also to regulation of the TCLS output.

There are a lot of articles related to the topic of tuneable colour light sources based on LEDs, and also how to fit the synthesized spectrum as close to the wanted spectrum as possible. Different studies have tried to find the best way to mimic a spectrum of different CIE standard sources and other illuminants. Fryc et al. [2] proposed a tuneable light source using LEDs in the (380–780) nm region, with a simple but slow iterative optimization procedure. Wu et al. [3] introduced a pruning process to achieve the smallest difference between optimized and wanted spectrums by removing improper LEDs, thereby finding an optimal set of LEDs. The results in the paper are very promising, but unfortunately, we were unable to recreate the procedure as not all steps are fully described in the paper. Luo et al. [4] proposed a stochastic radial basis function algorithm for nonlinear optimization of an LED-based spectrum, where a minimization of colour difference equation was included.

Procedures in the mentioned papers are all derived from the Gaussian optimization method, which is based on a minimization of the sum of squared differences between the spectrum synthesized by TCLS and the target spectrum. The least squares solution does indeed give the optimal result, but it can also contain some negative values of coefficients, which cannot be realized in the case of TCLS, because in this case the obtained coefficients actually represent light outputs of LEDs, where negative coefficients would mean negative light output subtracting this from synthesized light which is physically not possible. Therefore, an enhanced or a different optimization method, which would give the best result by taking into consideration that calculated values of coefficients need to be positive or equal to zero, needed to be found.

On the other hand, the Gaussian optimization method which is a basic mathematical procedure for the calculations of best fit solution coefficients – or at least their initial values – is very simple. According to [5], the Gaussian optimization method can also be used to find a constrained solution, but only if we define these constraints correctly and in a proper way. The ability of Gaussian optimization method to solve least squares problems with linear inequality constraints allowed us to base our synthesizing procedure on Gaussian optimization method also.

3. OPTIMIZATION METHODS WITH CONSTRAINTS

A lot of different optimization methods, which take into consideration some sort of constraints, are described in available articles. The one by Tosic and

Frossard [6] presented the main challenges in the research field of dictionary learning for dimensionality reduction. They focused on the development of novel algorithms for building dictionaries of subspaces that provide efficient representations of classes of signals. Since sparsity constraints are the keys for solving dictionary learning problems, they are all based on sparse approximation. Chun et al. [7] tested optimization methods to minimize reconstruction error and the number of LED sources using these sparse coding techniques from Tosic and Frossard [6]. Lawson and Hanson [5] described a procedure of a non-negative least squares (NNLS) problem which proved to be optimal for a non-negative problem with certain inequality constraints. Bro and De Jong [8] proposed a fast non-negativity-constrained least-squares algorithm, which is based on a standard NNLS algorithm in [5]. In some cases, it converges faster, but the basis of the procedure stays very similar. However, Cantarella and Piatek [9] announced a freely available C implementation of a sparse constrained least-squares problem. The code matches the accuracy of Matlab's function lsqnonneg [10], which is again based on method described in [5]. Cantarella's and Piatek's code works much faster than Matlab's function, and it is more suitable for very large problems.

Due to the fact that many articles use the non-negative least squares (NNLS) method for solving different problems, we can assume that this method gives an optimal solution for the non-negativity least squares problem with certain inequality constraints. This is why we also used it for optimization of TCLS output spectra. Below, we first present a brief description of the Gauss least squares optimization algorithm and second, we present an overview of the main algorithm that uses the NNLS method.

3.1. Gauss Optimization Method

The Gauss algorithm is used to solve non-linear least squares problems. The problem is called 'least squares' because we are minimizing the sum of squares of residuals. In case of TCLS the residuals are differences between the obtained output spectrum of TCLS and target spectrum at the observed wavelengths. The output spectrum of TCLS, denoted with $S_o(\lambda)$ is synthesized from M spectra of LEDs, so it can be represented with the help of the following equation:

$$S_o(\lambda) = \sum_{i=1}^{M} k_i \cdot S_i(\lambda), \tag{1}$$

where $S_i(\lambda)$ denotes the SPD of the i-th LED in the set of LEDs, k_i are their synthesis coefficients and M is the number of LEDs in set. The SPDs of used LEDs can be defined at chosen wavelength e.g. at every 1 nm from 380 nm to 780 nm if we want to use TCLS in the visible part of the spectrum only. The sampled target spectrum can be denoted by $S_t(\lambda)$. So the residual function R, which represents sum of squared differences between target and output spectrum can be written as:

$$R = \sum_{\lambda=380}^{780} \left(S_t(\lambda) - S_o(\lambda)\right)^2. \tag{2}$$

Taking into consideration equation 1, R can be further written as:

$$R = \sum_{\lambda=380}^{780} \left[S_t\ \lambda) - \sum_{i=1}^{M} k_i \cdot S_i(\lambda) \right]^2, \tag{3}$$

or in matrix form:

$$R = \left\| \mathbf{S_t} - \mathbf{S_{LED}}\,\mathbf{K} \right\|^2, \tag{4}$$

where $\mathbf{S_t}$ is a target spectrum in a vector form with values defined at chosen wavelengths, $\mathbf{K}$ is a vector of synthesis coefficients and $\mathbf{S_{LED}}$ is a matrix composed of spectra of used LEDs defined at the same wavelengths as $\mathbf{S_t}$. Taking into consideration the wavelengths between 380 nm and 780 nm with step of 1 nm vectors $\mathbf{K}$ and $\mathbf{S_t}$ have 401 elements and $\mathbf{S_{LED}}$ is a matrix with 401 x M elements like presented below:

$$\mathbf{S_{LED}} = \begin{bmatrix} d_1\ 1) & d_2(1) & \cdots & d_M(1) \\ d_1(2) & d_2(2) & \cdots & d_M(2) \\ \vdots & \vdots & \ddots & \vdots \\ d_1(401) & d_2(401) & \cdots & d_M(401) \end{bmatrix}, \tag{5}$$

where $d_n(i)$ is the value of spectrum of n-th LED at i-th wavelength.

The expression in (4) represents the over-determined system of 401 linear equations with M unknowns. Based on Gauss and Legendre discovery

the solution for **K**, which minimize the expression in (4), can be found by:

$$\mathbf{K} = \left(\mathbf{S}_{\mathbf{LED}}^{\mathbf{T}} \cdot \mathbf{S}_{\mathbf{LED}}\right)^{-1} \cdot \mathbf{S}_{\mathbf{LED}} \cdot \mathbf{S}_{\mathbf{t}}, \tag{6}$$

where

$$\mathbf{S}_{\mathbf{LED}}^{\mathbf{T}} \cdot \mathbf{S}_{\mathbf{LED}}\Big)^{-1} \cdot \mathbf{S}_{\mathbf{LED}} = \mathbf{S}_{\mathbf{LED}}^{+} \tag{7}$$

is the Moore-Penrose [11, 12, 13] pseudo-inverse of spectra matrix $\mathbf{S}_{\mathbf{LED}}$..

Unfortunately, in our case the synthesis coefficient vector **K** obtained may or may not be the optimal solution. This is, because in general **K** may contain some negative coefficients which would mean that these LEDs need to produce a negative amount of light. As this is not possible, thus calculated optimal output spectrum cannot be realized practically. This is the reason why we need to include additional constraints in our calculation: the optimal output spectrum will be the one with the smallest *R* and only positive synthesis coefficients.

3.2. Algorithm for Non-negative Least Square Problems

The resulting problem is so called non-negative least squares problem (NNLS) and can be in general defined by the statement:

$$\text{minimize } \|\mathbf{Ax} - \mathbf{b}\|, \text{ subject to } \mathbf{x} \geq 0, \tag{8}$$

where **A** is the *m x n* matrix, where $m \geq n$, **b** is the *m* element data vector, and **x** is the *n* element solution vector. An optimal solution for the set of linear equations $\mathbf{Ax} \approx \mathbf{b}$ must be found, where $\mathbf{x} \geq 0$. In our case the matrix **A** represent the matrix of LEDs spectra ($\mathbf{S}_{\mathbf{LED}}$) of the used (and measured) LEDs, where *n* is the number of LEDs and *m = 401* is the size of the sampled SPD vector with data at 1 nm step from 380 to 780 nm. The vector **b** represents the target spectrum $\mathbf{S}_{\mathbf{t}}$ and has the same size *m = 401* and **x** contains the optimal solution, in our case optimal synthesis coefficients **K**.

The NNLS problem can be solved with different algorithms. The first widely used algorithm was described by Lawson and Hanson in [5] and has nine steps. The procedure starts with setting all elements of **x** to zero, creating set **Z**, containing all indices, and empty set **P**. In the main loop the gradient vector **w** is calculated with the current value of **x**, with the equation

$$\mathbf{w} = \mathbf{A}^{\mathbf{T}} \ \mathbf{b} - \mathbf{Ax}\big). \tag{9}$$

If **Z** is empty or if all elements of **w**, with indices in **Z**, have values ≤ 0, we have a solution, therefore the procedure terminates. Otherwise in the next step the maximum element of **w** is moved from set **Z** to **P**. If any of the elements have negative values, only a fraction of **Z** can be accepted as a trial solution. So we need to find an index *q* such that

$$\alpha = \frac{x_q}{(x_q - z_q)} \tag{10}$$

is the minimum of all such expressions for negative elements of **Z**. With the expression α for this *q* the linear sum

$$\mathbf{x} = \mathbf{x} + \alpha \ \ \mathbf{z} - \mathbf{x}\big) \tag{11}$$

can be calculated. In the last step all indices for which the corresponding elements of *x* is zero, are moved from set **P** to **Z**. These will include x_q, but may also include other elements as well. When the procedure converges, set **P** is a vector of synthesis coefficients.

At the end not all elements of *x* are positive and in **P**. Some of them are left in **Z** with the value of 0. In the case of TCLS that means not all LEDs will contribute to the synthesized output spectrum. The needed ones will be supplied with the proper currents based on values of positive synthesis coefficients in **P** (or in **K** in our case) and the other will be switched off as their synthesis coefficients have value 0.

3.3. Other Simpler Methods to Get the Optimal Solution

The described mathematical procedure is not very complicated but might cause some problems if we would need to implement it in some simple TCLS, e.g. controlled with microcontroller. Even when it was implemented within the LabVIEW program to control the TCLS, we had some difficulties and the control program was rather slow. That's why we also tested some simpler "optimization" procedures.

These additional procedures were designed to be easier to implement in the LabVIEW or even microcontroller environment. To shorten the calculation time, the Gauss optimization method was used as a starting point. As described in 3.1, the main problem of Gauss optimization procedure is that the vector of optimal coefficients that we get with equation (6) can contain some negative values, which cannot be realized practically. Hence, the first approach is to exclude the LEDs with negative coefficients from the used set of LEDs and synthesize the output spectrum only with LEDs with positive coefficients. This is a very fast and simple method but the results are in most cases not very good. As we use only a small number of LEDs to synthesize the target spectrum the residual *R* (equation 4) is in most cases rather large.

Beside this basic method, which excludes all LEDs with negative values at once (no iterations), we also tested four other methods, which exclude LEDs with negative values step by step until only LEDs with positive values are left in the set and Gauss optimization procedure gives only positive synthesis coefficients. The three tested procedures of excluding LEDs with negative values step by step differ only in the way of excluding the first LED with a negative value. In the first procedure we excluded first the LED with the most negative value of synthesis coefficient. In the second procedure, the LED, which was excluded first, was the one with the least negative synthesis coefficient. In the third and fourth procedure we just excluded the first (last in fourth procedure) LED on a list with the negative synthesis coefficient. At the end of the iterative process when Gauss optimization procedure results in only positive synthesis coefficients, a synthesized output spectrum can be calculated with equation (1), where only LEDs with positive synthesized coefficients are used.

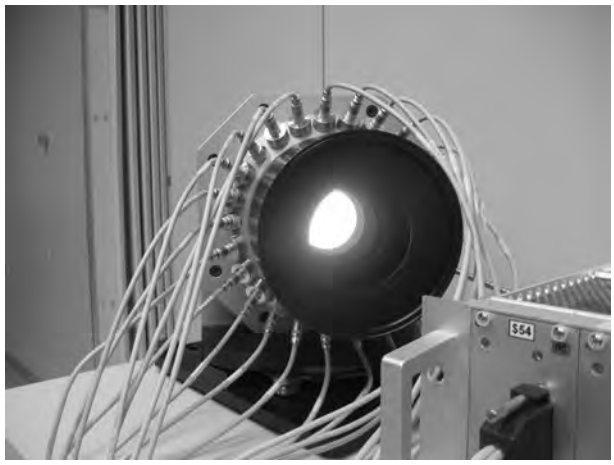

Fig.1. Realization of a tuneable colour light source based on integrating sphere and 24 LED placed around the output port

3.4. Comparison of Optimization Methods

All described methods were tested with the laboratory TCLS and with help of two different sets of LEDs. Since the size of the sphere is limited, the number of LEDs in one set is restricted to 24. The LEDs in the first set were all monochromatic and chosen so that their SPDs would be as evenly distributed throughout the whole visible spectrum range from 380 nm to 780 nm as possible. Such a distribution gives a continuous synthesized spectrum which could, at least in principle, be closer to the different target spectra. If coefficients of some LEDs are zero, when synthesizing target spectrum, currents of these LED's are set to zero. Therefore,

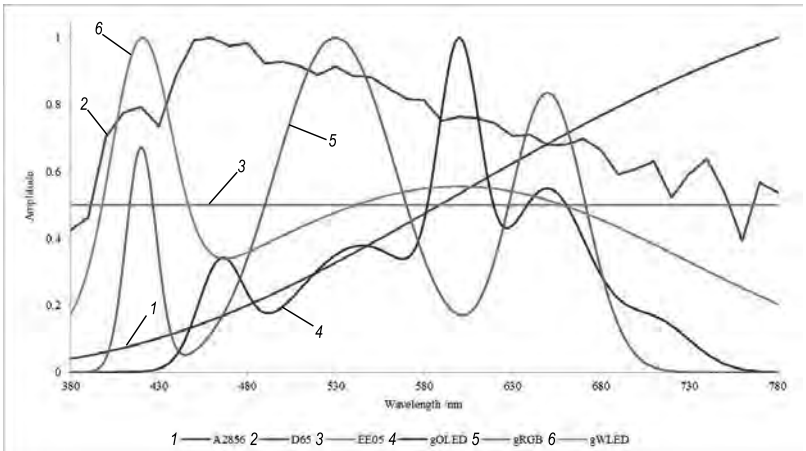

Fig.2. Six different target (wanted) spectra used for testing the TCLS optimization methods

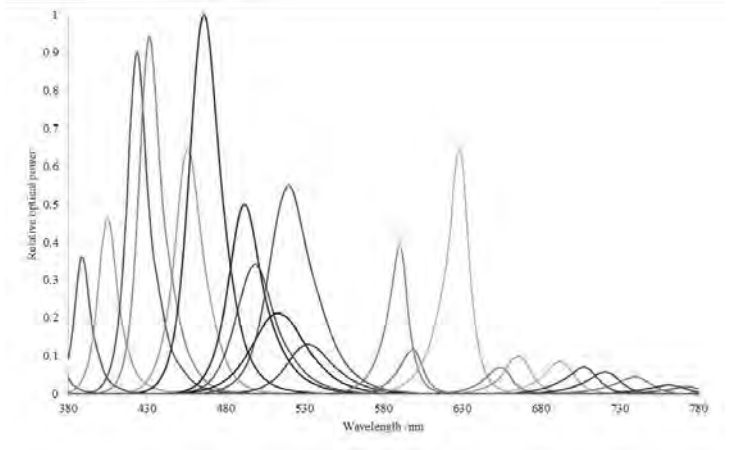

Fig.3. Relative spectra of 24 LEDs used in TCLS, measured at the nominal current of LEDs. Spectra were scaled so that the highest measured peak has a value of 1

these LEDs are not lit up but they stay mounted in TCLS. This is useful, when we want to use the TCLS for synthesizing more than one wanted spectrums. Hence, one LED might be turned off for one optimized spectrum, but is turned on in another synthesized spectrum. If calculations show, that one of the coefficients equals zero in all wanted spectrums, this LED can then be removed from the LED set, since it doesn't impact any of the wanted spectra. In such a case, a new LED can be installed in TCLS. Also in our first realization of TCLS one such LED emerged and it was later replaced with a white LED.

For first tests TCLS was equipped with 24 monochromatic LEDs. We tested it with six different target (wanted) spectra from various types of light sources: CIE standard illuminant A (T_{cc}= 2856 K) and D65 sources, an equal energy source (EE05), a generic OLED source (gOLED), a generic RGB source (gRGB), and a generic cold white LED source (gWLED). The used relative target spectra can be seen in Fig. 2. The spectra of the selected LEDs in the first set with 24 monochromatic LEDs are shown in Fig. 3.

As can be seen from Fig. 3 there is a lack of appropriate LEDs with peak wavelengths (WL) in the "green" region between 520 nm and 590 nm. As expected this caused rather significant deviation in synthesized spectrum from the target spectrum in that specific area.

In Table 1, the relative power of the individual LEDs used in set 1 is listed in the third and sixth columns to show different power outputs of the LEDs. Spectra were scaled according to the one with the maximum power output. Since LEDs with peak WL from 650 nm to 780 nm have rather low output compared to other LEDs, the maximal total luminous flux output of the TCLS may also be very low for some synthesized spectra. The first measu-

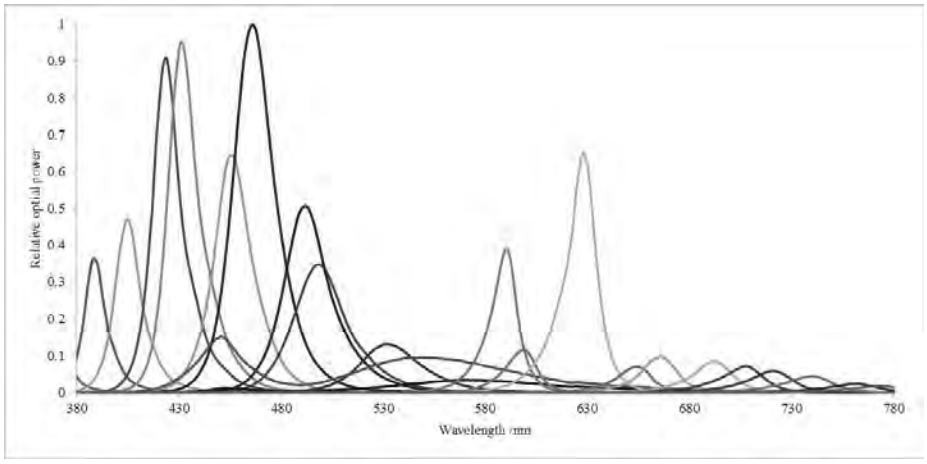

Fig.4. Relative spectra of 24 LEDs in set 2, where two monochromatic LEDs were replaced by warm white and cold white LEDs

Table 1. Peak WL (nm) and Relative Power of Chosen 24 LEDs

LED	Peak WL /nm	Relative peak power	LED	Peak WL /nm	Relative peak power
1	380	0,042	13	590	0,390
2	388	0,361	14	599	0,116
3	405	0,463	15	628	0,648
4	424	0,900	16	654	0,069
5	431	0,943	17	666	0,099
6	456	0,645	18	692	0,086
7	466	1	19	707	0,071
8	492	0,500	20	721	0,058
9	498	0,341	21	739	0,044
10	513	0,213	22	762	0,023
11	531	0,131	23	774	0,018
12	520	0,550	24	780	0,003

Table 2. Peak WL (nm) and Relative Power of White LEDs

LED	CCT /K	Peak WL /nm	Relative peak power
Warm white	3500	572	0.0339
Cool white	8700	451	0.1516

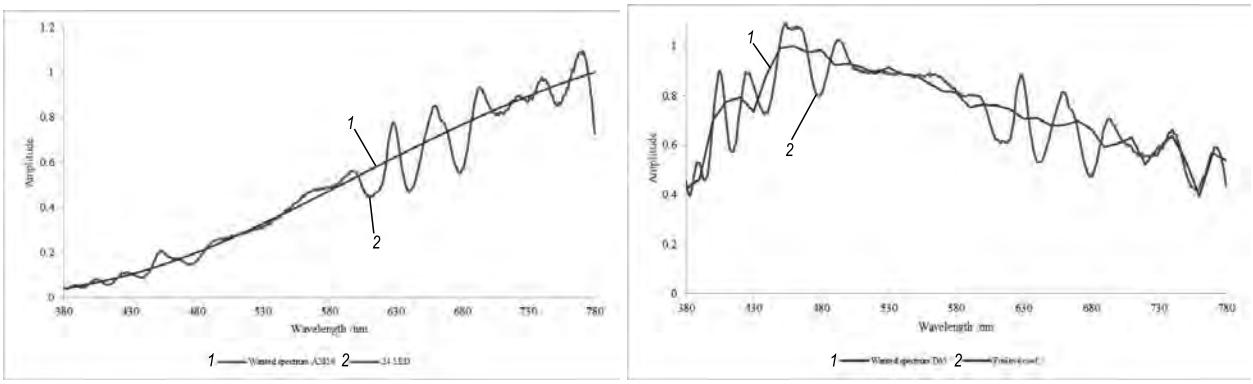

Fig.5. Results of synthesis of CIE Illuminant A spectrum (left) and D65 spectrum (right)

rements showed that the peak value of the 24th LED is very small, and with its peak WL of 780 nm it is also practically out of the visual spectrum. As the total luminous flux of the TCLS depends not only on the chosen target spectrum but also on peak powers of the used LEDs, the mentioned 24th LED always causes a rather low total luminous flux output. Therefore, this LED was not included in most of the tests and was later replaced.

To minimize the deviations from the target spectrum in the range between 520 nm and 590 nm, it was found out during the initial tests that two white LEDs (a warm white LED and cool white LED) will improve the spectrum. Hence, two phosphor-converted white LEDs, one cold-white and one warm white, were added to the set in the second step (Table 2). But because of the limited number of places for LEDs in the sphere, two existing LEDs had to be removed from the set. We removed LED no. 12, whose coefficient was zero with all synthesized test spectra and the LED no. 24, which was not included in most synthesized spectra due to its

Table 3. Comparison of Results of Used Methods with Two LED Sets – the Numbers in the Table are Calculated Residual Functions (*R*)

Synthesized Spectrum	A2856	D65	EE05	gOLED	gRGB	gWLED
Set with 23 monochromatic LEDs (No. 24 not used)						
NNLS	5,6745	15,725	5,847	3,9593	5,805	7,23419
all neg. to zero	132,94	868,42	262,0	92,380	278,2	252,666
most neg. first	5,6745	15,725	5,847	3,9593	5,805	7,23419
least neg. first	5,6824	15,839	5,888	4,1399	5,993	7,26875
first neg. first	5,6824	15,839	5,888	3,7566	5,206	7,26875
last neg. first	5,6745	15,725	5,847	3,9593	5,805	7,23419
Set with 22 monochromatic LEDs and two white LEDs						
NNLS	1,6819	2,6235	1,118	1,3999	2,916	1,71788
all neg. to zero	2,8366	9,5895	3,235	3,9093	6,052	4,28758
most neg. first	1,6819	2,6499	1,124	1,3999	2,916	1,72942
least neg. first	1,6837	2,8188	1,227	1,4000	2,926	1,85828
first neg. first	1,6819	2,6235	1,118	1,3999	2,916	1,71788
last neg. first	1.6837	2.6499	1.124	1.3999	2.916	1.72942

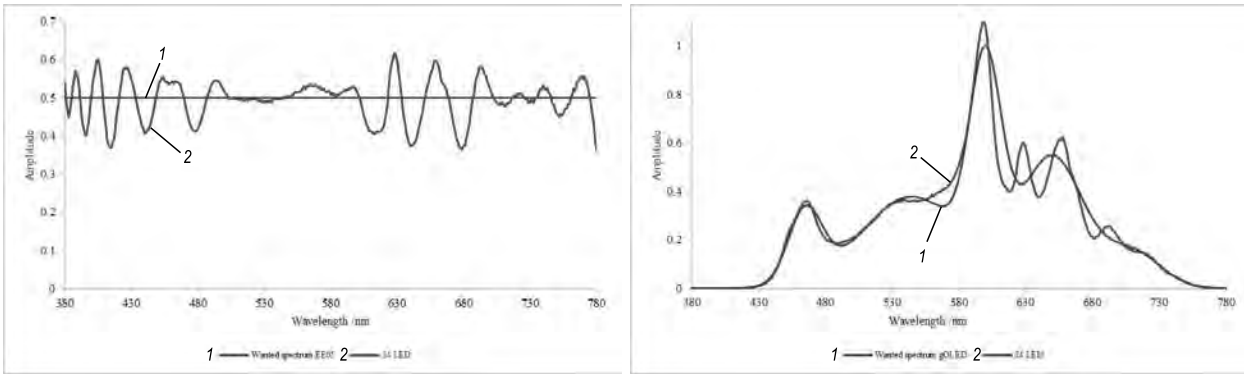

Fig.6. Synthesizes spectra of "equal energy" source (left) and generic OLED source (right)

very low light output. As shown in Fig. 4, the chosen two white LEDs do cover the area of the spectrum between 520 nm and 590 nm.

All described optimization methods were tested with both sets of LEDs. The spectra shown in Fig.2 were used as test target spectra. The comparison of the result is shown in Table 3. The NNLS method serves to find the smallest difference (smallest residual function R) between the synthesized and target spectrum for both LED sets, and hence, represents their best results. With both LED sets the results of at least one other (computing time improved) method (using different expelled LEDs) is equal to the results of the NNLS method. In the first LED set the best results are also given by two of the computing time improved methods, namely the method of excluding the LED with the most negative value first and the method of excluding the last LED with the negative value first. The method that also gives the best results with the second LED set is the method of excluding the first LED with negative value first. Other methods do not give comparable results.

4. RESULTS

The grey cells in Table 3 show the best results with the smallest obtained residual functions. On the basis of the results obtained in the tests, the above described method of NNLS does give the best results and therefore, the smallest deviations

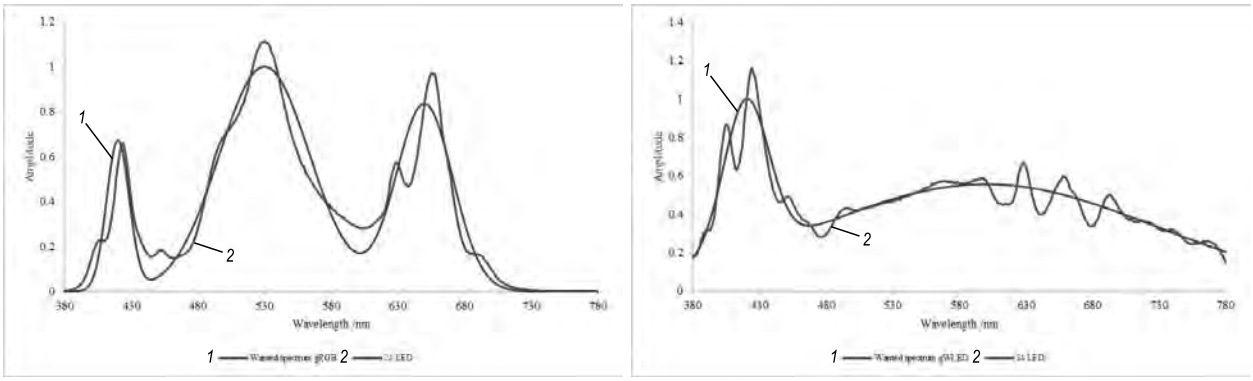

Fig.7. Results of synthesis of generic RGB LED (left) and generic white LED (right)

from the target spectrum with both LED sets. Only the method where all LEDs with negative values are excluded at once after first calculation of synthesis coefficients does not give comparable results, as the values of the residual functions are much higher in all synthesized spectrums. Beside NNLS method also the computing time improved optimization methods can be used equally, as the obtained results are the same or very close in most of cases. In particular, the method, where the LED with the most negative value is excluded first, is very promising. It's much faster and gives results almost all of which match those of the NNLS method

In the Figs. 5–7, the resulted optimized spectra are shown. They are all obtained with the NNLS optimization procedure and with the second set of LEDs containing 22 monochromatic LEDs and two white LEDs.

5. CONCLUSION

The aim of the research described in this paper is to find an optimal mathematical method which gives the synthesized spectrum of multiple LEDs light source as close to the wanted spectrum as possible. Based on literature review an optimization method for finding an optimal solution for the non-negativity least squares problem with certain inequality constraints was tested together with some more simple optimization methods. For the test purposes two different sets of LEDs were used to synthesize six target spectra. The described optimization procedure based on non-negative least square algorithm (NNLS) appears to be very useful for the tested setup, moreover it gives the best results for both tested sets of LEDs. Surprisingly, the results obtained with the much simpler methods, described in chapter 3.3. gave in most cases the same or very similar results compared to the sophisticated NNLS procedure. As expected, the only method with much worse results was the one, where already in the first optimization step all LEDs with the negative synthesis coefficients were taken out of the active set.

Despite the complexity of the NNLS procedure, it is the most adaptable tool for a laboratory tunable colour light source (TCLS) based on integrating sphere and controlled by a LabVIEW environment. However, due to the non-linearity of the current-dependent LED output characteristic which in addition depends on the temporal variation of the junction temperature of the LEDs, the realization of such a controlled TCLS usable for calibration is not so straight-forward as may be expected and it places some demands on the robustness of the NNLS procedure.

REFERENCES

1. Bizjak G, Lindemann M, Sperling A, et al. "Tunable LED colour source," *CIE Symp*, 2010.

2. Fryc I, Brown SW, Eppeldauer GP, et al. "LED-based spectrally tunable source for radiometric, photometric and colorimetric applications," *Opt. Eng.*, Vol. 44 (11), pp. 111309–111309–8, 2005.

3. Wu CC, Hu NC, Fong YC, et al. "Optimal pruning for selecting LEDs to synthesize tunable illumination spectra," *Light. Res. Technol.*, Vol. 44 (4), pp. 484–497, dec. 2012.

4. Luo MR, Xu L and Wang H. "An LED based spectrum design for surgical lighting," *Proc. 28th CIE Sess.*, 2015.

5. Lawson CL and Hanson RJ. "23. Linear least squares with linear inequality constrains," *Solving least squares problems*, Society for industrail and applied mathematics, 1995, pp. 158–173.

6. Tosic I and Frossard P. “Dictionary learning”, IEEE Signal Process. *Mag.*, Vol. 28 (2), pp. 27–38, mar. 2011.

7. Chun S, Kim JC and Lee CS. “Optimization for spectrally tunable lighting control, *Proc. 28th CIE Sess.*, 2015, pp. 2046–2055.

8. Bro R and Jong SD. “A fast non-negativity-constrained least squares algorithm,” *J. Chemom*, Vol. 11 (5), pp. 393–401, sep. 1997.

9. Cantarella J and Piatek M. “Tsnnls: A solver for large sparse least squares problems with non-negative vaiables,” *Comput. Res- Repos: CoRR*, 2004.

10. “Solve nonnegative least-squares constrains problem – lsqnonneg,” MATLAB – Maths Works Deutschland, [Online]. Accessible: http://www.mathworks.com/help/matlab/ref/lsqnonneg.html?requestedDomain=www.mathworks.com. [Accessed: 2-nov-2015].

11. Moore, E. H. (1920). “On the reciprocal of the general algebraic matrix”. Bulletin of the American Mathematical Society. 26 (9): 394–395.

12. Bjerhammar, Arne (1951). “Application of calculus of matrices to method of least squares; with special references to geodetic calculations”. Trans. Roy. Inst. Tech. Stockholm. 49.

13. Penrose, Roger (1955). “A generalized inverse for matrices”. Proceedings of the Cambridge Philosophical Society. 51: 406–413.

Nina Carli,
M. Sc.**,** studied at the Faculty of Electrical Engineering, University of Ljubljana in Slovenia. She graduated in Electrical Engineering with her diploma thesis about the spectrum optimization of tuneable colour light sources. She gathered academic experience during an internship at Physikalisch-Technische Bundesanstalt in Germany, and in Laboratory of lighting and photometry at the Faculty of Electrical Engineering in Ljubljana, Slovenia

Armin Sperling,
Ph.D, studied electrical engineering and semiconductor physics and optics. He received his doctoral degree from the TU Braunschweig in 1994. After six years in research and development in industry, he joined the Physikalisch-Technische Bundesanstalt PTB in 2001 and currently heads the Photometry and Spectroradiometry Department. He is associate Director of the Division 2 of the CIE, Chairman of the German National Committee of the CIE and member of the DIN advisory board of the standardization committee for Light

Grega Bizjak,
Prof., Ph.D**.,** is a Head of Laboratory of Lighting and Photometry at Faculty of Electrical Engineering, University of Ljubljana. He is active in the field of lighting and photometry as well as in the field of electrical power engineering. His main research interests in lighting are photometry, energy efficient indoor and outdoor lighting, use of daylight and use of LEDs in lighting applications. Prof. Bizjak is vice-president of CIE, president of Slovenian National Committee of CIE and representative of Slovenia in CIE Division 2

Light & Engineering
Vol. 26, No. 3, pp. 109–115, 2018

Svetotekhnika
No. 3, 2018, pp. 38–42

DIAMONDS COLOUR MEASUREMENTS

Tatyana V. Shirokikh and Valery E. Ivanov[1]

The Moscow Power Engineering Institute (MPEI NRU) branch in Smolensk
[1] E-mail: phizika@sbmpei.ru

ABSTRACT

As a rule, evaluation of diamond colour is carrying out visually, because creation of the measuring devices is a complex problem due to influence of defects in diamonds (irregularity of coloration, cracks and graphite inclusions). And elimination of this influence is a very difficult task. In this work, an analysis of visual diamond colour evaluation methods and assessment of known devices for objective diamond colour measurements is carried out. As a result, an installation for measuring diamond colour is offered, which as much as possible meets the visual evaluation conditions.

Keywords: diamond, colour, colour evaluation, colorimetry, devices for measurement of diamond colour

1. INTRODUCTION

The visual evaluation of diamond colour is carrying out at a white paper bookmark. The diamond is installed on it with the plane part down, and observation is carried out perpendicular to the diamond spike surface (Fig. 1). Traditionally colour is estimating when illuminating with light of the sky northern part not containing direct solar rays. Therefore, the room for diamond colour evaluation is usually placed in the building northern part. Spectrum of such natural light is characterised by colour temperature and can be classified as *D* type source. CIE [1] recommendation is to use D_{65} source in most cases.

There are several evaluation systems of diamond colour, of which the GIA system proposed by the Gemmological Institute of America is most widespread. In this system, every diamond colour is designating by a letter of Latin alphabet from *D* (completely colourless diamonds) to Z (diamonds with a pale yellow or brown shade). Each letter is followed by the colour description.

In Russia, diamond colour is designating by figures from 1 (colourless highest diamonds) to 9 (dark-brown and black diamonds). Each figure is followed by the colour description, Fig.2, [2].

Small diamonds are divided by colour groups according to Table 1, whereas middle and large diamonds are divided according to Table 2. A comparative analysis of diamond colour groups is presented in Table 3.

At present, diamond colour is estimated under artificial illumination conditions with application of standard light sources D_{65} against the background of white paper (photo – base is a substrate in accordance with GOST 30113) [2]. A working room intended for this purpose should have general illumination of 200 lx illuminance and a local illumination increasing the illumination to (1000–1200) lx [3]. In order to exclude influence of outside co-

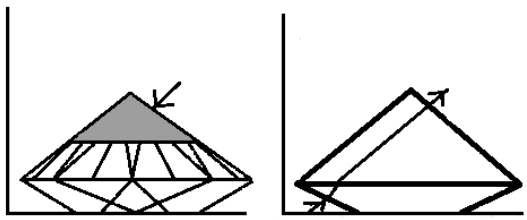

Fig. 1. A diagram of radiation travel through diamond in case of visual colour evaluation

Table 1. Colour Groups of Small Diamonds (to 0.29 carat)

Characteristic	Colour group
Colourless highest, colourless	1
With an insignificant shade	2
With a small yellowish, lilac, grey or scarcely perceptible brown shade	3
With an obviously visible yellow, lemon, grey or scarcely perceptible brown shade	4
Yellow with yellow or lemon colour in the whole diamond, as well as yellow with an insignificant brown shade	5
With a visible brown shade and grey diamonds	6
Brown, yellow-brown and black	7

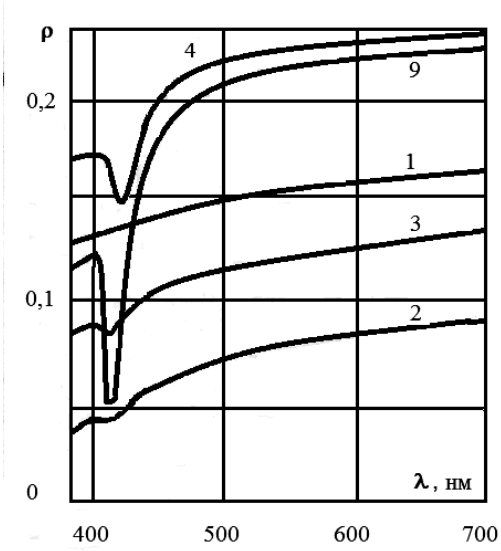

Fig. 2. Spectral reflection factors of diamonds (curve figures designate colour diamond group according to the Russian classification)

lour flare spots on the evaluation results, the room should be painted using an achromatic light paint, and estimators should work in the special white gowns.

2. DEVICES FOR MEASUREMENT OF DIAMOND COLOUR

For an objective diamond colour evaluation, devices not measure colour parameters (colour co-ordinates, colour purity, etc.) but are generally using for correlated values (statistical connected with colour) measuring. Most of such devices measure a relation of direct transmission factors in blue and yellow-green spectrum parts, which is statistically connected with the colour gradations characterising colour saturation of yellow tonality. Transmission factors are usually measured with illumination through the subject plane with a subsequent integration of the rays outgoing through top edges in the integrating sphere. Sometimes, when illuminating through the subject plane, integrating sphere is not applying. In this case, scattered radiation outgoing through bottom edges is measured.

A reason of such measurement method (according to the transmission factor relation) is a specific nature of spectral distribution of diamond transmission factor.

Among foreign devices operating by the principle of measuring a colour correlated value, one can

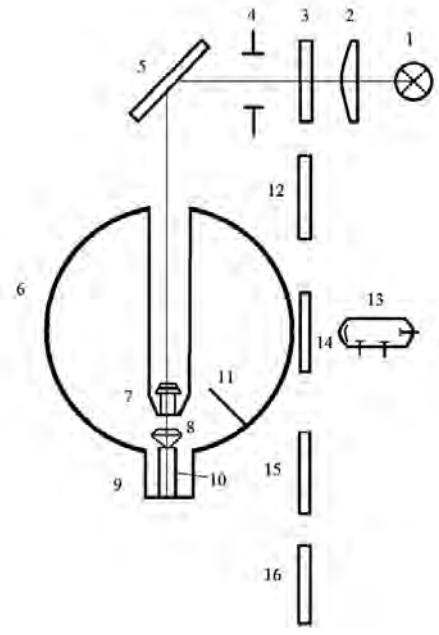

Fig. 3. Optical circuit of the Brilliant-1 device

Table 2. Colour Groups of Middle and Large Diamonds (from 0.30 carat)

Characteristic	Colour group
Colourless highest, as well as with a bluish shade	1
Colourless	2
With a scarcely perceptible shade	3
With an insignificant shade	4
With a small yellowish, lilac or grey shade, as well as with an insignificant brown shade	5
With visible yellow or grey shade	6
With visible brown shade	6–1
With cleary visible yellow, lemon or grey shade	7
Very light-coloured yellow	8–1
Slightly light-coloured yellow	8–2
Little-coloured yellow	8–3
Light-yellow	8–4
Yellow	8–5
Light-coloured brown	9–1
Little-coloured brown	9–2
Brown	9–3
Dark brown and black	9–4

name *Electronic Colorimeter* [5], in which spectral ranges are selected by filters, and the relation is calculated by a computer built in the device. Another device based on interference filters, which name is *Diamond Photometer*, has an indicator, which indications are used to calculate transmission factors, and according to their relation transmission coefficient is calculated.

In Russia, based on such method, the Brilliant-1 device was developed, which layout is given in Fig. 3 [6]. The device basis is integrating sphere 6, in which diamond 8 is installed on support 10 with the plane up. A light beam focused by micro lens 7 is directed to the plane. The micro lens is fixed in the draw-tube and operates in the illuminator circuit with incandescent lamp 1 located in condenser 2 focus, with aperture diaphragm 4 and mirror 5. The radiation outgoing through the top faces is integrating by the sphere and partly passes to radiation receiver (photo multiplier) 13, and the radiation outgoing down falls in nielloed light trap 9. Two pairs of interference filters 3 and 14 or 12 and 15 collect radiation with wave length of 550 nm or 390 nm providing double monochromatization and excluding influence of a possible fluorescence on the measurement results. Gate 16 is used to shut-off light when checking the device “zero”. The sphere has screen 11 excluding incidence of direct rays from a specimen to the receiver.

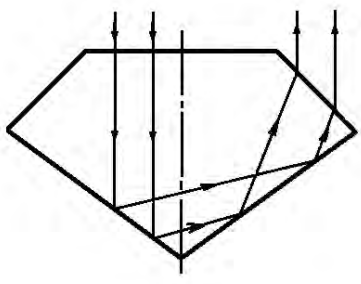

Fig. 4. Travel of light rays in round diamonds

With such illumination and measurement version, the radiation passes a distance within a diamond, which is approximately equal to 1.5 D (where D is diameter of the diamond along the girdle[1]), Fig. 4. This is surpassing radiation distance in case

[1] Girdle is a narrow band determining a diamond configuration, which plane separates the stone bottom from top

Table 3. Comparative Analysis of Diamond Colour Groups

Russian classification		*GIA*	**Characteristic**
To 0.30 carat	**From 0,30 carat**		
1	1 2	*D* *E*	Bluish-white
2	3	*F*	With a scarcely perceptible shade
3	4 5	*G* *H*	Grayish-white, yellowish-white. With a scarcely perceptible yellowness shade
4	6 7	*I* *J*	White with a scarcely perceptible colour shade
5	8 (1–5)	*K-L*	Pale-yellowish shade
6	6 (1)	*M-N*	Yellowish shade
7	9 (1–4)	*O-R* *S-Z*	Yellowish shade. Yellow

of a visual evaluation almost twice. As a result, colour of the measured stone will be more saturated and more yellow than with a visual evaluation. Besides, this installation is intended to measure defectless diamonds. Radiation reflection at cracks, graphite points and smoky inclusions significantly affects the measured diamond colour.

In another correlation method, diamond colouration of yellow tonality caused by reflection factor reduction general for all diamonds in the blue spectrum part is connected with the observed local cavity near wavelength of 415 nm (see Fig. 2). Depth of this cavity is quantitatively characterised by so-called *F*-number (farb-index)

$$F = \frac{\rho_{412}\rho_{420}}{\rho_{415}^2},$$

where ρ_{412}, ρ_{415} and ρ_{420} are reflection factors at the correspondent wavelengths.

Of objective colorimeters adapted to measure classical cut diamond colour, one can name electronic comparator ЭКЦ –1 [7] upgraded in the Scientific Research Institute of Introscopy (SRIIN), Fig. 5.

An initial device is intended to measure colour co-ordinates of diffusely reflecting specimens by the comparison method. In this case, colour co-ordinates differences of the specimen under test and of the compared specimen are measured. The second specimen colour co-ordinates are known in advance. The comparator works in the XYZ system.

The upgradated device is constructed according to a dual-beam principle, which allows alternately illuminating two compared specimens 8 and 10 by means of modulator disc 4 and of one incandescent lamp 1. Light from the lamp being source *A* is directed to the specimens (diamond plane) using a symmetric system containing lenses 2 and 6, prisms 3 and flexible multifiber light guides 7. Output end faces of the light guides are covered with plates of opal glass, which provides illumination of diamond plane part with scattered light, and plate size in this case do not exceed plane size. The radiation passed through specimens is integrated by the integrating sphere. A part of the integrated radiation passes to the radiation receiver (not shown in the figure) through output light guide of polished organic glass, which input end face 9 is at the centre of the sphere and, therefore, a direct incidence of the integrated radiation to the receiver is excluding. Between the output light guide and the radiation receiver replaceable filters are placed. They are intended to correct the receiver according to the colour mixture curves.

The measurements are reduced to an alignment of the radiation fluxes falling on the radiation receiver by both channels using nielloed meshed filters 5 adjusting the radiation flux without change of its spectral composition. An electronic circuit selects signals of both channels, and after luminous fluxes are aligned with an introduced correcting filter, an analogue circuit makes it possible to find the relation of colour co-ordinates.

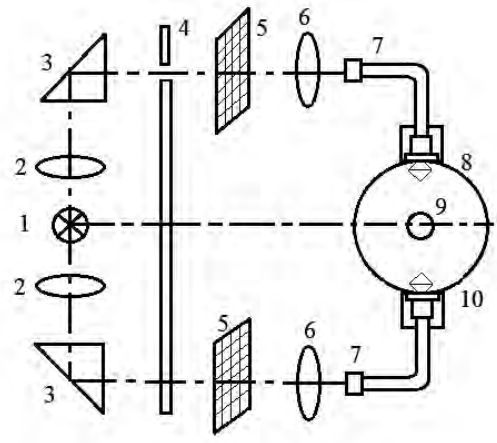

Fig. 5. Optical circuit of the ЭКЦ-1 device

In [7] is specified that this device provides a satisfactory reproducibility of diamond measurements but has a low sensitivity. According to the accepted comparison method, this device is used to measure colour difference of measured and standard (reference) specimens, which is providing maximum measurement accuracy. However, this requires a preliminary selection of a suitable comparison specimen, reduces measurement productivity and allows only comparing diamonds of yellow shades with specimens of yellow tonality.

In this installation, a disadvantage of diamond colour measurement connected with increase of radiation path length, which in this case is identical for reference and measured radiation, is eliminated. But deficiency of a diamond will still influence the stone colour, and as a result, its colour group will be determined incorrectly. It will be overestimated if a white smoky inclusion or reflection from a crack take place and it will be underestimated if graphite inclusions take place.

Great opportunities to measure diamond colour are provided by devices based on spectrophotometers. Among such devices, a spectrophotometer should be mentioned, which measures spectral distribution of diamond direct transmission factor when illuminating through the plane [5]. It is noticed in [5] that using this dependence, one can unambiguously and objectively determine colour of all gemstones.

In the SRIIN, a spectrophotometer based on the СИП-1 spectrometer was developed [8]. The СИП-1 spectrometer was earlier designed at the same place. An optical spectrophotometer circuit (Fig. 6) contains illuminator (1 – incandescent lamp, 2 – condenser), monochromator (3 – input

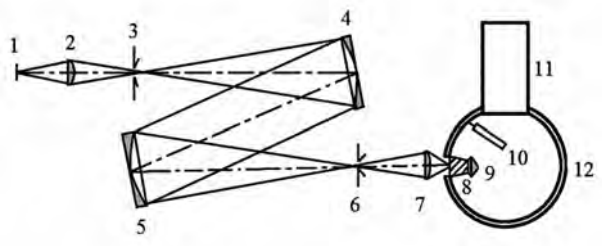

Fig. 6. A spectrophotometer developed by the NIIIN

slit, 4 – collimating mirror, 5 – diffractive grating, 6 – output slit) and an attachment for diamond measurement. The attachment contains microlens 7 by which radiation outgoing through the monochromator slit is directed to the photometric unit. In its turn, the photometric unit contains integrating sphere 10, focon (conic light guide) 8, to which diamond plane 9 is pressed, and radiation receiver 11 with a circuit to measure photocurrent. Diameter of the focon output end face is much less than diameter of the diamond plane. In the sphere, white screen 12, which is excluding radiation fall on the receiver directly from the specimen, is placed.

This device has the same disadvantages of diamond colour measurement, as the Brilliamt-1: the radiation passes path within a diamond twice exceeding the path in case of a visual evaluation, and the device is also intended to measure colour of defectless diamonds.

To measure diamond colour, *Adamas Gemmological Laboratory* Company, USA, manufactures a specialised laboratory spectrophotometric system SAS2000 (*Spectrometer Analysis System*) [9]. This is a two-channel fibre-optic spectrophotometer, which reference channel allows monitoring changes in radiation source spectrum. The device is intended to measure diamond spectral transmission factors with subsequent calculation by a computer built-in in the device and colorimetric parameters in the XYZ and CIELAB systems. Previously the device is calibrated according to *GIA* standards or to others at the request of the customer.

There is no detailed description of the device optical circuit in [9] to measure spectral transmission factor. One can assume that it is similar to the comparator (see Fig. 5). A diamond is placed on the light guide with the plane down, and ray path within the diamond is similar to the one given in Fig. 4. Hence the radiation portion outgoing from the diamond depends on the configuration and cut quality, on diamond size and on defects as various

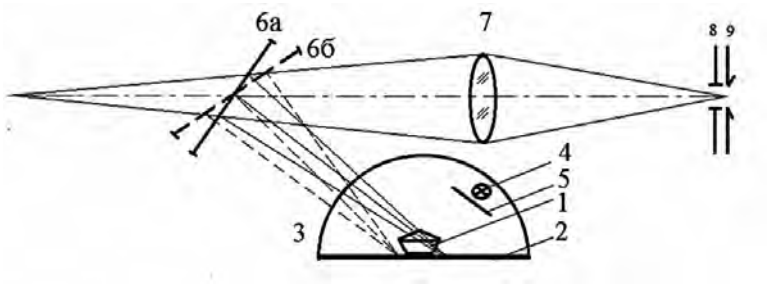

Fig. 7. Optical circuit of the recommended installation

inclusions and cracks. Therefore, the measurement results differ from the results of a visual evaluation. Diamond colour obtained in such a circuit is correlated, because radiation way length in a diamond surpass approximately twice the way length when visual diamond colour evaluating.

There are several common disadvantages inherent in all considered methods and devices using diamond illumination through the plane:

1. Radiation directed to the diamond plane comes back and in a greater degree falls into the illumination source, which leads to an incomplete radiation use;

2. Radiation portion outgoing from the diamond and falling to the light source is not constant and depends on the cut configuration and quality, as well as on presence of scattered light, defects and on diamond colouration irregularity, which can influence measurement results;

3. All devices using such illumination layout normally work with diamonds of a classical cut. Interpretation of the results of fancy cut diamond measurements, all the more of not cutted diamonds, is not obvious. It is not quite clear as well, what such devices measure in the event of the diamonds with internal defects;

4. The devices measure correlated colour since in each photometric layout, radiation way length within diamonds is different from the visual evaluation way length.

From this point of view, measurement layout corresponding to the visual evaluation conditions is most prospective. In this case, the diamond is placed with the plane down on a white substrate, and radiation falls on the receiver from the paper bookmark illuminated with scattered light. This radiation path length is equal to 0.65 D, which corresponds to the light ray pass length in case of diamond colour visual evaluation. The receiver is placed at an angle of 45° in relation to the substrate [5].

Such a layout can be implemented in the installation (Fig. 7), in which studied diamond 1 is located on base 2 of hemisphere 3. In this case, diffused illumination of the diamond and background is provided with radiation source 4 and with protection screen 5 excluding direct radiation falling onto the diamond. Such illumination system excludes influence of outside objects (room walls, appraiser's clothes, etc.), which radiation can be scattered on diamonds and change their colour.

In such a layout, one can determine spectral coefficient of a diamond luminance as a relation of spectral luminance concentration of radiation passed through the diamond to spectral luminance concentration of the background, for example of the paper bookmark. In doing so, the radiation spectrum makes no difference.

In photometry, this method is named a replacement method, and its accomplishment in this installation is enabled by mirror 6 turn, which allows by means of lens 7 projecting image either of the diamond (mirror position 6a), or of the substrate (mirror position 6b) on the monochromator input slit 9.

Hartmann's aperture diaphragm 8 at the monochromator input slit is intended to select by height a site necessary for the measurements within the diamond image, for example of a round diamond spike, which corresponds to the conditions of diamond colour visual evaluation.

Unlike known layouts, in this one the following takes place:

1. It is possible to measure specimens of any configuration, including diamonds and pastes; the known installations are as a rule intended to measure plain specimens;

2. In the measurement process, the specimen remains immovable, which provides a photometric measurements of the same site (in the known devices, a diamond is entered into the light ray and brought out of it with each change of the spec-

tral device wavelength); and since various colour, smoky, graphite inclusions and cracks are possible in diamonds, an insignificant diamond movement can lead to a measurement result distortion;

3. A device is used that allows to photometric measuring any diamond area (if necessary), id est one can measure the parts without defects.

REFERENCES

1. Meshkov V.V., Matveev A.B. Fundamental of Lighting Engineering: Manual for high education institutions: Of two volumes, part 2. Physiological optics and colourimetry. the 2nd revised edition, Moscow: Energoatomizdat, 1989. 432 p.

2. GOST P 52913–2008: "Diamonds Classification Technical requirements"

3. Building regulations 23–05–95: "Natural and artificial illumination".

4. Judd D., Vyshetskyi G. Colour in science and technology, Moscow: Mir, 1978, 592 p.

5. Pagel-Theisen V. Diamond Grading ABC, 12-th Edition, Antwerpen, Belgium, 2000, 290 p.

6. Yepifanov V.I., Pesina A. Ya., Zykov L.V. Technology of working diamonds, Moscow: Vyshaya Shkola, 1976, 319 p.

7. Rymov A.K., Shklover D.A. Electronic colour comparator ЭКЦ-1 // Svetotekhnika, 1961, #10, pp. 24–28.

8. Shelkova O.P., et. al. Study of a possibility to create installations of objective evaluation of diamonds and diamond raw materials by chromaticity and defects, Moscow: SRIIN, 1971, 70 p.

9. SAS2000 Spectrophotometer Analysis System // Adamas Gemmological Laboratory, 2000, # 4.

Tatyana V. Shirokikh,
Ph.D, Associate Professor, graduated from the Moscow Power Engineering Institute (Smolensk branch) in 1978. At present she is an Associate Professor of the Physics Chair of the Moscow Power Engineering Institute (NRU) in Smolensk. The scientific interest field: photometry and colorimetry

Valery E. Ivanov,
Ph.D., Associate Professor, graduated from the Smolensk State Pedagogical Institute (1974). At present he is an Associate Professor of the Physics Chair of the Moscow Power Engineering Institute (NRU) in Smolensk. The scientific interest field: photometry and semiconductor photo-converters

Light & Engineering
Vol. 26, No. 3, pp. 116–123, 2018

Svetotekhnika
No. 3, 2018, pp. 17–23

LIGHT DECORATION OF A CITY AS AN ART INTERPRETATION OF ARCHITECTURAL BASIS (AS EXEMPLIFIED BY ASTANA)

Yuri V. Nazarov [1,*], Alla A. Kornilova [2], and Sergei M. Tyurin[1]

[1] *National Institute of Design Autonomous Non-commercial Organisation, Moscow, RF*
[2] *The Kazakh Agrotechnical University of S. Seyfullin, Astana, Republic of Kazakhstan*
** E-mail: nounid@mail.ru*

ABSTRACT

The article is dedicated to some features of design and light decoration arrangement of Astana City being the young capital of Republic of Kazakhstan. A specific character of artificial illumination use is revealed in the context of implementing the general plan of development of Astana designed by Kisho Kurokawa (黒川 紀章). By means of an on-site investigation, light use is studied as an expression facility taking an active part in formation of art-and-communication environment of the capital. Difficulties in the illumination arrangement at the present development stage are revealed. Conclusions are formulated and development prospective of the light decoration of the city is planned.

Keywords: light, colour, city light decoration, design culture, art-and-communication environment

1. INTRODUCTION

In the XXIth century, it is difficult to overestimate the light role in a city environment formation. The light is one of the most important of the seven main expressiveness facilities forming city environment aesthetics as a whole [1]. These facilities are as follows: colour and light, landscape design (paving, “green architecture”, etc.), city design to a great extent determining bridge, parapet, lattice, etc. pattern, easily built structures (pavilions, booths, etc.), creations of monumental and decorative art and outdoor advertising. A competent use of artificial light in a city space turns architecture objects and the city landscape into fantastic images of the night-time city.

Today, an artificial light extensively influences formation of art-and-communication environment of a city as it is a powerful tool in hands of specialists, which allows simulating various aspects of the environment aesthetic perception.

Retrospectively, aesthetic function of the artificial light in external illumination of objects, including advertising, became dominating already in the twenties of the XXth century. In the XXth century, understanding of artificial illumination as an independent element or section of architecture, and of light as an architectural material and a mean of art expressiveness for city environment was gradually formed.

Studying of illumination of the cities in most different contexts is considered in works of such scientists as C. Bartenbach, N. Bystryantseva, F. Vanaverbeck, C. Vinkels, A. Guillo, V. Glazychev, N. Gusev, P. Zumter, A. Ikonnikov, G. Kamenskaya, W. Köhler, M. Klaasen, A. Kornilov, V. Luckhardt, V. Makarevich, M. Marini, M. Major, S. Mikhaylov, B. Munari, Yu. Nazarov, N. Obolensky, R. Narboni, D. Ponti, C. Santen, R. Sonnetto, M. Huber, V. Shimko, N. Shchepetkov, etc.

A. Kornilova, V. Laptev, E. Hvan and E. Horovetskaya turned to the question of light decoration of Astana in their studies. However, questions of the current state of illumination of Astana are studied insufficiently.

Leaving out of the brackets of this article such questions as visual perception psychology, interac-

tion of illumination types, safety, security and free orientation of citizens in space, sanitary and hygienic standards and economic problems of illumination, we will concentrate on art and aesthetic role and features of arranging artificial illumination as a part of arrangement of art-and-communication environment of Astana being the capital of Republic of Kazakhstan.

A purpose of this work was to reveal features of arrangement of artificial illumination in an interaction with development of architectural environment of Astana at the present stage. And the following tasks were set:

– To determine art and aesthetic outline of light decoration of Astana;

– To reveal interrelation of arrangement and application of artificial illumination in a modern city with development of art-and-communication environment of Astana;

– To study light use as an expression facility taking an active part in formation of art-and-communication environment of the capital.

2. LIGHT IN THE CONTEXT OF MODERN DESIGN CULTURE[1]

With an active use of light as an expression facility of arranging social and spatial environment of a city "diverse multistylish architecture is now perceived as a uniform city ensemble to a large extent due to absolutely special, dynamic, constantly changing atmosphere of the streets depending not so much on architecture…" [2]. An artificial light interacts with architecture in four its main types and categories: space, volume, plasticity and colour. As a result, a light environment with new visual qualities is formed [3, p.190].

Within the modern science, most different terms in relation to light decoration of a city are used: "light decoration", "light-decorative formation", "light environment of a city", "architectural and light image", "light-art image", "light urbanism", "light design".

In foreign design, the *lighting design* concept is used. In the informative sense, it is much wider than the light decoration and the local illumination of architectural objects. It means an intensely developing field at the boundary of design, architecture, lighting engineering and decorative art. Such a modern direction of design development requires an entire system of town-building, architectural and design approaches, as well as a separate competence of the specialists. A confirmation of the light urbanism importance as a culture phenomenon is N.V. Bystryantseva's conclusion that at the town-building level, it is a large-scale "work" of light within entire cities, in particular creation of general light plans of the cities and of their light frameworks [4, p.5].

Thus, an importance of light use in forming city environment is indisputable, and implementation of a competent, professionally verified artificial illumination is possible under the condition of attraction to illumination design of various direction specialists: architects and designers, lighting and electric engineers, as well as sociologists and psychologists. In such case, taking into account peculiarity of the specific city, identification of city space, psychological perception of the city by the population and guests are of a great importance [3, p.191]. Along with this, art and aesthetic properties of the light environment, which include integrity of light composition, informative efficiency, imaginative expressiveness and rationality of the light solution, are important [4, p. 14].

3. LIGHT DECORATION AS AN EXPRESSION FACILITY OF FORMING IMAGE OF THE CAPITAL OF REPUBLIC OF KAZAKHSTAN

The light decoration of Astana being the capital of Kazakhstan has its specific character, first of all in the historical context. From the beginning of 1991 and during the first years of independence of Kazakhstan, in all aspects of the city life connected with the search of the national identity, a new interpretation of the history from its various sides, with a choice of the further way of development, which was also reflected in light decoration of the city environment, cardinal changes began. After the capital was transferred from Almaty to Akmola (1997) renamed in 1998 into Astana, a swift city building was started. Light decoration as a part of the new art-and-communication environment of the city was

[1] Design culture is the highest level of the design sphere building itself over current design process of transformation and/or reconstruction of environment, over such its components as designing communities, design economy, designed parts of the environment and certainly over the design infrastructure, id est over the functional services providing a normal flow of the design process.

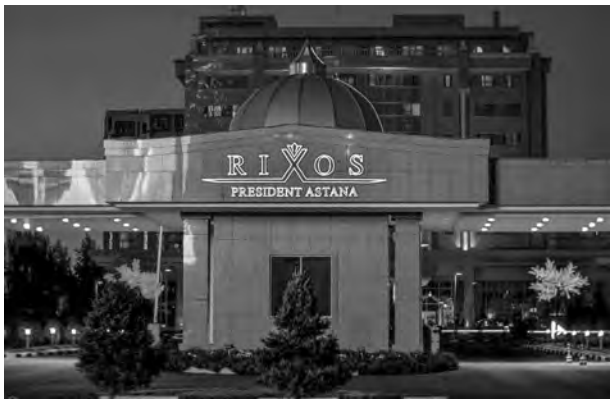

Fig. 1. The *Rixos President Astana* hotel. Photo of D. Chistoprudov, *http://www.titus.kz/*

intensely developed. Among other things, advertising information objects, various sign-boards, posters, decoration of building facades of the central highways, new symbols as memorials, small architectural forms, etc. have become to play a special role in it. In this context together with the change of style and aesthetic preferences, colour and light, as well as various details connecting concepts of presentation, comfort, usefulness, advertising and decorations have appeared in the city streets.

The general plan of Astana development designed by Kisho Kurokawa had been approved and started in 2001, and the city-building situation, the regional position of the city, the relief, climatic conditions and elements of the city space-planning composition had been took into consideration. This plan along with red lines[2], and with architectural and communication axes, determines features of the light solution of the new representative part of the city, which building was begun on Esil river left bank. Thus in the project of Kisho Kurokawa, light is included in the general plan of the city development at a level of the city concept.

All these components considerable influenced art-and-communication image of the capital. Two directions were used when forming artificial illumination of architectural objects of Astana:

– The illumination arrangement of building facades, show-windows, canopies and marquees over entrances during day time;

– An arrangement of the city illumination during evening and night time.

The day-time illumination arrangement is a local illumination of signs, entrance elements, symbols, indicators, running lines and of most various promotional and informational objects. Methods of the day-time artificial illumination are most actively implemented in commercial public places: restaurants, supermarkets, shopping and entertaining centres. Along with it, in the main streets corresponding installations are used, which have a functional value and an obvious art advantages. So, positive solution examples of light decoration in Astana are boutiques, shops, restaurants, hotels of world brands, which using integral approaches to the problem solution, showed a competent light forming show-windows, sign-board, and marquees (Fig. 1). As a result, local illumination accentuates architectural features of buildings, at the same time, keeping show-windows and sign-boards at the forefront.

Illumination of the city at evening and night time is rapidly formed emphasising the city-building size, and places of interest [1]. Light panorama of evening Astana gains the peculiar art expres-

[2] The red lines are the lines, which designate existing, planned (changeable and newly formed) boundaries of public territories, boundaries of land sites, on which power lines, communication lines, pipelines, highways, railway lines and other similar constructions are located.

Fig. 2. Panorama of evening Astana. Photo of D. Chistoprudov, *http://www.titus.kz/*

siveness, draws attention of the capital inhabitants and guests (Fig. 2)

According to N.I. Shchepetkov's conclusions, architectural-and-art expressiveness of city ensembles and objects for all people whose attention is attracted by the evening city can be provided in the two conditions: initial creation of a "scenario" or of an art concept of the main composition and lighting methods, as well as coordination of all illumination systems [2]. It should be noticed in this context that light design of Astana has such facilities as lighting devices, different types of art local illumination, light-and-colour and dynamic effects, as well as light advertising. The above listed facilities have different potentials of form-building and of visual exposure on the city environment.

The performed field study showed that the most aesthetically expressive part of the light solution of the new left-bank part of the city is the Nur zhol boulevard (water-green boulevard), which is an axis of the whole city, from the Ak-orda president palace to the Aray garden (Fig. 3).

The basis of the composite light solution of the Nur zhol boulevard is a light ensemble with the Astana-Bayterek monument being a dominant of the light panorama (Fig. 4).

From 9 p.m. to 1 a.m., this structure of metal, glass and concrete of 105 metres general height is illuminated with 16 LED searchlights of a new generation, which are installed along the site perimeter. A modern system of the dynamic LED illumination based on the *Philips Colour Kinetics* equipment united into a general circuit by means of wireless *Wi-Fi* connection is put into operation in 2014. There are more than the 50 illumination scenarios in the system creating a uniform colourful filling. Easiness of adaptation of the local illumination to any scenarios gives a peculiar aesthetic attractiveness and gives tone to dynamic light effects of the whole boulevard.

A special individual light-composition interpretation of government and public buildings, as well as of multi-storey high-rise buildings of residential clusters of the left-bank part of the city, allows making architectural advantages of the building facades to be visible and expressive at the night time, and on the other hand, creates a peculiar visual version of the boulevard even it is under reconstruction.

The unique unparalleled in Kazakhstan project is a light-music fountain at the Nur Zhol boulevard. Luminous LED local illumination and numerous

Fig. 3. Evening illumination of the Ak-orda president palace. Photo of D. Chistoprudov, *http://www.titus.kz/*

modes of water effects give evidence of possibilities of the design thought in cooperation of architects, designers and light engineers. A harmonious merge of water and light following a magnificent classic music or the modern composer music, create a real water performance attracting the hundreds spectators.

The Nur Zhol boulevard general light ensemble is formed by a variety of the lighting installations, which are placed practically along all perimeters and themselves became a split-level small architectural forms setting a specific light rhythm to the whole boulevard.

From the other side of the boulevard Nur Zhol a unique ensemble of the Khan-shatyr shopping

Fig. 4. The Astana-Bayterek monument. This is an art and expressive dominant of the Nur Zhol boulevard. Photo of D. Chistoprudov, *http://www.titus.kz/*

Fig. 5. An evening view of the Khan-shatyr shopping and entertaining centre. Photo of D. Chistoprudov, *http://www.titus.kz/*

Fig. 6. Evening illumination of the Saryarka bridge. Photo of the *Forbes.kz.* official site *http://forbes.kz/process/*

centre is located to complete the general light panorama (architect Norman Foster). This ensemble has a unique light decoration creating an illusion of a certain unreality and lightness of a building-dome as though soaring in air and shining from within (Fig. 5).

In process of an on-site investigation, it was found out that the following main features of the lighting arrangement of the Nur Zhol central boulevard city environment can be noticed:

– The light is an active composite element of the boulevard;

– An illumination devices form evening and night environment of the boulevard, and at the same time, they themselves are objects of specific small architectural forms;

– The functional separation of light sources takes place:

a) A lot of sodium lamps are placed along the whole boulevard, and they create a peculiar split-level horizontal illumination;

b) The sodium and LED lamps illuminate separate objects, first of all government and public buildings;

c) LED lamps are used to illuminate separate dominant architectural objects, such as the Astana-Bayterek monument.

Among other advantages, endurance of the used lighting equipment to atmospheric effects is an important quality, because this is significant taking into account complex climate conditions of Astana.

Design of the luminaires, formation of the light pattern and light rhythm, as well as creation of light-and-colour optical fields determine art features of the comprehensive illumination of the new left-bank part of the city.

Light decoration of the Saryarka and Maral-2 bridges through Esil river connecting new left-bank and historical right-bank parts of Astana is an outstanding light solution of a highly professional level.

The bridge Saryarka is decorated with steles; its handrails are decorated with a national ornament. The narrow-directed light sources made the bridge one of the most beautiful places of the evening capital. Numerous variations of the light decoration create a theatrical scenery effect and emphasise a singularity of the national patterns (Fig. 6).

The bridge Maral-2 is the longest in Astana, and its light arrangement may accept interesting aesthetic embodiments. Within the light-and-colour solution of the bridge Maral-2, more than 40 scenarios of local illumination are used, which are change depending on the season. During winter months, the basic colour tone is red, because it creates a sensation of heat; during summer months, a blue shade is used.

Presence of a wide range of luminaires with *Philips* Company LEDs allowed "… designing a system of local illumination, which not only changed the bridges from the aesthetic point of view advantageously accentuating the national colouration of architectural and sculptural elements of these constructions but also increased their functionality" [5]. The possibility to take into account wishes of guests and of the residents when developing new variations of light decoration of the bridges is a reflection of the modern approach to creation of a comfortable visual environment of Astana.

Concerning the left-bank historical part of the city, its light decoration was embodied in some objects, such as the Kazakhstan sports ensemble, central embankment, and public gardens with small

architectural forms. As an example, the public garden at the Ministry of Finance, which light dominant is the Tree of Life fountain, can be mentioned. The used dynamic illumination and the changing colour solutions emphasise bizarre shapes of the fountain and create a fabulous sensation at the evening time. Light design of the fountain turned it into a cultural object and a resting place for city people. Together with it, besides an aesthetic value, the fountain bears a certain information load referring to the cultural and national traditions and reflecting the national idea.

By means of various spectra and of illumination dynamics, different versions or "scenarios" of the city illumination are used in Astana. The festive light decoration of the city deserves a special attention. The architecture itself, as if deviates to the second place during such days, to be a background for festive symbols of the capital.

In festive projects of temporary light decoration of Astana, architectural and art local illumination of buildings, light graphics on building facades, light-decorative structures, illumination of highways, bridge constructions and of city lighting supports are used. Light-dynamics panels, illumination light systems, such as garlands, light cords, mesh works like "duralight", "kliplight" and "beltlights", as well as strobe lamps are also applied.

The history of the festive light decoration of Astana already includes brilliant measures. So, in 2013 during celebration of Nauryz being a holiday of the vernal equinox, a unique two-hour light-dynamics show took place at one city square. It was presented by a team of professionals under the leadership of a world famous designer Kurt Vermeulen. An artistic embodiment of the designer ideas by means of the latest lighting equipment was a delightful by visual perception action for inhabitants and guests of the capital. "We always experiment with new methods of developing the new methods of visual design… Attention is paid to several key elements within our projects. There are singularity, visual exposure, uniqueness and integration into the existing architecture among them. We are experimenting with new configurations, technologies and materials from unique places. Strengthening of symbiosis between our skills will allow us taking advantage of the available art experience in order to materialise our unique vision of light and creating works of art using light", – Kurt Vermeulen says [6].

Supporting the capital status, measures during such holidays as the Republic Independence Day, the Capital Day, the Day of the first president of Republic of Kazakhstan and others, are widely carried out and generously formed using light-and-colour objects. In all three districts of the city, light-dynamics panels are usually installed and highway and city space illumination is arranged. Facades of office and residential buildings, small architectural forms, which decorate parks and public gardens of the capital, are shaped by means of light.

So for example, in honour of the Day of the capital in 2017, more than 70 festive events took place, most of which were arranged on open sites, and they all in their turn had a light decoration. More than 60 light-dynamic panels were installed; festive compositions and fountain LED installations were arranged, which metal frameworks were braided with LED tapes of blue and white cold colours with twinkle effect. More than 500 arm panels were installed.

A bright event was in Astana during the International specialised EXPO-2017 exhibition, which illumination solved functional, architectural, art and emotional tasks. A dynamic schedule of the three months period of the exhibition (from June 10 to September 10) reflecting every minute directly determined the light scenario.

Dynamic light according to the saturated rhythm of the exhibition life, created an event-and-spatial outline, which helped the participants and guests of the exhibition to understand intuitively location, sequence and order of the events, as well as to feel themselves being in the centre of festive exhibition events and to perceive an emotional lift transfused among other things by light.

Kazakhstan national pavilion shaped as a sphere (Fig. 7) was the central architectural and expressive object of the international specialised EXPO-2017 exhibition.

Facade of the national pavilion sphere was decorated with the 126 thousand LED bulbs, which "worked" together with a unique glass coating, for which special illumination design was developed. A gift for the townspeople to the EXPO-2017 exhibition opening day became a light arch installed on the central embankment. This structure of more than 100 metres long with a dynamic illumination and sound, which is beginning from the Astana Nury restaurant, became an aesthetically expressive bright spot.

Fig. 7. Evening illumination of the Kazakhstan national pavilion of the international specialised EXPO-2017 exhibition. Photo of the EXPO-2017 official site *http://www.expo2017astana.com/*

Thus, an attractive luxury of the most various light decorations gives the city a festive art image and aesthetics, and sets a special psychological perception. It should be noticed that in Astana namely in 2002, light dynamics was applied for the first time on a snow and ice construction as a festive decoration or a light arrangement.

The all aforesaid demonstrates development of an essentially new understanding of city environment in the young capital of Republic of Kazakhstan. Light becomes one of those universals of the modern world, which can be the basis of strategy of a new humanity including solution of the following problems:

– Formation of a social request for increase of aesthetic, art and ecological quality of a city environment;

– Revival of the public nature of public space, which now is a space of private interests;

– Affirmation of such categories as "place spirit", "context" and "time spirit", which are necessary conditions for group and personal identification in modern space of society and culture [7].

4. PRESENT DIFFICULTIES IN THE CITY DECORATION BY LIGHT AND PROSPECTIVES OF THE CITY LIGHT DESIGN DEVELOPMENT

The results of the performed study showed that despite positive trends of light decoration of a city, nevertheless, there are some difficulties in its arrangement at the present stage. They are as follows:

1. Local illumination of majority of the city objects is arranged in such a way that it switching on and switching off are only automated in most cases. At the present time, a modern lighting equipment of new generation, which is able to change colour and luminance, to give dynamics, to add additional light elements is used only at some objects.

2. There are some objects in the city where illumination is behind the high level of building architecture. Among such objects are follows: Palace of Peace and Harmony, the Ministry of Transport and Communications (Transport Tower) building, the Family Town and Armand Kala buildings.

3. To create safety and comfort feelings of the city dwellers, light environment of the city is necessary to create, which preserves their health and solves problems of light support of building lower levels. As a rule, light decoration in the city only concerns top floors of high-rise buildings.

At present, an active work is performed in order to change-over to energy-effective LED illumination of the city. In 2015 a development of the town-building project of uniform light environment of the Astana city was started, which purpose was to change the practice of isolated and not interconnected design of external utilitarian, architectural, landscape and decorative illumination. Such a practice allowed forming in some cases disharmonious light spaces. The result was creation of the Light Environment Concept of the city, which was adopted in January, 2018. This is a reflection of practical steps of Republic of Kazakhstan towards the "green economics" transition. Using the state and private partnership mechanism, a system of intellectual illumination will be created in the capital. Use of energy saving technologies with a possibility to adjust radiation colour within a centralised RGB system control is provided for. Implementation of the new concept will become a basis to improve modern art and expressive energy-effective safe city space of Astana.

5. CONCLUSION

Thus, the performed studies allow drawing conclusions as follows:

1. Art and aesthetic outline of light decoration of Astana is determined by dynamic and extensive nature of its development.

2. The main factors influencing light decoration of the city as a part of the art-and-communication environment are as follows: administrative and territorial transformations (change of the city status), architectural and city-building transformations

(intensive construction of a new representative part of the city), historical and cultural motivations (recovery of own history and determination of further way of the development). One should also remember climate features (extreme continental climate) and relief conditions of free city spaces (rather long distances between architectural objects determining a specific character of light decoration).

3. Artificial illumination within the context of development of art-and-communication environment of Astana at the present stage is applied in two versions:

– Daily i.e. stationary illumination, with minimum facilities to use a prevailing white-yellow colour with a comparatively simple pattern. At some objects significant from the architectural point of view dynamic mode is used;

– Festive i.e. temporary thematic illumination during holidays.

4. Light as a mean of expression, which takes an active part in formation of art-and-communication environment of the city is used as follows:

– By means of aesthetically competent art and expressive light solutions at a level of separate architectural and expressive ensembles and objects;

– Using aesthetic expressiveness of two types of relations between light and architecture: a contrast opposition and shade coherence.

5. A conceptual competent maintenance of light use as a mean of expression when forming art-and-communication environment of the modern capital will allow with due performance giving a "frame basis" the all unique image of the city and accentuating its national colouration: ornament, symbolism, mythology, imagery, and metaphorical in dynamics of its historical and cultural development.

REFERENCES

1. Nazarov Yu.V. Light in a city – problems and prospectives // Svetotekhnika, 2013, #2, pp. 54–57.

2. Yermolaev A.P., Minervin G.B., Yefimov A.V., Gavrilina A.A., Shchepetkov N.I., Kudryashov N.K., Shimko V.T. Design of architectural environment. Moskow: Arkhitektura-C, 2004, 504 p.

3. Kornilova A.A., Horovetskaya E.M. A theoretical model of light and decorative arrangement of architectural environment // Bulletin of KazGas, 2006, #4 (43), pp.190–195.

4. Bystryantseva N.V. An integrated approach to creation of light environment of an evening city // Thesis of architecture Ph.D. Moscow 2015, 27 p.

5. Lights of evening Astana [An electronic resource]// Nur.kz. Official site. News of Astana. 9/6/2014. // Access mode: https://www.nur.kz/330044-ogni-vechernej-astany-foto.html (Addressing date: 2/5/2018)

6. In anticipation of Nauryz, a unique light show of a famous designer will take place in Astana [An electronic resource] // Zakon.kz Information service with a reference to the Bayterek media centre. 3/15/2013. // Access mode: http://online.zakon.kz/Document/(Addressing date: 2/5/2018)

7. Lekus E. Yu. City environment: light design versus light culture // Philosophy. Tolerance. Globalisation. The East and the West – a dialogue of outlooks: theses of reports of the VI-Ith Russian philosophical congress (Ufa, October 6–10, 2015). Three volumes. V.III, Ufa: RITs BashSU, 2015, pp. 309–310.

Yuri V. Nazarov,
Dr. of Art History, Professor. At present, he is a Rector of the National Institute of Design Autonomous none-commercial organisation of higher education, a corresponding member of the Russian Academy of Arts. During 25 years he was the Head of the Union of designers of the Russian Federation, a winner of the State prize of the Russian Federation. A honoured worker of arts of the Russian Federation, his scientific interest field: history, theory and methodology of design as a culture phenomenon

Alla A. Kornilova,
Dr. of Architecture, Professor of the Design Chair of the Kazakh Agrotechnical University of S. Seyfullin (KazATU), honourable education worker of Republic of Kazakhstan (RK), honourable architect of RK, honourable member of the International Public Organization of Assistance to Architectural Education (IPOAAE). Her scientific interest field: architecture of Kazakhstan

Sergei M. Tyurin,
Architecture designer, Master Degree (2014), graduated from the National Institute of Design Autonomous none-commercial organisation of higher education. His scientific interest field: design of city environment

Light & Engineering
Vol. 26, No. 3, pp. 124–131, 2018

Svetotekhnika
No. 3, 2018, pp. 32–36

COMFORT LIGHT ENVIRONMENT UNDER NATURAL AND COMBINED LIGHTING: METHOD OF THEIR CHARACTERISTICS DEFINITION WITH SUBJECTIVE EXPERT APPRAISAL USING

Nina A. Muraviova, Alexei K. Soloviev, and Sergei V. Stetsky

[1] University of Civil Engineering (NRU MGSU), Moscow
[2] X5 Retail Group, Moscow
E-mail: agpz@mgsu.ru; melamory740@gmail.com

ABSTRACTS

Light comfort in the room is characterized by the conditions of visual work, which are determined by the levels of illumination of the workplace and the saturation of the entire room with light. The related problems were solved mainly for artificial illumination. The article examines the results of research in our country and abroad by determining the criterion for the comfort of lighting rooms with artificial and natural light. It is pointed out that such studies are obviously insufficient, and suggestions are given on their development.

Keywords: expert evaluation, comfort, light environment, psychophysical methods, room lighting, visual work, room light saturation, subjective assessment, observers

1. INTRODUCTION

Requirements for the light environment in buildings are characterized by the levels of illumination sufficient for performing visual work, as well as high light saturation, providing light comfort. In addition, light comfort is ensured by the uniform distribution of light flows in the interiors and by the absence of sharp contrasts in the field of view. The listed parameters are static characteristics. However, numerous studies prove that a constant light environment in the room has a negative effect on people's health [1]. Human being accustomed to the dynamics of lighting for thousands of years. Change of day and night affects the production of hormones in the human body, affecting the state of wakefulness and fatigue [2]. These studies conducted in Russia and abroad showed the advantages of natural lighting. However, only natural lighting of interiors is impossible in principle, since at low levels of outdoor natural illumination it is necessary to include artificial light. Even at high levels of external natural illumination, one cannot avoid the use of artificial light. Modern production requires high levels of illumination, which in high-rise multi-storey buildings can not be provided at the expense of one natural light. In such premises, most part of a day natural and artificial light act together.

2. THE CONCEPT OF PERMANENT SUPPLEMENTARY ARTIFICIAL LIGHTING OF INTERIORS (PSALI)

This is the first concept of the combined effect of artificial and natural light, developed by R. Hopkinson back in 1959. [3, 4]. Prerequisites for this concept were the contradictions that arose during the normalization of artificial illumination of that time for school classes and offices in the UK. Normalized levels of illumination (160–200) lx caused a sharp contrast between the dark interior surfaces in the deep-most area of the premise and the bright sky, visible through the windows. In order to avoid this unpleasant phenomenon, it was necessary to in-

crease the levels of additional artificial illumination. Moreover, this increase should correspond to an increase in the external natural illumination.

2.1. The Concept of Automatically Adjustable Supplementary Artificial Lighting (AASAL)

Modern means of regulation of artificial illumination have allowed putting on forward the second concept of the combined illumination. This is automatically adjusted combined illumination. The main idea of this concept is the addition of natural light to the normalized value under artificial illumination in areas with insufficient natural light. In this case, the premise is divided into zones according to the levels of D.F. (day light factor), which change their area and location, depending on the change in the external illumination. In these zones, photodetectors are located in specially designated areas, fixing the illumination in these zones and sending signals to automat that turn on and off the luminaires, thus increase or decrease the luminous flux of these luminaires so that the total illumination from natural and artificial light is within the normative standard. Photodetectors can also be placed on the windows, with protecting them from direct sun exposure. In this case, it is necessary to elaborate a program for changing the zone with sufficient natural illumination, depending on the change in ambient light, and to turn on and off the rows of lighting fixtures in accordance with this program. In order to calculate the energy savings for artificial lighting in such systems, it must be assumed that the rows of lamps are parallel to the windows in such remises. It is believed that the levels of internal natural light, at which it is necessary to turn on or off the rows of lamps, must correspond to the normative requirements for artificial lighting. If a premises has a uniform distribution of natural light, for example in large halls with skylights evenly distributed on the roof, then the regulation of additional artificial lighting is carried out by switching on or off groups of luminaires that create the same levels of artificial illumination depending on the amount of external illumination (discrete regulation). Modern technology can also provide a smooth (continuous) regulation of the luminaires luminous flux.

The second concept is also not modern and does not meet the needs of a person. It is largely mechanistic. At the modern level of the science of lighting, we can calculate the levels of illumination and other lighting parameters in any room. But we know almost nothing about the needs of a person relating to the indoor light environment. For example, we do not know what is best for a person: discrete or continuous regulation. Continuous – creates a constant level of illumination at low levels of outdoor lighting. Discrete – supports in some measure the natural dynamics of natural light.

The design of combined lighting should solve two problems: creating the necessary conditions for visual work at the workplace and creating a light environment in a premise that would be characterized by people who are in it, as comfortable. It is believed that this can be achieved by recreating the psychological and aesthetic sense that the interior is flooded with natural light [5]. The provision of the required conditions for visual work is a necessary, but not sufficient requirement. A requirement representing the result of linking the solution of two tasks to each other is sufficient. The first problem is solved with reference to the combined lighting in the Research Institute of Building Physics of the RAASN [6], in the All-Russian Scientific Research Lighting Institute (VNISI) and in the Research University – the Moscow State University of Civil Engineering [7]. The second task is devoted to the work carried out in the laboratory of building physics at the Moscow State University of Civil Engineering, the methodology of which we tried to present in general terms in this article.

3. RESEARCH OF NATURAL AND COMBINED LIGHTING WITH USING CRITERION OF THE LIGHT ENVIRONMENT COMFORT IN WORKING PREMISES

Comfort of the light environment is a subjective concept. Physical quantities, which we learned to calculate, are secondary, leading to normalization. But first you need to determine – is what the person needs, what parameters of the light environment are comfortable for most people. In the second half of the twentieth century, a new approach to the design of natural lighting of premises using the method of subjective expert appraisal was outlined and gradually developed [8–14]. This method is based on subjective assessment by observers of the quality of the light environment. At the same time, emphasis is placed on higher quality parameters of na-

tural light in comparison with artificial light. These parameters are the spectral composition of natural light and the dynamics of its change. In addition, an important role in the subjective perception of natural light is played by the information link with the outdoor environment, which can only be carried out with side or, to a lesser extent, the roof light openings. At the same time, most of the qualitative parameters can recede to the background in comparison with the view from the windows. Through the skylights of the roof natural light system, information is received only about the weather and the time of the day. For some types of skylights, information on the season year due to the condition of the snow cover of the roof and the presence of snow on the glazing is added too. This is the minimum requirement for communication with the outdoor environment. Authors have revealed this during the installation of roof lights in the work shop of steel wire production of the Cherepovets Steel Mill and in the weaving shop of the Kherson Textile Mill by method of questionnaires conducted in the 1970 years.

In the domestic practice, the questions of the subjective evaluation of the light environment have been considered and are considered not sufficiently. Episodic studies that have been conducted in our country since the middle of the last century (in NIISF RAASN, MISI–MSCIU) unfortunately could not lay the fundamentals of this new scientific direction [15–19]. Therefore, this article aims to attract attention of domestic researchers in the field of architectural and building lighting technologies to the relevance of this scientific direction, which can effectively combine the results of engineering developments with the results of developments in the field of psychology, hygiene, etc. The method of subjective expert evaluation must pass from the category of auxiliary and testing to the category of the main one, which operates not so much with objective data on the working capacity of people, but also with data on their subjective preferences. This approach fully corresponds to the current world trend in the priority of individual interests, assessments and requests.

Studies on the subjective appraisal of the lighting environment in the premises, conducted at the Department Architecture of Civil and Industrial Buildings of the Institute for Civil Engineering named after V.V. Kuibyshev (now the Moscow State University for Civil Engineering) at the end of the last century were based on the works of leading Russian scientists, psychologists, hygienists, lighting engineers. In particular, the main influence on this was based on the theory of adaptation, developed by H. Helson (USA) [20]. The formula he proposed, determines the level of adaptation, depending on the focus, background and residual stimuli and their weighting factors.

$$A = X^p B^q P^r, \tag{1}$$

where A is the level of adaptation of the system, upon which the most complete acceptance of the stimulus occurs and its greatest correspondence to the human responses is achieved. X, B and P are, respectively, focal, background and residual stimuli, p, q and r are weighing coefficients taking into account the intensity of the influence of the corresponding stimuli. For some studies in the field of natural and artificial lighting, one can use a simplified version of the Helson formula:

$$A = X^p B^q. \tag{2}$$

Here, the residual stimulus is taken into account in the values of the background stimulus. The conditions of illumination and the research tasks determine the values of the focus and background stimuli. For example, in studies of the required conditions for performing visual work, the focus stimulus (X) is the amount of illumination, at which the highest operability and the lowest fatigue occur. The background stimulus (B) is the amount of total illumination in the interior to which the subject adapts. For artificial lighting, X is the level of local illumination and B is the level of general lighting. For natural lighting, X is the level of natural light, at which maximum performance and minimal fatigue are observed. B is the average level of natural illumination in the premise. However, under natural lighting, these parameters change all the time, and it is required to switch on and turn off artificial light. Therefore, with combined lighting, X is the level of natural illumination at a given time, with the addition of the necessary amount of artificial light to ensure maximum performance and minimal fatigue in this visual work. B is the level of additional artificial illumination.

The weighing coefficients p, q and r in formula (1) can vary in their significance, depending on the situations being evaluated. The focal stimulus in one case, may be background or residual for

Table 1. Values Assigned to the Rating Scale

№	Characteristics	Score in points				
		1	2	3	4	5
1	Overall appraisal of the light environment	Very bad	Bad	Satisfactory	Good	Very good
2	Predominance of natural or artificial ligh	Artificial	More artificial than natural	Equally	More natural than artificial	Natural
3	Combination of natural and artificial light	Very bad	Bad	Satisfactory	Good	Very good
4	Feeling of Twilight	No	Minor	Average	The twilight presents	Large
5	Contrast between windows and wall piers	Very Small	Small	Average	big	Very big
6	Distribution of brightness over the room	Monotone	Almost Monotone	pleasant	Almost Contrast	Contrast

another situation. So, for example, when assessing lighting conditions in the workplace, lighting in the workplace is considered a focal stimulus, the overall light environment is a background one, and the residual stimulus is characterized by past experience and observer habits. When assessing the light environment of the premise as a whole, the background stimulus passes into the focus category. The complete adaptation is indicated by neutralization of the applied energy and that is the best estimation of the stimulus.

For example, in administrative offices, focus and background stimuli can be estimated by weight coefficients p and q equal to 0.5. This is determined on based of on the analysis of working time of the office employees. Complete adaptation is based on the results of questionnaires with A = 600 lx. Normalized artificial illumination (we shall consider it as the background stimulus) B = 300 lx. According to formula (2), the saturation degree of the interior X with light (we shall consider it as a focal stimulus) can be determined from the expression:

$$600 = X^{0.5} \times 300^{0.5};\ X = 1200\ lx. \qquad (3)$$

This suggests that for full adaptation, i.e. feeling of comfort of the light environment, it is necessary that the levels of illumination in the workplaces in total with the overall level of illumination in the premise should be summed up.

In the studies conducted, the subjective appraisal of the light environment in the rooms was carried out by the most common method – a ball score, based on a given scale. The assignment of scores to one or another characteristic was the coding of visual sensations. For example, the evaluation of an explored feature with a maximum score indicates that a "comfort zone" has been reached. With a decrease or increase in the parameters of the evaluated feature, the score decreases, which indicates discomfort of the sensations (Table 1 and Fig. 1) [20]. The complete adaptation is indicated by neutralization of the applied energy that is the best estimate of the stimulus. There is an optimal value of the stimulus, which in psychophysics is expressed by the so-called "U-hypothesis". This hypothesis

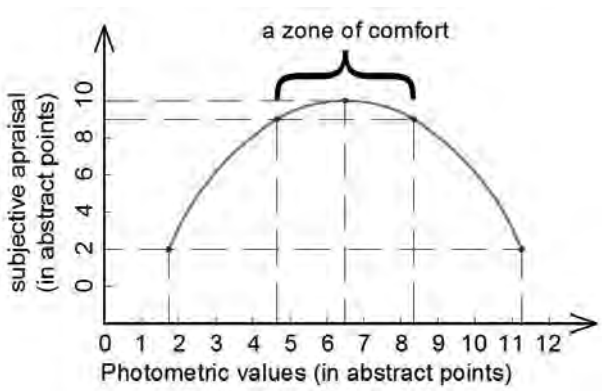

Fig. 1. Scheme of the dependence of the subjective appraisal of the light environment on the change in the photometric value

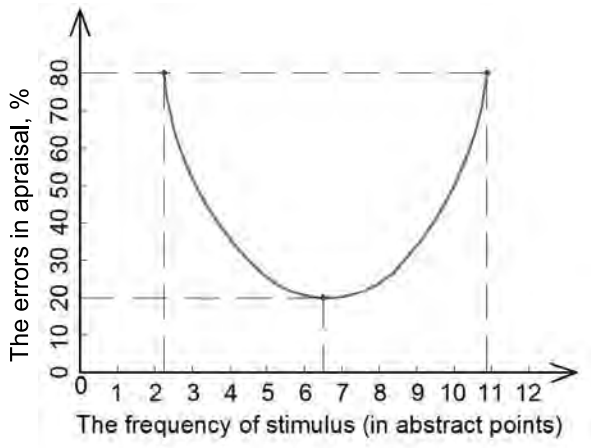

Fig. 2. "U" – functional dependence

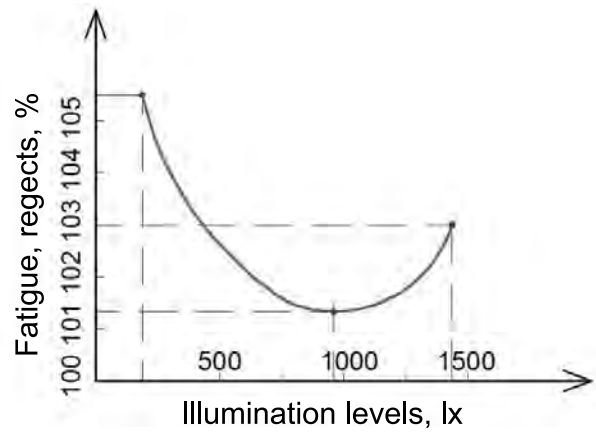

Fig. 3. Dependence of the amount of rejects on levels of artificial illumination

assumes that the character of the process change is described by the graph of the frequency of the stimulation in form of the Latin letter "U". The optimal value of the stimulus is the range of minimal erroneous solutions, where the minimum is at the point that is the adaptation level of the system under consideration (Fig. 2) [21–22].

The principal use of the main provisions of the theory of adaptation, which confirms the "U-functional" relationship between stimuli and reactions, can be traced in the basic works of foreign and domestic researchers since the end of the last century. Thus, Fig. 3 represents a graph showing the change in the amount of rejects in the work due to fatigue of the workers when the illumination levels change, similar to the graph in Fig. 2. The graph in Fig. 4 shows that when the illumination is increased to a certain limit, the productivity of labour increases, which is also the analogy of the graph in Fig. 1.

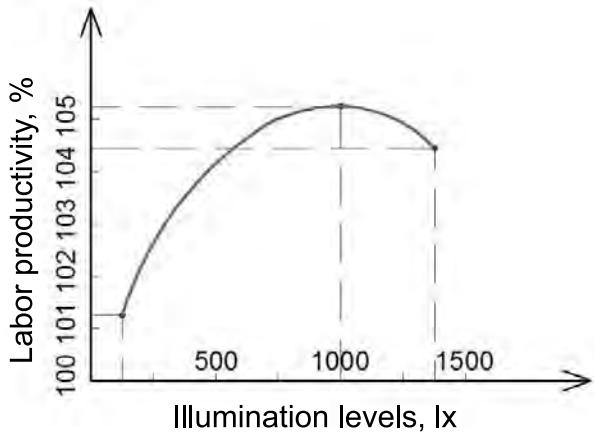

Fig. 4. Dependence of labour productivity on levels of artificial illumination

Objective data on the change in the degree of fatigue and labour productivity when the illumination in the workplace is changing correspond to a subjective evaluation of the overall light environment for the premise which was obtained in a series of studies conducted later on, according to the method of expert evaluation. The basics of this technique are the following actions, namely:

1. Selection of a group of observers by quantity;
2. Selection of a group of observers for quality;
3. Determination of the objectives of the experiment and the formulation of the corresponding tasks;
4. Correct processing of experimental results.

The necessary number of observers (n) should be determined in accordance with the selected values of the feature, which estimates the accuracy of the experiment by the formula of G.F. Lakin [23]:

$$n = (t_z^2/z^2) + 3, \quad (4)$$

where t_z is the normalized deviation from a given level of significance, z is the auxiliary value for estimating the values of the correlation coefficient, and it is determined from the table [23]. To obtain more reliable statistics, a group of observers should consist of persons of different sex, age, vocational training, fatigue conditions of, visual analyzer, etc. It is necessary to develop a special manual (the so-called "introduction to the experiment"), with which observers are introduced before the beginning of observations. The purpose and objectives of the experiment largely determine the methodology for conducting it. Therefore, this item should be worked out with great care. Finally, correct processing of the results of observations should be en-

Table 2. The Composition of the Expert Group (75 observers, 99 sessions of observations)

№№	Number of observations	Classification	Subgrouping					
1	99	Gender	Men			Women		
			66			33		
2	99	Professionalism	Experts		Specialists		Amateurs	
			22		33		44	
3	99	The state of the visual analyzer	Normal	Myopia		Hyperopia		Astigmatism
			47	26		18		8
4	99	Age	<20	20–30	30–40	40–50	50–60	>60
			9	37	31	11	7	4
5	99	Degree of fatigue	Minimum		Average		Maximum	
			33		48		18	
6	99	Time of the experiment	9 a.m. – noon	noon – 3 p.m.		3 p.m.– 6 p.m.		6 p.m.– 9 p.m.
			16	41		30		12

sured with the help of modern electronic methods of mathematical statistics [24, 25]. In particular, as an example, the composition of the expert group with which the experiment was conducted on the subjective evaluation of the light environment on models of premises, in which levels and zones of additional artificial lighting in premises with side light openings were determined, could be cited as an example. With a total number of observers 99, men were 66 and women – 33. This ratio was chosen as a real one in accordance with the specific task of the experiment to determine the levels of additional artificial lighting in the premises of design organizations. Those with normal vision were 47 people. The number of observers by age groups varied as follows: Individuals under 30 years old – 46, from 30 to 50 years – 42, over 50 years – 11 observers.

The further development of the methodology for conducting psychophysical experiments using questionnaires and an interactive method, when the subjects themselves establish the desired parameters of the light environment, was obtained during a number of full-scale experiments conducted by the new generation of young researchers at the Chair of Architecture, and then the Chair of Design of Buildings and Structures NRU MGSU. An example is the last study carried out by former postgraduate student of the Department of Design of Buildings of the Moscow State University of Civil Engineering, N.A. Muraviova [26]. She established the dependence of the subjective appraisal of the quality of the natural light environment on the value of the daylight factor of cylindrical illumination (DFCI). As studies have shown, this factor, which is the ratio of natural cylindrical illumination in the centre of the room to simultaneous outdoor illumination on a horizontal plane, characterizes the light field around the observer. Having determined this value, at which observers regard the light environment as comfortable, one can proceed to normalize Daylight factor or spatial characteristics of the light field in the premise.

4. CONCLUSIONS

1. The development of modern building physics poses new challenges for researchers, which can be successfully solved only on the basis of using the basic principles and methods, which are characteristic for other fields of science. In particular, in recent years, methods of subjective expert evaluation of both the internal light environment in the premise as a whole and its individual parameters are increasingly widely and actively used, which are the prerogative of psychophysics.

2. The current state of lighting engineering makes it possible to determine and calculate any characteristics of the light environment. Technical

capabilities using mathematical formulas and modern computer technology ensure high accuracy of calculations. However, we almost do not know what is required for a person when creating a light environment in the premises. Studies of the light environment in the workplace allowed us to normalize the levels of artificial illumination for performing certain visual tasks. Visual workability was also studied under natural light. Scientific works on the study of a comfortable light environment in the entire premise were conducted only a few. Now there is a need to conduct such studies that will allow obtaining data for the normalization of natural light in premises where visual work is not determinative, and the comfort of the natural light environment is the determining one.

3. The methodology for carrying out studies by the method of expert evaluation largely depends on the goals and objectives set in the specific work. Therefore, the general methodology for researching coverage issues by expert evaluation method does not make sense. Here we proposed only the fundamentals of the methodology. A specification should be for each individual task, which will be presented in the future.

REFERENCES

1. Goncharov N.N., Kireev N.N. Visual performance under natural and artificial light. // Svetotechnika, 1977, № 9. pp. 5–8.

2. Van den Böld G. Light and health / / Svetotechnika, 2003, № 1. pp. 4–8.

3. R.G. Hopkinson and J. Longmore. The permanent supplementary artificial lighting of interiors // Trans. Illuminat. Engineering Society, 1959, 24 (3), 121 p.

4. R.G. Hopkinson. Architectural physics: Lighting. HMSO, 1963.

5. Gusev N.M., Kireev N.N. Lighting of industrial buildings. M. Stroiizdat. 1968. 160p.

6. Semenikhin N.I. Subjective assessment of the quality of lighting installations of reflected light. // NIISF. Proceedings of the Institute// Building Lighting Engineering, Issue 13, 1975.

7. Stetsky S.V., Lobatovkina Ye.G. Perfection of the method of subjective expert evaluation of the factors of the internal microclimate // Industrial and civil construction, 2013 № 12, pp 69–72.

8. Yurov S.G. Some question of the metrics and methods of expert subjective assessments of psycho-esthetic parameters of the ligt-color environment. // Svetotechnika, 1974, № 9, pp.2–4.

9. Irens A.N. Light and Productivity /Transactions of Illuminating Engineering Society (London), 1960, V.25, No.2, pp.53–68.

10. Manning P. Lighting in Relation to other Components of the total Environment/ Transactions of Illuminating Engineering Society (London), 1968, V.33, No.4,. pp.159–168.

11. Bodmann H.V. Light and total Energy Input to a Building. // Light and Lighting, September 1970, pp.240–245.

12. Ne'eman E., Hopkinson R.G. Critical minimum acceptable Window Sice: A Study of Window Design and Provision of a View. // Lighting Research and Technology, 1970, V.2, No.1, pp.17–27.

13. Lay S.D. Appraisal of the visual Environment. // IES Lighting Review, October 1970, pp.129–138.

14. Cockram A.H., Collins J.B. A study of User Preferences for fluorescent Lamp Colors for Daytime and Nighttime Lighting. // Lighting Research and Technology, 1970, V.2, No.4,. pp.249–256.

15. Solovyov AK, Stetsky S.V. Creating a comfortable light environment in classrooms. // Collection of special and scientific works of the Polytechnic Institute of Brno (Czechoslovakia), 1979, pp. 113–124.

16. Stetsky S.V. Subjective appraisal of the quality parameters of combined lighting. // Architectural education. Intercollegiate collection of the Moscow Architectural Institute, 1979, 206p.

17. Solovyov AK, Stetsky S.V. Determination of the parameters of combined lighting by subjective appraisal of the light environment in the premises. // Designing and scientific research. M. Stroiizdat, 1984, № 6, pp 36–38.

18. Stetsky S.V., Porublev S.A. Subjective appraisal of the light environment in the work shops of small auto repair enterprises for the climatic conditions of the North Caucasus. // Industrial and civil construction, 2011, № 1, pp 46–48.

19. Soloviev A.K. Die Anvendung der Lichtfeldtheorie bei der Projektierung der Beleuchtung von Arbeitstaetten. // Licht, 1996, № 5.

20. Helson H. Adaptation Level Theory: An experimental and Systematic Approach to Bechavior. // Harper and Row, USA, 1974, 732 p.

21. Report of the ICE No. 19. "A recommended method for appraisal aspects of lighting associated with visual perception." Washington – London. 1971.

22. Study of performance and fatigue under various lighting conditions. // Publication of the Society for the Study of Light. Lichttechnik. 1965, No.8.

23. Lakin G.F. Biometrics. Moscow, High school, 1973.

24. Bardin K.V. The problem of sensitivity thresholds and psychophysical methods, Moscow, Science. 1976.

25. Leontyev P.D. Statistical processing of measurement results, Moscow, Goslesbumizdat, 1952.

26. Muraviova N. A, Soloviev A.K. Investigations of the nature of the distribution of natural cylindrical illumination in rooms with side natural illumination // Svetotechnika, 2015, № 6, pp. 27–30

Nina A. Muraviova,
Ph.D. in technical sciences, graduated from NRU MGSU in 2012. At present time, she is employee of the retail company X5 Retail Group

Alexei K. Soloviev,
Prof., Dr. of technical sciences. He graduated in 1965 from Moscow Institute named after V.V. Kuibyshev. At present, he is the Professor of the department "Design of buildings and structures" (former department of "Architecture of civil and industrial buildings") of the NRU "MGSU". He is a Member of the European Academy of Sciences and Arts and the editorial board of the "Lighting Engineering" and "Svetotekhnika", has the titles of "Honorary Builder of the Russian Federation" and "Honoured Worker of the Higher School of Russia"

Sergei V. Stetsky,
Ph.D. in technical sciences, Associate Professor, graduated from Moscow Institute named after V.V. Kuibyshev in 1970. At present, he is an Associate Professor at the chair "Design of Buildings and Structures" (former department of "Architecture of Civil and Industrial Buildings") NRU "MGSU"

Light & Engineering
Vol. 26, No. 3, pp. 132–139, 2018

Svetotekhnika
No. 5, 2018

ENERGY EFFICIENCY RETROFITTING OF LIGHTING IN UNIVERSITY LIBRARIES BASED ON ILLUMINATION SUITABILITY ANALYSIS

Bojun WANG[1, 2], Xiaojun LIU[1*], and Yanping YANG[1, 2]

[1]School of Management, Xi'an University of Architecture & Technology, Xi'an, China;
[2]College of Zhangjiagang, Jangsu University of Science & Technology, Suzhou, China;
** E-mail: wbj7266996@163.com*

ABSTRACT

Taking the lighting energy efficiency retrofitting of a university library as a case study, this study aims to solve the existing problems in energy efficiency retrofitting in library lighting, such as one-sided consideration of factors, deviation from reality, and rebound of energy use. On the basis of illuminance suitability analysis, this study considers the technology and economy factors into the decision-making process and constructs a decision-making system for realizing the energy saving goal of the system. Findings show that using the illuminance suitability analysis data to determine the illuminance trigger threshold of energy saving light source and intelligent lighting system can guarantee the lighting energy saving rate and lighting visual environment, eliminate the "energy use rebound effect", and achieve good technical and economic results.

Keywords: intelligent lighting, energy efficiency retrofitting, illuminance analysis, economic evaluation

1. INTRODUCTION

Building energy consumption accounts for approximately 40 % of total energy consumption, which makes the building the main target of energy efficiency retrofitting [1]. A primary means to reduce building energy consumption is energy efficiency retrofitting of existing buildings, the important part of which is the lighting energy efficiency retrofitting. The measured data from Tsinghua University show that lighting power consumption accounts for (20–40)% of the total energy consumption of large public buildings [2]. Swedish researchers found that the actual average annual energy consumption of lighting systems in office buildings was 21 kW·h/m^2, whereas theoretical calculations and simulation experiments showed that the annual average energy consumption of lighting systems reached 10 kW·h/m^2, which could satisfy the demand for office lighting, and the energy saving space was 50 % [3]. Particularly, the lighting energy consumption in a university library is higher than that of common public buildings, and reducing the lighting energy consumption of a university library has obvious effect on building energy saving.

Many buildings only consider lowering the lighting power but neglect the change of illuminance value after retrofitting due to the lack of systematic consideration. Other studies have shown that users tend to exert minimal effort on energy saving and have an "energy use rebound" effect after energy efficiency retrofitting due to the reduction of energy consumption [4], which results in a decline in the effectiveness of energy efficiency retrofitting. Meanwhile, some schemes of lighting energy efficiency retrofitting only focus on the high standard of lighting system but ignore the economic feasibility, which results in the failure of the energy efficiency retrofitting.

According to the above analysis, this study takes a university library as an example to optimize the

process of lighting energy efficiency retrofitting completely and achieve its overall goal

2. RELATED WORKS

Scholars at home and abroad have studied lighting energy conservation from theory and practice. In the development of lighting energy saving technology, some scholars have attempted to apply outdoor intelligent lighting control systems to green and intelligent buildings [5], use energy saving control sensors in changing the brightness of luminaires [6] and lighting system composed of multiple control devices [7], and apply remote traffic engineering modelling technology to lighting control systems [8].

In terms of illumination analysis, using intelligent management system can maintain maximum visual comfort [9]; using energy saving glass to reduce reflection and astigmatism can save lighting energy consumption [10]; utilizing a hyperbolic lens can improve the uniformity of the illumination of light emitting diode (LED) light source [11]; and using of daylight reasonably can improve visual comfort [12].

In view of the energy use rebound effect, the design and test of ecological feedback system, simulation of lighting consumption [13] and lighting feedback [14], deployment of new energy monitoring system, and investigation of new energy use behaviours [15] can adjust human energy use behaviour and improve lighting system for reducing energy consumption.

From the existing literature, most scholars at home and abroad lack a systematic and comprehensive perspective by focusing on certain type of technology or a certain phenomenon to study the unilateral problems of lighting energy saving. However, the actual lighting energy efficiency retrofitting is a comprehensive system engineering that integrates technology, economy, and management. Moreover, the lack of analysis of key elements brings risks to project implementation. Therefore, this study comprehensively considers all elements of lighting energy efficiency retrofitting of university libraries and their relations starting from the engineering practice and formulates practical and feasible retrofit schemes to address the shortcomings of previous studies.

3. DESIGN OF ENERGY SAVING SCHEME FOR LIGHTING

3.1. Research Ideas

The present work adopts the research method for combining practical test with theoretical analysis to design and verify the scheme of lighting energy efficiency retrofitting of a university library. First, an irradiance test is conducted to ensure that the illuminance of energy saving lamps after retrofitting is not lower than the original illumination level, and the amount of energy saving produced by luminaires replacement is analyzed. Second, the intelligent lighting system suitable for the university library is replaced by manual management to overcome the energy use rebound effect while improving energy efficiency. Finally, the economic benefits of lighting energy efficiency retrofitting are verified by calculating the dynamic investment payback period.

3.2. Analysis of Illuminance Suitability

This study aims to solve the current problem that the lighting energy efficiency retrofitting only pays attention to the change of lighting power and neglects the illumination suitability by analyzing the illuminance and power of energy saving luminaire via field test. The luminaire is selected as the light source after energy efficiency retrofitting to satisfy the requirements of illuminance and amount of energy saving.

The analysis shows that the reading room and the stacks have the largest lighting area, and the reading room has the highest requirements for the illumination comfort. Therefore, this experiment selects the reading room to perform the illuminance test and analyzes the energy saving of changing the lighting equipment under the same illuminance. The uniformity ratio of the illuminance is then analyzed, and the fitting degree between the measured and theoretical illuminance is compared to correct the value of correlation coefficient in the illumination theory formula (1) as the basis for related calculations.

In theory, indoor illuminance is usually used as the evaluation index of illuminance suitability. On the basis of “utilization coefficient method” for indoor illumination analysis, the theoretical calcu-

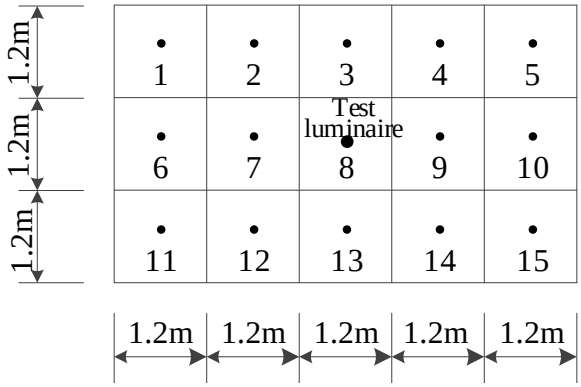

Fig. 1. Scheme of test points

lation formula for the illuminance of the test point on the working surface is as follows:

$$E_{ti} = \frac{(\phi \times U \times M)}{A}, \tag{1}$$

where E_{ti} is the theoretical calculation value of the illumination of the test point i on the test face [lx], ϕ is the luminous flux parameter of luminaire itself [lm], U is the utilization factor, M is the maintenance factor, and A is the area of the illuminated surface in the room.

Formula (1) indicates that when the illuminance test is conducted, the influences of the parameters of the luminaire itself and the room environment factors on the indoor illuminance should be considered.

According to the testing requirements of illuminance in "Measurement methods for lighting" (GB/T 5700–2008), the central point method is used in this experiment to design the testing environment and arrange the measuring points. The field average illuminance measured by the centre point method is calculated as

$$E_{av} = \frac{\sum E_i^a}{M \times N}, \tag{2}$$

where E_{av} is the average illuminance on the test surface [lx], E_i^a is the measured illuminance of point i on the test surface [lx], M is the vertical number of distribution points, and N is the horizontal number of distribution points.

In the experiment, an illumination test platform with three horizontal and five vertical squares is constructed, and the test points are established at the centre of each square, as shown in Fig. 1. The distance between measured points is 1.2 m longitudinally and laterally; the height of the test face from the ground is 0.75 m; and the distance from the luminaires to the test face is 2.05 m. TES-1339 illuminance meter is used, and the test time selected is after 22:00 when the room is unaffected by other light sources.

All six types of lamp being used and the five types of LED lamp as alternative light sources are selected for grouping comparison test to select the new light source on the basis of the illumination suitability and energy saving rate. The luminaire numbers, grouping, test comparison parameters, and replacement results are shown in Table 1.

Table 1 indicates that when the illumination requirements are satisfied, the LED series luminaires that replace the original luminaires as the energy-saving light source can save energy remarkably.

The test results are the average value of illuminance of every single lamp in each point, and the uniformity ratio of illuminance of the test platform is reflected by the actual illumination distribution of each measuring point. The actual test data of T8 LED are considered as the representative, formula (1) is used for the theoretical calculation and simulation, and the actual and calculated illuminance and their distribution of each T8 LED measured point are obtained (Fig. 2(a)). In addition, whether the entire illumination value, uniformity ratio of illuminance, and lighting power density (LPD) of the room with energy saving luminaires meet the requirements must be tested and identified. Taking the first reading room as an example, the overall illumination and LPD of the room before and after the retrofitting are compared. Theoretical calculations show that if the reading room's lamp positions and its number remain unchanged, and each lamp position is replaced by three T8 LED tubes in parallel installations, then the reading room will be equipped with 116 sets of lamps, and the power of each set of lamps is 56 W. Hence, the requirements for illuminance and power density of the reading room can be completely satisfied, and the construction cost can be avoided by changing the lamps power and quantity. To verify whether the relevant indexes after lighting energy efficiency retrofitting satisfy the design requirements, the test platform is arranged, as shown in Fig. 2. Table 2 presents the related parameters and test, and Fig. 2(b) shows the calculated and measured values of the entire illuminance of the reconstructed room.

Table 2 shows that the power of three T8 fluorescent tubes in parallel installations and electro-

Table 1. Illuminance Test and Replacement Result of Luminaires

NO.	Luminaire Model	Power, W	Luminous flux, lm	Average illuminance, lx	Replacement result	Energy saving rate, %
1	T5Fluorescent lamp	28	1720	49.6	T5 LED	46
2	T5 LED	15	1860	53.9		
3	T8Fluorescent lamp	36	1800	52.3	T8 LED	50
4	T8 LED	18	2070	60.7		
5	3U Energy saving lamp	20	1260	37.8	11W LED bulb	45
6	3U Energy saving lamp	14	730	21.1	6W LED bulb	57
7	Spiral energy saving lamp	13	670	19.7	6W LED bulb	54
8	Spiral energy saving lamp	6	346	10.9	4W LED bulb	33
9	LED bulb	11	1070	42.2		
10	LED bulb	6	590	22.4		
11	LED bulb	4	430	13.6		

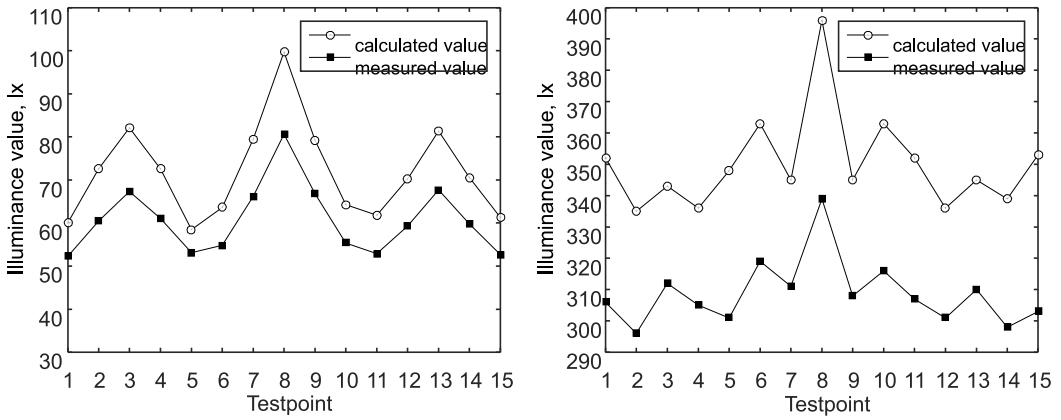

Fig. 2. Calculated and actual values of illuminance and its distribution

nic ballast used before retrofitting is 120 W per set. Although the illuminance conforms to the standard, the LDP value exceeds it. After replacing three T8 LED tubes in parallel installations, each index is better than the target value.

The distribution trend of the two types of test data and the calculated results at each measuring point are consistent (Fig. 2), which verifies the correctness of formula (1). The overall calculation result is slightly higher than the measured value because of the high value of the utilization coefficient *U* and the maintenance coefficient *M*, such that the empirical values of *U* and *M* must be revised according to the actual situation.

3.3. Design of Intelligent Lighting

Illumination testing is an important link in the implementation of lighting energy efficiency retrofitting. However, automatic control of lighting system, that is, intelligent lighting must be implemented to achieve the goal of lighting energy efficiency retrofitting. First, the traditional manual control lighting system not only increases the cost of labour

Table 2. Uniformity Ratio of Illuminance and LPD Analysis

Light Source Model	Combination mode of luminaires	Power per set, W	Luminous flux per set, lm	Illuminance, lx		LDP, W/m^2	
				target value	measured value	target value	measured value
T8 fluorescent lamp	3 lamps in parallel	120	6210	300	283.2	9	16.98
T8 LED	3 lamps in parallel	56	5400	300	308.8	8	7.91

but also loses control of the opening of light source according to the actual demand of each room, thereby wasting considerable electric energy. Second, people tend to desalinate the consciousness of energy saving and the phenomenon of energy use rebound becomes evident because of the decrease of lighting power. However, the manual control lighting system cannot overcome this phenomenon. Finally, manual control can neither effectively identify the effect of outdoor natural light on illuminance nor fully use natural light to reduce lighting energy consumption.

The analysis of the electricity utilization data of each room before the lighting energy efficiency retrofitting of the library indicates that the stacks and the reading room have large lighting area, dense light source, and high demand for illuminance, accounting for over 85 % of the total lighting power consumption of the library, which is the key point of lighting energy saving control. Therefore, the intelligent lighting control system, which is designed for the stacks and the reading room, provides three control modes or their combination, that is, timing, inductive, and illuminance control. Inductive control is adopted for the other public rooms or passageways. The stacks adopt the combined mode of timing and inductive. During opening hours, only the luminaires of the main channels are opened. The bookshelf and reading areas are equipped with dual technology detector to sense the activity of the personnel. The lighting system in the area is automatically turned on when someone looks up for books and periodicals, and the lighting system automatically shuts down otherwise. The reading room adopts the illuminance control preferentially, supplemented by the induction control mode. During regular opening hours of the reading room, the brightness of the artificial light source is reduced automatically when the illuminance is higher than the set value. Correspondingly, the induction control mode is activated when the illuminance is below the set value and automatically turns on the lighting for people's reading activities. The illumination detection of the reading area near the outer window is strengthened to maximize the use of natural light, obtain comfortable visual environment, and save electricity for lighting. Generally, the closer the reading area is to the window, the higher the illuminance of the natural light and the weaker the artificial illumination. By adjusting the illuminance of artificial light source through intelligent control system, the synthetic illuminance can be maintained within the set range.

The management platform of the intelligent lighting system is designed according to the network control mode, and the lighting trigger threshold is set simultaneously with the illuminance test. The trigger threshold of the dual technology detector is set according to the sensitivity requirement. Intelligent meter is set up in each lighting control area to realize acquisition, statistics, and transmission of energy consumption data. The intelligent lighting controller in the system has the function of conventional/intelligent mode switching, which can automatically switch to normal mode in case of network failure and improve the reliability of the system. Fig. 3 shows the structure of the intelligent lighting system.

To test the energy saving effect of the intelligent lighting system, the intelligent lighting system is divided according to the floor and kept running according to the conventional control mode and the intelligent lighting mode for one week after completing the retrofitting and the trial operation of the intelligent lighting system. The opening time of luminaires per day, the average rate of lights off, and the amount of electricity consumed are recorded, and the data obtained are compared with those obtained before lighting energy efficiency retrofitting. Table 3 shows the test results.

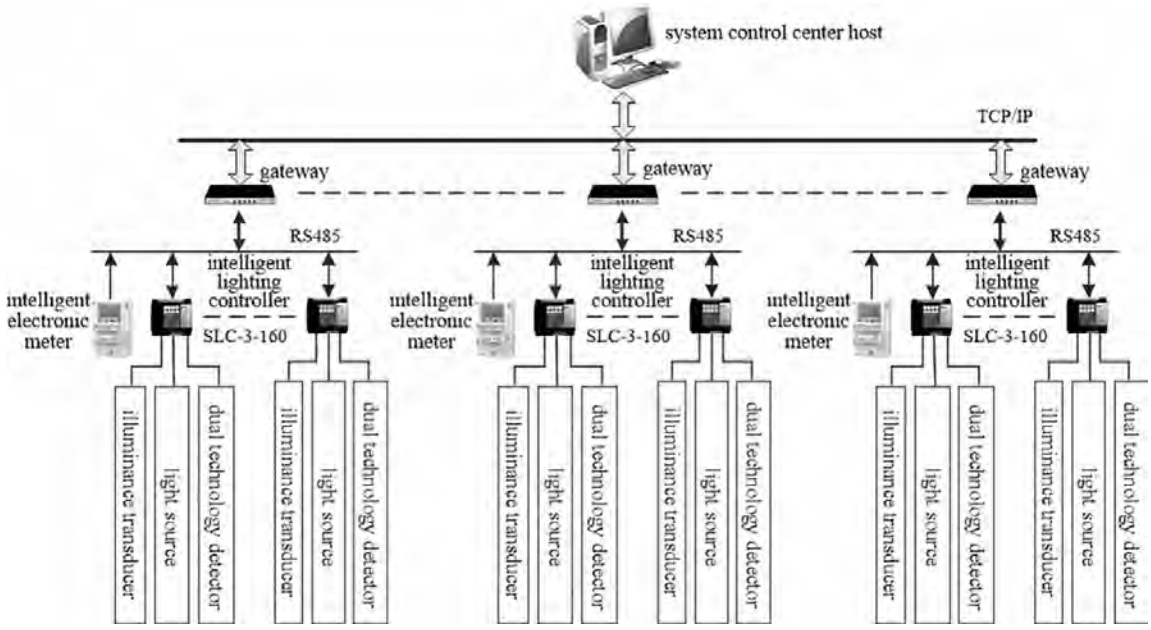

Fig. 3. Structural diagram of the intelligent lighting system

Table 3 shows that the total electricity consumption of the intelligent mode for one week after retrofitting is 49.61 less than that before retrofitting. If the conventional mode is adopted, then it is only 28.47 % less than before retrofitting. The opening time of luminaires after retrofitting evidently increases, whereas the ratio of lights off decreases. This result is the main reason for the significant increase in energy consumption of the intelligent mode and is a typical phenomenon of energy use rebound.

3.4. Economic Effect Evaluation

On the basis of the energy consumption bill of three consecutive years before lighting energy efficiency retrofitting of the library, the average annual lighting power consumption is 545,569.65 kW·h after the lighting energy efficiency retrofitting and the average weekly electricity consumption is 5,288.32 kW·h under intelligent mode for 36 weeks. With the library being open for 48 weeks a year, the annual saving power consumption is 291,730.29 kW·h. If the average electricity price is 0.89 yuan, then 259,640 yuan will be saved every year. Given the long service life and low failure rate of replaced LED lamps, maintenance cost can be saved. In addition, the use of intelligent lighting system can save on labour management fees and increase the operation and maintenance costs of intelligent system. Table 4 shows the costs details.

The planned payback period is 3.5 years. Given the opportunity cost of investment and the average social return rate, the dynamic investment payback period is calculated as

$$C_E = \frac{B\left[i\ 1+i\right)^n\right]}{\left(1+i\right)^n - 1}, \tag{3}$$

where C_E is the total investment; B is the total revenue; i is the social benchmark rate of return, which is assumed to be 8 %; and N is the dynamic investment payback period. After introducing C_E=776,573, B=364,520, and i=8 % into formula (3), n (2.44 years) is less than 3.5 years, and the investment returns are significant.

4. RESULT ANALYSIS AND DISCUSSION

According to the functional characteristics of the rooms on each floor of the library, the lighting energy efficiency retrofitting system is established based on illumination suitability analysis, and the intelligent lighting system is used to control the system. The overall energy savings rate reaches 50 %, the dynamic investment payback period is 2.44 years, and the effect of energy efficiency retrofitting is good.

The project is based on the illuminance test data to design the retrofit scheme. Through the illumination test, the performance of the energy sa-

Table 3. Experimental Data of Lighting Energy Consumption for One Week in Different Control Modes

	Conventional mode before retrofitting			Intelligent mode after retrofitting			Conventional mode after retrofitting		
Floor	Opening time of luminaires per day, h	Average ratio of lights off,%	Electricity consumed per week, kW·h)	Opening time of luminaires per day, h	Average ratio of lights off,%	electricity consumed per week, kW·h	opening time of luminaires per day, h	Average ratio of lights off,%	Electricity consumed per week, kW·h
5F	8	11	836.32	6	33	425.68	10	6	585.36
4F	13	13	2657.76	11	35	1372.29	15	8	1964.44
3F	14	12	2825.56	11.5	29	1413.75	16	7	1958.47
2F	14	11	3019.17	12	26.5	1516.13	16	7.5	2152.92
1F	11	10	1358.86	9	31	662.83	13.5	9	989.76

Table 4 Cost Benefit Details of Lighting Energy Efficiency Retrofitting (Yuan/Year)

Cost name	Total investment (CE)	Save electricity	Save labour costs	Save maintenance expenses	Maintenance expenses of the intelligent system	Total revenue (B)
amount of money	776573	259640	76560	65200	36880	364520

ving lamps, the overall illumination uniformity ratio, and power density of the room are guaranteed. In the intelligent lighting system with illuminance priority, the setting and modification of the illuminance sensor trigger threshold must be based on the data of the illuminance suitability analysis, and the synergistic optimization of the lighting environment comfort and energy saving effect is achieved.

In view of the energy use rebound effect, scholars at home and abroad have overcame this phenomenon by means of ecological feedback and adjustment of human energy use behaviour. Although the effect is not ideal, the use of intelligent lighting system eliminates this phenomenon well. In addition, this study only considers the dominant cost and income items in the analysis of economic benefits based on the conservatism principle; however, LED is a cold light source, which will inevitably reduce the energy of refrigeration of the air conditioning in summer. If these factors are considered, then the benefits of lighting energy efficiency retrofitting will be highly considerably.

5. CONCLUSION

On the basis of the lighting energy efficiency retrofitting project of a university library, this study aims to address the problem in which people only pay attention to the energy saving rate, ignore the illuminance standard after the retrofitting, and only pursue the high standard of the design but ignore the economy feasibility. This paper establishes a feasible decision system based on illuminance suitability analysis to achieve the overall goal optimization of multiple factors and avoid the phenomenon of “only caring for one thing” in the retrofit scheme.

The results show that using illumination test to select energy-saving lamps can simultaneously meet the requirements of illuminance and power density target value. The intelligent lighting system based on illuminance test can improve energy efficiency, achieve a comfortable visual environment, and overcome the energy use rebound effect. Finally, the calculation of the dynamic investment payback period verifies the feasibility of the retrofit scheme. The results not only apply to the lighting energy efficiency retrofitting of the library but also provide some reference value for energy efficiency retrofitting of other public buildings.

ACKNOWLEDGEMENTS

The authors are grateful for the support provided by the special scientific research founda-

tion of doctorate in colleges and universities (No. 20116120110010), the soft science research project of the ministry of housing and urban-rural development (No. 2015-R1–010).

REFERENCES

1. Nan L, Zheng Y, Becerik-Gerber B, Chao T, Nanlin C. Why is the reliability of building simulation limited as a tool for evaluating energy conservation measures? Applied Energy, 2015. V159, #12, pp.196–205.

2. Xin Z, Da Y, Tianzhen H, Xiaoxin R. Data analysis and stochastic modeling of lighting energy use in large office buildings in China. Energy and Buildings, 2015. V86, #1, pp.275–287.

3. Marie-Claude D, Åke B. Energy saving potential and strategies for electric lighting in future North European, low energy office buildings: A literature review. Energy and Buildings, 2011. V43, #10, pp. 2572–2582.

4. Guofeng M, Jing L, Nan L, Junjie Zhou. Cross-cultural assessment of the effectiveness of eco-feedback in building energy conservation. Energy and Buildings, 2017. V134, #1, pp. 329–338.

5. Selcuk A, Nazmi E. Development of an outdoor lighting control system using expert system. Energy and Buildings, 2016. V130, #10, pp.773–786.

6. Lvan C, Vineetha K, Naing Win O, Jussi P. Design of an energy-saving controller for an intelligent LED lighting system. Energy and Buildings, 2016. V120, #5, pp.1–9.

7. Diaz-Mendez S E, Torres-Rodríguez A A, Abatal M, Escalante Soberanis M A, Bassam A. Economic, environmental and health co-benefits of the use of advanced control strategies for lighting in buildings of Mexico. Energy Policy, 2018. V113, #2, pp.401–409.

8. Xuejun L. Application of teletraffic engineering modelling techniques for studying smart lighting systems for energy saving. Lighting Research and Technol, 2014. V46, #2, pp.113–127.

9. Juan F. De Paz, Javier B, Sara R, Gabriel V, Juan M. Corchado. Intelligent system for lighting control in smart cities. Information Sciences, 2016. V372, #12, pp.241–255.

10. Chih-Ling H, Chichun H, Yubin Chen. Development of an energy-saving glass using two-dimensional periodic nano-structures. Energy and Buildings, 2015. V86, #1197, pp. 589–594.

11. Heng W, Xianmin Z, Peng G. Double freeform surfaces lens design for LED uniform illumination with high distance–height ratio. Optics & Laser Technology, 2015. V73, #10, pp.166–172.

12. Danny H W Li, Angela C K Cheung, Stanley K H Chow, Eric W M Lee. Study of daylight data and lighting energy savings for atrium corridors with lighting dimming controls. Energy and Buildings, 2014. V72, #4, pp. 457–464.

13. Palacios-García E J, Chen A, Santiago I, Bellido-Outeiriño F J, Flores-Arias J M. Stochastic model for lighting's electricity consumption in the residential sector. Impact of energy saving actions. Energy and Buildings, 2015. V89, #2, pp.245–259.

14. Shengnan L, Jaap H, Cees M. The influence of color association strength and consistency on ease of processing of ambient lighting feedback. Journal of Environmental Psychology, 2016. V47, #9, pp.204–212.

15. Victor L. Chen, Magali A. Delmas, William J. Kaiser. Real-time, appliance-level electricity use feedback system: How to engage users? Energy and Buildings, 2014. V70, #2, pp. 455–462.

Bojun WANG,
Ph.D., candidate of Engineering Economy and Management, Associate Professor. Study at Xi'an University of Architectural Science and Technology

Yanping YANG,
Ph.D., candidate of Engineering Economy and Management, Economic Engineer. Study at Xi'an University of Architectural Science and Technology

Xiaojun LIU,
Doctor of Management, Professor, Doctoral Supervisor. Graduated from the Xi'an Jiao Tong University

Light & Engineering
Vol. 26, No. 3, pp. 140–142, 2018

Svetotekhnika
No. 2, 2018, pp. 75–77

ELECTRODE-LESS FERRITE-FREE CLOSED-LOOP INDUCTIVELY-COUPLED FLUORESCENT LAMP

Oleg A. Popov, Pavel V. Starshinov, and Victoriya N. Vasina

National Research University Moscow Power Engineering Institute (NRU MPEI)
E-mail: popovoleg445@yahoo.com

ABSTRACT

Electrode-less ferrite-free inductively-coupled low pressure discharge was excited in the mixture of mercury vapour (~10^{-2} Torr) and argon (0.1 Torr) at a frequency of 2.0 MHz and lamp *RF* powers of (150–202) W with the help of a 6-turn induction coil. The discharge lamp of rectangular shape (50 cm in length and 7 cm in height) employed a closed-loop glass tube of 30 mm in diam. Tube walls inner surface was coated with three-color phosphor (T_{cc} = 3100 K, R_a = 80). The induction coil made from silver-coated copper wire (ρ_w = 2.2x10^{-3} Ohm/cm) was disposed on the atmospheric side of tube walls, along closed-loop lamp tube perimeter. As plasma power, P_{pl}, grew from 127W to 180 W, coil power losses practically were unchanged, P_{coil} = (25–22) W. Lamp luminous flux, Φ_v, grew with plasma power from 10430 lm (P_{pl} =127 W) to 13500 lm (P_{pl} =180 W), while plasma efficacy, $\eta_{pl} = \Phi_v/P_{pl}$, decreased from 82 to 75 lm/W, and lamp efficacy $\eta_V = \Phi_v/(P_{pl} + P_{coil})$ decreased from 70 to 67 lm/W.

Keywords: ferrite-free inductive discharge, fluorescent lamp, low pressure mercury plasma, coil power losses, lamp and plasma efficacy, radiofrequency voltage (*RF*)

1. INTRODUCTION

Transformer-type inductively-coupled light sources excited in the mixture of low pressure mercury vapour and inert gas at *RF* frequencies (0.1–13.56) MHz and *RF* power (50–500) W have shown excellent characteristics: high luminous efficacy (up to 100 lm/W) and very high life-time (> 60000 h) [1, 2]. However, transformer-type lamp has one but substantial disadvantage: expensive and fragile ferrite cores encircling a closed-loop discharge tube. Meanwhile, ferrite-free inductively-coupled discharges could be excited at *RF* frequencies in a closed-loop lamp made from a tube of (50–70) mm in diameter with the help of an induction coil disposed on the atmospheric side of lamp walls, along its "inner" perimeter [3].

Here, we present results of an experimental study of ferrite-free closed-loop inductively-coupled lamp employing discharge tube of 30 mm in diameter excited with the help of an induction coil encircling the lamp around its "outer" perimeter.

2. EXPERIMENTAL SET-UP AND MEASUREMENT TECHNIQUES

An inductive plasma was excited and maintained at a frequency f = 2.0 MHz and *RF* power of P_{pl} = (127–180) W in the mixture of mercury vapour and argon in a closed-loop lamp made from cylindrical glass tube of 30 mm in diam. Tube walls inner (vacuum) surface was coated with three-colour phosphors (T_{cc} = 3100 K, R_a = 80). The lamp has rectangular shape of 500 mm in length and of 70 mm in height; the distance between two discharge tubes was H_2 = 6 mm (Fig. 1). A 6-turn induction coil made from silver-coated copper wire (ρ_w = 2.2x10^{-3} Ohm/cm) encircled the closed-loop discharge lamp along its perimeter. Mercury vapour was maintained at optimum pressure of ~ 10^{-2} Torr by con-

trolling amalgam (Bi-In-Hg) temperature; argon pressure was 0.1 Torr.

Sinusoidal *RF* voltage at a frequency of 2,0 MHz was sent from the signal generator (PM 5193, Philips) to the wideband amplifier (A-300, ENI), and further to the directional coupler (C5100, Werlatone). Forward and reflected *RF* power, P_{for} and P_{ref}, were measured with the help of *RF* power meter (NAP Z8, Rhode-Schwartz). The transferred *RF* power $P_{tr} = P_{for} - P_{ref}$ comprised plasma absorbed power, P_{pl}, induction coil power losses, P_{coil}, and *RF* power P_{cap} dissipated in low loss (<1 W) matching network ceramic capacitors C_{ser} and C_{par}. Induction coil *RF* voltage and current, U_c and I_c, phase shift between them, φ, and lamp and matching network powers, P_{lamp} and P_{cap}, were measured with the help of high voltage probe, current transformer, and 4-channel oscilloscope HP 54503A. Lamp luminous flux, Φ_v, spectrum, and lamp colour characteristics, T_{cc} and R_a were measured with the help of the computerized photometrical sphere. Plasma and lamp efficacy were calculated as $\eta_{pl} = \Phi_v/P_{pl}$, and $\eta_v = \Phi_v/P_{lamp} = \Phi_v/(P_{pl} + P_{coil})$, respectively.

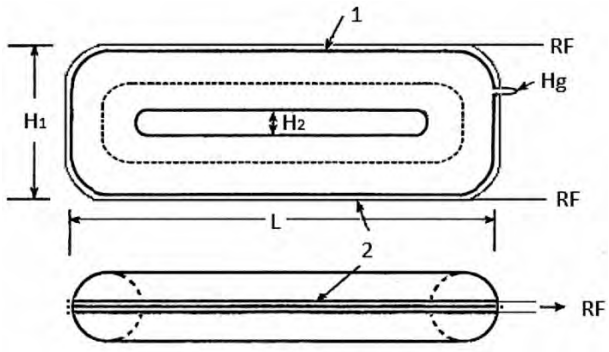

Fig. 1. Schematic drawing of ferrite-free closed-loop inductively-coupled lamp: 1 – discharge tube; 2 – induction coil; Hg – exhaust tubing with amalgam; RF – radio-frequency voltage

2. EXPERIMENTAL RESULTS AND DISCUSSION

The results of measurements are shown in Figs. 2, 3. It is seen from Fig. 2 that coil power losses, P_{coil}, did not show dependence from plasma power, P_{pl}, and had values of (22–25) W. Lamp luminous flux, Φ_v, grew as plasma power increased from 10430 lm (P_{pl} =127 W) to 13500 lm (P_{pl} = 180 W). Coil power efficiency $\eta_c = 1 - P_{coil}/(P_{pl} + P_{coil})$ increased with plasma power from 0,85 (P_{pl} = 127 W) to 0,89 (P_{pl} = 180 W), while lamp and plasma efficacies, η_v and η_{pl}, decreased from 70 to 67 lm/W, and from 82 to 75 lm/W, respectively (Fig. 3). The decrease of plasma efficacy η_{pl} as plasma power grew was due to the growth of the frequency of quenching collisions of resonantly excited mercury atoms with plasma electrons [3, 4].

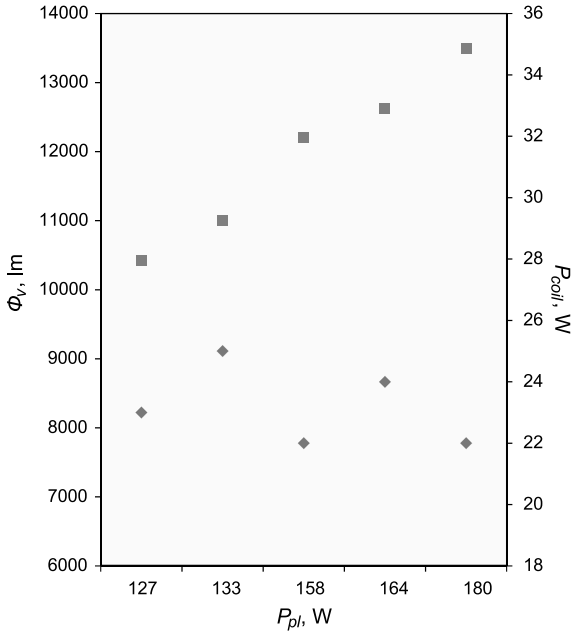

Fig. 2. Lamp luminous frux, Φ_V, and induction coil power losses, P_{coil}, as functions of plasma power, P_{pl}. ■ – Φ_V; ♦ – P_{coil}

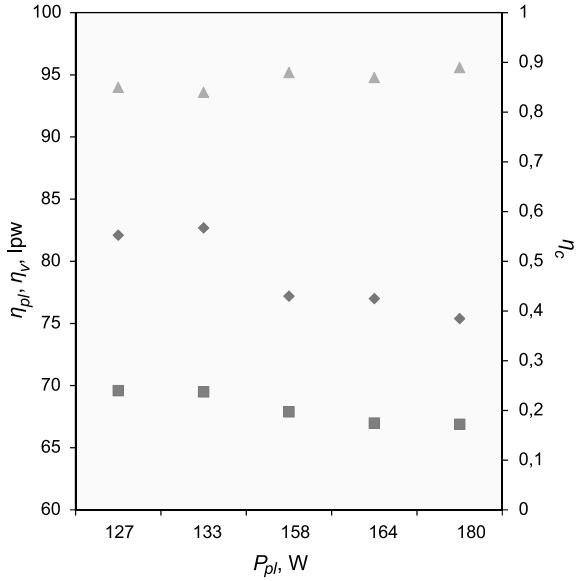

Fig. 3. Lamp and plasma efficacies, η_v and η_{pl}, and induction coil power efficiency, η_c, as functions of plasma power, P_{pl}. ♦ – η_{pl}; ■ – η_v; ▲ - η_c

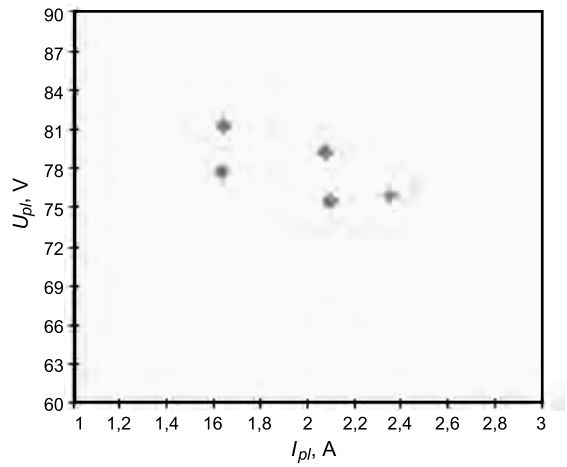

Fig. 4. Lamp volt-ampere characteristic, U_{pl} *vs* I_{pl}

Discharge current, I_{pl}, calculated within the framework of inductive discharge transformer model grew with plasma power from 1.63 A (P_{pl} = 127 W) to 2.35 A (P_{pl} = 180 W). While *RF* electric field, $\bar{E}_{pl}$, averaged across plasma diameter, decreased insignificantly from 0.76 to 0.72 V/cm. These values are essentially the same as *RF* electric fields (E_{pl} = (0.73–0.78) V/cm) in the transformer lamp plasma excited in mixture of mercury vapour (~10^{-2} Torr) and argon (0.1–0.12 Torr) in the closed-loop tube of 16.6 mm in diam. at a frequency of f = 265 kHz and plasma power of P_{pl} =180 W [5]. The dependence of plasma *RF* voltage, U_{pl}, from discharge current, I_{pl}, plotted in Fig. 4 has negative character and is in good agreement with the dependence of $\bar{E}_{pl}$ from P_{pl} that is typical for high density low pressure mercury discharges [4].

3. CONCLUSION

It was experimentally shown that plasma efficacy 80 lm/W and lamp efficacy 70 lm/W could be obtained in a ferrite-free closed-loop inductively-coupled mercury low pressure fluorescent lamp with discharge tube of 30 mm in diam. The further increase of plasma efficacy η_{pl} could be achieved by rising argon pressure to (0.2–0.3) Torr, at which ultraviolet UV (λ = 254 nm) radiation generation in the inductive discharge in the closed-loop lamp with tube of 16,6 mm in diameter operated at the same power level was found to be maximal [5]. To substantially increase lamp efficacy, $\eta_V = \eta_c\eta_{pl}$, induction coil efficiency, η_c, should be increased to 0,95–0,97 by reducing coil power losses to (4–5) W. This could be done by using in induction coil low loss ($\rho_w \leq 5x10^{-4}$ Ohm/cm) Litz wire [3].

REFERENCES

1. Shaffer J.W. and Godyak V.A. The Development of low frequency high output electrode-less fluorescent lamp // J. Illum. Eng. Soc., 1999, № 28, p.142.

2. Popov O.A., Chandler R.T. Inductively-coupled transformer-type light source operated at frequencies of 150–400 kHz and RF power of (200–500) W // High Temp. Phys. 2007, № 4, p. 795.

3. Popov O.A., Chandler R. Ferrite-free high power electrodeless fluorescent lamp operated at a frequency of 160–1000 kHz // Plasma Sources Sci. Technol. 2002, Vol. 11, № 2, p.218.

4. Elenbaas W. Light Sources. – New York: Crane, Russak & Co. 1972, p. 240.

5. Levchenko V.A., Popov O.A., Svitnev S.A., Starshinov P.V. Electrical and Emission Characteristics of a transformer type lamp with discharge tube of 16.6 mm in diam. // Light & Engineering, 2016, № 2, pp. 77–81.

Oleg A. Popov,
Prof., Dr. of Science, graduated from MPEI in 1965, Professor at the chair "Light and Engineering" NRU MPEI

Pavel V. Starshinov,
M. Sc., graduated from NRU MPEI in 2015, post graduate student at the chair "Light and Engineering" NRU MPEI

Victoriya N. Vasina,
student of the chair "Light and Engineering" NRU MPEI

Light & Engineering
Vol. 26, No. 3, pp. 143–149, 2018

Svetotekhnika
No. 6, 2017, pp. 15–19

ON THE EFFECTIVENESS OF MODERN LOW-PRESSURE AMALGAM LAMPS

Michiel van der Meer [1], Fred van Lierop [2], and Dmitry Sokolov [3,4]

[1] *Philips Lighting Company, Belgium*
[2] *UV Lamp Consulting Company, USA*
[3] *LIT Scientific and Production Association, Moscow, Russia*
[4] *E-mail: sokoloff@npo.lit.ru*

ABSTRACT

A lot of attention is paid to the efficiency questions of modern amalgam lamps of low pressure in connection with more and more growing relevance of increasing energy efficiency of installations for water, air and surface disinfection. The real efficiency of a radiation source, as well as of the whole UV disinfection system, is an operational parameter much important for the customers. In this work, factors influencing efficiency of low pressure lamps are considered in detail. It is shown that efficiency of the modern amalgam lamps at the beginning of their lifetime is about (30–40)%.

Keywords: efficiency, performance factor, low pressure amalgam lamp, UV disinfection

Ultra-violet radiation is extensively applying in various fields of human activity and actively uses as a method of bactericidal treatment of water, air and surfaces [1]. For the last twenty years, UV disinfection method manifested a rapid growth. The technology is allowed the cardinal changing approaches to disinfection of environments, and in this case the UV disinfection method most considerably has been developed as a method of water disinfection [2]. Besides water supply and wastewater disposal, the UV disinfection is also widely used in various industries: food, pharmacological and electronic industry, medicine, recycling water supply, fish breeding etc., [1].

It is possible to say confidently that a certain equipment market is formed, and the most large-scale manufacturers of which are such companies, as *Trojan* (Canada), *Wedeco Xylem* (USA-Germany), *LIT Technology (Russia-Germany)*, *HALMA Fluid Technology Group* (Great Britain) and many others.

The UV technology success would be impossible without a significant progress of the bactericidal UV radiation sources. During the last twenty years, gas-discharge UV radiation sources and especially amalgam lamps of low pressure made a huge sudden scientific and technological change in their development. One can remember that ten or fifteen years ago lamps of up to 100 W power, generally lamps of so-called uviol glass (soft glass) or the same mercury lamps but made of quartz glass named *standard low pressure mercury lamps* (standard mercury lamps of low pressure) were basic sources for UV installations. Then quartz mercury lamps of an increased power (high output) arose, and finally amalgam lamps appeared. With technology progress, amalgam sources of 200, 300, 700 and even 1000 W power appeared. This made it possible to decrease essentially capital investment costs due to the UV machine cost reduction when decreasing number of lamp needs at the same disinfection level and at the same water consumption passing through the disinfection installation. The most large-scale manufacturers of the modern amalgam lamps of low pressure are the following: *Heraeus Noblelight* (Germany), *LSI/Lighttech* (USA-Hunga-

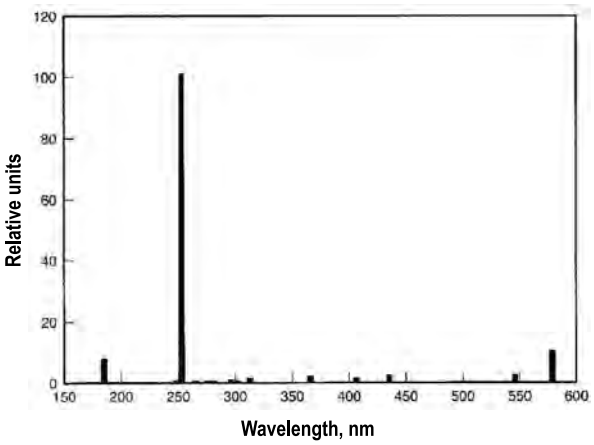

Fig. 1. Spectrum of the low pressure mercury discharge, the 254 nm line is accepted to be 100 %

ry), *Philips Lighting* (Belgium-China), LITAS (Russia), *Wedeco Xylem* (Germany), *UV-Technik/Hoenle group* (Germany), *First Light* (USA), as well as numerous Asian manufacturers [2].

The core of any UV machine is the UV radiation source, and this work is dedicated to UV amalgam lamps of low pressure. What is amalgam lamp? UV radiation source in mercury lamps of low pressure and in the amalgam lamps, which are widely used for disinfection, there is an arc discharge of low pressure in mercury vapour and in inert gases. The difference between them is a mercury vapour source: a small amount of liquid metal mercury is placed in envelopes of mercury lamps, and in amalgam lamps, amalgam is used, which is a solid alloy of mercury with metals. An optimum pressure of mercury vapour is about (0.7–1.5) Pa, and pressure of inert gases (most often neon or argon, or their mixtures) is (100–300) Pa. Under such conditions, (30–40)% of the discharge electric power transforms into radiation of mercury resonant line of 253.7 nm wavelength, which is near maximum of the bactericidal efficiency curve. The spectrum is linear (Fig. 1), and UV radiation portion at 185 nm and 254 nm lines is (90–98)% of all discharge radiation.

It should be noticed that lamp characteristics of many manufacturers are often very close to each other. For example, if to compare well-known standard lamps of about 300 W, such as *UV3000+, XPT240, DB300, UVI260, GPHVA1554T6L,* then it appears that their current, electric power, efficiency and UV radiation output are very close. Indeed, lamp current fluctuates from 1.8 A to 2.0 A, UV radiation power is within 87 W and 95 W, and electric power is within the range of (230–260) W. Thus, efficiency of these sources is approximately identical and lies in an interval of (35–38)%.

With increase of power and working current, the lamp characteristics are changing. The following operational characteristics of the lamps are reached to date: electric power is up to 1 kW, life time resource is (12000–16000) h, UV radiation decrease by the life time end is (5–10)%.

Many lighting companies actively co-operate and technology information exchange on lamp parameters, because such parameters as UV radiation power, efficiency of the source, lamp resource, the radiation decrease in the operation process are very important information for the customers. Almost all fore-quoted companies are members *of IUVA* (*International Ultraviolet Association)* and took part in development of a standardised protocol to measure low pressure amalgam lamps [4] based on the so-called *Robin Round* test. This allowed closer co-operating in terms of information exchange on the lamp characteristics.

It should be noticed that over the last years, an increasing attention is paid to efficiency of UV sources, which taking into account growth of electric energy tariffs and economics of treating environment (for example, water) has the great significance. And if UV radiation reduction/retention purpose or lamp lifetime increase are solvable engineering tasks, then lamp efficiency question is a question of the gas discharge physics.

What is UV lamp efficiency? Traditionally lamp efficiency is a relation of full UV radiation flux to electric power:

$$\eta = \frac{\Phi_{254}}{\Phi_{el}} \cdot 100\ \%. \qquad (1)$$

Are the (35–38)% efficiencies big or small, such as, for example, in the case of a standard lamp the *DB*300 type? Based on a comparison with other light sources, one can say confident that this is a much high efficiency, and this is an exceptional case when nature helped people, especially taking into account that 254 nm line lies close to the efficiency maximum of microorganism inactivation on the bactericidal curve.

An alternative in this UV area can only be xenon excimer sources with the correspondent phosphor or other sources with exciplex molecules, which efficiency can reach high values of (10–20)% under certain conditions [4, 5] as well, as UV light

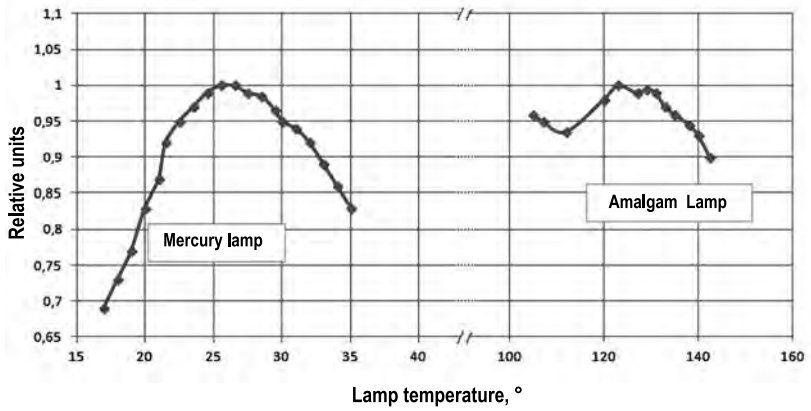

Fig. 2. Mercury vapour pressure depending on the temperature in a mercury and in amalgam lamps

emitting diodes of (260–275) nm wavelengths, which efficiency at present does not exceed several percents, and commercially available crystals have efficiency lower than 1 %. [6.7]

Let's consider factors influencing efficiency of low pressure amalgam lamps. From the view point of physical processes in the lamps, the following factors influence the radiation output: lamp current and frequency, the envelope diameter, thickness of the envelope wall, the lamp envelope coating, composition and pressure of ballast gas, isotope composition of mercury.

In our opinion, detailed and deep from the view point of the gas discharge physics consideration of influence of different factors on the radiation output (full flux) with wavelength of 254 nm is rather laborious, therefore we will only consider these processes qualitatively.

PRESSURE OF MERCURY VAPOUR

Whether mercury vapour pressure influences UV radiation output of amalgam lamps? Of course, when mercury vapour pressure increases and other discharge parameters are invariable, UV radiation output also increases as number of the excited and radiating atoms grows. However, when some optimum level is exceeded, efficiency decreases again (Fig. 2). This is caused by influence of re-absorption of resonant radiation and by increase of effective life time of the excited level, as well as by decrease of electronic temperature.

It should be also noticed that a part of energy is lost due to collisions of the excited atoms with each other and with electrons.

Method of achieving an optimum pressure of mercury vapour, for example, maintenance of a certain temperature mode of the amalgam is only an engineering problem and is implemented in each case differently by the manufacturer of a specific lamp type (multicomponent amalgams, pellet technology, cold point). To obtain UV radiation output higher than some maximum is impossible at an optimum mercury vapour pressure in the lamp.

FILLING THE LAMP WITH GAS, ITS COMPOSITION AND PRESSURE

It is possible to show that the main factor to pump a needed 6^3P_1 level is electronic temperature of plasma. The problem is to reach its optimum value. Whether mercury vapour discharge can work without ballast gas in general? Of course and moreover, the first mercury lamps were constructed in such a way. Without ballast gas, electrons and then ions, under influence of ambipolar diffusion go to the wall too quickly, and to maintain a balance of the particles, plasma provides a high speed of forming ion – electronic couples. And this leads to an increase of electronic temperature. A high electronic temperature allows pumping energy not only into the 254 nm needed line but also into other unnecessary lines, which leads to losses.

The most important function of inert gases is reduction of the electron diffusion rate towards the wall. One can adjust electron temperature up to an optimum level by changing pressure of the inert gas. The optimum level is the one, at which energy portion for excitation and radiation of mercury atoms considerably surpasses the energy losses portion for elastic impacts. Excitation and radiation losses depend on the electron temperature exponentially, and elastic impact losses depend linearly. Electron temperature should not be too high

Fig. 3. Quartz walls of a new lamp envelope (above) and of an exhausted lamp envelope

since it is necessary that 6^3P states were mainly excited, and that more high levels were not noticeably excited. To some limit, reduction of the inert gas pressure leads to increase of discharge UV radiation generation efficiency and energy distribution over the spectrum can change. However, this dependence has a non-monotonic character, and, among other things, because of the previously mentioned influence of the inert gas on the absorption processes of the resonant radiation. If the lamp pressure is too low, ion and electron flow towards the wall is abruptly increasing, and the ionisation energy losses portion is growing.

It should be noticed that if the pressure is lower than 1 mm Hg, resource of the oxide cathode becomes a limiting factor: barium oxide particles due to high values of diffusion coefficient "go" into plasma, thereby reducing the electrode resource to unacceptable values. Mechanisms of emission substance consumption of the low pressure lamp oxide cathodes are fully described in [8].

Thus, it is possible to say that the typical pressure interval of buffer gas is rather narrow and is within (0.8–2) mm Hg.

A high electron temperature required for the UV radiation optimum output can be reached by replacement of one buffer gas with another, in which mercury electron and ion diffusion speed is greater, and by use of lower pressure with retention of the same tube diameter. Indeed, velocity of electron and ion disappearance changes according to change of ambipolar diffusion coefficient of ions in inert gases, which in this case is determined by mobility of ions. Approximate values of mercury ion mobility in three lightest gases at 0 °C and with pressure equal to 100 kPa (760 mm Hg) are equal to the following: for helium – 19.6 $cm^2/(V \cdot s)$, for neon – 5.9 $cm^2/(V \cdot s)$, for argon – 1.85 $cm^2/(V \cdot s)$. Respectively, mobility of mercury ions in krypton and xenon is evens less. The lighter gas is, the mercury ion mobility is higher in it. Thus, temperature of electrons and consequently UV radiation output saturation level are maximum in helium and minimum in xenon.

From the practical point of view, xenon and krypton are inapplicable because of a low radiation output, and helium is extremely fluid and can be only considered here theoretically. Therefore in practice, argon, neon and their mixtures are used. Certainly, an important factor is gas purity.

LAMP ENVELOPE COATING

One of the most important characteristics of the lamps is UV radiations decrease at the lamp service end. To ensure a confident disinfection even after (12000–16000) h of operation, the UV machine design is calculated so that to take into consideration a possible weakening of the full bactericidal lamp flux. Certainly, the less is radiation decrease, the more profitable is the source from practical point of view and the higher is its efficiency by the end of the lifetime. It does not matter for a customer, what source efficiency was at the operation beginning but it is important what will be lamp efficiency at its end. So, all UV installations are calculated for their operation end.

Darkening mechanism of inner surface of a lamp quartz tube (Fig. 3) was studied and discussed in [9, 10]. It is connected with formation of mercury oxide on the quartz tube inner surface. This process is caused by the ambipolar diffusion, which is initiated by formation of electric field between plasma column and tube wall. Mercury ions are accelerated in this electric field, obtain kinetic energy and affect the quartz wall. This leads to formation of *Hg-O* links. Mercury oxide (*HgO*) intensely absorbs UV radiation.

Thus, a mercury oxide layer of only 10 nm thickness absorbs approximately 50 % of UVC radiation generated by the discharge.

For which purpose envelope inner surface is covered? The coating is needed to solve the problem of quartz glass surface effective protection against interaction with the discharge plasma. There are many methods and approaches to create a protect cover. The main approach is protection using a layer transparent for UVC radiation being more resistant to chemical exposure of mercury ions. As a rule, various metal oxides are used for this purpose. In total,

the layer structure obtained using different coating methods can be divided into two groups: layers of nanoparticles and mesoporous layers as oxide films.

Each method has its advantages: use of nanopowders is an easy, technological and inexpensive way, whereas creation of thin and strong mesoporous coatings is much more complex technology, which means use of decomposition reactions at a high temperature, or of so-called sol-gel technology. The results of use of such technologies also differ. Decrease of UVC full flux of a lamp during the lifetime is connected with the protection cover type, filling of the lamp, current loading of the lamp, etc. After (12000–16000) hours of lamp operation, the decrease is from 5 % to 10 % for mesoporous coatings and from 15 % to 20 % for nanopowders (Fig. 4).

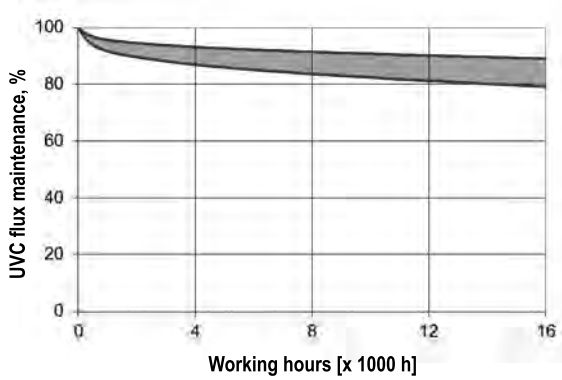

Fig. 4. Typical curves of UV radiation decrease for amalgam lamps of high power with mesoporous coating (above) and with coating of nanopowder (below)

CURRENT OF THE LAMP

With any filling of a lamp when current increasing, power of UV radiation grows first till r it achieves the saturation, or a speed of this increase is significantly reduce. In such a case, UV radiation efficiency due to discharge generation decreases. This is caused by increase of the electron concentration and by increase of contribution into gas heating of electron elastic collisions with atoms of inert gas and mercury, as well as by increase of suppressing excited states of mercury atoms by means of electrons during inelastic impacts of the second kind. The one more reason being the most important is a decrease of electric field strength and of electron energy owing to increase of concentration of metastable mercury atoms and to strengthening step process role.

LAMP CURRENT FREQUENCY

Influence of the lamp current frequency was repeatedly studied [11, 12]. It is known that in the low pressure discharge, the main losses of charged particles occur due to ambipolar diffusion onto the envelope wall. Duration of ambipolar diffusion is milliseconds, and it is less than the mains voltage period in the event of the industrial frequency use of (50–60) Hz. Therefore, the discharge extinguishes at the end of each half-cycle and lights up at the beginning of each next half-cycle. With such mode, configurations of the discharge current and of the lamp voltage do not coincide. Use of an electromagnetic throttle as a current stabilizer is a traditional but outdated solution because of a small number of switches on, a relatively low lamp resource, a lesser energy contribution into plasma and a low power factor. In practice, for powerful amalgam lamps electronic ballasts are used, which operate with quasi-sinusoidal current of (20–70) kHz frequency. This allows eliminating the above listed defects of electromagnetic ballasts. However, a further frequency increase is not prospective. First, this does not lead to an essential increase of the 254 nm line output as the near-electrode losses reduction reserve is not infinitely big. Secondly, this leads to the wire noticeable capacitive losses. The practical limit is (60–70) kHz interval, and most often (30–40) kHz interval is used in view of an insignificant difference of the discharge efficiency in these frequency intervals, as well as proceeding from a necessary reserve for the systems of adjusting power, with which the lamp current frequency significantly increases.

Current configuration also influences discharge characteristics. For example, instead of sinusoid, one can apply rectangular pulses of meander type, which can theoretically lead to increase of discharge input efficiency into plasma. However, one can show that for the 254 nm line this efficiency additive is small (1–3)%, and wire losses due to use of such current configuration because of the higher harmonics may be very essential, so it can lead not to increase of the system general efficiency but to its decrease.

CHANGE OF DIAMETER

A change of the discharge diameter is influence the discharge in two ways. On the one hand, reduc-

tion of the diameter leads to increase in losses of charged particles, and on the other, it leads to increase in current density. Therefore, when increasing the discharge tube diameter, efficiency first is raise as charged particle losses decrease, and then is reduce as the electronic temperature falls.

THICKNESS OF THE LAMP ENVELOPE WALL

A lamp envelope wall thickness is determined by two major factors: mechanical strength and transmission factor of the quartz glass. From the view point of UV radiation output, minimum thicknesses are most advantageous, because depending on absorption factor (quality) of quartz glass, UV radiation output keeps in with the Beer–Bouger – Lambert law. However, traditionally proceeding from the reasons of mechanical strength, the wall thickness is selected though minimum but sufficient. Practically it is from 1mm to 2 mm. Transmission of a good quartz glass is (87–89)% relative to 1 mm of the thickness. A pure quartz glass allows obtaining transmission values even above 90 %, however alloying additives (100–200) *ppm* TiO_2 are specially added into quartz to block the 185 nm line, and in such case an insignificant decrease of the 254 nm line also takes place.

ISOTOPE COMPOSITION

Due to presence of seven isotopes in natural mercury: ^{196}Hg (0.146 %), ^{198}Hg (10.02 %), ^{199}Hg (16.84 %), ^{200}Hg (23.13 %), ^{201}Hg (13.22 %), ^{202}Hg (29.80 %) and ^{204}Hg (6.85 %), an effective capture of resonant radiation is less than if mercury would consisted of the one isotope. The studies of the mercury isotope composition influence on the resonant radiation output shows that its increase is possible, approximately by 10 %, using change of the isotopes ratio [13]. However, because of high prices of the photochemical method of isotope separation, this task is not topical.

We have considered characteristics, which to the maximum extent determine lamp operation efficiency. As it was already shown above, many factors limit UV radiation output. Theoretically, the efficiency of gas discharge in mercury vapour may be very high [14]. One can show that with very low pressure of some mixtures of buffer gases, as well as with low current density, it is possible to obtain the source efficiency close to (50–55)%. However, such sources do not have a practical sense in view of either short lifetime, or a low UV radiation flux.

CONCLUSION

Anyway, the data provided by lighting companies are very important for designers and manufacturers of UV equipment. On the basis of a wide practical experience, of theoretical studies, mutual lamp measurements in laboratories and of the reasons presented above, we declare that efficiency of modern powerful sources is within (30–40)% at the beginning of the lifetime. These data are generally accepted, multiply checked by mutual measurements and published in official catalogues of the fore-quoted companies.

Sometimes UV equipment manufacturers for the marketing purposes declare ultrahigh efficiency of their lamps, thereby consciously or unconsciously misleading the consumers, for example specifying efficiency of a lamp without regard to electron ballast losses and extending this efficiency to all UV system as a whole. Or they give the data obtaining with a special ballast, which can only provide such efficiency in some conditions (for example, being located near the lamp, which is often inconveniently and isn't applied), etc.

The consumers should remember that they should estimate the UV system energy efficiency proceeding from all consumed power carefully considering all its operation modes and should not believe the fore-quoted marketing statements.

REFERENCES

1. Karmazinov F.V., Kostyuchenko S.V., Kudryavtsev N.N., Hramenkov S.V. Ultra-violet technologies in the modern world: A collective monograph, Dolgoprudny: Intellekt Publishing House, 2012, 392 p.

2. Vasilyev A. I, Kostyuchenko S.V., Kudryavtsev N.N., Sobur N.N., Sokolov D.V. UV disinfection technologies for water, air and surfaces treatment, // Svetotekhnika, 2007, #5, pp. 6–11.

3. Lawal, O., Dussert B., et al. Proposed method for measurement of the output of monochromatic (254 nm) low pressure uv lamps // IUVA News, 2008, V. 10, No.1, pp. 14–18.

4. Beleznai, S., Mihajlik, G., Agod, A., Maros, I., Juhasz, R., Nemeth, Z., Jakab, L., Richter, P. High-efficiency dielectric barrier Xe discharge lamp: theoretical and ex-

perimental investigations // J. Phys. D: Appl. Phys., 2006, V. 39, pp. 3777–3787. 5. Lomayev M.I., Skakun V.S., Sosnin E.A., Tarasenko V.F., Shitts D.V., Erofeyev M.V. Exilamps are effective sources of UV and VUV radiation // Uspekhi Fizicheskikh Nauk (Achievements of Physical Sciences), 2003, V. 173, #2, pp. 201–217.

6. Pagan, J., Lawal, O. Coming of age – UVC–LED Technology Update // IUVA news, 2015, V. 17, No. 1, pp. 21–24.

7. Moe, C. RADTECH REPORT, 2014, ISUE1, pp.45–49.

8. Rokhlin G.N. Discharge light sources. Moscow: Energoatomizdat, 1991, pp. 328–337.

9. Vasil'ev A.I. at al. Effect of a Protective Layer on the Lifetime and Output Radiation Intensity Decay Rate of Quartz Low-Pressure Gas Discharge Lamps // Technical Physics Letters, 2006, V. 32, No. 1, p. 42.

10. Pecherkin V. Ya. Ph.D. Thesis "Study of mechanisms of decreasing UV radiation and operation resource of UV radiation sources with mercury arc of a low pressure", Moscow, 2007. 11. Litvinov V.S., Troitsky A.M., Holopov G.K. Characteristics of domestic fluorescence lamps when working at increased frequencies // Svetotekhnika, 1961, #1, pp. 5–10.

2. Milenin V.M., Timofeev N.A. Concerning a possibility of increase of low pressure gas-discharge light sources luminous efficacy // Svetotekhnika, 1981, #4, pp. 6–7.

13. Petrov, G.M., Giuliani, J.L. Inhomogeneous model of Ar-Hg direct current column discharge // Journal of Applied Physics, 2003, V. 94, No. 1, pp. 62–74.

14. Grossman, M.W., Lagushenko, R., Maya, J. Isotope effects in low-pressure Hg-rare-gas discharges // Physical Review A, 1986, V. 34, No. 5, p. 4094.

Michiel van der Meer,
Ph.D. Since 2000 he works in the Development Central Department of Philips Company, since 2004 – in the UV lamp field, and, at present, – in the UV diode new application field

Fred van Lierop,
Ph.D., chemical engineer. During 25 years he worked in different divisions of Philips Company, (Holland, Belgium, the USA and China) in the field of light source development and production. Since 2011 he is the owner of F&Consulting Company. At present, he is the chief scientific specialist of UV Lamp Consulting Company (USA)

Dmitry V. Sokolov,
Ph.D., graduated from Moscow MPEI University, Chief of the Development Department at the LIT Scientific and Production Association

Light & Engineering
Vol. 26, No. 3, pp. 150–154, 2018

Svetotekhnika
No. 3, 2018, pp. 56–59

PULSE IGNITION DEVICES WITH NEW CIRCUIT SOLUTIONS

Alexander M. Mayorov and Michael I. Mayorov

Ogarev Mordovia State University, Saransk
E-mails: allexx1383@mail.ru; mayorovmi@mail.ru

ABSTRACT

The most of three-lead domestic pulse ignition devices (PID) do not provide parameters of high-voltage pulses determined by the lamp operation manuals. New circuit solutions are presented, which meet the requirements to HP sodium lamps used in street illumination and greenhouse irradiation. It is proposed to separate two functions of the three-lead PID pulse transformers: generation of high-voltage pulses and transmission of the lamp full current. To generate high-voltage pulses, transformers with a big turn number of thin wire should be used. And to transmit lamp full current, high-frequency throttles with a low resistance should be applied. A version of calculating parameters of a high-frequency throttle and oscillograms of pulses generated by the PID are given.

Keywords: discharge lamp, pulse ignition device, high-voltage pulse

It is known that production volume of ballasts, especially for high pressure sodium lamps (HPSL) and metal halogen lamp (MHL) are still big and such situation will remain for a long time [1].

For ignition of HP discharge lamps in circuits with electromagnetic ballast, it is necessary that the PID generates pulses with certain voltage amplitude and duration. So for some types of such lamps, pulse parameters specified in the Table are necessary.

Parameters of pulses generated by a PID are determined by the PID electronic circuit features, and the pulse transformer parameters, such as transformation coefficient, inductance of primary and secondary windings, as well as saturation current.

Domestic enterprises only manufacture PIDs providing high-voltage pulse parameters corresponding to the given in the Table with a parallel ignition circuit (the pulse oscillogram is given in Fig. 1, curve *1*).

Such PIDs have two leads and are connected in parallel to the lamp switched to the circuit in series with the ballast throttle, which is a ballast element limiting lamp current. Lamp current in this circuit does not flow through the PID, which causes its simplicity, low cost and universality. A disadvantage of such PID is that high-voltage pulses influence not only the lamp but also the ballast throttle, as well as the connecting wires between the throttle and the lamp. This reduces ballast reliability, causes a necessity to strengthen insulation of the ballast

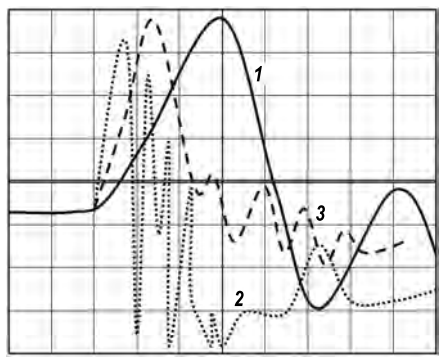

Fig. 1. Oscillogram of pulses generated by different type PIDs:
1 – PID-T 70–1000 PID (two-lead); *2* – 400/220V-012 PID; *3* – *Z 1000 S* PID;
(1000 V/div 1 μs /div; 0 is one square lower than the screen middle)

throttle and leads to a dependence of the PID output pulse parameters on the input wire length and on the ballast throttle structure [2].

Fig. 1 also shows oscillograms of the pulses generated by a sequential ignition PID (curves *2* and *3*). One can see from these oscillograms that such PIDs do not provide high-voltage pulse parameters according to the Table. So pulse duration at a level of 3 kV generated by PID400/220V-012 is 0.5 μs, and by PID *Z 1000 S* it is equal to *1* μs. Application of these PIDs causes a necessity of pre-term replacement of operable lamps, which are not ignited because of insufficient pulse duration. Sequential ignition PIDs have three leads, two of which are connected in series with the lamp [2]. Sequential ignition PIDs have certain power losses, big size and mass (as pulse transformer secondary winding should be designed for the lamp current passing through it). However, such PIDs are most widespread as they do not require strengthening insulation of the ballast throttles.

PID circuits without a pulse transformer are known, because functions of the latter are performed using a ballast throttle with a drop wire [2]. On the one hand this allows obtaining a big amplitude voltage wide pulses and reducing PID size, mass and cost. Such PID circuits are widely used abroad, for example in the *ZRM 2300C201* PID and in *ZRM 4000B101* (see also article [3]). But they require presence of special ballast throttles with drop wires and strengthened insulation.

It is also known a circuit of serial-parallel three-lead PIDs [4], which were produced in large quantities since eighties, for example, 250–400ДНаТ/220 PID. The throttle voltage when generating ignition pulses by these PIDs did not exceed 2000 V, which did not require special ballast's throttles with strengthened insulation. But by mass-dimensional factors, these devices did not differ much from sequential ignition PIDs. Therefore, the problem of creating an effective and cheap three-lead PID for HP discharge lamps of a big power is topical until now. It can be solved by a little addition, which turns a two-lead PID into three-lead eliminating defects of two-lead PIDs [5]. It is proposed to separate two functions of three-lead PID pulse transformers: generation of high-voltage pulses and transmission of a lamp full current by means of two separate inductors. An apparent complication of the structure allows generating pulses with characteristics selected in advance using a pulse transformer with

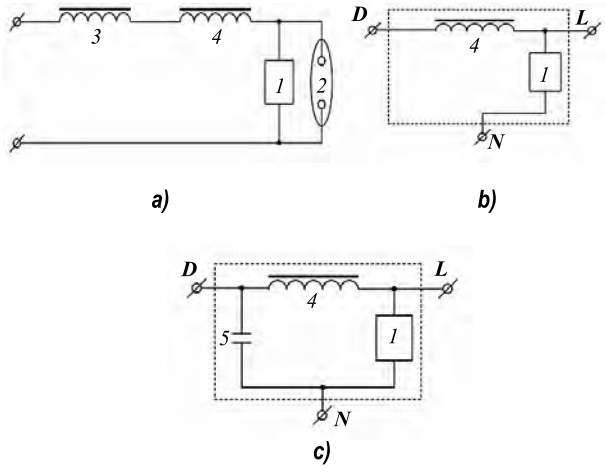

Fig. 2. PID circuit versions [5]

a large number of thin wire's turns. And to pass the lamp full current, one should use a high-frequency throttle with a small resistance protecting the throttle ballast against a breakdown. This separation is especially effective for PIDs designed for big currents and big pulse durations.

Fig. 2 *a* shows a circuit ballast with PID. This circuit contains two-lead PID1, connected in parallel with discharge lamp *2* switched to the circuit in series with ballast throttle *3* and with high-frequency throttle *4* complementary added in order to protect ballast throttle *3* against breakdown by the PID high-voltage pulses. PID1 and high-frequency throttle *4* can be placed in the same case with three leads (Fig. 2, *b*.)

The ballast within a PID operates as follows. When switching on, PID1 generates high-voltage pulses mainly with 3–5 kV amplitude. These pulses create a conducting channel in the interelectrode gap of lamp *2*. In this channel, high-current discharge plasma is formed then. The discharge is supplied through ballast throttle *3* and high-frequency throttle *4* from a power-line. Throttle *4* limits pulse voltage affecting ballast throttle *3* during pulse generation to maximum permissible for this ballast throttle 3 (usually it is 2 kV. After lamp *2* is ignited, it shunts PID1 charge circuit, in consequence of which it is automatically switched off. In the event lamp *2* is not ignited or it is just absent, PID1 continues pulse generation. In some cases, this PID is equipped with a disconnection unit stopping pulse generation within several minutes, if lamp *2* is not ignited. This time depends on type and power of the lamp and is equal to (1–2) min for HPSLs and (10–15) min for MHLs [2]).

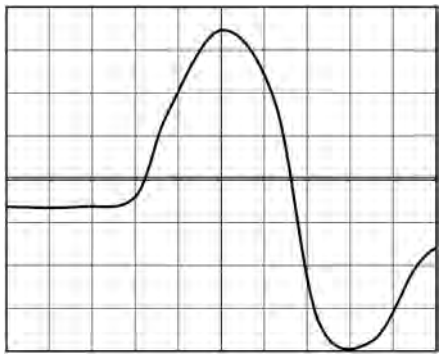

Fig. 3. Oscillogram of a pulse generated by PID #1 with a high-frequency throttle based on the ETD44 core. (1000 V/div; 1 μs /div; 0 is one square lower than the screen middle)

Not only the high-frequency throttle, but also an own ballast throttle capacity takes part in the limitation of pulse voltage influencing the ballast throttle during pulse generation. However in some cases, in order to limit the pulse voltage influencing the ballast throttle, one should add a varistor or an additional capacitor *5* (mainly up to 2000 pF) as it is shown in Fig. 2, *c*.

For rectangular shape high-voltage pulses generated using a closed magnet conductor pulse transformer, pulse duration by amplitude product is limited by size and by maximum achievable magnetic induction B_{max} of the pulse transformer core.

According to it, high-frequency throttle parameters are mainly selected by means of the following expression:

$$\Delta B \cdot S \cdot w \geq 0{,}5 \cdot \int_{t_1}^{t_2} \varepsilon(t)\,dt, \qquad (1)$$

where ΔB is the change of magnetic induction in the high-frequency throttle during PID pulse action maximum possible in this circuit; $\varepsilon(t)$ is the function describing voltage dependence on time of the pulses generated by the PID; integral is the pulse "area" (for example, in V·s dimension); $(t_2 - t_1)$ is the pulse duration; S is the cross-section area of the high-frequency throttle magnet conductor; w is the turn number of the high-frequency throttle winding.

The 0.5 coefficient forward of the integral means that a part of the high-voltage pulse generated by the two-lead PID (Fig. 2, *a*) only, "falls" on the high-frequency throttle, and the other part is applied to the ballast throttle. When calculating, one should watch that this part do not exceed a maximum permissible voltage for this ballast throttle.

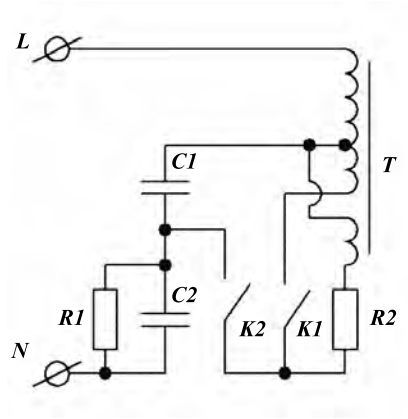

Fig. 4. Electric circuit od two-lead PID applied in PID#3

In the PID (PID #1) version according to Fig. 2, *b*, the high-frequency throttle was made based on the *ETD44* ferrite core (S = 173 mm^2) without a gap of material #87 with μ = 1650 relative magnetic permeability. With ignition pulse "area" of 4000 $V \cdot 2$ μs and ΔB = 0.4 T, according to (1), w > 58. An oscillogram of the pulse generated by this PID version is shown in Fig. 3. As two-lead PID1 (Fig. 2, *b*) of the ИЗУ-Т 70–1000 type is applied, which pulse oscillogram is shown in Fig. 1.

It follows from the presented data that pulse parameters meet requirements of the operation manual given in the Table. And ballast throttle pulse amplitude does not exceed 2000 V.

In comparison with high-voltage pulses generated by the *Z1000S* PID (Fig. 1), in which the ferrite *ETD44* core without a gap made of material #87 is also used, the pulse duration in the proposed PID version is twice more, and at a level of 3 kV it exceeds 2 μs.

In accordance with (1), pulse "area" depends on ΔB. In order to minimise size and mass of the high-frequency throttle, it is expedient to use magnetic conductors of a material with a high maximum achievable magnetic induction B_{max} [6]. For ferrites, B_{max} does not exceed 0.5 T, and for amorphous metal alloys based on iron it reaches 1.5 *T*. It means that size of a magnetic conductor made of amorphous metal alloys based on iron in comparison with a magnetic conductor made of ferrite can be reduced up to three times. And in doing so, identical parameters of high-voltage pulses are achieved. A reduction of magnetic conductor size will allow reducing resistance of the pulse transformer due to a decrease of the winding wire length, which will lead to a decrease of losses at the pulse transformer winding and to saving copper wire.

Table

HPSL(ДНаТ) Power, W	Pulse amplitude, V		Pulse duration at the 0.5 level, μs, no less	Pulse energy, J, no less
	no less than	no more than		
600	4000	5000	2.0	0.002
1000				

In another PID version (PID #2), according to Fig. 2(*b),* the high-frequency throttle was made on the basis of a ring magnetic conductor AMET 5B32·20·10 with S = 90 mm^2, which material had $B > 1.2$ T at magnetic field strength of 5 A/m and $\mu > 50{,}000$ at 0.1 A/m. With $w = 45$ and in case of application as two-lead PID1 (Fig. 2, *b*) of PID-T 70–1000 type, an oscillogram of the pulses generated by this PID version coincides with the presented in Fig. 3. Mass of the high-frequency throttle does not exceed 50 g, and its active resistance is equal to 0.03 Ohm.

A reduction of high-frequency throttle magnetic conductor size at the same high-voltage pulse parameters is achievable in case, if its magnetic reversal is made not from zero to B_{max} (as it is implemented in PID #1 and PID #2) but from $-B_{max}$ to B_{max} (or from B_{max} to $-B_{max}$) thereby twice amplifying ΔB [7]. In accordance with (1), it will allow reducing S twice having saved pulse former "area".

These solutions were implemented in PID #3, in which two-lead PID1 (Fig. 2, *b*) were performed according to Fig. 4. In this case, operating capacitor *C1* charged via current-limiting element *R1-C2* was connected using a switching element in parallel to the pulse transformer *T* primary winding.

The switching element consisted of two keys *K1* and *K2* connected in series. General point of the keys connected to each other via a current-limiting resistor *R2* is switched to the end-point of an additional primary winding, which beginning is joined with the primary end-point. Key *K1* is connected to the beginning of the primary winding, and key *K2* – to the operating capacitor and to the current-limiting element. Key *K1* is switched on in (0.1–10) μs (in the event of PID #3 – in 2 μs (Fig. 5)) after key *K2* is switched on [7]. Key *K2* is only switched on, if the working capacitor is charged to a necessary level. Power part of keys *K1* and *K2* is made based on triacs connected to the correspondent control circuits. It is proposed in patent [7] to use a saturable throttle as *K1* key. Due to the circuit solution according to Fig. 4, two-lead PID1 (Fig. 2) generates a bipolar pulse, which first magnetises high-frequency throttle 4 (Fig. 2) into one polarity (for example, to $-B_{max}$), and then, when polarity changing, the basic high-voltage pulse is generated. In doing so, the high-frequency throttle is re-magnetised from $-B_{max}$ to B_{max} and reliably protects the ballast throttle from breakdowns maintaining its voltage at a level less than 2000 V when generating an ignition pulse of up to 5 kV amplitude.

Fig. 5 (curve *1*) shows an oscillogram of the pulses generated by PID #3 intended to ignite HPSLs according to the Table with use of the foregoing circuit solutions [5, 7, 8]. It is seen that pulse parameters meet the Table requirements: the pulse duration at the 0.5 level is more than 2 μs. With that, high-frequency throttle *4* (Fig. 2) consists of two throttles connected in parallel; ETD29 ferrite cores of material #87 are used without a gap, and pulse transformer *T* (Fig. 4) has mass of 20 g. Due to a little material consumption s, this provides a high economic efficiency of this PID. Foreign PIDs with similar parameters, *ZRM 12ES/B* for example, have

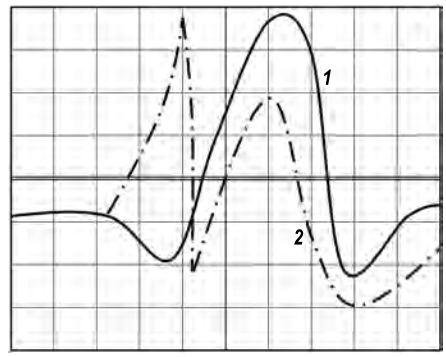

Fig. 5. Oscillogram of a pulse generated by PID #3 with a high-frequency throttle based on the ETD29 core with connected (1) and disconnected (2) additional primary winding. (1000 V/div; 1 μs /div; 0 is one square lower than the screen middle)

twice greater mass, and their cost is significantly more.

Fig 5 also shows an oscillogram of a pulse generated by PID #3 (curve 2) with disconnected additional primary winding of the two-lead PID (Fig. 4). It is seen that pulse duration at the 0.5 level in this case is less than 1 μs.

PIDs with pulse parameters meeting the Table requirements were developed to be introduced into production together with Kadoshkinsky Electrotechnical Factory JSC being a part of BL GROUP International Lighting Corporation.

REFERENCES

1. Klykov Mikhail E. and Agafonova Tatyana A. LED drivers and Discharge lamps control gears: present state and future development// Light & Engineering, @017, V25, #4, pp.32–40.

2. Reference book on lighting engineering / Edited by Yu.B. Ayzenberg.The 3rd revised edition, Moscow: Znak, 2006, 972 p.

3. Rajat Mandal, Santosh Upadhyay, Saswati Mazumdar, Asit Kumar Sur, Chetan M. Sankhla, and Susanta Bhaumik " Igniter Issues with High Intensity Discharge Llighting Applications"// Light & Engineering, 2012, V.20, #4, pp. 90–96.

4. Reference book on lighting engineering / Editerd by Yu.B. Ayzenberg, Moscow: Energoatomizdat,1983, 472 p.

5. Mayorov M. I, Mayorov A.M. A ballast with pulse ignition device / Patent #167448 of the RF, 2017.

6. Mayorov M. I, Mayorov A.M., Goryunov V.A. A device for ignition of gas-discharge lamps/ Patent #103436 of the RF, 2011.

7. Mayorov M. I, Mayorov A.M., Goryunov V.A. A device for ignition of gas-discharge lamps/ Patent #2567739 of the RF, 2015.

8. Mayzenberg S.I., Polyakov A.G. An airfield searchlight / Patent of the USSR #739307, 1980.

Alexander M. Mayorov,
Ph.D., graduated from Physical Faculty of the Ogarev MSU in 2005. At present, he is an Associate Professor of the Structure and Technology Informatics Chair of the Ogarev MSU

Michael I. Mayorov,
Dr. of Technical Science, Associate Professor, graduated from Physical Faculty of the Ogarev MSU in 1970. At present, he is a Professor of the Structure and Technology Informatics Chair of the same university

Light & Engineering
Vol. 26, No. 3, pp. 155–162, 2018

Svetotekhnika
No. 1, 2018, pp. 71–78

RESEARCH AND MODELLING ON ELECTRICAL AND THERMAL MODE OF LEDS OPERATION IN THE LUMINAIRE

Sergei S. Kapitonov, Anastasia V. Kapitonova, Sergei Yu. Grigorovich, Sergei A. Medvedev, and Taher Sobhy

Ogarev Mordovia State University, Saransk
E-mail: kapss88@mail.ru

ABSTRACT

In the article, the electrical and thermal processes in the LED lamp with varied parameters are investigated. Voltage and current measurements on all LEDs of the luminaire are carried out in the nominal operating mode. The power allocated to each LED is determined. The calculation of the LED crystal temperature was carried out using the developed thermal LED model based on the results of the measurements and by using "Multisim" program. It has been established that the temperature of the crystals of individual LEDs in the luminaire differ significantly, which leads to unfavourable thermal conditions for them and an increased likelihood of premature failure.

Keywords: LED, LED luminaire, voltage, current, power, current-voltage characteristic, crystal temperature

1. INTRODUCTION

Ensuring high reliability and the service life of LEDs lamps and luminaires declared by the manufacturer is one of the main tasks of modern electronics and lighting technology. The service life of an individual LED operating in nominal mode can reach 100 thousand hours. Many manufacturers of LED light sources indicate a similar lifetime for their products without conducting the relevant studies. The main deception for the consumer is this, because at the moment the real life of LED lamps and lamps does not exceed 50 thousand hours. On the one hand, this is due to the reliability of the driver, in which many manufacturers of LED products are trying to save by using substandard devices. On the other hand, there are problems associated with ensuring the reliability of the LEDs themselves, even if the ideal driver is used for their power supply.

The values of electrical and thermal parameters of LEDs can vary within 10 % due to the instability of the technological process of production. In order to determine the effect of variation in the values of the parameters on the operation modes and the service life of the LED light source, a study was made of the processes taking place in the real lamp. The luminaire of the Russian-Korean company NEPES RUS is selected as the test sample. The rated power is 50 watts. The luminaire includes 40 LEDs, which are included in a series-parallel group. Lifetime of the lamp, according to the manufacturer, is 70 thousand hours [1, 2]. Operating temperature range is from –20 ºC to +50 ºC. Blue LEDs, produced by the company Semi LEDs, are used in the luminaire. The LEDs are rated for a rated direct current of 350 mA and a power rating of 1 W [3]. The scheme of switching on the LEDs in the luminaire is shown in Fig. 1.

The electrical circuit of connecting the LEDs in the luminaire is a parallel connection of four branches, each of which contains ten LEDs in series. The photograph of the design of the LEDs light module is shown in Fig. 2.

All the LEDs are located on the same printed circuit board, made of fibre glass. LEDs are mounted

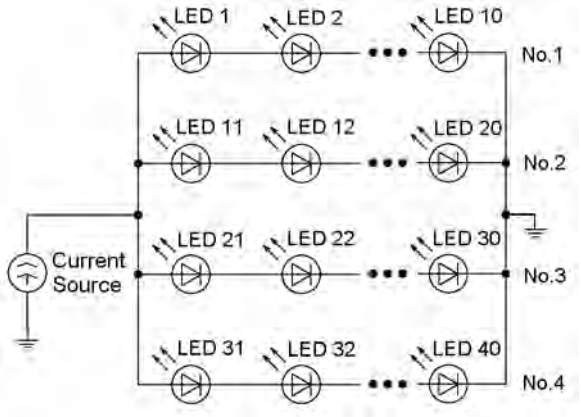

Fig. 1. Diagram of LEDs in the luminaire

on the surface of the printed circuit board using surface mounted technology. The circuit board is attached to the metal housing of the luminaire. Additional measures for cooling LEDs are not provided [3].

2. METHOD

Measuring the thermal processes in the luminaire and LEDs is quite difficult. The solution is to calculate the thermal processes based on the measurement of electrical processes and data on the design of the luminaire and LEDs. The thermal processes occurring in the LED are calculated according to the theory of heat transfer. The methods for determining the temperature fields in the construction of the LED are based on this theory. Thermal processes are described by a system of differential equations of heat conduction. The number of elements in the construction of the LED housing determines the order of the system [3]. Three main methods exist for solving the system of differential heat equation:

1) Analytical method;
2) Approximate numerical methods;
3) The method of electro thermal analogy.

The first method is used when it comes to bodies with simple geometry and structure, with unchanged values of thermo physical parameters, a simple analytical expression of boundary conditions and a source of thermal energy. However, when using the presented method for real light emitting diodes, it is necessary to simplify considerably the mathematical description of thermal processes. This affects the final result, which makes it possible only to assess the nature of the course of the heat transfer process.

Numerical or analogy solution methods are used to improve the accuracy of calculations. These methods are mathematical and physical modelling. The result of numerical methods is only an approximate solution. The temperature field is calculated for the specific points of the element and is represented as a tabular value.

The method of electro thermal analogy (ETA) is based on the analogy of differential equations of the electric and temperature fields. The ETA method provides that the heat capacity of the structural element is replaced by the electrical capacity proportional to it, and the thermal resistance by the electrical resistance. The electric current is taken as the analogue of the power released when an electric current flows through the LED chip in the ETA method. The potentials of the circuit nodes correspond to the superheat temperature of the corresponding structural element. Each element of the device design in the model is replaced by a T-shaped RC-chain. The combination of these RC-circuits forms a thermal model of the LED design. All the electrical processes taking place in this scheme reflect the thermal processes in the LED [4].

The following assumptions were adopted in the development of the thermal model:

1. The temperature field in the structure and the electric field in the model are one-dimensional;

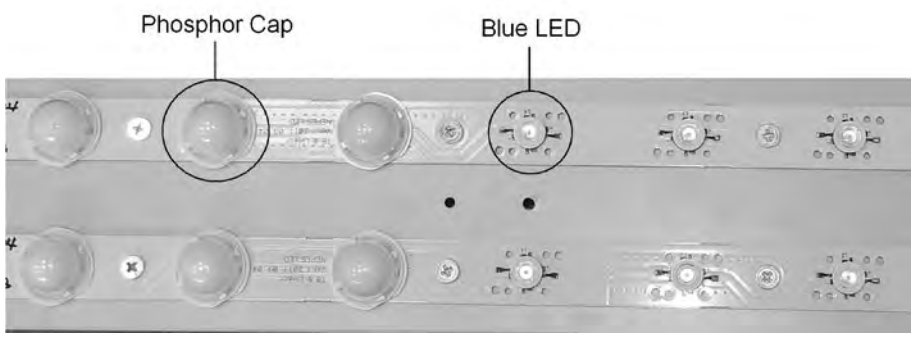

Fig. 2. The design of the LEDs light module

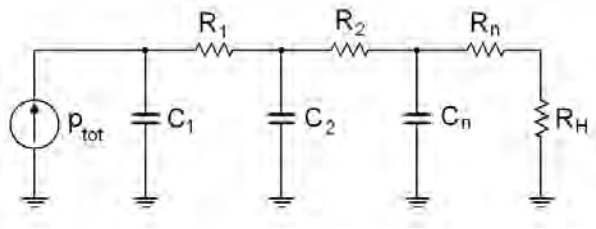

Fig. 3. Generalized analogue of the LED design

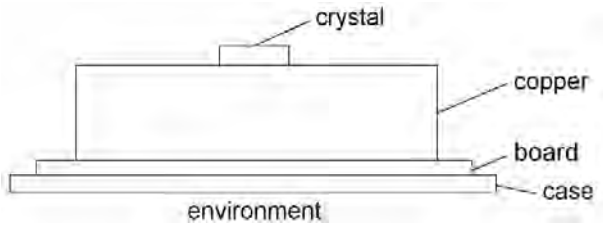

Fig. 4. Simplified LED design

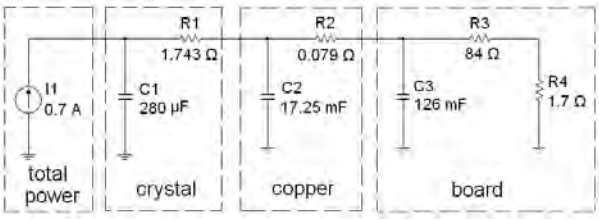

Fig. 5. Thermal model of the LED in "Multisim"

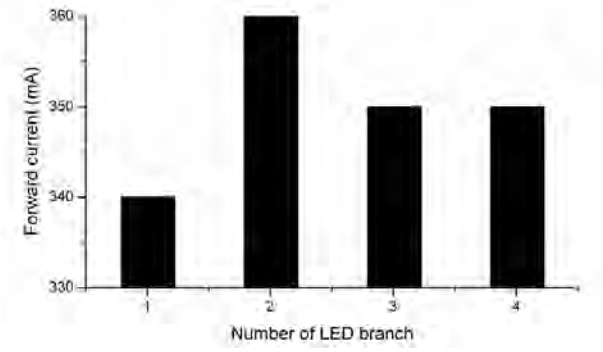

Fig. 6. Current distribution along the parallel branches of the luminaire

2. The material of the crystal and other elements of the LED design is homogeneous and isotropic with respect to thermo physical properties, and these properties do not depend on temperature;

3. All thermal energy is dissipated in a layer of an infinitesimally thin crystal passing through its centre parallel to the ends;

4. The temperature of all elements of the structure is steady and identical at the initial moment.

The equivalent T-shaped RC-chain corresponds to a certain element of the LED design in the model. The circuit consists of two series resistors RI and a capacitor CI. Capacitance capacitor CI corresponds to the heat capacity of the I-TH element of the structure. Resistance RI corresponds to the thermal resistance of this element. The values of resistance RI and capacity CI for an element of area S and length l were calculated as follows [5, 6]:

$$R_i = \frac{l_i}{k_i \cdot S_i}, \tag{1}$$

$$c_i = \rho_i \cdot c_0 \cdot S_i \cdot l_i, \tag{2}$$

where ρ is the density; c_0 is the specific heat; k is the coefficient of thermal conductivity.

The resulting model of the LED is an electrical circuit (Fig. 1) consisting of series-connected T-shaped RC-circuits.

The following notation is introduced in Fig. 3: P_{tot} is the loss capacity; Rn is the equivalents of the element's thermal resistance; C_n is the equivalent heat capacity of the element; $R_н$ is the edge cooling conditions on the radiator side.

The creation of a complete electro thermal LED model is possible in a certain environment of mathematical modelling of electrical processes using the ETA method. Thermal parameters are represented by their electrical analogies, which allows for a reverse thermal connection between the electric and thermal models taking into account the scale factors for the recalculation of these quantities. A similar feature of the application of the ETA method makes it possible to investigate the electro thermal processes taking place in both individual LEDs and in LED lamps and luminaires in general. This can not be obtained by using standard element libraries that exist in simulation programs for electrical processes.

The proposed approach is the basis for the thermal model of the LED, which is part of the electro thermal model created in the "Multisim" program. Let us consider in more detail the process of developing this thermal model.

The simplified design of this LED is shown in Fig. 4, given that it is attached to a printed circuit board that acts as a cooler.

The LED design is a crystal based on gallium nitride (*GaN*), which is located on a copper substrate. The printed circuit board, on which the LEDs are located, quite often acts as a cooler for modern LED

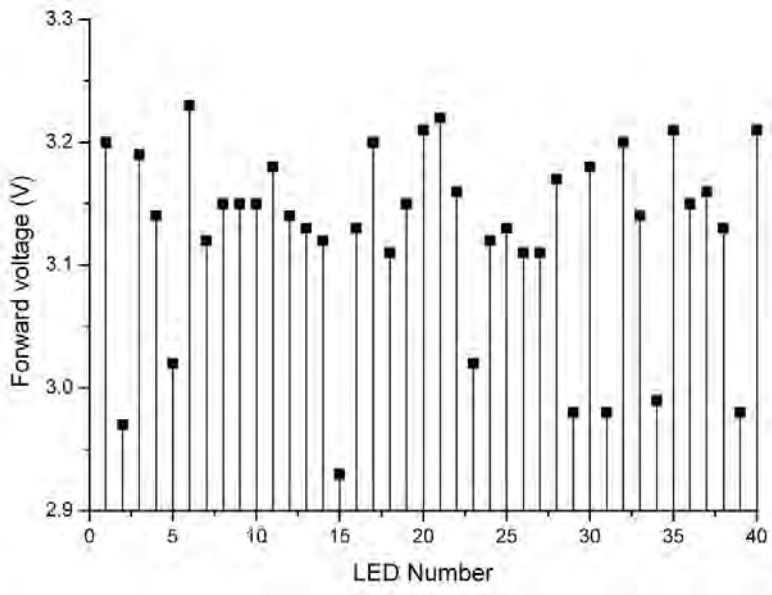

Fig. 7. Distribution of values of direct voltage on the LEDs of the luminaire

light fixtures. The calculation is carried out for this case.

The substitution scheme for the thermal model, performed using the ETA method in the "Multisim" software environment, is shown in Fig. 5 [7, 8].

Fig. 5 shows that the DC source is at the input of the circuit and is analogous to the electrical power loss, which is released on the LED. The value of this power is 0.7 W, taking into account the efficiency of the LED, equal to 30 %. Further, RC circuits, which are analogies of a crystal, a metal substrate and a printed circuit board, follow in the model. The values of resistors and capacitors in the developed model were calculated as follows [9].

The crystal dimensions are for the selected LED: height 0.145 mm, length 0.8 mm, width 0.8 mm. The specific heat conductivity of *GaN* is 130 W / m • K, the specific heat is 0.49 J / g • ºC, the density is 6.15 g / cm3. Substituting these values into formulas (1) and (2), the following values of the thermal resistance of the crystal-metal substrate and the heat capacity of the crystal are: R1 = 1.743 ºC / W and C1 = 280 μJ / ºC.

The dimensions of the copper substrate are equal: height 0.4 mm, diameter 4 mm. The specific thermal conductivity of copper is 401 W / m • K, the specific heat is 385 J / g • ºC, the density is 8.92 g / cm^3. Substituting these values into formulas (1) and (2), the following values of the thermal resistance of the metal substrate-printed circuit board and the heat capacity of the copper substrate yield: R2 = 0.079 ºC / W and C2 = 17.25 mJ / ºC.

The dimensions of the section of the printed circuit board made of fiberglass, which is involved in the heat exchange process are: height 1.2 mm, diameter 7 mm. The specific thermal conductivity of the fibreglass is 0.37 W / m • K, the specific heat is 1470 J / g • ºC, the density is 0.185 g / cm^3. Substituting these values into formulas (1) and (2), the following values of the thermal resistance of the printed circuit board-environment and the heat capacity of the printed circuit board yield: R3 = 85.7 °C / W and C3 = 126 mJ / °C.

Thus, the calculation of the main components of the thermal model is carried out. The temperature value of each structural element can be measured with the XSC1 oscilloscope, since the voltage is the equivalent of temperature.

3. RESULTS

Investigation of the luminaire (Fig. 2) was carried out in the nominal mode of its operation, when a current of 1.4 A flows through it. This current should be evenly distributed across each parallel branch of the LEDs when there is no variation in the values of the LED parameters. Thus, the current flowing through each LED should be equal to the nominal value of 350 mA. However, the current values are distributed differently in real light fixtures. The measurement is based on the values of the current flowing in each parallel branch of the LEDs in the luminaire. The driver current distribution along the parallel branches is shown in Fig. 6.

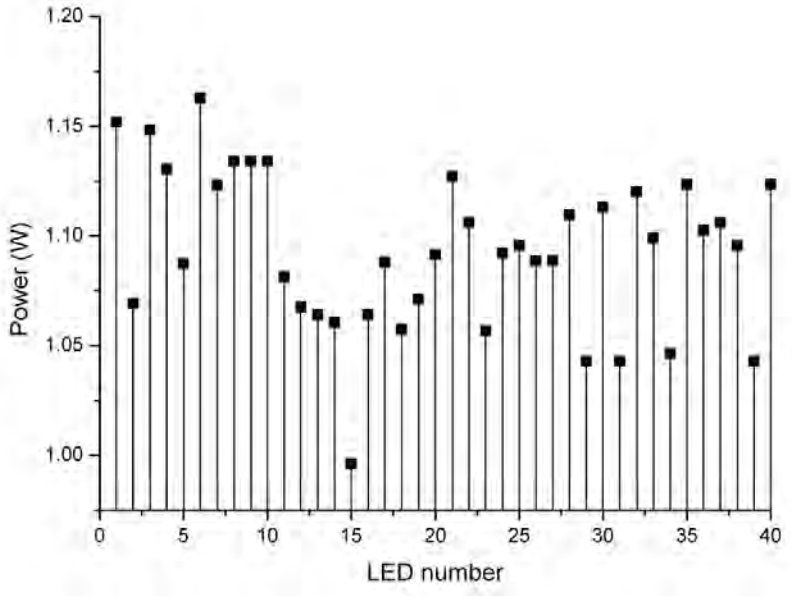

Fig. 8. Variation of the power, which is released in the LEDs crystals

Fig. 6 shows that the currents flowing through parallel branches No. 2 and 3 differ from the nominal value of 350 mA and are equal, respectively, to 360 mA and 340 mA. Thus, the LEDs of these branches operate in modes other than the nominal mode, due to the presence of a technological spread of the values of their parameters.

Consider the processes that occur in the LEDs of each parallel branch. Since the current flowing through the LEDs of the branch is the same, it is of interest to consider the variation of the values of the direct voltage drop across them. Measurement of voltage values is carried out on each LED of the luminaire at the values of the current flowing through them, shown in Fig. 6. The results of the measurement are shown in Fig 7.

Fig. 7 shows that a significant variation in the values of direct voltage on the LEDs is observed in the luminaire. The maximum value of the forward voltage is observed on the LED № 6 ($U_{F№\,6}$ = 3.23 V). The minimum value of voltage was obtained on the LED № 15 ($U_{F№\,15}$ = 2.93 V). The values of the forward voltage vary considerably within a single branch of the LEDs, despite the fact that the same current flows through them. The maximum variation in the values of the forward voltage is observed in branch No. 2 and it is equal to 0.25 V.

Variations in the magnitude of the current flowing through the parallel branches of the LEDs and the direct voltage on them lead to the release of different power values in their crystals. Variations in the power values, which are released in the crystals of the LEDs of the light, are shown in Fig. 8.

It can be concluded from Fig. 8 that a significant variation in the power values emitted in LED crystals is observed in the lamp under study. The power value did not exceed the nominal value of 1 W and was 0.99 W on the LED No. 15. Power significantly exceeding the nominal value of 1 W is allocated on the LEDs of parallel branches No. 1 and 4, through which the rated current of 350 mA flows. The maximum power value is allocated in the crystal of LED No. 6 and is 1.16 W, which is 16 % higher than the nominal value.

Thus, the variation and excess of the nominal value of the power released in the crystals of the luminaire's LEDs leads to the appearance of unfavourable thermal regimes of their operation.

The electro thermal model of the LED used in the test fixture was developed to investigate the thermal operating conditions in the Multisim software environment. The design of the luminaire was also taken into account when creating a thermal model. The results of simulation of the transient process of changing the temperature of LEDs No. 5, 6 and 15 are shown in Fig. 9. The maximum (1.16 W), average (1.08 W) and minimum (0.99 W) power is allocated in the crystals of these LEDs (Fig. 8). The initial value of the crystal temperature of the LEDs is 20 °C. The efficiency of the LEDs, equal to 30 %, was taken into account in the simulation. This efficiency shows that 70 % of all energy supplied to the LED is allocated as heat in the crystal.

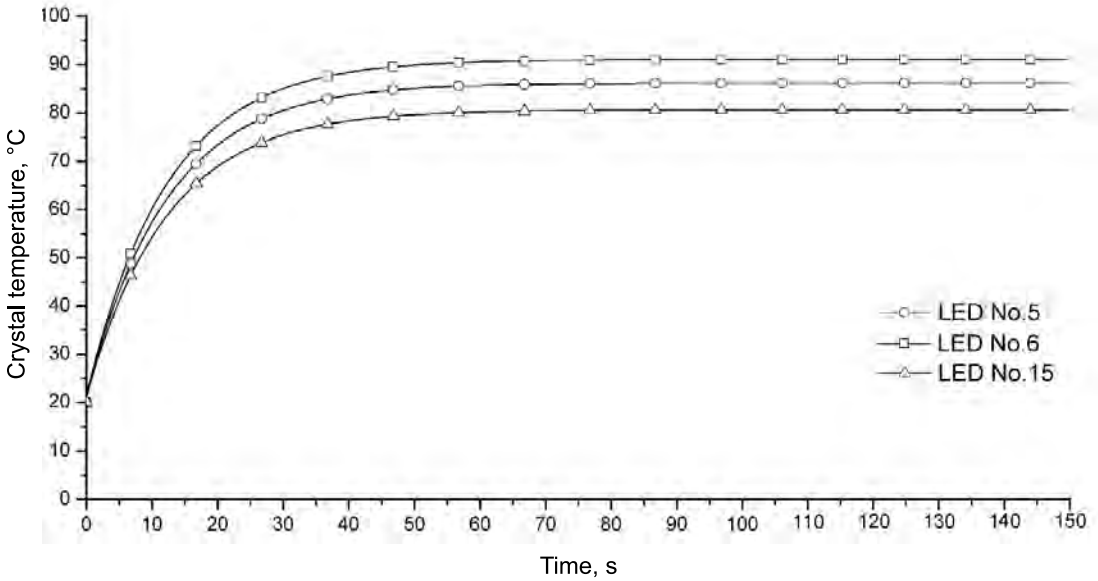

Fig. 9. Time dependences of crystal LED temperature

Fig. 9 shows that the transient process ends at the instant of time equal to 150 s, and the temperature of the LED crystals reaches the following values: $T_{j№\,6}$ = 92 ºC; $T_{j№\,5}$ = 87 ºC; $T_{j№\,15}$ = 82 ºC. The maximum scatter in the crystal temperature of the luminaire's LEDs was ΔT_{jmax} = 10 ºC.

4. DISCUSSION

Such a variation of crystal temperature values, at first glance, does not pose a danger to LEDs, since the maximum permissible temperature of the crystal is +125 ºC in accordance with the passport data. However, LEDs degrade over time, and their parameters and characteristics deteriorate significantly during operation. In [10, 11], a study was made of the dependence of the lifetime of various LEDs on the crystal temperature. It is established that the service life of the blue LED is 25 thousand hours longer at a crystal temperature of 80 °C than at a temperature of 90 °C. In addition, the variation in the values of the parameters of the LEDs will increase due to the spread of the crystal temperature values, which will lead to an even greater discrepancy in the temperature values. Thus, the likelihood that the lamp will work claimed by the manufacturer 70 thousand hours, is extremely small.

There are no specific methods and ways to solve this issue for manufacturers of LED products at the moment. Only attempts are made to correct the effect of the problem, while nothing is done to prevent the cause. It is easier for manufacturers to provide the customer with favourable warranty conditions and in case of failures replace defective lamps with new ones. However, not every consumer has the ability and desire to periodically disassemble the lighting system to replace the fixtures. This problem causes a significant impact on the reputation of LED products in general.

4. CONCLUSIONS

Preliminary studies have shown that for the same electrical and thermal operating modes of the LEDs as close as possible to the nominal, it is necessary, first of all, start exercising binning on a complex light, electrical and thermal properties at the stage of their production. LED lamps are formed from LEDs belonging to one bin at the present time. However, light emitting diodes are blown mainly by light parameters, such as luminous flux, brightness and correlated colour temperature. The main electrical parameter, by which the bin is made, is a direct voltage drop. Despite this, the conducted research revealed the presence of a variation of this parameter in the LEDs of the luminaire. Binning is not conducted at all on the values of thermal parameters. As a result, LEDs with identical values of the parameters of light, but with significantly different values of the electrical and thermal properties, can be branches in the same lamp. Accordingly, different energy will be released as heat in the crystals of such LEDs. The heat from the crystal will also be at different intensities, due to the variation in the valu-

es of the thermal parameters, the most important of which is the thermal resistance of the crystal-shell in the steady state. This leads to differences in the thermal conditions of the individual LEDs of the luminaire and a reduction in its service life.

A study conducted on the example of a Russian-Korean LED lamp showed that the problem of variation in the values of the parameters of LEDs in luminaires does exist. This leads to a discrepancy between the thermal operating modes of the LEDs. These processes will lead to a reduction in lamp life. The amount by which the service life will be shortened depends on the degree of divergence of the thermal regimes of the individual LEDs. Thus, the LED luminaire can work out declared by the manufacturer 70 or 100 thousand hours only in the event that all its LEDs work in the same nominal modes. This can not be achieved at the moment in practice, taking into account the applied methods of the bin.

REFERENCES

1. Hamon B., van Driel W.D. LED degradation: From component to system/ Microelectronics Reliability, 2016, 64, pp. 599–604.

2. Qu X., Wang, H., Zhan X., Blaabjerg F., Chung H.S.-H. A Lifetime prediction method for leds considering real mission profiles/ IEEE Transactions on Power Electronics, 2017, 32, pp. 8718–8727.

3. Bespalov N.N., Kapitonov S.S., Kapitonova A.V. Research of processes in the LEDs luminaire in case of the voltage temperature coefficient of separate LEDs variation/ Light & Engineering, 2016, V.24, #4, pp. 72–75.

4. Bespalov Nikolai N., Ilyin Mikhail V., Kapitonov Sergei S. Testing equipment for LED luminaire control devices and fluorescent lamp electron ballasts/ Light & Engineering, 2017, V. 25, no. 4, pp. 86–91.

5. Kapitonov Sergei S., Kapitonova Anastasia V., Grigorovich Sergei Y. Temperature dependence modeling for powerful LED characteristics in Multisim/ ARPN Journal of Engineering and Applied Sciences, 2017, V. 12, no. 10, pp. 3328–3334.

6. Bai K., Wu L.G., Nie Q.H., Dai S.X., Zhou B.Y., Ma X.J., Zheng Z.Y., Zhang F.W. Thermal simulation and optimization of high-power white LED lamps / International Conference on Electronics, Communications, and Control, ICECC Proceedings, 2011, pp. 573–576.

7. Kapitonov S. S., Kapitonova A.V., Grigorovich S.Y. Development of thermal LED model / Journal of Fundamental and Applied Sciences, 2017, V. 9(7S), pp. 752–762.

8. Alexeev V.P., Belousov A.V. Features of electric and mechanical systems electrothermal models in the method of electrothermal analogy. Proceedings of the 8th International Scientific and Practical Conference of Students, Post-Graduates and Young Scientists: Modern Technique and Technologies 2002, pp. 93–95.

9. Ishizaki S., Kimura H., Sugimoto M. Lifetime estimation of high power white LEDs / Journal of Light and Visual Environment, 2007, 31, pp. 11–18.

10. Yang L., Hu J.b, Shin M.W. Degradation of high power LEDs at dynamic working conditions / Solid-State Electronics 2009, 53, pp. 567–570.

11. Koh S., Yuan C., Sun B., Li B., Fan X., Zhang G.Q. Product level accelerated lifetime test for indoor LED luminaires / 2013, 14th International Conference on Thermal, Mechanical and Multi-Physics Simulation and Experiments in Microelectronics and Microsystems 2013, pp. 652–999.

Sergei S. Kapitonov,
Ph.D. in Technical Science, graduated from the National Research Ogarev Mordovia State University in 2010 year. At present, he is an Associate Professor of Department of Electronics and Nanoelectronics at the same university. His scientific interests are research and development of LED light sources and control systems for LED light sources

Anastasia V. Kapitonova,
postgraduate, graduated from the National Research Ogarev Mordovia State University in 2013 year, scientific interests are research and development of LED light sources and control systems for LED light sources

Sergei Yu. Grigorovich,
postgraduate, graduated from the National Research Ogarev Mordovia State University in 2010 year, scientific interests are research and development of LED light sources and control systems for LED light sources

Sergei A. Medvedev,
student of the National Research Ogarev Mordovia State University, graduated from the Physics and Mathematics Lyceum, scientific interests are research and development of LED light sources and control systems for LED light sources

Taher Sobhy,
higher education, graduated from the University of Texas at Austin. At present, he is a student of National Research Ogarev Mordovia State University. His scientific interests are microcontrollers and microprocessor technology, research and development of LED light sources and control systems for LED light sources

Light & Engineering
Vol. 26, No. 3, pp. 163–166, 2018

Svetotekhnika
No. 2, 2018б, pp. 84–86

RADIANT HEAT CONDUCTION IN THE HEAT INSULATING LIGHTWEIGHT MATERIALS

Eugene Yu. Shamparov, Inna N. Zhagrina, and Sergei V. Rode

Kosygin Russian State University (Technologies, Design, Art), Moscow
E-mails: shamparov@bk.ru, jagrina@mail.ru, rode-s-v@mail.ru

ABSTRACT

An evaluation of scattering and absorbing abilities of light heat insulating materials in the IR spectrum range is given. The generalized form of Fourier equation application to such materials with taking into account radiant environment heat conduction is shown. Convection-less measurements of material specimen thermal resistance of different thickness are performed. Theoretical substantiations and ideas concerning heat-protective material properties are reliably confirmed. Exact values of total material heat conduction are obtained, and values of material radiant heat conduction, as well as of thermal radiation penetration depth into them are estimated.

Keywords: thermal radiation, environment scattering and absorption, Kirchhoff's law, radiant heat conduction, Fourier equation, radiation-conductive heat transport, material thermal resistance

Tasks of diffuse radiation scattering are met in optics relatively seldom and, therefore, are rather complex. Nevertheless, sometimes they should be solved when influence of diffuse radiation is significant. In this regard, this work is dedicated to distribution of thermal radiation in an incidentally scattering environment.

As it is known, there are three mechanisms of heat transfer: conduction, convection and thermal radiation. The latter only makes an essential contribution to heat transport in transparent environment, which under nature conditions is air only. The conductive component contribution is essential at a small air layer thickness, about several millimetres. In the case of the bigger air thickness, the radiation component dominates over the conductive.

Convection contribution to a significant extent depends on geometry of the system transferring heat and is extremely complex to be analysed. So, when measuring, we tried to make it insignificant.

Diffuse scattering occurs on environment random non-uniformities. If non-uniformity typical size is less than radiation wavelength, then scattering is frequency-dependent; the lower wavelength is, the scattering is more. For this reason namely, sunlight scattering on microscopic dust particles in atmosphere within the short-wave spectrum part is more intensive, and we see the blue sky.

And on the contrary, if non-uniformity size as in the case of drops or snowflakes in clouds is much more than radiation wavelength, scattering intensity does not depend on frequency, and we see white clouds respectively.

Modern light heat insulating materials have on the average almost isotropic structure, and for thermal radiation they can be considered a random scattering environment. There are two main types of such materials: foamed and fibrous. In the either case, bubble typical size (of about 100 μm) and fibre diameter (~ 20 μm) are more than the radiation wavelength (~ 10 μm). For our measurements, specimens were selected as follows:

- Foamed polyethylene of 2.2 mm thickness of 16.5 kg/m^3 density, of (0.1–0.3) mm bubble size and with the volume portion filled with polyethylene of 1.74 %;
- Foamed polystyrene (foamed plastics) of 5.0 mm thickness of 32 kg/m^3 density, 0.05–

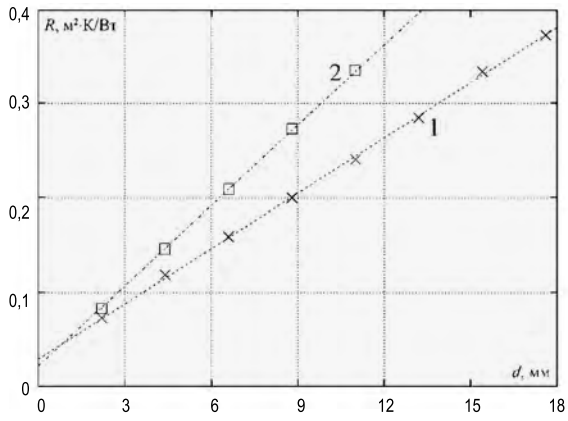

Fig.1. Thermal resistance dependences of foamed polyethylene specimen piles on thickness of the pile: 1 – without foil, 2 – for the pile interlaid from above, from below and between all layers with specula aluminium foil

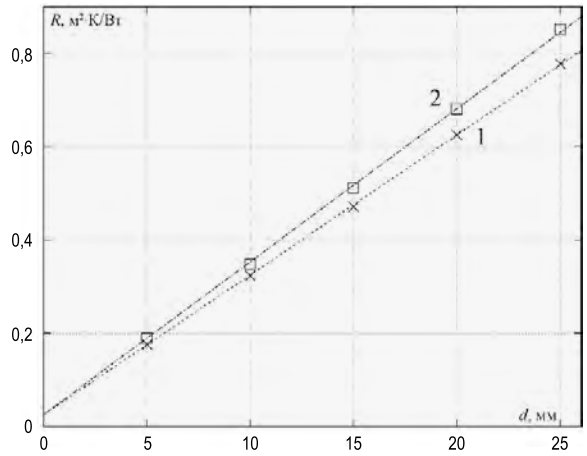

Fig.2. Thermal resistance dependences of foamed polystyrene specimen piles on thickness of the pile: 1 – without foil, 2 – for the pile interlaid from above, from below and between all layers with specula aluminium foil

0.15 mm bubble size and with the volume portion filled with polystyrene of 2.56 %;

• Nonwoven material manufactured under *Hollowfibre* brand of 6.0 mm thickness of 11.7 kg/m^3 density made of poliethylene terephtalate hollow fibres of 32 μ thickness and with the volume portion filled with it of 0.9 %.

As non-uniformity dimensions of all specimens are much more than the wavelength, thermal radiation scattering in them should be frequency-independent.

Though polyethylene, polystyrene and poliethylene terephtalate have a number of absorption lines, their transparency in the IR range is comparatively high (average penetration depth is about 1 mm) [1]. As portion of porous materials space filled with solid substance is (1–2)% only, their thickness equivalent by absorption should be (5–10) cm. From the visual evaluation of porous materials characteristics, it is easy to understand that radiation scattering occurs at a "thickness" of about 5 mm, i.e. much lesser than 5 cm. In the case of a simultaneous presence of absorption and scattering, penetration depth of radiation is determined by two parameters: scattering factor v and absorption factor χ [2]:

$$a = (v + \chi)^{-1}. \tag{}$$

The scattering factor v of the selected materials is obviously much more than the absorption factor χ, and respectively, one should consider that a does not practically depend on the wavelength within the IR range, and each material can be considered as a diffuse grey environment.

Dynamics of radiant heat distribution in a diffuse grey environment is considered according to the Kirchhoff's law for thermal radiation. The radiation component of heat transport within such environment is characterised by its radiant heat conduction [3]

$$L = 16 \cdot \sigma \cdot T^3 \cdot a/3, \tag{1}$$

where σ is the Stefan-Boltzmann constant and T is the absolute temperature. If to consider that optical environment thickness is big at the distances from the boundaries significantly greater than thermal radiation penetration depths, radiant flux density Φ is directly proportional to temperature gradient ∇T, similar to the Fourier equation for conductive heat transfer. Therefore, in case of radiation-and-conductive heat transport in such materials, Fourier equation in a generalised configuration should be met

$$\Phi = -(L + D)\nabla T, \tag{2}$$

where D is the environment conductive heat transfer.

Respectively thermal resistance R of a material layer should be proportional to its thickness d:

$$R = \Delta T/\Phi = d/(L + D). \tag{3}$$

Using an installation developed for convection less measurements of thermal permeability [4] "in plane-parallel geometry", dependences of specimen pile thermal resistance on material layer number (thickness) have been determined. The results are presented in Figs. 1–3 (dependence #1). At

the same place, to demonstrate presence of radiant heat conduction, thermal resistance dependences of the same specimen piles are given with the difference that between the layers, the thin aluminium foil (10 μ) is laid from above and from below the piles and between all layers (dependence #2).

A feature of this installation is that operation plain elements, between which a temperature difference is created, are manufactured of the transparent within the IR spectrum range single-crystal silicon. This significantly weakens surface effects, because of which environment boundaries influence is almost imperceptible.

The fact that thermal resistance dependence on environment thickness for all materials is close to a straight line with a high precision (of about 1 %), confirms our ideas about properties of the studied materials with a high reliability (3). Approximation of radiant heat conduction (2) is quite applicable to such environments. A value reciprocal of inclination coefficient of straight lines, is equal to environment total heat conduction $L + D$. Its correspondent values for foamed polyethylene, polystyrene and for Hollowfiber are as follows: – 0.0514 ± 0.0003, 0.0333 ± 0.0005 and 0.0610 ± 0.0005 W / m · *K*.

Aluminium foil almost completely (for 99 %) reflects thermal radiation. And with such a small thickness, its contribution to heat conductive transport is negligible. Respectively a result of foil addition between material layer should only be reduction of the heat transport radiation component. Differences of the dependences for specimens with foil and without foil (Fig. 1–3) show that contribution of the radiation component is comparable with contribution of the conductive. As well as in the event with specimens without foil, in the second case several specimens with identical thermal resistance were installed sequentially. Therefore diagrammes of thermal resistance dependences on pile thickness with foil were straight lines too. In this case, the diagramme inclination increased, and "heat conduction" decreased. Total heat conduction of materials with foil is 0.0353 ± 0.0003 for foamed polyethylene, 0.0305 ± 0.0005 for foamed polystyrene and 0.0490 ± 0.0005 W/m · K for Hollofiber. The less distance between the foil screens is, the more essential reduction of heat transport radiation component should be. Therefore for foamed polyethylene of 2.2 mm thickness, relative "heat conduction" change (31.3 %) was significantly

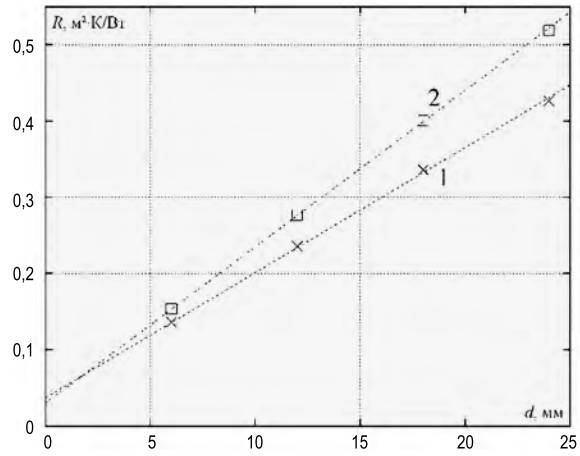

Fig.3. Thermal resistance dependences of foamed *Hollowfibre* specimen piles on thickness of the pile: 1 – without foil, 2 – for the pile interlaid from above, from below and between all layers with specula aluminium foil

greater than for 5 mm thickness foamed polystyrene (8.4 %) and for 6 mm thickness Hollofiber (19.7 %).

Conductive heat transfer of polymers is comparatively low. Therefore among the studied materials, the main role in conductive heat transfer is played by air occupying 99 % of the total volume. Air heat conduction at average temperature measurements is 0.0272 W/(m·K) [5]. Radiant heat conduction of foamed polyethylene and of the *Hollowfibre* is approximately equal to conductive. According to formula (1), it is easy to estimate depth of thermal radiation penetration into these materials: $a \approx 3.5$mm. This rather good coincides both with visually observed material transparency and with the measurement results for specimen piles with foil. A more dense and finely-divided foamed polystyrene is significantly less transparent for thermal radiation. Its radiant heat conduction is (3–5) times less than of two other materials, and, respectively, $a \approx 1$ mm. So, despite a lesser thickness (5 mm) than of the *Hollowfibre* (6 mm), its "heat conduction" relative change (8.4 %) (for specimens with foil) was considerably lesser than of the *Hollowfibre* (19.7 %).

Thus our measurement results demonstrate a role of radiant heat conduction in light heat insulating materials. The formed concepts and correct measurements allow finding characteristics of heat-protective material properties exactly enough. At what it is possible to do by using visual material characteristics. In the attempts to make heat insulating materials as light as possible, the manufacturers have already reached such a level when the radiation component contribution to the thermal transport is comparable with the conductive component

contribution. Material upgrade in respect of reducing their heat conduction radiation component is a significant reserve of improving their heat-protective properties and an important direction of development of the correspondent production in the near future.

REFERENCES

1. Crystal polyolefins: Collection of monograph articles / Edited by R.A. Ruff and K.V. Duck, Vol. 2, Structure and properties. Moscow: Khimiya, 1970, 469 p.

2. Ziegel R., Howell Dj. Heat exchange by radiation, Moscow: Mir, 1975, 934 p.

3. Kutateladze S.S. Fundamental of the heat exchange theory. The 5th revised edition, Moscow: Atomizdat, 1979, 416 p.

4. Shamparov E. Yu., Zhagrina I.N. Installation for precision convectionless measurements of thermal permeability of materials at a temperature close to the room / Useful model RF #166709. 2016. Bulletin #34.

5. Physical values: A handbook / Edited by I.S. Grigoriev and E.Z. Meylikhov, Moscow: Energoatomizdat, 1991, 1232 p.

Eugene Yu. Shamparov,
Ph.D., Associate Professor, graduated from the General and Applied Physics Faculty of the MIPT in 1994. At present, he is the Associate Professor of the Physics Chair of the RSU of A.N. Kosygin. His scientific interest fields are physical optics, material science of productions of textile and consumer industry

Inna N. Zhagrina,
Ph.D., Associate professor, graduated from the Skin Product Technology and Design Faculty of the Moscow Technological Institute of Consumer Industry in 1993. At present, she is the Associate Professor of the Materials Science and Commodity Examination of the RSU of A.N. Kosygin. Her scientific interest fields are physical optics, material science of productions of textile and consumer industry, quality control

Sergei V. Rode,
Prof., Dr. of Technical Science, graduated from the Physical Faculty of Lomonosov Moscow State University in 1964. At present, he is the Head of the Physics Chair of the RSU of A.N. Kosygin. His scientific interest fields are physical optics, material science of productions of textile and consumer industry

Light & Engineering
Vol. 26, No. 3, pp. 167–173, 2018

Svetotekhnika
No. 5, 2018

MANUFACTURING COST OPTIMIZATION OF PHOTOVOLTAIC ENTERPRISES BASED ON NEURAL NETWORK

Weiping ZHANG[1,2], Shuming LI[2], Junfeng YU[2], and Yihua MAO[3]*

[1]*Department of Electronic Information Engineering, Nanchang University, China*
[2]*Binhai Industrial Technology Research Institute of Zhejiang University, Tianjin, China;*
[3]*Zhejiang University College of Civil Engineering and Architecture, Hangzhou, China;*
** E-mail: kxtbi1337@163.com*

ABSTRACT

How to reduce the cost of photovoltaic power generation is the core issue of the survival and development of photovoltaic enterprises. Based on this, the manufacturing cost optimization of photovoltaic enterprises is studied based on neural network. Through the design of cost accounting control of photovoltaic enterprises, a genetic algorithm is proposed to optimize the manufacturing cost of photovoltaic enterprises, which is predicted at the maximum power point of the same photovoltaic power generation system. The results show that the RBF neural network optimized by genetic algorithm not only improves the prediction speed, but also improves the prediction accuracy. Thus, the maximum power point tracking control of photovoltaic power generation can be achieved better, and the manufacturing cost of photovoltaic enterprises can be optimized.

Keywords: RBF neural network (Radial basis function network), EPR system database, analytic network process (ANP), photovoltaic enterprises, optimization of manufacturing cost

1. INTRODUCTION

The development of photovoltaic industry is in its infancy. The idea of reducing the cost of products is mainly to reduce product costs through the revolution of new technologies and the development of new materials, which reduces the overall cost from the previous 10 yuan/W to the current 4 yuan/W, and realizes the unit cost of electricity generation 0.8 yuan per kWh contribution [1]. This change plays a vital role in promoting the rapid development of the photovoltaic industry, and thus bringing about the new energy revolution and solving the environmental pollution problems of the traditional energy [2]. However, in the next few years, the development speed of new technology and new materials will slow down. In order to support the continued decline in PV generation costs needs to open up new space for reduction. The study found that through the refinement of the cost management and control of photovoltaic companies, relying on the internal management of enterprises to promote cost reduction and efficiency increase, is an important support point for the reduction of photovoltaic costs in the future. The most basic work of cost control is scientific and effective cost accounting analysis. Through accounting and analysis, there is a waste in the company's operations, which in turn drives cost improvement [3]. Therefore, the following research questions are put forward and solved through the cost accounting operation in photovoltaic enterprises. Reducing manufacturing costs is a management act. Only by identifying and improving the project on the basis of cost accounting and analysis can the cost be optimized and controlled. The main research area is the cost accounting application of photovoltaic enterprises. Through the combination of ERP system and the application of two cost accounting methods (standard cost method and activity-based costing),

the cost data can be exported timely and effectively, and the waste in the cost is analyzed [4].

2. STATE OF THE ART

After systematically studying the relevant literature, it is found that the study of standard cost method and activity-based costing by domestic and foreign scholars focuses on the analysis of the method [5]. Standard cost method is widely used in enterprises, and most enterprises use this method in accounting costs. However, the shortcomings of the standard cost method are very prominent, which is not conducive to the company's comparison of manufacturing links and products. Moreover, the cost accounting cycle is long, and enterprises respond slowly to cost improvement. The operating flow of the activity-based costing method is complex, and the process involved is many and complex. It is difficult for general enterprises to carry out this work in operation [6]. ERP system in the current environment, the application of enterprises is relatively popular [7]. However, most companies mainly use the software in simple invoicing management, and simple standard costing has been used. Most studies only analyze problems in a single field, ignoring the integration of cost management. Empirical research has great limitations, poor replicable ability, inability to intuitively guide companies to solve practical problems, and lacks a comprehensive conceptual framework that integrates existing theoretical research and empirical research [8]. There are few cases of integration and integration of several cost management theories, and lack of analysis and use of information means, especially advanced ERP systems, to optimize the depth of cost management. For how to effectively combine the advantages of the standard cost method and the activity-based costing method under the ERP system, it is relatively less to develop a simple method of cost accounting and cost analysis. In particular, there is little research on the cost management of photovoltaic products and process characteristics.

3. METHODOLOGY

3.1. PV Enterprise Manufacturing Cost Accounting Control Design and its Optimization Algorithm

The algorithm of direct material cost in the standard cost method is: For example, if A product is 10 pieces and the direct material cost is 500 yuan, then the direct material cost per unit A product is 500/10=50 yuan. The disadvantages of this algorithm are: first, the business unit only knows the cost of the unit material 50 yuan / blocks, it is difficult to know which material is abnormal. The second is the long accounting cycle, which requires financial data to be available after the financial closing at the end of the month. Thirdly, there are many influencing factors of direct material cost, which are caused by fluctuations in raw material prices and the actual consumption of materials and the change of standard dosage. The combination of factors in direct material costs makes it difficult to find improvements in the above financial data. Unit direct material cost = art material unit price * (unit material theory consumption + excess loss dosage). Manufacturing costs consist of three parts: direct materials, direct labour and manufacturing costs. When calculating the manufacturing cost, the standard cost method takes the product as the accounting object, and obtains the unit manufacturing cost through the total manufacturing cost divided by the output quantity. The activity-based costing method is based on the standard costing method to increase the calculation of the process costs. In designing the manufacturing cost accounting of A PV enterprises, the following requirements are realized:

– First, the manufacturing cost data must be reported every day;

– Second, it is necessary to account for the manufacturing costs of different products, different times, different production workshops, and different sales orders.

To achieve the first requirement, it is necessary to report the data from time to time, and to respond to every ERP data in a timely manner through the use of the ERP system.

The implementation of the second requirement requires the addition of cost accounting objects and the introduction of the concept of work order here. The work order is the production instruction issued by the enterprise to the production department according to the sales order, which includes production workshop, production time, and material list and so on. At the same time, it is also used as a carrier for ERP system to issue materials and warehouse [9]. Therefore, according to the design of manufacturing cost accounting of A PV enterprises, the manufacturing cost accounting of unique work orders is constructed through the ad-

dition of processing orders as accounting objects [10]. In addition, the traditional cost accounting is relatively simple for the apportionment of the amortization cost, such as the direct labour and the manufacturing cost, and is generally distributed directly according to the quantity of the products. Due to the different labour costs and processes of different products, the simple distribution according to the amount directly leads to the unreality of cost accounting. For example, the direct labour cost, the traditional algorithm is that the total labour cost for the month is 10,000 yuan, the monthly output A product is 4000 W, the B product is 1000 W, and the unit cost per W = 10000/(4000+1000) = 2 yuan/W. The drawback of this accounting method is that the default products A and B and the cost per unit of labour per unit is the same. In fact, it is possible that the employment cost of the product A is 1.5 times that of the product B. According to the above algorithm, the unit cost calculated is the cost underestimation of product A, and the cost of product B is overestimated. By analogy, the above problems also exist in the allocation of manufacturing costs. When designing the manufacturing cost of a work order, the following principles should be followed. First, in the work order cost report, the sales order corresponds to the corresponding production work order, which truly reflects the material picking cost of each production work order. Second, it is necessary to standardize the ERP operation of the enterprise and to enter the system data in real time. Third, according to the product's different processes and differences, design and share standards, truly reflect the characteristics of the product. After determining the weights of various processing parameters, the optimal processing cost can be determined by the following function:

$$F(x) = \min \sum_{\substack{i=1,\ldots,m \\ j=1,\ldots,n}} (Pc_{IJ} X_{IJ} C_{IJ} / \sum Pc_{IJ}), \quad (1)$$

where *m* is the total number of processing processes, that is, the total number of characteristics of substitute processing, and *n* is the number of feasible processing methods corresponding to each process. Pc_{IJ} is the weight of the processing parameter to the total cost calculated by ANP, and C_{IJ} is the corresponding cost of the processing technology. X_{IJ} is a decision variable for processing methods:

$$X_{IJ} = \begin{cases} 1, \text{Perform this processing} \\ 0, \text{Do not perform this processing} \end{cases}. \quad (2)$$

And the processing of a feature must meet the requirement of machining accuracy.

$$\sum_{j=1,\ldots,n} X_{IJ} Pq_{IJ} \geq \eta Pq_I . \quad (3)$$

Among them, Pq_{IJ} is the accuracy coefficient corresponding to each processing process, and Pq_I is the characteristic *i*, the minimum precision coefficient required to achieve the processing, η is the weight of machining accuracy corresponding to different reliability requirements. This is a combinatorial optimization problem. This type of problem has a very precise mathematical description, high computational complexity, and is arsenic. The conventional methods for solving combinatorial optimization problems include problem transformation, branch and bound method, hill climbing method and so on. When the problem size is small, applying these methods generally can get better feasible solution. When the size of the problem increases, the number of feasible solutions increases exponentially, leading to the combined explosion of search space. In actual production, the processing parameters that affect the total cost are often complicated, and the solution by traditional methods is no longer effective. Here a genetic algorithm is chosen to solve this problem. To determine the Group Scale (integer) and the algebra (integer) of the genetic operation, the initial algebra k=1, using the random method or other methods to produce the *n* possible solutions $X(1 \leq i \leq n, k = 1)$ to form the initial solution group.

For each individual $X_t(k)$ in the group, the fitness $f(X_t(k))$ is calculated. For each individual $X_t(k)$ in a group, the probability of survival is $P_t(k)$. According to the survival profile $P_t(k)$, the parent is selected to perform genetic operations in the group, including replication, crossover, and variation to obtain a new solution group. At this point *k=k+1*, the condition is satisfied and the operation ends. Compared with traditional optimization methods, genetic algorithm has the following characteristics:

– Genetic algorithm does not directly deal with the design variables of the problem itself, but the

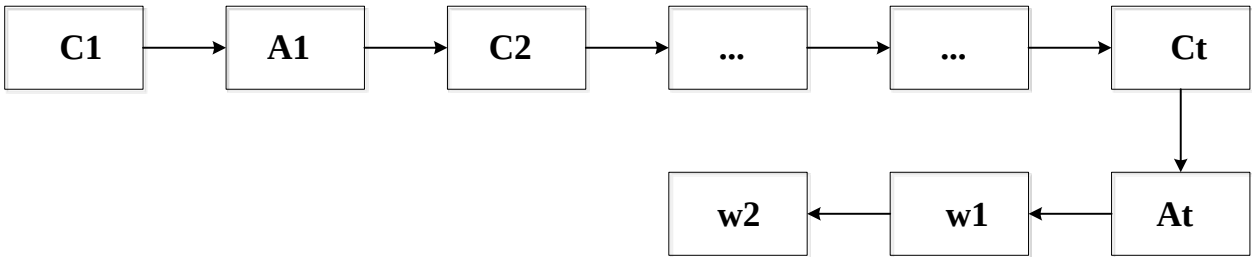

Fig.1. Genetic algorithm chromosome structure

coding of the design variables, which improves the universality of the algorithm;

– The search process of genetic algorithms begins with an initial group, rather than from a single individual, and has a parallel search feature, which greatly reduces the possibility of falling into the local optimal;

– Genetic operations used by genetic algorithms are all random operations. At the same time, it searches according to individual adaptation information and does not need other derivative information, so it has wide adaptability;

– Genetic algorithm has global search ability, has a strong and high computational efficiency, and is good at solving complex problems such as combination optimization;

– The genetic algorithm interacts with the same generation or the front and back groups through proper genetic manipulation to maintain the information that has been searched, which is incomparable to the optimization method based on the single search process.

3.2. Genetic Algorithm for Optimizing RBF Neural Network

The output layer, hidden layer, and RBF neural network output layer have different functions. When designing the network, the most critical step is the hidden layer data centre C_i expansion constant δ_i and the choice of w between the hidden layer and the output layer. Only by selecting the most accurate parameter values the RBF neural network can get the best approximation effect. Therefore, the genetic algorithm is used to optimize the network, that is the best choice of the three parameters. The specific optimization steps are as follows: select chromosomes and encode them. RBF network design is generally divided into two independent steps. First, the data centre ink stone and the expansion constant of the network are selected through the *k*-means clustering method, and then the weight w is solved through the least square method. In this way, the required solution is computed, which is not conducive to the unity of the whole algorithm. The genetic algorithm is encoded by the three parameters, such as C_i, δ_i, and w_i; and the chromosome string is formed. The data centre of the hidden layer plays an important role in the input and output layer in the radial basis function. Because the base function of RBF neural network is Gauss's function, the changes of two parameters of data centre C_i and extension constant δ_i Bare closely related, and the change of data centre will affect the extension constant change. Therefore, the genetic algorithm will intersect two parameters of C_i and δ_i, that is, a data centre is composed of a set of expansion constants. Then put the weights w in the last order, which can increase the probability that data centres and extension constants will change simultaneously in the genetic process. The chromosome structure of the genetic algorithm is shown in Fig. 1.

If the number of hidden layer neurons in the RBF neural network is *P*, the number of input layer neurons is *M*, and the number of output layer neurons is *N*, the number of weights is *MN*. The data centre and width are *PN+P*, and the total length of chromosomes is *MN+PN+P*. In addition, the number of neurons in the hidden layer will vary

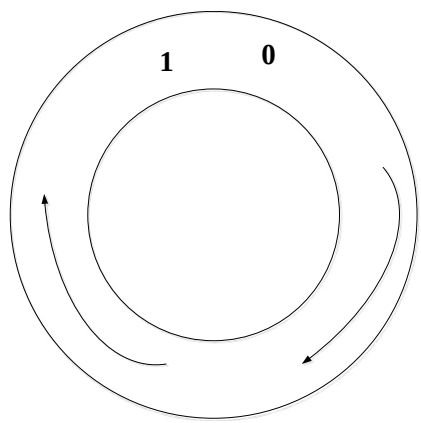

Fig.2. Intersection and selection diagram in genetic algorithm

Table 1. Before and After Improvement

	Manufacturing cost, yuan/W	Overall cost, yuan/W	Profit
2012	3.8	45000	12 %
2013	3.6	42000	14 %
Ring than	5 %	7 %	17 %

with the approximation ability of the RBF neural network in the course of heredity. The ratio of fitness calculated to each individual corresponds to each other. During the random number is generated in the range of [0, 1], the number that the pointer points will be selected. The schematic diagram of the selection operation is shown in Fig.2. In this operation, the higher fitness of individuals is higher probability of pointer selection, which indicates that the three parameters corresponding to C_i, δ_i and w_i are better.

4. RESULT ANALYSIS AND DISCUSSION

4.1. Data acquisition and preprocessing

In this part, we use the algorithm and model to calculate. The specific idea is: firstly, we get the data from photovoltaic enterprises, and summarize the data, then compare the two numerical prediction methods, get the best method, and finally carry out numerical prediction.After introducing new cost accounting schemes, PV enterprises get good profits in the actual business operation. XX enterprises formally introduces the cost management plan in 2013, and achieves better returns from the completion of various economic indicators, as shown in Table 1.

As shown in Table 1, the cost of manufacturing is down by 5 %. In 2012, the manufacturing cost was 3.8 yuan per watt. In 2013, the manufacturing cost was 3.6 yuan per watt, which was 5 % lower than the previous quarter. In order to make the data more comparative, the same material prices as in 2012 were used to account for 2013 manufacturing costs for the study). Four major costs (financial costs, administrative costs, R&D expenses, sales costs). The ring fell 7 %, and the gross profit increased by 17 %. From the above economic data is not difficult to obtain, there is a significant improvement before and after the import. A real and effective accounting method brings enterprise management with the exception of quantitative data. More derivative benefits can be summed up as four points: cost accounting

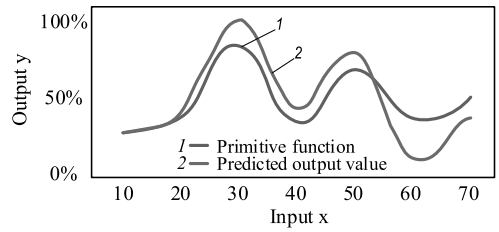

Fig.3. RBF neural network output graph based on randomly selected centre method

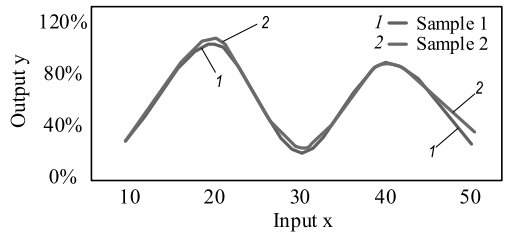

Fig.4. RBF neural network output graph based on k-means clustering

and business operation. Costing is based on a principle of consistency with business processes. According to the different products, the real allocation coefficient is used to ensure that the accounting data are not distorted. In this way, the acceptance of business units is relatively high.

4.2. Numerical prediction

Then we choose K-means clustering method and random center selection method to simulate the function, and compare the results to confirm the most suitable function simulation method.

The random selection centre method can randomly select data as data centre through random number, then the data centre is fixed and its corresponding extension constant is no longer changed. Then the weights are determined by the least square method. Fig. 3 shows the RBF neural network's ability to approximate the function after training based on the randomly selected centre method. The dotted curve is the original function, and the solid curve is the predicted output value of the network.

Table 2. Partial RBF Neural Network Training Data

Time	W/m^2	^{0}C	V	W
6.083	63.4720	25.2756	28.9800	9.9357
6.167	103.066	25.3657	29.2500	19.0074
6.250	87.6348	25.4578	29.5600	15.2387
6.330	127.8117	25.4135	29.9400	23.4470

After initializing the network, the samples are categorized into different categories in order of distance from near to far. Save old cluster centres and generate new cluster centres. The data centre is determined by comparing whether the two central locations coincide and the weight is determined by least square method. The predicted output is shown in the curve in Fig. 4.

From the comparative analysis of Figs 3 and 4, it is shown that the *k*-means clustering method can simulate the original function more accurately than the random selection centre method. There is a close relationship between the prediction degree of RBF neural network and the number and location of the data centre, and the random selection centre method is more random to the data centre. Therefore, *k*-means clustering and least square method are used to determine the data centre and weights of RBF neural network. After choosing the appropriate function simulation method, this paper uses the random center selection method to carry out function simulation and numerical prediction. In the numerical prediction, we first normalize the target vector, and then predict.

The selected target vector is X=[(time (Ct), light intensity (Sun), temperature (T_{ac})], while the counter normalized output vector is required to be the corresponding voltage of the maximum power point. Part of the training data and prediction data of the network are shown in Table 2.

A total of 145 sets of data for forecasting PV MPPT were collected from 6:00 a.m. to 18:00 p.m. on May 2, 2013. The average is divided into one group every 5 minutes. The first 100 groups are the training data of the RBF neural network, and the other 45 groups are the prediction data of the network. After the input data is determined, the centre and weights of the RBF neural network are determined by the *k*-means clustering method and the least square method. Select the first 100 sets of data as samples to input data for training, and then use the 45 sets of data to predict, in order to test the accuracy and practicability of the network. The result of network prediction is the voltage corresponding to the maximum power point in photovoltaic generation when the time, intensity and temperature are changing.

5. CONCLUSION

The development of photovoltaic industry is in its infancy. On the way of lowering the cost of products, it is mainly through the revolution of new technology and the development of new materials to reduce the cost of products and reduce the overall cost. This change plays a vital role in solving the problem of environmental pollution of traditional energy sources. Based on this, the manufacturing cost optimization of photovoltaic enterprises is studied based on neural network. First of all, the status and problems of the research are expounded. Secondly, based on neural network algorithm, this paper puts forward the design and optimization algorithm of manufacturing cost accounting control of photovoltaic enterprises, and then takes the A enterprise as an example to test it. The models and algorithms can be effectively applied in enterprises. Only by identifying and improving the project on the basis of cost accounting and analysis can the cost be optimized and controlled. Through the combination of ERP system and the application of two cost accounting methods (standard cost method and activity-based costing), the cost data can be output in time and effectively, and the waste in the cost is analyzed.

REFERENCES:

1. Baptista D, Abreu S, Travieso-González C, et al. Hardware implementation of an artificial neural network model to predict the energy production of a photovoltaic system. Microprocessors and Microsystems, 2017. V49, pp.77–86.

2. Dumitru C D, Gligor A, Enachescu C. Solar photovoltaic energy production forecast using neural networks. Procedia Technology, 2016. V22, pp.808–815.

3. Kayri I, Gencoglu M T. Predicting power production from a photovoltaic panel through artificial neural networks using atmospheric indicators. Neural Computing & Applications, 2017, pp.1–14.

4. Kane P V, Andhare A B. Application of psychoacoustics for gear fault diagnosis using artificial neural

network. Journal of Low Frequency Noise, Vibration and Active Control, 2016. V35, #3, pp.207–220.

5. Zheng M, Horowitz K, Woodhouse M, et al. III-Vs at scale: a PV manufacturing cost analysis of the thin film vapour–liquid–solid growth mode. Progress in Photovoltaic: Research and Applications, 2016. V24, #6, pp.871–878.

6. Haiying Li, Xian Li, Xinyue Xu, Jun Liu, Bin Ran. Modelling departure time choice of metro passengers with a smart corrected mixed logit model – A case study in Beijing. Transport Policy. 2018, #69, pp.106–121.

7. Moon S, Yoon S G, Park J H. A new low-cost centralized MPPT controller system for multiply distributed photovoltaic power conditioning modules. IEEE Transactions on Smart Grid, 2015. V6, #6, pp.2649–2658.

8. Jain S, Agarwal V. A single-stage grid connected inverter topology for solar PV systems with maximum power point tracking. IEEE transactions on power electronics, 2007. V22, #5, pp.1928–1940.

9. Goti-Elordi, Aitor; de-la-Calle-Vicente, Alberto; Gil-Larrea, Mara-Jose, et al. Application of a business intelligence tool within the context of big data in a food industry company. DYNA, 2018. V92, #3, pp. 347–353.

10. Oman S, Leskovar R, Rosi B, et al. Integration of MES and ERP in supply chains: effect assessment in the case of the automotive industry. Tehnički vjesnik, 2017. V24, #6, pp.1889–1896.

Weiping ZHANG
received the Ph.D. degree in computer science from Rostock University, Rostock, Germany. From 2014 to 2016, he was a Research Scientist with the Institute of BCRT in Berlin, Humboldt University, Berlin, Germany. He is currently a Uni-Professor with the School of Information Engineering, Nanchang University, Nanchang, China. His research interests include machine learning, process information management systems and real-time mobile measurements of physiological parameters

Shuming LI, Post Dr. She has received Ph.D. degree in Beijing Forestry University in 2013. From 2017 till now, she began her postdoctoral research at Binhai Industrial Technology Research Institute of Zhejiang University. Her research interests include high value utilization of biomass, technology innovation management and commercialization of research findings

Junfeng YU received the master's degree in communication and information system from Beijing Jiaotong University, Beijing, China. He has more than 5 years development and operation experience in the internet industry, particularly in domain name system and routing technology. He is currently an R&D engineer in Binhai Industrial Technology Research Institute of Zhejiang University, Tianjin, China. His research interests include machine learning and data analysis

Yihua MAO, Ph.D, Professor. He has got Ph.D. degree from Zhejiang University. Now he serves in College of Civil Engineering and Architectural of Zhejiang University. He also serves as the deputy dean of Industrial Technology Research Institute of Zhejiang University and the dean of Binhai Industrial Technology Research Institute of Zhejiang University. His main research fields: the engineering economy and project cost, construction project management, system design and large data analysis technology; enterprise strategy and technology innovation management

Light & Engineering
Vol. 26, No. 3, pp. 174–180, 2018

Svetotekhnika
No. 5, 2018

BIG DATA SURVEY ON EMPLOYEE EXERCISE IN NEW HIGH-TECH PHOTOVOLTAIC ENTERPRISES: HIGHLIGHTS ON START-UP PHOTOVOLTAIC COMPANIES

Zewen WANG

Capital University of Physical Education and Sports, Beijing Province, 100191, China;
E-mail: sbjuu5635@163.com

ABSTRACT

Numerous studies show that scientific and reasonable physical exercise can promote human health. Reasonable exercise prescriptions based on an individual's physical condition is important in improving one's health. On this basis and through the investigation on the big data of emerging high-tech photovoltaic enterprises, the development and design of a human health model and science in sports are developed based on ant colony optimization algorithm. Finally, the requirement analysis, design, specific application, and model algorithm testing of the physical fitness exercise prescription model can provide a scientific strategy for human health and scientific movement.

Keywords: high-tech, photovoltaic, physical exercise, fitness function, fitness value

1. INTRODUCTION

The photovoltaic (PV) industry in emerging strategic industries has recently experienced an explosive growth trend, which has led to economic growth in related regions. At present, the capacity of China's PV industry has reached 35 GW, which exceeds the total installed capacity of the world. Overcapacity has become a major problem that cannot be ignored in China's PV industry [1]. China's PV industry has sold more than 90 % of its products to developed countries, such as Europe and the United States, because their governments provide many subsidies for solar power enterprises. However, the government's subsidy for solar power companies has been greatly reduced due to the European debt crisis and other issues, which has seriously affected the sales of Chinese PV products abroad [2]. For example, Germany reduced the on-grid tariff of solar energy by 15 %, and Spain, France, the Czech Republic, and other European countries are also reducing their support for the solar power industry. In 2012, China's PV products suffered another round of anti-dumping investigation abroad. Under the pressure of a series of problems, such as the reduction of foreign demand, the large margin of profit, the collapse of enterprises, and the intensification of international trade disputes, China's PV industry has encountered an unprecedented crisis [3]. Under such enormous pressure of "foreign invasion" China's PV industry must turn its attention to the domestic market to escape the crisis. At present, although the output of PV modules in China has reached 80 % of the world's output, its installed capacity of PV accounts for only 8 % of the world's total. At the end of 2011, the total installed capacity of PV was less than 4 GW. For emerging high-tech PV companies, talent is critical. The cultivation of talents in emerging high-tech PV companies not only requires high comprehensive skills but also a healthy body [4]. On this basis, the investigation on the big data of the employees of high-tech PV start-ups is launched.

2. STATE OF THE ART

Since 1991, China has successively established 53 state-level high-tech industrial development

zones (hereinafter referred to as high-tech zones). By the end of 2000, the number of high-tech enterprises in the country was 20,796, employing 2.5 million people and increasing by 38 % annually [5]. As an important part of the national "Torch Program" for developing high and new technology industry, the National Hi-tech Zone has become the most dynamic economic growth point in the country and an important force to pull the regional economy. Emerging industries are mostly transformed from high-tech industries. The destructive effect of technological innovation on the traditional market has led to emerging strategic companies to face conflicts with traditional industries, the market, and the original system in the process of gradual growth [6]. Under the background of the increasing energy crisis and environmental problems, the PV industry, as an important part of the new energy industry, has been highly valued by all countries in the world, and it is one of the relatively fully developed industries in the emerging strategic industrial system. Under the existing market mechanism and industrial environment in China, the experience and lessons of the PV industry in the process of development are of considerable importance for the PV industry itself, as well as other emerging strategic industries [7].

3. METHODOLOGY

3.1. Model of the Physical Training Prescription for New and High-Tech PV Enterprises

The technical principle of "two-dimensional dynamic exercise intervention program" is based on the theory of sports health promotion of the American Sports Medicine Association [8]. According to the index of the current physical state of the body (e.g., body weight and body composition), body strength, muscle strength and endurance, blood pressure, blood sugar, and energy consumption, this personal index dimension is analyzed in combination with external environmental factor indicators (e.g., temperature, humidity, season, geographic location, and project suitability). Through the learning mode, the intelligent decision fits an individual's exercise program. The route is as follows. Samples are tested, and the error of each sample is calculated to determine the fitness value:

$$E = \frac{1}{2}\sum_{k=1}^{n}\sum_{j=1}^{p}(y_j^k - o_j^k), \quad (1)$$

where n is the number of training samples, p is the number of output nodes, and $y_j^k - o_j^k$ is the error of the k^{th} sample relative to the j^{th} output unit. The fitness function is set to fitness equal to l/E. The selection operation uses a sorting method. According to the fitness value of each individual sample sorted from smallest to largest, the individual with the smallest fitness value corresponds to a serial number of *1*, and the individual with the largest fitness value corresponds to a serial number of M. After sorting, the sample with the serial number i corresponds to a relative fitness value $fitness_i$, as shown as follows:

$$fitness_i = \max - [(\max - \min)(i-1)(M-1)], \quad (2)$$

where max is [1.3, 1.7] and min is [0.2, 0.6]. Subsequently, on the basis of the relative fitness value of each sample, the selection probability of the sample is calculated according to the fitness proportion selection (stake) method, as shown as follows:

$$P = fitness_i / \sum_{i=1}^{M} fitness_i. \quad (3)$$

Cross operation adopts mathematical crossover, followed by probability P_c to cross select two samples, XI and X2 and obtain two new individuals, X1 and X2, where I is the crossing point adopted, 1 or less than i n; n is the chromosome length; and a is the predetermined real number, $0 < a < l$.

$$X_1 = aX_{1i} + (1-a)X_{2i}. \quad (4)$$

$$X_2 = (1-a)X_{1i} + aX_{2i}. \quad (5)$$

The variant operation uses the non-uniform variation to set the variant parent $X = wlw2w3...$ $wk...$ wl. Using the non-uniform variation, the variation point wk is randomly determined by the probability Pm. The range of the value of wk is $\left[U_{min}^k, U_{max}^k\right]$, and the new gene value w_k is determined as follows:

$$w_k = \begin{cases} w_k + \Delta(t, U_{max}^k - w_k) random(0,1) = 0 \\ w_k + \Delta(t, w_k - U_{min}^k) random(0,1) = 1 \end{cases}. \quad (6)$$

Random (0, 1) represents the probability of equality from 0 to 1, and *t* denotes evolutionary algebra. In delta (T, Y) (Y represents $U_{max}^k - w_k$ and $w_k - U_{min}^k$ represents [0, y], which range conforms to the non-uniform distribution of random numbers with the increase of evolutionary algebra T), the probability of delta (T, Y) approaching 0 also increases. T is the largest evolution algebra; *r* whose range is [0, 1] meets a random number of uniform probability distribution; and *b* is the coefficient of determining non-uniformity [2, 7]. Therefore, the non-uniform mutation allows the operator to search uniformly in the solution space at the beginning (*t* is less), whereas it has partial search property in the later stage (*t* is close to T). The two-dimensional dynamic exercise intervention program should include sport types, exercise intensity, exercise time, exercise frequency, exercise progress, and precautions.

Sports Type

Common types of exercise may generally include endurance (aerobic), strength, stretching (flexible), balance, agility, and speed exercises.

Exercise intensity. Exercise intensity is the core of exercise prescription and the most difficult part in designing exercise prescription. The corresponding exercise intensity can be determined on the basis of the result of exercise load test.

Duration

The interval training method, continuous training method, and intermittent continuous combination training method can be used in the exercise prescription to enhance cardiopulmonary endurance. The effective time of the exercise, that is, the time during which the exercise is performed, must be maintained.

Number of repetitions, number of completed sets, and interval time

In the exercise prescription for enhancing cardiopulmonary endurance, when the interval training method is used, specifying the running distance, the completion time of each running distance, the interval time, the number of completions, and so, the total number of completions becomes possible.

Exercise frequency

Exercise frequency refers to the number of exercises per week. One only needs to exercise once a day, 3–4 times a week, or once every other day.

Precautions

Attention must be paid to the safety of sports in implementing exercise prescriptions. The safety of venues, facilities, clothing, and the environment must be ensured. The safety instructions in the exercise prescription should also be followed during the exercise. For example, exercise intensity should not exceed the prescribed prescription, proper exercise, and exercise time.

3.2. Ant Colony Optimization Algorithm

First, the weights are determined. Each enterprise is abstracted into an antill, which must have memory capability. The weights are determined by comparing the data in the relational model G. A taboo list of PGs for each ant is used to record whether the current ant has been allocated. PG tables must be updated constantly and must be emptied before the next start. Second, a match between the employee and the physical exercise program is then observed. For an employee who can perform multiple sports, the relationship model must determine which employee is most suitable for which sports event. This condition is similar to the ants performing a match in the ant colony algorithm and comparing it with the last best match to determine which of the edges with weights has the largest weight. Third, pheromone is selected. Pheromones are the degrees of influence exerted by employees who have exercised on those who have not. The volatilization characteristics of pheromones include the mood, the state, and the working condition of the employee on that day, and the effective use of positive and negative feedback algorithms. The pheromone strategy in the MMAS algorithm is selected to prevent the premature convergence of the algorithm and lengthy computation time. Furthermore, probability selection is applied in the algorithm to satisfy the randomness requirements.

$$P_{ij}^k(t) = \begin{cases} \dfrac{[\tau_{ij}(t)]^\alpha [\eta_{ij}]^\beta}{\sum\limits_{s \in allowed} [\tau_{is}(t)]^\alpha [\eta_{is}]^\beta} & j \in allowed_k \\ 0 \end{cases}, \quad (7)$$

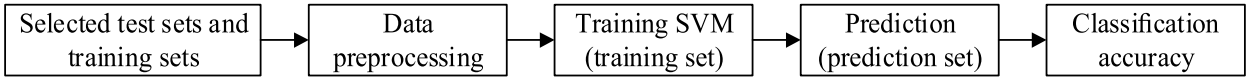

Fig.1. Algorithm flow chart

where $tabu_k (k = 1, 2, 3, \ldots n)$ represents the set of all nodes that ant k is currently walking through, and $allowed_k$ represents the set of ants that has not passed the point.

$$\tau_{ij}(t+n) = (1-\rho)\cdot\tau_{ij}(t) + \Delta\tau_{ij}, \tag{8}$$

$$\Delta\tau_{ij} = \sum_{k=1}^{m} \Delta\tau_{ij}^{k}, \tag{9}$$

where ρ denotes the pheromone volatilization coefficient i, (1-ρ) denotes the pheromone residual factor, and $\Delta\tau_{ij}$ denotes the pheromone increment on the path in the current cycle and the amount of information that the k^{th} ant remains on the path in the current cycle.

$$\Delta\tau_{ij}^{k} = \begin{cases} \dfrac{Q}{L_k}, & \text{If } K \text{ only ants pass through this cycle } (i,j) \\ 0 & \end{cases}, \tag{10}$$

$$\eta_{ij} = \frac{1}{(100 - d_{ij})}, \tag{11}$$

where d_{ij} is the degree of employee satisfaction with a certain sporting activity. The heuristic factor α, expected heuristic factor β, number of ants m, and coefficient of volatility ρ of the algorithm are derived from the eil51 in the TSPLIB simulation experiment and Zhao's research on arranging classes based on the ant colony algorithm. The following values are used in the algorithm: $m = 5$, maximum number of iterations = 40, $\alpha = 1$, $\beta = 5$, $\rho = 0.3$, $\tau_{\max} = 1000$, $\tau_{\min} = 0.01$, and $Q = 20$. For the MMAS pheromone, only one ant performs pheromone updates after each cycle. The value range of each pheromone is limited to $[\tau_{\min}, \tau_{\max}]$. When the pheromone value is $\tau > \tau_{\max}$, $\tau = \tau_{\max}$ is considered; when the pheromone value is $\tau < \tau_{\min}$, $\tau = \tau_{\min}$ is taken. For the maximum matching of bipartite graphs, the graph is a mathematical model that uses dots and lines to characterize discrete objects d_{ij} collections, and objects in some way.

The main steps of program algorithm are presented in Fig.1.

Health fitness management can be divided into five aspects, namely, personal health test, physical fitness assessment, intervention effectiveness assessment, physical fitness intervention, and physical fitness training and guidance.

Healthy fitness, the basic information of managers: the management platform functions as a questionnaire, and managers can use the Internet to fill out questionnaires and determine their basic information. Survey questionnaires can use the software's own questionnaire model, and users can also edit the questionnaires to learn useful information from the managers.

Physical fitness assessment: the evaluation of employees' physical fitness mainly includes items stipulated by the standards for physical fitness testing of the employees. These items include indicators of reaction morphology and indicators of responsiveness. Indicators of responsiveness can be used as the basis for evaluating physical fitness.

Exercise load test evaluation: the incremental load exercise program and the synchronous testing of the relevant physiological and biochemical indicators as the basis for the development of exercise intervention can be utilized based on actual needs. Health-related indicators include muscle strength and muscle endurance, cardiopulmonary function, bone density, and body composition. Through these test items, the purpose of the intervention can be determined from the perspective of healthy physical fitness.

Physical fitness intervention: after formulating corresponding exercise prescriptions, relevant physical fitness interventions are performed according to exercise prescriptions. The supervision function of the software and the monitoring function of the terminal equipment are optimized to perform related exercise interventions effectively and reasonably. In the physical fitness management evaluation, about 4–6 weeks of exercise intervention and timely evaluation confirm the effectiveness of the intervention and the effect of the evaluation and adjust the intervention program to perform well in the subsequent intervention and management.

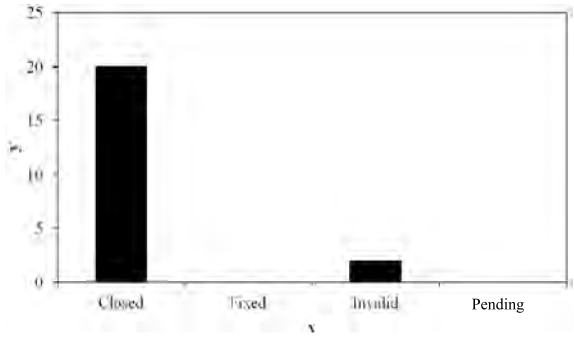

Fig.2. Bug distribution

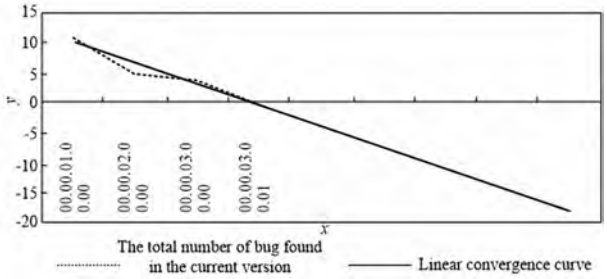

Fig.3. Bug convergence curve with the change of version

Physical fitness training and guidance: most of physical fitness management uses external factors for management and supervision. The managers must be supplemented by teaching and instruction for the internal factors to work and let them think about the importance of the health ideology and then consciously exercise. Education and counselling can take the form of DIY software, books, newspapers, conversations, or using the Internet. Managers should use their own characteristics to conduct healthy physical fitness assessment in the actual work.

4. RESULT ANALYSIS AND DISCUSSION

The test cases verify the normal implementation of the entire system function through several major points, such as member registration, selection of test items, and verification of test item functions, personal analysis, print report, and interface. A simple explanation of the use case of "Verification Test Item Function" is shown in Table 1. The testing methods of other function points are the same as the testing methods of this function point. They all consider whether the verification testing program can be selected normally and whether the input data can be saved normally.

Each version of bug distribution (bug with the version of the convergence curve) is shown in Figs. 2,3.

As shown in Fig. 3, the number of problems discovered converges with the version. Among them, the test focus of version 00.00.01.00.00 to 00.00.03.00.01 mainly focuses on functional testing and verifying whether the business process of its management software is correct and whether the test project screening scheme is correct, including personal analysis and report verification. Bug severity distribution is shown in Fig. 4.

As shown in Figs. 4,5 among the 20 valid bugs, none have "4-Critical" level, fatal problems, stable functions, and excessive abnormalities; the 3-Serious and 2-Medium are 20 % and 30 %, respectively. This result is mainly caused by the function settings and the actual implementation of the performance, which do not match the error after the interface switching. Moreover, the level of 1-Low ratio is 50 %, which mainly aids information and prompts information error, Table 2. The ETT test officially began entering the testing phase on May 17, 2017. During the project testing process, four test versions were made, resulting in 20 effective bugs. Through the six aspects of the test in the use case, the software function was realized normally, the operation was stable, the operation and use were in accordance with the common user's operating habits, the friendliness promptness was clear, and the use of the user was well guided.

Weight reduction exercise prescription has the highest priority in this system. From the aspect of the direct relationship between body weight and body weight, weight reduction belongs to the in-

Table 1. Function Testing

Functional testing				
Test phase	Test cycle	Working hours (human hours)	Total number of problems	Problem discovery rate (per hour)
Functional test stage	2012.5.17 ~ 2012.5.24	63	20	0.33

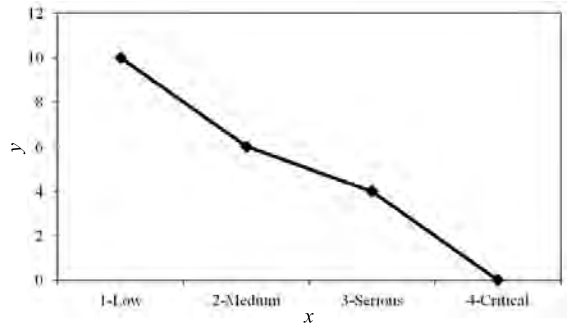

Fig.4. Severity degree distribution of bug

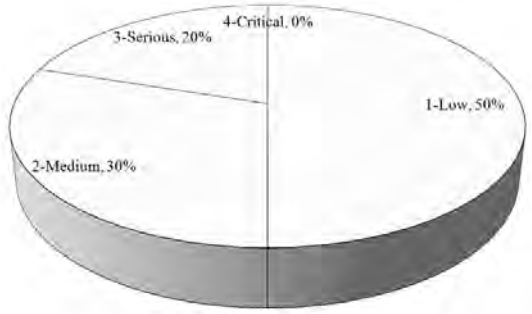

Fig.5. Severity distribution

Table 2. Severity Degree Distribution of Bug

Severity	Number	Percentage, %
1-Low	10	50
2-Medium	6	30
3-Serious	4	20
4-Critical	0	0
Total	*20*	*100*

dex of the body shape subsystem. Therefore, the related parameter equations are set in the body shape subsystem. Similarly, a 50-year-old male ID with wg656 as an example (weight exercise prescription) was employed to perform a system dynamics analysis of the effects of exercise prescriptions. The ID with wg656 user-related fitness test information is entered into the model, related parameters are set according to age and gender, and a system dynamics model is established. The user needs to lose weight, and the difference between his actual and ideal weight is 21.99 kg, which is an unscientific goal in the 12-week exercise prescription cycle.

Through the system dynamics simulation of weight-loss exercise prescription, the results of changes in the secondary indicators of physical fitness, and the improvement of body shape, the physiological function changes to a certain extent, which can be understood as the physiological function produced with the change of body shape. Changes in fitness, body shape, and physiological function result in comprehensive changes in physical fitness, that is, changes in body shape affect the comprehensive changes in physical fitness. The weight-loss exercise prescription for body shape change is insensitive to changes in physical fitness. It is manifested as a change in body shape, and the change in physical fitness is small and shows no change (physical fitness is a straight line). Setting a weight-reduction exercise prescription has minimal significance in the development of physical fitness. Therefore, in the development of weight-loss exercise prescription, the desire to achieve good results in physical fitness necessitates performing special quality exercises to obtain good overall physical fitness evaluation results.

5. CONCLUSION

The analysis on the big data of the high-tech PV start-ups' employees shows that the individual differences in the quality of the employees' quality inspections, together with the degree and methods of physical exercise, have different results. Therefore, how to cultivate employees' life-long sports awareness based on their individual differences should be a top priority for emerging high-tech PV companies. An exercise prescription software system wherein employees routinely load their own characteristics is designed, that is, an employee physical fitness exercise prescription system. This system, combined with the physical exercise model, plays an active role in the employees' daily exercise and forms good exercise awareness. Endurance exercise has a significant training effect on enhancing the capability of the respiratory system to take up oxygen, the cardiovascular system load and the capability to deliver oxygen, and the capability of the tissue to use oxygen for aerobic metabolism; thus, endurance training and endurance training are designed for endurance training.

REFERENCES:

1. Alferov Z. I., Andreev V.M., Rumyantsev V.D. III–V Heterostructures in photovoltaic. Springer Series in Optical Sciences, 2007. V130, p.25.

2. Sur C. Study on the Impact of Grid Electricity in Powering the Expansion of Healthcare Services and Facil-

ities in Sagar Island. Journal of Rural Development, 2017. V36, #3, pp.397–418.

3. Gopal Y, Kumar K, Birla D, et al. Banes and boons of perturb & observe, incremental conductance and modified regula falsi methods for sustainable PV energy generation. Journal of Power Technologies, 2017. V97, #1, pp. 35–43.

4. Deenik J, Kruisdijk F, Tenback D, et al. Physical activity and quality of life in long-term hospitalized patients with severe mental illness: a cross-sectional study. BMC psychiatry, 2017. V 17, #1, p.298.

5. Van Zutphen M., Winkels R.M., van Duijnhoven F.J. B., et al. An increase in physical activity after colorectal cancer surgery is associated with improved recovery of physical functioning: a prospective cohort study. BMC cancer, 2017. V 17, #1, p.74.

6. Pirtea M, Botoc C, Jurcut C. Risk and return analysis: evidence from emerging markets. Transformations in Business & Economics, 2014. V13, #2B, pp.637–647.

7. Haiying Li, Xian Li, Xinyue Xu, Jun Liu, Bin Ran. Modelling departure time choice of metro passengers with a smart corrected mixed logit model – A case study in Beijing. Transport Policy. 2018, #69, pp.106–121.

8. Xu, X., Xie, L., Li, H., & Qin, L. Learning the route choice behaviour of subway passengers from AFC data. Expert Systems with Applications, 2018. #95, pp. 324–332.

Zewen WANG,
Master of education, postgraduate student, graduated from the Capital University of Physical Education and Sports in 2016, Studied in Capital University of Physical Education and Sports. His research interests include athletic performance and health promotion

Light & Engineering
Vol. 26, No. 3, pp. 181–187, 2018

Svetotekhnika
No. 3, 2018, pp. 50–55

OPERATION FIELD ILLUMINANCE IN DENTISTRY

Anna Yu. Turkina[1], Irina A. Novikova[1], Andrei N. Turkin[2], and Galina N. Shelemetieva[3]

[1] Sechenov University, Mocow
[2]Lomonosov Moscow State University
[3]Private Organization, Blagoveshchensk
E-mail: andrey@turkin.su

ABSTRACT

Dental treatment zone and operation field illuminance estimation were made in this study. Treatment zone illuminance was 500 lx under conventional fluorescent lamp based lighting and 1000 lx in a case of additional ceiling light use. Operation field illuminance under a dental operating light varied from 4000 lx to 14000 lx in dependence on an oral cavity zone and a patient position. The maximal illuminance level was achieved at upper incisors in a patient supine position, the minimal one was achieved at upper molars in patient upright position. Using of light emitting diode (LED) headlight increased the illuminance up to 2000 lx in average. The use of intraoral light sources provided adequate operating field illuminance in range (7000–18000) lx in molars area where illumination of dental operating light are not enough.

The study results allow recommendation of ceiling lights and intraoral lights as additional light sources.

Keywords: illuminance, operating field, dental office, luxmeter

1. INTRODUCTION

In modern dentistry, high-tech treatment methods are widely used providing a broad range of possibilities. At the same time, a dentist mostly deals with extremely small sizes, about (0.1–0.3) mm objects ant this fact allows qualification of a dental treatment process as a high precise class work [1]. However, high precise manipulations require proper operating field lighting. Standard and additional light sources rational using provides high quality treatment and prevents dentist vision disturbance caused by eye strain [2, 3].

Every dental office has general and point source illumination. Fluorescent lamps with good colour rendering index are recommended for general lighting. Moreover, all dental units have operating lights for direct oral cavity illumination. For this task, high brightness LEDs are mostly used as light sources [4].

At present time, operating field direct illumination equipment is widely presented in dental market. It is possible to qualify this equipment with three groups:

– Additional general illumination lights having wide light distribution, for example ceiling lights used for dental unit and treatment area illumination;

– Additional extra oral direct illumination lights, for example different LED based headlights and dental operating microscope light providing additional one dental range (5–6 teeth) illumination;

– Additional intraoral illumination lights used for indirect vision areas illumination, for example LED dental hand pieces, dental mirrors with LED light and suction & lighting systems (MaxBite, Isolite).

In Russian Federation standard, the dental office overall illuminance is equal to 500 lx [5]. In actual health & sanitation rules the operation field illuminance value isn't established but it's noted that local light level doesn't have to exceed overall one

Fig. 1. The illuminance measurement at the lower molar occlusal surface

Fig. 2. Additional ceiling light

in more than 10 times. Basing on this requirement it's possible to suppose that the recommended operation field illuminance value is 5000 lx.

For any activity three illuminance zones exist [6]:

1. Operating zone (in dentistry – oral cavity). Oral cavity illuminance standard value is up to 20000 lx;

2. Transition – middle zone (patient chin). Middle zone illuminance is in range from 6500 lx to 10000 lx;

3. Overall illuminance zone (treatment zone illumination). Instrument table surface illuminance is close to (1500–2000) lx.

According to European Standards DIN5035–3:2006–07 ("Lighting of health care premises") and DIN EN12464–1:2011 ("Lighting of work places. Indoor work places") the recommended operating field illuminance value is 5000 lx, the treatment zone one is 1000 lx and overall dental office illuminance is 500 lx [7,8].

According to study made in 2006, dentist instrument table surface illuminance for fluorescent lamps based overall illumination was 450±20 lx, that is lower than standard value, and operating field (oral cavity) illuminance was in range (5280–6140) lx, that is higher than standard value [1]. Basing on study 2013, dentist operating field illuminance in state clinics was 4930±8,2 lx, and in private ones it was 8850±7,6 lx [9].

Treatment zone and operating field illuminance values can be significantly varied in dependence on dental operating light power and on additional light sources used. According to ISO 9680:2014 "Dentistry: Operating Lights", dental lights must provide adjustable operating field illuminance close to range (8000–20000) lx [10]. In the RF National State Standard: GOST 26368–90 "Medical luminaires. General technical requirements and test methods", the maximal operating field illuminance is stated as not more than 2800 lx at recommended distance in range (0.7–1.0) meter (at the patient eyes level – not more than 1000 lx) [11]. Several manufacturer promotional materials announce that dental operation light is able to provide a surface illuminance up to 30000 lx at a distance 0.7 meter. However, it's necessary to note that it's much difficult to provide a direct tooth surface illumination, so a real molar illuminance level usually will be lower.

The aim of this study was a dental treatment zone and operating field illuminance determination in dependence on used lighting devices.

2. METHOD AND RESULTS OF THE STUDY

The study was performed at the restorative dentistry department of Sechenov University, Moscow.

The treatment zone and operating field illuminance values were measured with luxmeter TKA-PKM (08) ("Scientific & Research company TKA LTD, Russia). The luxmeter includes a measurement sensor, LCD display module and connecting stranded flexible cable. For treatment zone illuminance measurement the sensor was placed at the surface of instrument table. For operating field illuminance value measurement the sensor was protected with disposable digital x-ray sensor sleeve and placed in oral cavity (Fig. 1).

The measurements of treatment zone illuminance were made under natural light, under standard fluorescent lamp based lighting and with additional ceiling light for dental office. The operating field illuminance was measured under fallowing light sources:

Fig. 3. Dental unit operating light

Fig. 5. Colour filter for LED headlights

– Conventional fluorescent lamp based lighting;

– Additional ceiling light for dental office D-TEC (manufacturer listed the illuminance value 5800 lx at the distance of 1.2 m) (Fig. 2);

– Dental operating light of the dental units: A-DEC200, A-Dec Int., USA (according to manufacturer, LED light provides the illuminance value 8000–17000 lx) and Darta 1605 M, Russia (according to manufacturer, LED light provides the illuminance value 3000–35000 lx) (Fig.3);

– LED headlights: Crystal LED Light and NOW. CLIP (NOW, China), providing the maximal illuminance 35000 lx (Fig, 4); colour filter for LED headlights DK – Cap (DKH Dr. Kim, Republic of Korea) (Fig. 5);

– Dental operating microscope with LED light Leica M 320 Hi-End (KaVo, Germany) (Fig. 6);

– Dental mirror with LED light LumiEst (Geosoft, Russia-Israel) (Fig. 7);

– LED dental turbine handpieces: SYNEA TG – 98 L (W&H Dental Werk, Austria) (Fig.8) NTKsd – 300 (BX-Taifun, Russia);

– Intraoral suction & lighting system MaxBite (China) (manufacturer listed the illuminance value 5000 lx) (Fig. 9).

Fig. 4. LED headlight

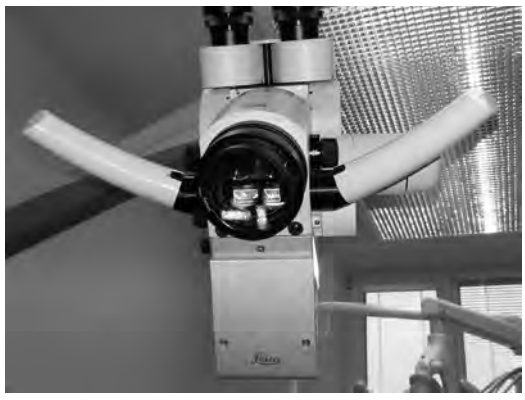

Fig. 6. Dental operating microscope

Fig. 7. LED dental mirror

The intraoral measurements were performed in upright and supine patient positions. The sensor was positioned at the upper incisors vestibular surfaces, lower molars occlusal surfaces and upper molars occlusal surfaces. In the each area 2 measurement series were performed under different light sources. Each series included 5 measurements. Totally it was performed 50 series of 5 measurements. Further illuminance average values and their standard deviations were calculated. Treatment zone illuminance values are presented in Table 1.

Table 1. Dental Office and Treatment Zone Illuminance Value

Light source	Illuminance, lx
Natural light* (by the window)	805±15
Natural light* (treatment zone)	232±20
Conventional fluorescent lamp based lighting	470±25
Additional ceiling light for dental office	1000±15
* the measurements were carried out at 11 a.m. in a cloudy autumn weather	

Fig. 8. Dental LED turbine handpiece

Fig. 9. Intraoral suction&lighting system MaxBite

Natural light is not enough for adequate illumination of dental treatment zone (232±20) lx, so it's not recommended to examine the patient under natural only. Though some authors recommend determining patients' teeth shade under natural light when direct or indirect esthetic restoration is planned. In that case it would be better to determine teeth colour near the window, where illumination is better (805±15 lx) and near the daylight.

Under conventional fluorescent lamp based lighting treatment zone illuminance was lower than recommended level (470±25) lx. The illuminance was depending on instrument table position. The maximum illumination level was achieved when the instrument table was positioned directly under the light source. Under additional ceiling light the treatment zone illuminance was (1000±15) lx and corresponded to European standards.

The operating field illuminance depends of the oral cavity zone, Table 2. When dental operating light is used, the maximum illuminance is determined on the upper incisors' vestibular surface (12300±2500) lx at upright position and (13200±1200) lx at supine position). So, there is no need to use any additional light sources to perform dental treatment in this area. Illuminance on the lower molars also depends on patient's position. When the patient is in the supine position, the dental operating light can be placed directly above the oral cavity (light incident angle is close to 90^{O}), so the illuminance value can be up to (10000±1000) lx. In the upright patient's position the light incident angle is less than 90^{O} and illiminance value decreases to (54000±500) lx. However, this illuminance value is more than 10 times higher than treatment zone illuminance level, provided by standard fluorescent lamp based lighting. The minimum illuminance was determined on the upper molars' occlusal surface in the patient's upright position, (2500±300) lx.

During dental treatment the tooth surface can be shaded with dental handpiece or any other instrument, so the illuminance level can decrease significantly. In the presented study when turbine handpiece was positioned in the oral cavity the illuminance value at the lower molars' occlusal surface was 250 lx in upright patient's position and 300 lx in supine position.

When additional light sources are used, the operation field illuminance varies from 2300 lx up to 12500 lx (Table 3).

LED operating light alone provides the illuminance in lower molars area (2300±30) lx. When LED head light and dental operating light are used

Table 2. Different Zones of Oral Cavity Illuminance Value, Provided by Dental Operating Light (the distance is 70 cm)

	Patient is in upright position, lx	Patient is in supine position
Upper incisors' vestibular surface	12300±2000	13200±1200
Upper molars' occlusal sirface	2500±300	3900±500
Lower molars' occlusal surface	5400±500	10000±1000
Lower molars' occlusal surface (the operation field is shaded with dental handpiece, positioned in oral cavity).	250±5	300±10

Table 3. The Operation Field* Illuminance with Additional Light Sources

	Dental operating light is off, lx	Dental operating light is on, lx
LED headlight	2300±300	12100±300
LED head light with colour filter	101±4	Not used
LED light source of dental operating microscope	6800±500 (40 cm distance)	12500±300

* The measurements were performed at lower molars' occlusal surface

Table 4. Operation Field Illuminance Provided with Intraoral Light Sources

	Dental operating light is off, lx	Dental operating light is on, lx
Dental mirror with LED light	950±12	11200±200
LED turbine handpiece	5200±500	6800±300
Intraoral suction & lighting system MaxBite*	Min* 3000±500 Max* 8000±500	Min* 13000±1500 Max* 18000±2100
* dimming		

together, the illuminance is (12100±300) lx, which is more than 20 times higher than treatment zone illuminance, provided by standard fluorescent lamp. However, the problem of operation field shading during dental treatment is not dissolved.

When direct tooth restoration is performed, the use of LED headlight can lead to composite resin premature polymerization due to high intensity blue spectra region [4]. So, for resin composite modelling special colour filter is recommended. In that case, operation field illuminance decreases up to 101 lx.

Nowadays endodontic treatment, microsurgery and many other procedures are performed under high magnification with dental operating microscope. Built-in LED light source provides the operation field illuminance value (6800±500) lx when used alone and (12500±300) lx when used together with dental operating light.

Intraoral light sources put the light directly to the operating field and provide a high illuminance value (Table 4).

Dental mirror with LED light provides illuminance (950±12) lx when used alone and (11200±200) lx when used together with dental operating light. So, with dental mirror with LED a good illumination of operation field can be reached even in zones of indirect vision.

When LED dental handpiece is used, the light beam is directed exactly to the tooth surface, but the handpiece itself partially obstructs the light from dental operating lamp. In this situation the operating field illuminance was (6800±300) lx, which was much better comparing to the dental handpiece without LED light, (300±10) lx.

Intraoral suction & lighting system MaxBite can provide the operating field illuminance from (3000±500) lx up to (5000±500) lx when

used alone and in range from (13000±1500) lx to (18000±2100) lx when used together with dental operating light. The system is fixed opposite to operating field (when the treatment is on the right side, MaxBite is on the left side), so the light can be partially obstructed with instruments used during dental treatment.

The results of the study demonstrate that the conventional overall illumination with fluorescent based lamps is not enough for adequate lighting of treatment zone. Recommended by standards illuminance value 1000 lx can be reached, when additional LED ceiling light is used.

The operation field illuminance depends on oral cavity area and patients position. The best illuminance level was achieved in patient's supine position. The dental operating light can provide illiuminance values from 12000 lx up to 14000 lx at the incisors and from 4000 lx up to 10000 lx at the molars. So, the difference between treatment zone and operating field illumination can be up to 12–14 times. During the working time, the dentist has to switch attention from operating field to instrument table many times. The significant difference between illuminance values leads to eye fatigue due to frequent adaptation to varying light levels [2]. This can have adverse effect on the vision of the dentist and assistant [12]. According to T.F. Danilina et al., 86.7 % of dentists note eye fatigue after the working shift [13]. According to A.V. Nemaeva et al. after the working shift 60 % of dentists note blurred vision and 20 % have eye redness [14].

The use of LED headlights together with dental operating light allows increasing illuminance up to 2000 lx. However, the dental operating light alone can provide illuminance relevant to European standards. So, there is no need to use LED headlight for conventional dental treatment, especially on the zone of indirect vision. Headlights have narrow angle light distribution. If a dentist turn his head to the instrument table and back during a treatment, it's necessary to refocus a headlight. Headlights using is the most efficient at long treatment procedures requiring a maximal dentist attention and high illuminance level (for example, endodontic surgery). It's also important to take into account that in cool white LEDs a royal blue band light intensity is significantly higher that yellow-green band one that is a cause of additional dentist eye strain [15].

It's necessary to note that maximal illuminance level is achieved only in front teeth group area. In molar area the illuminance is significantly lower. At first, it's impossible to provide a direct lighting in lower molar and especially upper molar area. At second, instruments shade the operating field in this region. In these cases intraoral light sources providing adequate operating field illuminance even in indirect vision zones are the most efficient.

The results, which were obtained in the upper research, allow recommending ceiling lights and intraoral light sources (dental mirrors with LED lights, LED dental handpieces and intraoral suction & lighting systems) as additional lighting in dentistry.

REFERENCES:

1. Nekhoroshev AS, Danilova NB. Characteristics of work conditions of dentists in therapeutic dentistry offices. Med Tr Prom Ekol. 2006;(11):42–3. [In Russ]

2. Demchenko TV. Professional visual impairments in the dentist. Syndrome of "dry eye". Causes, methods of prevention. Parodontologiya. 2012; (3): 62–7 [In Russ]

3. Iacomussi P., Carcieri P., Rossi G., Migliario M. The factors affecting visual discomfort of dental hygienist. Measurment. 2017; Vol 98: 92–102.

4. Walsh L. LED operating lights in dental practice. Ausralasian Dental Practice; May/June 2009:48–54

5. Health and safety rules and standards 2.1.3.2630–10 (SanPin 2.1.3.2630–10) "Sanitary-epidemiological requirements for organizations engaged in medical activities", № 58, 08.05.2010 [In Russ]

6. Dyachenko VG, Galesa SA, Pietrokh MT, Pavlenko IV. Introduction to general practice in dentistry. – Khabarovsk, 2009: 312 p. [In Russ]

7. CSN EN12464–1:2011. Light and lighting – Lighting of work places – Part 1: Indoor work places

8. DIN5035–3:2006–07 Artificial lighting – Part 3: Lighting of health care premises

9. Khamidova TM, Shamsiddinov AT, Daburov KN Sanitary and hygienic assessment of working conditions in dental institutions of various forms of ownership. Nauchno-prakticheskij zhurnal TIPPMK. 2013; (2):202–3. [In Russ]

10. ISO 9680:2014 Dentistry – Operating lights.

11. GOST 26368–90 "Medical lights" [In Russ]

12. Garbin A.J.I., Garbin C.A.S., Ferreira N.F., Ferreria N.L., Saliba Jr. O.A. Illumination in the dental office. Acta Cientifica Venezolana. 2007; Vol 58(1):29–32.

13. Danilina TF, Slivina LP, Dallakyan LA, Kolesova TV. The influence of hygienic and ergonomic labor as-

pects on the dentist's health. Health & Education Millenium. 2016; Vol. 18 (1):234–6. [In Russ]

14. Nemaeva AV, Alpatova VG, Bukhtiyarov IV, Gritsay IG, Selyagina AS, Batyukov NM. Ergonomic aspects analysis of using the magnification systems in endodontic treatment. The Dental Institute. 2017; (1):16–7 [In Russ]

15. Stamatacos C, Harrison JL. The possible ocular hazards of LED dental illumination applications. J Tenn Dent Assoc. 2013, Fall-Winter; 93(2):25–9

Anna Yu. Turkina,
Ph.D., graduated from Moscow State University of Medicine and Dentistry in 2001, Associate Professor of the Department of Therapeutic Stomatology of I.M. Sechenov First Moscow State Medical University (Sechenov University)

Irina A. Novikova,
Ph.D, Associated Professor, graduated from Moscow State University of Medicine and Dentistry in 1989. At present, she is an Associate Professor of the Department of Therapeutic Stomatology of I.M. Sechenov First Moscow State Medical University (Sechenov University)

Andrei N. Turkin,
Ph.D., raduated from Faculty of Physics of M.V. Lomonosov Moscow State University (MSU) in 1995. At present, he is an Associated Professor of the Department of Optics, Spectroscopy and Nanosystem Physics of Faculty of Physics of Lomonosov State University

Galina N. Shelemetieva,
Ph.D., graduated from Dental Faculty of the Irkutsk State Medical University in 1984. At present, she is a practitioner dentist in private practice in Blagoveshchensk city, Russia

Light & Engineering
Vol. 26, No. 3, pp. 188–193, 2018

Svetotekhnika
No. 4, 2018, pp. 51–55

THE USE OF LED-BASED DIGITAL OPTICAL MINISTICKS AS MULTI-FUNCTIONAL CONTROLS OF UNIFIED HUMAN-MACHINE INTERFACES

Sergei A. Golubin, Vladimir S. Nikitin, and Roman B. Belov

Research, Development and Manufacturing enterprise "Tensosensor"
E-mail: 507z@mail.ru

ABSTRACT

The active development of robotics requires increasingly complex remote control devices. The remote control devices are increasingly large, complex, and expensive. They decrease economic efficiency of robotics and increase their price.

The scientific task is the research into possibility of applying optical mini-sticks on the basis of light emitting diodes as the new type basic multi-functional controls of unified human-machine interfaces allowing us to control commonly known robotic equipment types using identical devices.

During the research original ergonomic methods of purposeful combination of two mini-sticks on two actuating levers were used so that to provide convenience of tactile control of various robots without visual contact with controls.

As a result of the research**,** new controls were created and patented. They became known as "poly-joysticks" (patent of Russian Federation No. 2497177) and allow controlling engineering facilities having up to 20 degrees of freedom which exceeds the similar parameters of known controls by factor of 3 to 5. Due to combined use of optical mini-sticks, two poly-joysticks and a video mask, a new general-purpose generation human-machine interface was created. It allows controlling various robots and vehicles, from tractor to aircraft.

The discussion of the obtained results was carried out by comparing them with parameters of control panels of different robotics systems. The analysis of the comparison results has shown that the controls based on poly-joysticks and digital optical mini-sticks on the basis of light emitting diodes have the best indices in terms of implemented among known control devices, in terms of ratio of functionality to weight and volume of the devices. New interfaces have already been applied for developing multi-agent robotic system control system for fire forest extinguishing.

Keywords: optical mini-stick, LED, photo diode, optical system, poly-joystick, control system, unified human-machine interface

1. INTRODUCTION

Nowadays complex robotics is being developed for fire extinguishing, emergency and rescue activities, carrying out dangerous operations in mining industry, etc. The robotic systems are increasingly complex and multi-purpose. The existing control panels created using traditional joysticks and buttons are increasingly large and expensive, but their functionality is still insufficient and they are inconvenient. Therefore, the developer companies often have to copy the whole cab of a vehicle to be robotized. For instance, this is the way they followed in Komatzu and BELAZ companies for controlling robotic dump trucks [1, 2]. Such solutions, in which the cost of control facilities is comparable with the cost of robots, decrease economic efficiency of robotics. It is possible to solve this problem by developing cheap and ergonomic human-machine interfaces on the basis of new multi-purpose controls. Such controls were invented in Research, Develop-

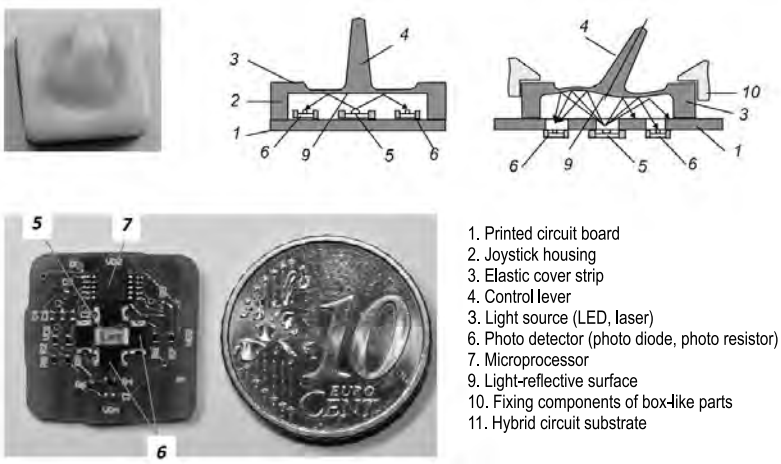

Fig. 1. Optical mini-stick DMR4I–Ch developed by Research, Development and Manufacturing enterprise "TENSOSENSOR"

ment and Manufacturing enterprise "TENSOSENSOR" and patented in Russia (patents of the Russian Federation Nos. 2596576 and 2594992).

The scientific task of this paper is the research into possibility of applying digital optical mini-sticks on the basis of LEDs as the basic controls of unified human-machine interfaces.

2. PROPOSED METHODOLOGY AND DISCUSSION

The optical system of a digital mini-stick is shown in Fig. 1. The mini-stick contains LEDs and a photo diode above which an elastic deformation element is located. It is made of an elastic polymer with a control lever. It is an optical modulator changing the intensity of the reflected light flux impinging on the photo diode as the handle is tilted. The mini-stick processor calculates the mini-stick angle and inclination direction and transmits the information to the control system.

The use of an optical circuit and a microprocessor allowed creating a digital optical mini-stick DMR4I–Ch [3]. The mini-stick has high output signal linearity (Fig. 2), convenient digital signal output, compact size (16 x 19 x 13.5 mm), about 2.3 g weight, long service life – about 1.5 million presses. The control lever deviation range is 5 mm in any direction. The optical mini-stick characteristics research results are provided on articles [4–8].

The most important advantage of the created mini-stick is its polymorphy, i.e. its applicability as a multi-purpose device capable of performing several functions simultaneously, for example, as a button, toggle switch, multi-position switch, regulator and a joystick. The functionality can be changed immediately during operation that is on-line. The digital mini-stick is "intelligent", it is capable of distinguishing long-time and short-time pushes, single and double pushes, circular rotational movements, which is beyond the functionality of other types of switches.

During the research original ergonomic methods of purposeful combination of two mini-sticks on two robot actuating levers were used so that to provide convenience of tactile control of various robots without visual contact with controls. As a result of multiple screening of combinations of mini-stick positions and ergonomic tests of different control lever designs involving experienced experts the unique controls were created and patented. They were called "poly-joysticks" (patent of the Russian Federation No. 2497177).

Fig. 3 illustrates a poly-joystick with optimum layout of mini-sticks. Two mini-sticks (M1 and M2) are located under the thumb. Mini-stick M1 is very convenient for controlling the vehicle direction movement (turns, U-turns). Mini-stick M2 is convenient to be used for controlling the rotation of the direction video camera along the direction. It

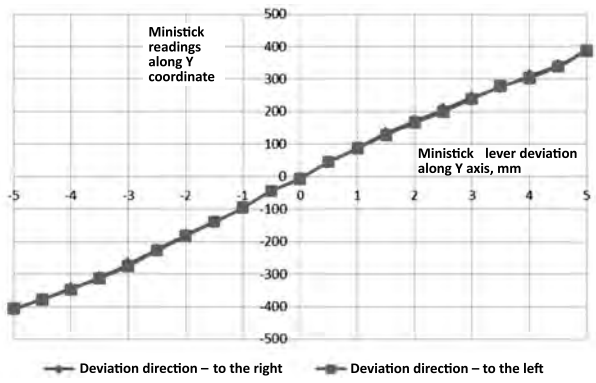

Fig. 2. Mini-stick output signal as a function of control lever deviation value

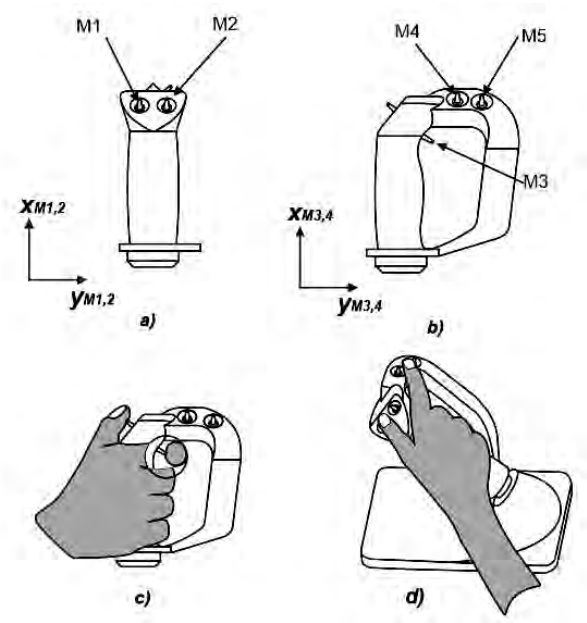

Fig. 3. The final version of mini-stick combination in the design of a poly-joystick with 5 mini-sticks (the mini-sticks are designated as M1, M2, M3, M4 и M5)

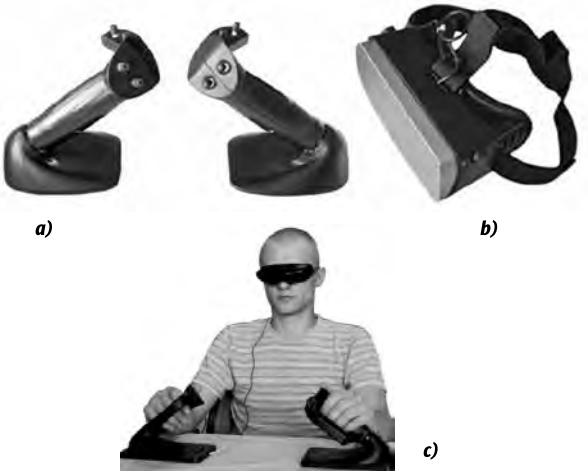

Fig. 4. – Unified human-machine interface
a) – poly-joysticks PD-002, b) video-mask, c) operator with a new unified human-machine interface

suits for air drones and ground robots. The third mini-stick M3 is located just like a pistol trigger, it is very convenient for emergency situations – abrupt deceleration, taking photos, shutter release, etc. The pointer finger reaction is very fast. Two more mini-sticks are located in the upper part of the poly-joystick (M4 and M5). These mini-sticks can be used for long-term special equipment control operations, effector guidance, switching over of operation modes or navigation.

To increase functionality, it is expedient to use two poly-joysticks with non-symmetrical function distribution simultaneously, i.e. to control one set of functions with the left poly-joystick and to control the other one with the right poly-joystick. In this case it is possible to switch over the functionality symmetry using special control software. For right-handers one functionality order can be set, and for left-handers the mirror order can be used.

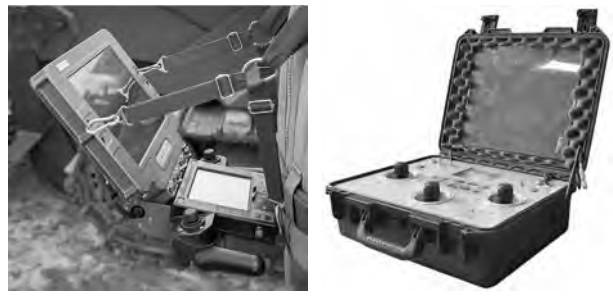

Fig. 5. Specialized panels for robot control

Poly-joysticks PD-002 type were created on the basis of the conducted research. Their specifications are posted on the TENSOSENSOR company web site [7].

3. RESULTS OF THE EXPERIMENTS

The experimental research into functionality of poly-joysticks have shown that they allow controlling both aerospace (shuttles, aircraft, helicopters, drones), and various ground and aquatic facilities – motor vehicles, tractors, excavators, harvesters, reaper threshers, skimming boats, etc. 10 two-coordinate mini-sticks operating in joystick mode allow controlling robots requiring control of 20 degrees of freedom. It is a very high functionality index.

The unified human-machine interface includes two control poly-joysticks, a video-mask and a unit interfacing with the control system. The video cameras image, tactical environment and different control instruments and switches are displayed in the video-mask display. Multi-functional controls – digital optical mini-sticks are located on poly-joysticks. The use of polyjoysticks allows carrying out the reliable visual contact with handling devices.

A demonstration video with examples of various equipment controlling is available on the web site of the company (see http://www.tenzosensor.ru/images/TenzosensorPJ.mp4).

An experimental research has shown that poly-joysticks of the unified human-machine interface ensure high ergonomic standards and con-

Fig. 6. PonsseComfort interface

venience of operation for both right-handers and left-handers.

The use of video-mask of the original design allowed doing without bulky displays sensitive to flare, vibration and jerks.

4. COMPARING PARAMETERS OF DIFFERENT ROBOTIC SYSTEMS' CONTROL PANELS

The HOTAS (hands on throttle-and-stick) concept used by the authors for creation of the new interface is fairly popular. Its development follows the trend of increasing the quantity and nomenclature of operational aircraft controls on the aircraft actuating levers for both left and right hands of the pilot.

However, such an approach to HOTAS concept implementation has serious drawbacks. Essentially, only one fixed-functionality operational control can be located on the grip. Off-the-shelf items and original solutions are used to control robotic systems.

From the off-the-shelf products the mobile platform developers usually select various joysticks, game pads, control panels, etc. The advantages of such products are absence of costs of their development and guaranteed operating life. The drawbacks are the fixed functionality of devices and ergonomic solutions which are not always in line with the developer's wishes.

The original solutions of control facilities in the form of specialized control panels are generally used by major developers, Fig. 5..

The advantages of specialized control panels are expanded functionality. Low ergonomic properties are drawbacks of such systems.

The interface of harvester produced by *Ponsse* – *PonsseComfort* company [8] (Fig 6) can be considered to be a close equivalent of poly-joysticks manufactured by Research Development and Manufacturing enterprise "TENSOSENSOR". It contains joysticks, armrests and a side instrument panel.

Analogical mini-joysticks are located on side surfaces of huge basic joystick levers under operator's thumbs. There are many programmable buttons for execution of different operations in range of thumbs access zone. Despite high functionality, the use of standard component parts demanded a high cost; the interface *PonsseComfort* has significant drawbacks: large overall dimensions and weight, and high price.

Table 1 contains specifications of known robot control systems.

Fig. 7 illustrates the quantity of freedom degrees for joysticks used in control devices shown

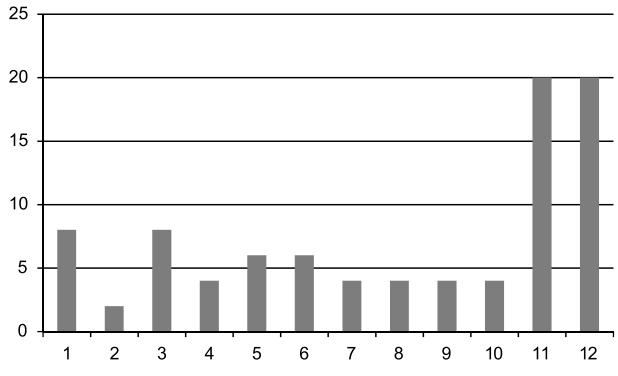

Fig. 7. Quantity of freedom degrees for joysticks (Device numbers correspond to the order in Table 1)

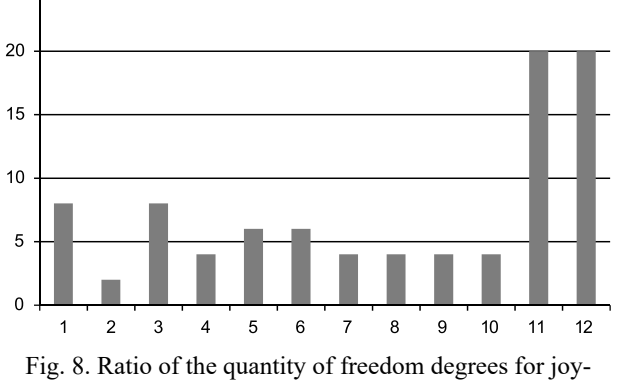

Fig. 8. Ratio of the quantity of freedom degrees for joysticks to the volume of control devices (the device numbers correspond to the order in Table 1)

Table 1. Specifications of Known Robot Control Systems

Item No.	Manufacturer or product name	Quantity of joysticks, pcs	Quantity of switches, pcs	Length/ width/ height, dm	Volume/ Weight, l/kg
1	Platform TALON/SWORDS robot	4	23	4/4/1.5	24/12
2	Robotic board SWAT-Bot	1	5	0.8/0.5/1.2	0.48/0.8
3	Panel HBC Radiomatic Palfinger	4	1	4/2/1.5	12/3
4	Panels of Russian State Scientific Center for Robotics and technical Cybernetics	2	20	4/4/1.5	24/8
5	Control panel for robot “VARAN” – Scientific and Training Center of Bauman Moscow State Technical University	3	22	4/4.5	24/8
6	Control panel for robots “Varyag” – Scientific and Training Centre of Bauman Moscow State Technical University	3	24	4/4/1.5	24/8
7	Control panel for multi-purpose robotic system “Metallist” (Kovrov)	2	24	3.5/3.5/0.7	8.58/4
8	Control panel for “Tigr” vehicle, OJSC Elins	2	12	4/2/2.5	5/12
9	Control panel for robot manufactured by OJSC Spetstekhnika pozharotusheniya	2	25	4/4/1.5	24/12
10	Control panel for robot “Tral-Patrul”:	2	6	3.5/1.5/1.5	7.88/3
11	Poly-joysticks manufactured by Research, Development and Manufacturing enterprise “TENSOSENSOR”	**10**	-	**0.2/1.8/1.2**	0.86/1.2
12	Hand-wheels based on poly-joysticks	**10**	-	**3/1.8/1.8**	9.72/2.5

in Table 1. Fig. 8 illustrates the ratio of quantity of freedom degrees for joysticks to the volume of the devices shown in Table 1.

The discussion of the obtained results was carried out by comparing them with parameters of control panels of different robotics systems. The analysis of the comparison results has shown that the controls based on poly-joysticks and digital optical mini-sticks on the basis of light emitting diodes have the best indices in terms of implemented among researched robot control devices, in terms of ratio of functionality to weight and volume of the devices.

5. CONCLUSIONS AND RECOMMENDATION

The results of the conducted research allow concluding that the use of LED-based digital optical mini-sticks as multi-functional controls enables creating up-to-date ergonomic human-machine interfaces with expanded functionality.

The comparison of the up-to-date robot control systems and advanced developments in the field of human-machine interfaces shows expediency of use of unified human-machine interfaces developed by Research, Development and Manufacturing enterprise “TENSOSENSOR” on the basis of digital optical mini-sticks in control systems of robotic systems of various applications. On the basis of the conducted research it was decided to use the developed interface in the control system of the multi-agent robotic system for forest fire extinguishing [9].

6. ACKNOWLEDGEMENTS

The research works are conducted with financial support of the government represented by the Ministry of Education and Science of the Russian Federation within the framework of fulfilment of the Agreement dated the 26th of September, 2017 No. 14.579.21.0151. Unique identifier of applied scientific research and experimental development is

the RFMEFI57917X0151. The authors are grateful to monitors and experts of Scientific and Engineering Enterprise Directorate for correct and well-wishing discussion of the obtained results. The authors thank D. Sc. (Engineering) Semenov E.I. for valuable recommendations provided by him during the work.

7. REFERENCES

1. Kulula, M.I. and Akande, J.M. (2018) Effects of Machine Parameter and Natural Factors on the Productivity of Loading and Haulage Equipment. Journal of Minerals and Materials Characterization and Engineering, 6, 139–153. doi: 10.4236/jmmce.2018.61011.

2. Potapenko A. N., Gaidukov K.Y., Medvedev V.V. Peculiarities of automation of quarry dump trucks within automated dispatch control system, FSBEI of HPE V.G. Shukhov Belgorod State University, journal "Fundamental Research", 2016, No. 9 (part 1), – pp. 56–51).

3. Digital optical ministick /Datasheet/Research, Development and Manufacturing enterprise "Tensosensor" LLC /2016/) http://www.tenzosensor.ru/images/DMR4I–Ch%20Data%20Sheet.pdf.

4. Experimental research on the performance of optical ministicks with a common receiver/ Sergei A. Golubin, Alexei N. Lomanov, Vladimir S. Nikitin and Valery M. Komarov // Light & Engineering. 2015. Volume 23, Number 4, pp. 81–87.

5. Experimental study of how lighting patterns affect optical ministicks characteristics / Sergei A. Golubin, Alexei N. Lomanov, Vladimir S. Nikitin, Valery M. Komarov, and Ernst I. Semenov // Light &Engineering. 2016. Volume 24, Number 4, pp. 105–110.

6. Study of Characteristics of VCSEL-based Optical Ministicks / Sergei A. Golubin, Alexei N. Lomanov, Vladimir S. Nikitin, Valery M. Komarov, and Ernst I. Semenov. Study of Characteristics of VCSEL-based Optical Ministicks // Light & Engineering. 2016. Volume 24, Number 4, pp. 111–116.

7. Polyjoystick/Datasheet/Research, Development and Manufacturing enterprise "Tensosensor" LLC/ 2017/) http://www.tenzosensor.ru/images/PD-002 %20Data%20Sheet.pdf.

8. Matti Lahtinen, Ergonomics evaluation of Cut-To-Length forest harvesters, Master's thesis Management and Economy in the International Forest Sector, June 2017/ https://www.theseus.fi/bitstream/handle/10024/130914/Lahtinen_Matti.pdf?sequence=1&isAllowed=y.

9. Nikitin V. S., Belov R.B., Robotic system for forest fire extinguishing, Research, Development and Manufacturing enterprise "Tensosensor" LLC), MATERIALS OF THE XIII INTERNATIONAL SCIENTIFIC AND PRACTICAL CONFERENCE, October 30 – November 7, 2017, c 24 Robotics, http://www.rusnauka.com/books/2017–10–28-A4-tom-3.pdf.

Sergey A, Golubin,
post-graduate of Federal State-Financed Educational Institution of Higher Professional Education «P.A. Solovyov Rybinsk State Aviation Technical University» (RSATU). He is graduated from RSATU in 2013. At present, he is a systems engineer in Tenzosensor LLC

Vladimir S. Nikitin,
Ph.D. and CEO&founder of Tenzosensor LLC. Inventor and idea man, leading expert in the field of R&D organization and performance, strategy development, organization of project team work. Miscellaneous expert in the field of Physics, Chemistry, Electronics, Material Sciences, highly qualified designer. At present, he is the director of LLC «Scientific and Technical Centre "Introphysics"»

Roman B. Belov,
Deputy General Director, Chief Designer of the Scientific and Production Enterprise "Tenzosensor", and a research engineer, a highly skilled designer and an experienced manager, has extensive experience in a senior position in the central design bureau, oversees the development and production of innovative products, and is fluently active in modern CAD systems

CONTENTS

VOLUME 26 **NUMBER 4** **2018**

LIGHT & ENGINEERING
(SVETOTEKHNIKA)

PARTNERS OF LIGHT & ENGINEERING JOURNAL

Editorial Board with big gratitude would like to inform international lighting community about the Journal Partners Institute establishment. The list with our partners and their Logo see below. The description of partner's collaboration you can found at journal site *www.sveto-tekhnika.ru*

BL Group

BL GROUP holding

ЛИТ

REFLUX HID Lighting systems

PHAROS-ALEF

LIGHTING SOLUTIONS

enercon®
СОЗДАЕМ ЛИДЕРОВ В ЭНЕРГОСБЕРЕЖЕНИИ

ГСТЗ г. Гагарин

FAGERHULT

Светотехнический завод ВЛАДАСВЕТ

TS TENZOSENSOR

СВЕТОВЫЕ СИСТЕМЫ

СОЛАР® МАГИЧЕСКИЙ СВЕТ

ВНИСИ

НИИ